



## University of Bradford eThesis

This thesis is hosted in [Bradford Scholars](#) – The University of Bradford Open Access repository. Visit the repository for full metadata or to contact the repository team



© University of Bradford. This work is licenced for reuse under a [Creative Commons Licence](#).

THERMO-ECONOMIC MODELLING OF MICRO-  
COGENERATION SYSTEMS

N. KALANTZIS

PHD

2015

Thermo-Economic Modelling of Micro-Cogeneration Systems

System Design for Sustainable Power Decentralization by Multi-Physics  
System Modelling and Micro-Cogeneration Systems Performance Analysis  
for the UK Domestic Housing Sector

Nikolaos KALANTZIS

Submitted for the degree of Doctor of Philosophy

Faculty of Engineering and Informatics

University of Bradford

2015

## **Abstract**

Nikolaos Kalantzis

Thermo-Economic Modelling of Micro-Cogeneration Systems

System Design for Sustainable Power Decentralization by multi-physics system Modelling and Micro-Cogeneration Systems Performance analysis for the UK Domestic housing Sector

*Keywords: Sizing, Selection, micro-CHP, Combustion Engine, Residential, Simulation, Modelling, Performance, Emissions*

Micro-cogeneration is one of the technologies promoted as a response to the global call for the reduction of carbon emissions. Due to its recent application in the residential sector, the implications of its usage have not yet been fully explored, while at the same time, the available simulation tools are not designed for conducting research that focuses on the study of this technology.

This thesis develops a virtual prototyping environment, using a dynamic multi-physics simulation tool. The model based procedure in its current form focuses on ICE based micro-CHP systems. In the process of developing the models, new approaches on general system, engine, heat exchanger, and dwelling thermal modelling are being introduced to cater for the special nature of the subject. The developed software is a unique modular simulation tool platform linking a number of independent energy generation systems, and presents a new approach in the study and design of the multi node distributed energy system (DES) with the option of further development into a real-time residential energy management system capable of reducing fuel consumption and CO<sub>2</sub> emissions in the domestic sector.

In the final chapters, the developed software is used to simulate various internal combustion engine based micro-CHP configurations in order to conclude on the system design characteristics, as well as the conditions,

necessary to achieve a high technical, economic and environmental performance in the UK residential sector with the purpose of making micro-CHP a viable alternative to the conventional means of heat & power supply.

## **Acknowledgements**

*This thesis cannot be complete without acknowledging the people whose support played a key role in this undertaking.*

*I would like to thank my principal supervisor Professor K. M. Ebrahimi for trusting me with this project and offering invaluable support in the form of excellent guidance and advice, as well as in the form of necessary materials for the development and completion of this thesis.*

*I would like to thank and dedicate this thesis to my family, whose unconditional love and support made it possible for me to pursue my dreams and be in the current position of completing this personal milestone.*

## Table of contents

Abstract.....	i
Acknowledgements.....	iii
Table of contents .....	iv
Table of figures.....	xii
Table of tables .....	xviii
Nomenclature .....	xix
<b>Chapter 1 Introduction .....</b>	<b>1</b>
1.1. Model based energy analysis and design .....	3
1.2. Power generation and waste heat .....	4
1.3. Waste heat recovery in combustion engines .....	5
1.4. Definition of cogeneration .....	5
1.5. Micro Cogeneration .....	6
1.6. An overview of existing $\mu$ CHP types .....	9
1.7. Obstacles to the proliferation of $\mu$ CHP systems.....	9
1.8. Contribution of the Thesis .....	12
1.9. Structure of Report .....	14
<b>Chapter 2 Background Knowledge .....</b>	<b>17</b>
2.1. Heat and power supply .....	17
2.2. Combined Heat and Power.....	20
2.3. Energetic, environmental, and economic performance (EEEP) .....	23
2.3.1. Device efficiency vs. overall efficiency.....	24
2.3.2. Energy stream in an ICE based systems.....	25
2.3.3. EEEP Indicators .....	27
2.4. Summary .....	32

<b>Chapter 3 Literature Review</b> .....	33
3.1. System viability and factors that affect it.....	33
3.1.1. Geographical location.....	33
3.1.2. Season of the year .....	34
3.1.3. Building type and construction method.....	35
3.1.4. Heat to Power Ratio ( <i>HPR</i> ).....	36
3.1.5. System electrical efficiency.....	38
3.1.6. Morphology of load patterns .....	40
3.1.7. Device fuel utilization efficiency .....	41
3.1.8. Performance of the conventional heat and power supply .....	41
3.1.9. Control strategy .....	42
3.1.10. System size.....	44
3.1.11. Energy prices .....	45
3.1.12. Electricity export prices .....	46
3.1.13. Government subsidies.....	46
3.1.14. Loads and system inertia .....	47
3.1.15. Useful operating life.....	49
3.2. Improving $\mu$ CHP fuel conversion efficiency.....	49
3.2.1. High performing internal combustion engines.....	49
3.2.2. Combined cycles .....	50
3.3. Managing heat and power surplus and deficiency .....	51
3.3.1. Electricity surplus.....	51
3.3.2. Electricity deficiency and import .....	52
3.3.3. Thermal surplus and heat rejection .....	52
3.3.4. Thermal deficiency and the auxiliary burner .....	53
3.3.4.1. Thermal Storage.....	53
3.3.4.2. Heat recovery system and fluid temperatures .....	55



3.3.5.	Indoor temperature settings.....	56
3.4.	Modelling and Simulation of micro - CHP systems .....	57
3.4.1.	Micro – CHP studies with building simulation packages.....	57
3.4.2.	CHP System Modelling.....	58
3.4.2.1.	Constant coefficient CHP models.....	58
3.4.2.2.	Quasi-stationary CHP models .....	59
3.4.2.3.	Thermodynamic ICE model.....	60
3.4.2.4.	Transient ICE behaviour and micro – CHP engine modelling. .	60
3.4.2.5.	Generator Shaft dynamics.....	61
3.4.2.6.	ICE Exhaust Temperature calculation .....	62
3.4.2.7.	Waste heat in the engine coolant .....	64
3.4.3.	Heat exchanger modelling .....	64
3.4.4.	Heat Storage Tank Models .....	65
3.5.	Load profiles .....	66
3.5.1.	Energy demand in single family dwellings .....	66
3.5.2.	Representative electrical load profiles and their usage .....	67
3.5.3.	IWEC weather data .....	69
3.5.4.	Domestic Hot Water (DHW) Profiles.....	69
3.5.5.	Occupancy Pattern and heating period .....	70
3.6.	Summary .....	71
<b>Chapter 4 Modelling the ICE based generator set .....</b>		<b>73</b>
4.1.	System Model .....	75
4.2.	The stoichiometric combustion of fuels.....	86
4.2.1.	n – Octane .....	88
4.2.2.	Stoichiometric Combustion of Natural Gas.....	88
4.3.	Parameter Identification .....	89

4.4.	Energy based model of the electric generator .....	92
4.5.	Simulation and Validation .....	99
4.6.	Design and Analysis .....	104
4.7.	Thermal load on the cooling system of SI ICEs .....	106
4.8.	Natural Gas as an ICE fuel .....	107
4.9.	Categories of Natural Gas fuelled ICEs .....	108
4.10.	Fuel modified performance surfaces .....	109
4.11.	Proposed engine model variations .....	111
4.11.1.	Low CR Petrol engine converted to NG .....	111
4.11.2.	High CR purpose designed NG exclusive engine.....	112
4.12.	Summary .....	113
 <b>Chapter 5 Heat Exchanging Systems.....</b>		<b>114</b>
5.1.	Flow circuit types .....	114
5.2.	Heat Exchanger Modelling.....	116
5.3.	Shell & tube heat exchanger.....	118
5.3.1.	Forced convection and heat transfer .....	118
5.3.2.	Heat transfer coefficients.....	123
5.3.3.	Flow conditions and heat transfer.....	124
5.3.4.	Laminar flow .....	124
5.3.5.	Turbulent flow .....	125
5.3.6.	Exhaust gas side - pulsated flow .....	126
5.4.	The discretised heat exchanger model on Simulink.....	128
5.5.	Coil type heat exchanger .....	131
5.6.	Modelling the heating radiators.....	135
5.7.	Heat Exchanger Simulation and Mapping Tool.....	137
5.8.	Lookup table based quasi - stationary models.....	140

5.8.1.	The shell and tube heat exchangers.....	140
5.8.2.	The storage tank coils .....	142
5.8.3.	The radiator .....	143
5.9.	Summary .....	143
<b>Chapter 6 UK Dwelling Models .....</b>		<b>145</b>
6.1.	Dwelling models for simulation .....	145
6.2.	The importance of dwelling model diversity .....	146
6.3.	Geometrical characteristics of typical UK dwellings .....	146
6.4.	Statistical data on UK dwellings .....	147
6.5.	An overview of heat loss calculations .....	150
6.7.	Dwelling age groups .....	155
6.8.	Dwelling Fabric .....	156
6.8.1.	Walls.....	156
6.8.2.	Roof.....	157
6.8.3.	Ground Floor .....	157
6.8.4.	Windows.....	157
6.9.	Model Validation .....	157
6.10.	Generated curves .....	160
6.11.	Summary .....	164
<b>Chapter 7 Modelling structure .....</b>		<b>165</b>
7.1.	General layout .....	165
7.1.1.	The Load Block.....	167
7.1.2.	The dwelling .....	168
7.1.3.	Transient system thermal characteristics .....	172
7.1.4.	The system Controller .....	175

7.1.5.	The $\mu$ CHP System block .....	178
7.1.6.	The Heat Storage System block.....	179
7.1.7.	The “Cogeneration Unit” block.....	181
7.1.8.	The “Heat Recovery System” block.....	183
7.1.9.	The Generator Set block .....	183
7.2.	Micro – CHP Energy Simulation Tool .....	185
7.2.1.	Simulation parameters.....	185
7.2.1.1.	Engine displacement.....	185
7.2.1.2.	Engine type .....	185
7.2.1.3.	Electric machine conversion efficiency at maximum load.....	185
7.2.1.4.	CHP system configuration.....	186
7.2.1.5.	Design Heat Exchanger temperatures .....	186
7.2.1.6.	Design radiator temperatures.....	186
7.2.1.7.	Dwelling Location .....	186
7.2.1.8.	Dwelling configuration .....	187
7.2.1.9.	Generation of representative dwelling combinations.....	187
7.2.1.10.	Dwelling thermal mass.....	188
7.2.1.11.	System operating mode .....	188
7.2.1.12.	Indoor temperature limits .....	188
7.2.1.13.	Thermal storage tank size.....	189
7.2.1.14.	Auxiliary burner capacity.....	189
7.2.1.15.	System inspection panel.....	190
7.3.	Total required thermal capacity of heating systems.....	191
7.3.1.	Case 1 HPC, no auxiliary boiler, no heat storage .....	192
7.3.2.	Case 2 HPC with auxiliary boiler, no heat storage.....	193
7.3.3.	Case 3 HPC with auxiliary boiler and heat storage.....	193
7.4.	Post Processing Window .....	194

7.5.	Model functionality .....	196
7.6.	Summary .....	202
<b>Chapter 8 Heat Priority Control Analysis.....</b>		<b>203</b>
8.1.	Engine Grade.....	203
8.2.	Dwelling Type .....	208
8.3.	Dwelling Location.....	217
8.4.	Summary .....	225
<b>Chapter 9 Electricity Priority Control Analysis .....</b>		<b>227</b>
9.1.	Engine Grade.....	227
9.2.	Heat Storage Size.....	235
9.3.	Heat storage tank water temperature limits .....	242
9.4.	Dwelling Type .....	250
9.5.	Dwelling Location.....	259
9.6.	Summary .....	265
<b>Chapter 10 Results and Strategy Comparison .....</b>		<b>268</b>
10.1.	Energetic and Environmental Performance .....	268
10.2.	Operating Patterns .....	271
10.3.	Economic Performance .....	275
10.4.	Summary .....	278
<b>Chapter 11 Conclusions and Recommendations for Future Work.....</b>		<b>280</b>
11.1.	Observations .....	280
11.2.	General Conclusions .....	283

11.3. Recommendations for future work.....	287
<b>References</b> .....	290
<b>Appendix 1 Types of micro-CHP</b> .....	304
A.1.1 Stirling .....	304
A.1.2. Rankine .....	304
A.1.3. Micro Turbines.....	305
A.1.4. Fuel Cells .....	305
A.1.5. Thermo - Photovoltaic .....	306
A.1.6. ICE based systems .....	306
<b>Appendix 2. A discussion on Bottoming cycles</b> .....	308
A.2.1. Rankine Cycle .....	308
A.2.2. Turbocompounding .....	309
A.2.3. Turbo generator.....	310
A.2.4. Thermoelectric Exhaust Heat Recovery .....	311
A.2.5. A combination of technologies.....	312
<b>Appendix 3 Sensible Enthalpy Plots</b> .....	313
<b>Appendix 4 UK Location Factors</b> .....	314

## Table of figures

Figure 1.1 Schematic of an I.C.E. based Micro-CHP system.....	7
Figure 2.1 Energy flow under conventional supply of heat and power.....	20
Figure 2.2 Schematic of a basic cogeneration layout.....	22
Figure 2.3 Energy flow between the CHP, the environment and the user....	27
Figure 3.1 Dry bulb outdoor temperature vs. time of a day in January.....	34
Figure 3.2 Averaged load profiles of a detached and a mid - terraced house .....	36
Figure 3.3 Engine conversion efficiency vs. fraction of max. power.....	39
Figure 3.4 Electric machine efficiency vs. fraction of maximum power .....	39
Figure 3.5 Monthly cost savings for three different fuel prices .....	46
Figure 3.6 Response of the heat recovery system start up.....	48
Figure 3.7 Electrical load profiles during a workday and a holiday.....	66
Figure 3.8 Averaged electricity profile of mid terraced dwellings .....	67
Figure 3.9 Electrical profile generated by the Domestic Electricity Demand Model .....	68
Figure 4.1 Comparison between the input and outputs of a) a typical engine model (for non cogenerating applications), and b) the developed engine model .....	74
Figure 4.2 Diagram of the main routes of energy flow .....	75
Figure 4.3 Block diagram of the proposed engine model.....	77
Figure 4.4 Block diagram of the power component calculator subsystem ...	84
Figure 4.5 Layout of the shaft dynamics subsystem .....	85
Figure 4.6 Exhaust temperature vs. engine speed and volumetric efficiency .....	90
Figure 4.7 Q.R. vs. engine speed and volumetric efficiency .....	91
Figure 4.8 Schematic of a voltage regulated synchronous electric machine	93
Figure 4.9 The simplified diagram of the generator/load circuit .....	95
Figure 4.10 The electrical load placed on a 2.8kW alternator vs. the required mechanical power input .....	98
Figure 4.11 Alternator conversion efficiency vs. the percentage of maximum power output .....	99
Figure 4.12 Power component distribution vs. time .....	100

Figure 4.13 Electrical load and engine exhaust temperature vs. time.....	101
Figure 4.14 Simulated and tested heat inlet rate and electrical load vs. time .....	102
Figure 4.15 Relative error of the estimated fuel input by the model vs. time .....	102
Figure 4.16 Simulated and measured exhaust temperatures vs time .....	103
Figure 4.17 Relative error of the exhaust temperature predicted by the model vs. engine speed and volumetric efficiency.....	104
Figure 4.18 Percentage of fuel input that enters the cooling system vs. engine speed .....	106
Figure 5.1 Schematic of a basic micro - CHP layout.....	115
Figure 5.2 Input/Output diagram of a basic heat exchanger model.....	116
Figure 5.3 Schematic of the discretised counter flow heat exchanger model .....	118
Figure 5.4 Section of the heat exchanger tube profile.....	119
Figure 5.5 Schematic of the heat transfer relationship between the incremental mass node and the fluid streams.....	122
Figure 5.6 Simulink block diagram of the discretised exchanger model.....	128
Figure 5.7 Simulink block diagram of each heat exchanger cell .....	129
Figure 5.8 Simulink block diagram of the "tube side" block.....	130
Figure 5.9 Simulink block diagram of the "shell side" block .....	130
Figure 5.10 3d CAD model of a coil type heat exchanger.....	131
Figure 5.11 Schematic of the discretised coil type heat exchanger model.	133
Figure 5.12 Segment of the discretised coil type heat exchanger model on Simulink .....	133
Figure 5.13 Simulink block diagram of a coil type heat exchanger cell .....	134
Figure 5.14 Simulink block diagram of the "shell side" block .....	135
Figure 5.15 Schematic of the rectangular section representing one element of the radiator.....	135
Figure 5.16 Schematic of the of the radiator model rectangular element...	136
Figure 5.17 Parameter input panel.....	138
Figure 5.18 Results display and mapping panel .....	139
Figure 5.19 Block diagram of the lookup table based exhaust gas heat exchanger model .....	141



Figure 5.20 Block diagram of the lookup table based jacket water heat exchanger model .....	141
Figure 5.21 Block diagram of the primary circuit coil type heat exchanger model .....	142
Figure 5.22 Block diagram of the secondary circuit coil type heat exchanger model .....	142
Figure 5.23 Block diagram of the lookup table based radiator model .....	143
Figure 6.1 I/O Diagram of the building model of Peter F. Chapman [110] .	147
Figure 6.2 Representation of different dwelling layouts in space .....	148
Figure 6.3 Cross section of a heat transfer surface .....	151
Figure 6.4 Sketch of a wall fitted with a window.....	151
Figure 6.5 I/O block diagram of heat loss calculations.....	153
Figure 6.6 I/O block diagram of the developed dwelling model.....	161
Figure 6.7 <i>HLP</i> vs. Floor Area for Pre 1967 dwellings .....	161
Figure 6.8 <i>HLP</i> vs. Floor Area for Post 1967 dwellings.....	162
Figure 6.9 <i>HLP</i> vs. Floor Area for Pre - 1967 dwellings .....	163
Figure 6.10 <i>HPL</i> vs. Floor Area for Post - 1967 dwellings.....	163
Figure 7.1 Top level of the Simulink based CHP/Dwelling model .....	166
Figure 7.2 Block diagram of the "load block".....	167
Figure 7.3 Block diagram of the "Dwelling" block.....	168
Figure 7.4 Schematic of the 3-node discretised wall model.....	170
Figure 7.5 Block diagram of the "Dwelling Fabric" block.....	171
Figure 7.6 Block diagram of heat transfer "Layer" blocks 1 - 4 .....	172
Figure 7.7 Block diagram of the "inner", "mid", and "outer" "Wall Layer Mass" nodes .....	172
Figure 7.8 Block diagram of the water circuit segment that connects the radiator outlet to the heat storage coil.....	174
Figure 7.9 Block diagram of the controller block. The controller code is contained in the "Controller Code Loop" Embedded Matlab Function .....	177
Figure 7.10 Block Diagram of the "Micro – CHP System" block.....	179
Figure 7.11 Block diagram of the "Heat Storage System" .....	180
Figure 7.12 Block diagram of the block "Heat Storage (2-Coil)".....	181
Figure 7.13 Block diagram of the "Cogeneration Unit" block .....	182

Figure 7.14 Block diagram of the "Heat Recovery System" block.....	183
Figure 7.15 Block diagram of the "Generator Set" block.....	184
Figure 7.16 System configuration panel.....	190
Figure 7.17 System inspection panel.....	191
Figure 7.18 Segment of the post processing window.....	194
Figure 7.19 Plot selection panel.....	195
Figure 7.20 Simulated indoor temperature profile of a workday in March..	196
Figure 7.21 March workday outdoor, indoor, and wall layer temperature profiles .....	197
Figure 7.22 Simulated indoor temperature profile of a holiday in March....	198
Figure 7.23 Simulated engine speed profile of a March workday.....	198
Figure 7.24 Simulated engine speed profile of a March holiday .....	199
Figure 7.25 Storage tank temperature profile under heat priority control during a March workday.....	200
Figure 7.26 Simulated engine speed profile under an EPC operation .....	201
Figure 7.27 Storage tank temperature under EPC strategy during a March workday .....	201
Figure 8.1 PES vs. $R_q$ (Engine comparison, HPC).....	204
Figure 8.2 PES vs. $V_d$ (Engine comparison, HPC).....	205
Figure 8.3 CO <sub>2</sub> savings vs. $R_q$ (Engine comparison, HPC) .....	205
Figure 8.4 Cost savings (With FIT) vs. $R_q$ (Engine comparison, HPC) .....	206
Figure 8.5 Cost savings (No FIT) vs. $R_q$ (Engine comparison, HPC).....	207
Figure 8.6 PES vs. $R_q$ (Dwelling comparison, HPC) .....	209
Figure 8.7 CO <sub>2</sub> Savings vs. $R_q$ (Dwelling comparison, HPC).....	210
Figure 8.8 Engine starts vs. $R_q$ (Dwelling comparison, HPC).....	211
Figure 8.9 Engine operating hours vs. $R_q$ (Dwelling comparison, HPC) ....	212
Figure 8.10 Engine oper. hours vs. $V_d$ (Dwelling comparison, HPC) .....	212
Figure 8.11 Boiler starts vs. $R_q$ (Dwelling comparison, HPC).....	213
Figure 8.12 Boiler operating hours vs $R_q$ (Dwelling comparison, HPC).....	214
Figure 8.13 Cost savings vs. $R_q$ (Dwelling comparison, HPC) .....	216
Figure 8.14 Cost savings vs. $R_q$ (Dwelling comparison, HPC).....	217
Figure 8.15 PES vs. $R_q$ (Geog. comparison, HPC) .....	218
Figure 8.16 CO <sub>2</sub> Savings vs. $R_q$ (Geog. comparison, HPC).....	219
Figure 8.17 Engine starts vs. $R_q$ (Geog. comparison, HPC) .....	220

Figure 8.18 Engine operating hours vs. $R_q$ (Geog. comparison, HPC) .....	221
Figure 8.19 Boiler starts vs. $R_q$ (Geog. comparison, HPC) .....	222
Figure 8.20 Boiler operating hours vs. $R_q$ (Geog. comparison).....	223
Figure 8.21 Cost Savings (With FIT) vs. $R_q$ (Geog. comparison, HPC) .....	224
Figure 8.22 Cost Savings (No FIT) vs. $R_q$ (Geog. comparison, HPC).....	224
Figure 9.1 PES vs. $V_d$ (Engine comparison, EPC) .....	228
Figure 9.2 CO <sub>2</sub> Savings vs. $V_d$ (Engine comparison, EPC).....	229
Figure 9.3 Engine starts vs. $V_d$ (Engine comparison, EPC) .....	230
Figure 9.4 Engine operating hours vs. $V_d$ (Engine comparison, EPC) .....	231
Figure 9.5 Boiler starts vs. $V_d$ (Engine comparison, EPC) .....	232
Figure 9.6 Boiler operating hours vs. $V_d$ (Engine comparison, EPC) .....	233
Figure 9.7 Cost savings (With FIT) vs. $V_d$ (Engine comparison, EPC).....	234
Figure 9.8 Cost savings (No FIT) vs. $V_d$ (Engine comparison, EPC) .....	235
Figure 9.9 PES vs. $V_d$ (Tank size comparison, EPC).....	236
Figure 9.10 CO <sub>2</sub> savings vs. $V_d$ (Tank size comparison, EPC) .....	237
Figure 9.11 Engine starts vs. $V_d$ (Tank size comparison, EPC) .....	237
Figure 9.12 Engine operating hours vs. $V_d$ (Tank size comparison, EPC) .	238
Figure 9.13 Boiler starts vs. $V_d$ (Tank size comparison, EPC) .....	239
Figure 9.14 Boiler operating duration vs. $V_d$ (Tank size comparison, EPC)	240
Figure 9.15 Cost savings (With FIT) vs. $V_d$ (Tank size comparison, EPC) .	241
Figure 9.16 Cost savings (No FIT) vs. $V_d$ (Tank size comparison, EPC) ...	242
Figure 9.17 Tested storage tank temperature operating limits.....	243
Figure 9.18 PES vs. $V_d$ (Temp. limit comparison, EPC).....	245
Figure 9.19 CO <sub>2</sub> savings vs. $V_d$ (Temp. limit comparison, EPC).....	245
Figure 9.20 Boiler starts vs. $V_d$ (Temp. limit comparison, EPC) .....	247
Figure 9.21 Boiler operating duration vs. $V_d$ (Temp. limit comparison, EPC)	248
.....	
Figure 9.22 Cost savings (With FIT) vs. $V_d$ (Temp. limit comparison, EPC)	249
.....	
Figure 9.23 Cost savings (Without FIT) vs. $V_d$ (Temp. limit comparison, EPC)	250
.....	
Figure 9.24 PES vs. $V_d$ (Dwelling comparison, EPC).....	251
Figure 9.25 $Q_{rej}/Q_{used}$ vs. $V_d$ (Dwelling comparison, EPC) .....	251
Figure 9.26 CO <sub>2</sub> Savings vs. $V_d$ (Dwelling comparison, EPC) .....	252

Figure 9.27 Engine starts vs. $V_d$ (Dwelling comparison, EPC) .....	253
Figure 9.28 Engine operating hours vs. $V_d$ (Dwelling comparison, EPC) ...	254
Figure 9.29 $E_{imp}/E_{use}$ vs. $V_d$ (Dwelling comparison, EPC) .....	254
Figure 9.30 Boiler starts vs. $V_d$ (Dwelling comparison, EPC) .....	256
Figure 9.31 Boiler operating hours vs. $V_d$ (Dwelling comparison, EPC) .....	257
Figure 9.32 Cost savings (with FIT) vs. $V_d$ (Dwelling comparison, EPC) ...	258
Figure 9.33 Cost savings (No FIT) vs. $V_d$ (Dwelling comparison, EPC) .....	259
Figure 9.34 PES vs. $V_d$ (Geog. comparison, EPC) .....	260
Figure 9.35 CO <sub>2</sub> Savings vs. $V_d$ (Geog comparison, EPC) .....	261
Figure 9.36 Boiler starts vs. $V_d$ (Geog comparison, EPC) .....	262
Figure 9.37 Boiler operating hours vs. $V_d$ (Geog. comparison, EPC) .....	263
Figure 9.38 Cost Savings (With FIT) vs. $V_d$ (Geog. comparison, EPC) .....	264
Figure 9.39 Cost Savings (Without FIT) vs. $V_d$ (Geog. comparison, EPC) .	265
Figure 10.1 PES vs. $V_d$ (Strategy comparison) .....	269
Figure 10.2 PES vs. month of the year (Strategy comparison) .....	270
Figure 10.3 CO <sub>2</sub> vs. $V_d$ (Strategy comparison) .....	271
Figure 10.4 Engine starts vs. $V_d$ (Strategy comparison) .....	272
Figure 10.5 Engine operating duration vs. $V_d$ (Strategy comparison) .....	273
Figure 10.6 Boiler starts vs. $V_d$ (Strategy comparison) .....	274
Figure 10.7 Boiler operating duration vs. $V_d$ (Strategy comparison) .....	275
Figure 10.8 Cost savings (With FIT) vs. $V_d$ (Strategy comparison) .....	277
Figure 10.9 Cost savings (Without FIT) vs. $V_d$ (Strategy comparison) .....	278
Figure A.2.1 Schematic of the energy flow taking place between the components of a combined ICE-Rankine cycle based CHP system .....	308
Figure A.2.2 Schematic of the energy flow taking place between the components of a turbo-compound prime mover supplying power to an electric machine .....	310
Figure A.2.3 Schematic of the energy flow taking place between the components of an internal combustion engine with a turbogenerator in the role of the bottoming cycle. Both cycles supply power to a respective electric machine .....	311

Figure A.3.1 Sensible Enthalpy of CO <sub>2</sub> vs. temperature .....	313
Figure A.3.2 Sensible Enthalpy of H <sub>2</sub> O vs. temperature .....	313
Figure A.3.3 Sensible Enthalpy of N <sub>2</sub> vs. temperature .....	313

**Table of tables**

Table 1.1 Comparison of existing $\mu$ CHP technologies .....	11
Table 4.1 Characteristics and settings of the tested engine.....	90
Table 4.2 Coefficients of the 5th order polynomial surface fits on $T_{exh}$ , and $Q.R$ .....	92
Table 6.1 Statistical composition of UK dwellings per number of storeys ..	149
Table 6.2 Average Total Dwelling Areas per dwelling type .....	149
Table 6.3 Heat Loss Parameters for different dwelling types .....	158
Table 6.4 Representative UK dwelling characteristics .....	159
Table A.4.1 Table of UK Location Factors [116] .....	314

## Nomenclature

### Chapter 1: Introduction

CHP	Combined heat and power	
FIT	Feed-In Tariff	
DES	Distributed energy system	
HHV	Higher heating value	(kJ/kg)
LHV	Lower heating value	(kJ/kg)
PBP	Payback period	(years)
ICE	Internal combustion engine	
SI	Spark ignition	
CI	Compression Ignition	
MT	Micro-turbine	
ECE	External combustion engine	
StC	Stirling cycle	
FC	Fuel Cell	
TPV	Thermo-photovoltaic	
GUI	Graphical user interface	

### Chapter 2: Background Knowledge

$P_{el\_cent}$	Electrical power generated on the centralized power station	(kW)
$\dot{Q}_{tran}$	Transmission loss rate	(kW)
$P_{load\_el}$	Electrical load	(kW)
$\eta_{tran}$	Transmission efficiency	
$\dot{Q}_{in\_plant}$	Heat inlet rate to the power plant	(kW)
$\dot{Q}_{w\_plant}$	Rate of waste heat generated from the power plant	(kW)
$\dot{Q}_{in\_boil}$	Heat inlet rate to boiler	(kW)

$\dot{Q}_{load}$	Heat demand rate	(kW)
$\dot{Q}_{w_b}$	Rate of waste heat generated from boiler	(kW)
$\eta_b$	Boiler efficiency	
$\eta_{gen}$	Power generation efficiency	
$\dot{Q}_{w_{gen}}$	Rate of waste heat from power generation	(kW)
$\dot{Q}_{w_R}$	Rate of recoverable waste heat	(kW)
$\dot{Q}_{w_{NR}}$	Rate of Non – recoverable waste heat	(kW)
$\dot{Q}_{w_{CHP}}$	Rate of waste heat from CHP	(kW)
$\eta_{HR}$	Heat recovery efficiency	
$\dot{m}_{f_{CHP}}$	Fuel mass flow rate to CHP	(kg/s)
$\dot{m}_a$	Air mass flow rate	(kg/s)
$h_a$	Specific enthalpy of air	(kJ/kg)
$\dot{m}_{exh}$	Exhaust mass flow rate	(kg/s)
$h_{exh}$	Specific enthalpy of the exhaust	(kJ/kg)
$T_{a_{in}}$	Air inlet temperature	(°K)
$T_{exh_o}$	Exhaust outlet temperature after heat recovery	(°K)
EEEP	Energetic, environmental, and economic performance	
$\dot{Q}_{in_{CHP}}$	Heat inlet rate to CHP	(kW)
$\dot{Q}_{in_{sep_t}}$	Total heat inlet rate for the separate supply of heat and power	(kW)
$\dot{Q}_{in_{PM}}$	Heat inlet rate to prime mover	(kW)
$P_{mech}$	Mechanical power output	(kW)
$\dot{Q}_{cool}$	Flow rate of heat to coolant	(kW)
$\dot{Q}_{exh_{in}}$	Flow rate of exhaust heat to heat exchanger	(kW)
$\dot{Q}_{Rad}$	Rate of flow of radiated heat	(kW)
$\dot{Q}_{conv}$	Rate of flow of convected heat	(kW)
$\dot{Q}_{w_{EM}}$	Rate of waste heat generation from the electric machine	(kW)

$P_{el\_CHP}$	Electricity generated from the CHP	(kW)
$\epsilon_{CO2\_CHP}$	Specific CO <sub>2</sub> emissions of the CHP solution	(kg <sub>CO<sub>2</sub></sub> /kWh)
$\epsilon_{CO2\_conv}$	Specific CO <sub>2</sub> emissions of conventional boiler and grid	(kg <sub>CO<sub>2</sub></sub> /kWh)
$M_{CO2\_CHP}$	Mass of emitted CO <sub>2</sub> from the CHP	(kg)
$M_{CO2\_Aux\_b}$	Mass of emitted CO <sub>2</sub> from the auxiliary boiler	(kg)
$M_{CO2\_el\_imp}$	Mass of emitted CO <sub>2</sub> for the imported electricity	(kg)
$M_{CO2\_boiler}$	Mass of emitted CO <sub>2</sub> from the standalone boiler	(kg)
$Q_{space\_total}$	Total amount of used thermal energy for space heating	(kWh)
$Q_{DHW\_total}$	Total amount of used thermal energy for DHW	(kWh)
$E_{el\_CHP\_total}$	Total amount of produced electrical energy from CHP	(kWh)
$E_{el\_imp\_total}$	Total amount of imported electrical energy	(kWh)
$\eta_{oal}$	Overall efficiency	
$\eta_{dev}$	Device efficiency	
$\eta_{oal\_conv}$	Overall efficiency of conventional boiler & grid	
$\sum \dot{Q}_{use}$	Total rate of usable heat	(kW)
$\sum P_{out}$	Total rate of usable power	(kW)
$\sum \dot{Q}_{in}$	Total rate of primary energy inlet	(kW)
$Q_{in\_conv}$	Total heat inlet for the conventional boiler & grid	(kWh)
$Q_{in\_oal\_CHP}$	Total heat inlet for the CHP solution	(kWh)
$Q_{in\_PM}$	Total amount of thermal energy input to the prime mover	(kWh)



$Q_{in,b}$	Total amount of thermal energy input to boiler	( $kWh$ )
$Q_{in,imp}$	Heat input to central power station for imported electricity	( $kWh$ )
$\Delta C_{sys}$	Percentage cost savings	(%)
$C_{conv}$	Operating costs of conventional boiler & grid	(£)
$C_{CHP}$	Operating costs of the CHP application	(£)
$C_{pel,imp}(t)$	Costs of imported electricity	(£)
$C_{NG}(t)$	Costs of consumed natural gas	(£)
$R_{FIT}(t)$	Revenues generated by the feed in tariff scheme	(£)
$R_{exp}(t)$	Revenues generated by the electricity export	(£)
$P_{el,imp}(t)$	Imported electrical power	( $kW$ )
$c_{el}(t)$	Electricity price	(£/ $kWh$ )
$\dot{m}_{NG\_CHP}(t)$	Mass flow rates of natural gas to the CHP	( $kg/s$ )
$\dot{m}_{NG\_Boiler}(t)$	Mass flow rates of natural gas to the boiler	( $kg/s$ )
$P_{el,prod}(t)$	Produced power	( $kW$ )
$P_{el,exp}(t)$	Exported electrical power	( $kW$ )
$c_{NG}$	Natural Gas price	(£/ $kWh$ )
$r_{ex}$	Export price of electricity	(£/ $kWh$ )
$C_{marg}$	Marginal cost	(£)
$C_{conv\_1y}$	Total annual energy costs (conventional solution)	(£)
$C_{CHP\_1y}$	Total annual energy costs (CHP)	(£)
$GT$	Generation tariff	(£/ $kWh$ )
$\dot{Q}_{rec\_CHP}$	Rate of heat recovered from CHP	( $kW$ )
$\dot{Q}_{rec\_b}$	Rate of heat recovered from boiler	( $kW$ )
$P_{el\_CHP}$	Electricity generated from CHP	( $kW$ )

HPC	Heat priority control
EPC	Electricity priority control

### Chapter 3: Literature Review

$BSFC_{Mech}$	Mechanical brake specific fuel consumption	(g/kWh)
$P_{bottom}$	Power output of bottoming cycle	(kW)
$P_{PM}$	Power output of prime mover	(kW)
$\dot{m}_{f_{PM}}$	Fuel mass flow rate to prime mover	(kg/s)
$BSFC_{El}$	Electrical brake specific fuel consumption	(g/kWh)
$\eta_{bottom\_gen}$	Conversion efficiency of the bottoming cycle generator	
$M_{t_{ICE}}$	ICE torque	(Nm)
$M_{t_{gen}}$	Generator torque	(Nm)
$M_{t_{Fr}}$	Friction torque	(Nm)
$M_{t_{acc}}$	Accelerating torque	(Nm)
$P_{mech}$	Mechanical power	(kW)
$\omega$	Angular speed	(rad/s)
$J$	Moment of inertia	(kgm <sup>2</sup> )
$\dot{Q}_{exh}$	Rate of exhaust heat flow	(kW)
$T_{amb}$	Ambient temperature	(°K)
$X_{disp}$	Fraction of input power lost in the environment due to incomplete heat recovery	
$X_{exh}$	Exhaust heat fraction	
$c_{p\_exh}$	Specific heat capacity of the exhaust	(kJ/kg°K)
$AFR$	Air – fuel ratio	
$c_{p_{N_2}}$	Specific heat capacity of Nitrogen	(kJ/kg°K)
$T_{cool\_out}$	Coolant outlet temperature	(°K)
$\dot{m}_{cool}$	Coolant mass flow rate	(kg/s)

$c_{p\_cool}$	Specific heat capacity of the coolant	(kJ/kg $^{\circ}$ K)
$T_{cool\_in}$	Coolant inlet temperature	( $^{\circ}$ K)

#### Chapter 4: Modelling the ICE based generator set

$\dot{Q}_{in}$	Heat inlet rate	(kW)
$\dot{Q}_{conv}$	Rate of heat flowing through convection	(kW)
$f_{mep}$	Friction mean effective pressure	(kpa)
$\dot{Q}_{fr}$	Rate of heat generated through friction	(kW)
$\eta_{vp}$	Volumetric efficiency	
$N$	Engine speed	(rpm)
PID	Proportional – Integral – Derivative controller	
$\dot{m}_f$	Fuel mass flow rate	(kg/s)
$bsfc$	Brake specific fuel consumption	(g/kWh)
$AFR_{st}$	Stoichiometric air – fuel ratio	
$\dot{V}_{f\_vap}$	Volumetric flow rate of fuel vapour	(m $^3$ /s)
$v_{f\_vap}$	Specific volume of fuel vapour	(m $^3$ /kg)
$v_{ptr\_vap}$	Specific volume of petrol vapour	(m $^3$ /kg)
$\dot{V}_{ch}$	Volumetric flow rate of the charge	(m $^3$ /s)
$\dot{V}_{sw}$	Swept volumetric flow rate	(m $^3$ /s)
$V_d$	Engine displacement	(cm $^3$ )
$m_{ch}$	Charge mass	(kg)
$\rho_{ch}$	Charge density	(kg/m $^3$ )
$h_{exh}$	Specific enthalpy of the exhaust	(kJ/kg)
$P_{net}$	Net power output	(kW)
$P_{mech}$	Mechanical power output	(kW)
$P_{load}$	Load on the shaft	(kW)
$E_{rot}$	Rotational kinetic energy	(kJ)
$J_{eq}$	Equivalent moment of inertia	(kgm $^2$ )
$J_{eng}$	Engine moment of inertia	(kgm $^2$ )

$J_{EM}$	Moment of inertia of the electric machine	$(kgm^2)$
$n_{p_i}$	Moles of each product per mole of burned fuel	
$\bar{h}^o$	Reference specific molar enthalpy	$(kJ/Kmol)$
$n_r$	Number of reactants	
$(\bar{h})_{p_i}$	Specific molar enthalpy of each product	$kJ/Kmol$
$q_{exh}$	Specific molar enthalpy of the exhaust gas mixture per $kmol$ of burned fuel	$kJ/Kmol\ fuel$
$n_{CO_2}$	CO <sub>2</sub> moles per mole of burned fuel	
$\bar{h}_{CO_2}$	Specific molar enthalpy of CO <sub>2</sub>	$(kJ/Kmol)$
$n_{H_2O}$	H <sub>2</sub> O moles per mole of burned fuel	
$\bar{h}_{H_2O}$	Specific molar enthalpy of H <sub>2</sub> O	$(kJ/Kmol)$
$n_{N_2}$	N <sub>2</sub> moles per mole of burned fuel	
$\bar{h}_{N_2}$	Specific molar enthalpy of N <sub>2</sub>	$(kJ/Kmol)$
$\alpha$	Percentage of maximum throttle angle	
$EMF$	Electromotive force	$(V)$
$AC$	Alternating Current	
$\Phi_p$	magnetic field flux	$(Wb)$
$f_{me}$	in engine speed	$Hz$
$K_w$	field winding factor	
$N_{pp}$	the number of pole pairs	
$N_{ph}$	number of phases	
$R_A$	the armature resistance	$(\Omega)$
$R_i$	the equivalent internal resistance	$(\Omega)$
$\dot{Q}_{gen\_fr\_d}$	Design rate of windage and friction losses	$(kW)$
$\eta_{gen\_d}$	Design alternator conversion efficiency	
$P_{L\_d}$	Design alternator power output	$(kW)$
$P_{mech\_d}$	Design engine power output	$(kW)$
$\dot{Q}_{Loss\_gen\_t\_d}$	Total rate of design power losses	$(kW)$

$r_{fr\_d}$	Ratio of the design windage and friction power losses over the total design power losses	
$\dot{Q}_{gen\_fr\_d}$	Design rate of alternator windage and friction power losses	(kW)
$\dot{Q}_{Ri\_d}$	Design resistive loss rate	(kW)
$I_{L\_d}$	Design current	(A)
$P_L$	Generator load	(kW)
$V_{Ri}$	voltage drop	(V)
$\dot{Q}_{coolant}$	Rate of heat flowing to coolant	(kW)
$\dot{Q}_{radiant}$	Rate of radiated heat	(kW)
NG	Natural gas	
FCE	Fuel conversion efficiency	
CR	Compression ratio	
$BSFC_{model\_s\_new\_f}$	Break specific consumption of the fuel modified engine	(kg/kWh)
$BSFC_{map\_orig\_f}$	Break specific consumption of the original fuel engine	(kg/kWh)

## Chapter 5: Heat Exchanging Systems

$k_{tube}$	Tube thermal conductivity	(kW/m <sup>°K</sup> )
$d_i$	Tube internal diameter	(m)
$d_o$	Tube external diameter	(m)
$h_i$	Heat transfer coefficient of the inner boundary layer	(kW/m <sup>2°K</sup> )
$h_o$	Heat transfer coefficient of the outer boundary layer	(kW/m <sup>2°K</sup> )
$\dot{m}_{hot}$	Mass flow rate of the hot fluid	(kg/s)
$T_{hot\_j}$	Hot fluid cell temperature	(°K)
$\dot{Q}_{hot\_in\_j}$	Rate of heat inlet via mass inflow in the hot side	(kW)

$\dot{Q}_{hot\_out\_j}$	Rate of heat outlet via mass inflow in the hot side	(kW)
$\dot{Q}_{incr\_j}$	Rate of incremental heat transfer component	(kW)
$T_{hot\_j+1}$	Hot fluid cell outlet temperature	(°K)
$T_{cold\_j}$	Cold fluid cell inlet temperature (parallel flow)	(°K)
$T_{cold\_n-j}$	Cold fluid cell inlet temperature (counterflow)	(°K)
$\dot{Q}_{cold\_in\_j}$	Rate of heat inlet via mass inflow in the cold side	(kW)
$\dot{m}_{cold}$	Mass flow rate of the cold fluid	(kg/s)
$\dot{Q}_{incr}$	Rate of incremental heat transfer of a cell	(kW)
$L_{incr}$	Cell length	(m)
$U_{incr\_j}$	Heat transfer coefficient of a cell	(kW/m <sup>2</sup> )
$A_{incr}$	Heat transfer area of a cell	(m <sup>2</sup> )
$\Delta T_{incr\_j}$	Temperature difference of the cold and hot side	(°K)
$U_{oal\_j}$	Overall heat transfer coefficient of a cell	(kW/m <sup>2</sup> °K)
$h_{i\_j}$	Heat transfer coefficient of the inner boundary layer	(kW/m <sup>2</sup> °K)
$h_{o\_j}$	Heat transfer coefficient of the outer boundary layer	(kW/m <sup>2</sup> °K)
$M_{tube\_incr}$	Tube incremental mass	(kg)
$U_{incr\_i\_j}$	Inner heat transfer coefficient	(kW/m <sup>2</sup> °K)
$d_m$	Mean tube diameter	(kg)
$U_{incr\_o\_j}$	Outer heat transfer coefficient	(kW/m <sup>2</sup> °K)
$R_{incr\_i\_j}$	Inner thermal insulance	(m <sup>2</sup> °K/kW)
$R_{incr\_o\_j}$	Outer thermal insulance	(m <sup>2</sup> °K/kW)
$\dot{Q}_{tube\_in\_j}$	Rate of heat transferred to incremental tube mass	(kW)

$\dot{Q}_{tube\_out\_j}$	Rate of heat transferred out of the incremental tube mass	(kW)
$T_{tube\_j}$	Incremental tube mass temperature	(°K)
$\dot{Q}_{net\_j}$	Net heat transfer rate of the incremental tube mass	(kW)
$Q_{M\_incr\_j}$	Stored heat in the incremental mass	(kJ)
$cp_{tube}$	Specific heat capacity of the tube material	(kJ/kg°K)
$Nu$	Nusselt number	
$Re$	Reynolds number	
$D_H$	Hydraulic diameter of the flow	(m)
$\dot{m}_{flow}$	Mass flow rate	(kg/s)
$\mu$	Dynamic viscosity	Ns/m <sup>2</sup>
$A_{flow}$	Flow area	m <sup>2</sup>
$Gz$	Graetz number	
$f$	Darcy-Weisbach friction factor	
$Gr$	Grashof number	
$\rho$	Density of the surrounding fluid	kg/m <sup>3</sup>
$\beta$	Coefficient of volume expansion	1/°C
$Ra$	Rayleigh number	

## Chapter 6: UK Dwelling Models

$A_{total}$	Total exposed area	(m <sup>2</sup> )
$A_{floor}$	Total floor area	(m <sup>2</sup> )
$HLP$	Heat loss parameter	(kW/m <sup>2</sup> °K)
$n_s$	Number of storeys	
$T_{indoor}$	Indoor temperature	(°K)
$T_{outdoor}$	Outdoor temperature	(°K)
$q_{i\_fabric}$	Heat loss of any individual construction element	kW
$A_i$	Surface area if individual construction element	(m <sup>2</sup> )

$U_i$	Heat transfer coefficient of a construction element	$(kW/m^2\text{°K})$
$X_i$	Component thickness	$(m)$
$K_i$	Thermal conductivity of the material	$(kW/m\text{°K})$
$\dot{Q}_{fabric}$	Dwelling fabric heat loss rate	$(kW)$
$\dot{Q}_{win}$	Window heat loss rate	$(kW)$
$\dot{Q}_{wall}$	Wall heat loss rate	$(kW)$
$\dot{Q}_{roof}$	Roof heat loss rate	$(kW)$
$\dot{Q}_{ground}$	Ground heat loss rate	$(kW)$
$A_{win}$	Window area	$(m^2)$
$U_{win}$	Window heat transfer coefficient	$(kW/m^2\text{°K})$
$A_{wall}$	Wall area	$(m^2)$
$U_{wall}$	Wall heat transfer coefficient	$(kW/m^2\text{°K})$
$A_{roof}$	Roof area	$(m^2)$
$U_{roof}$	Roof heat transfer coefficient	$(kW/m^2\text{°K})$
$A_{ground}$	Ground area	$(m^2)$
$U_{ground}$	Ground heat transfer coefficient	$(kW/m^2\text{°K})$
$\dot{Q}_{inf}$	Rate of heat loss due to air infiltration	$(kW)$
$c_{p\_air}$	Specific heat capacity of air	$(kJ/kg\text{°K})$
$\rho_{air}$	Air density in room conditions	$kg/m^3$
$V_{intern}$	the internal volume of the building	$m^3$
$ACH$	Air changes per hour	
$U \times A$	the dwelling Heat Loss Coefficient	$(kW/\text{°K})$
$HLP_{det}$	Heat loss parameter of a detached house	$(kW/m^2\text{°K})$
$HLP_{semi}$	Heat loss parameter of a semi - detached house	$(kW/m^2\text{°K})$
$HLP_{terr}$	Heat loss parameter of a terraced house	$(kW/m^2\text{°K})$
$Y$	Length of the long side of the dwelling	$(m)$
$\epsilon$	the aspect ratio of the dwelling floor	
$h$	Dwelling height	$(m)$



## Chapter 7: Modelling structure

$X_{layer}$	Layer thickness	(m)
$X_{wall}$	Wall thickness	(m)
$R_{layer}$	Layer thermal insulance	( $m^2\text{°K}/kW$ )
$R_{wall}$	Wall thermal insulance	( $m^2\text{°K}/kW$ )
$R_{layer_o}$	Outer thermal insulance	( $m^2\text{°K}/kW$ )
$R_{layer_i}$	Inner thermal insulance	( $m^2\text{°K}/kW$ )
$U_{layer_o}$	Outer heat transfer coefficient	( $kW/m^2\text{°K}$ )
$U_{layer_i}$	Inner heat transfer coefficient	( $kW/m^2\text{°K}$ )
$T_1$	Control volume inlet temperature	( $\text{°K}$ )
$\dot{m}_{wat}$	Water mass flow rate	( $kg/s$ )
$\dot{Q}_{wat\_in}$	Rate of heat inlet in the control volume	( $kW$ )
$\dot{Q}_{wat\_out}$	Rate of heat leaving the control volume	( $kW$ )
$c_{p\_wat}$	Specific heat capacity of water	( $kJ/kg\text{°K}$ )
$Q_{cv}$	Enthalpy in the water mass of the control volume	( $kJ$ )
$m_{w\_cv}$	Mass of control volume	( $kg$ )
$Q_{node}$	Heat stored in the node	( $kJ$ )
$Q_{comp}$	Heat stored in the components	( $kJ$ )
$C_{comb}$	Heat capacity of the lumped components	( $kJ/\text{°K}$ )
$c_{p\_steel}$	Specific heat capacity of steel	( $kJ/kg\text{°K}$ )
$m_{rad}$	Radiator mass	( $kg$ )
$c_{p\_copper}$	Specific heat capacity of copper	( $kJ/kg\text{°K}$ )
$m_{tube}$	Tube mass	( $kg$ )
$c_{p\_alu}$	Specific heat capacity of aluminium	( $kJ/kg\text{°K}$ )
$m_{eng}$	the engine mass	( $kg$ )
$\dot{Q}_{total\_cap}$	Total thermal capacity	( $kW$ )
$L.F.$	Load factor	
$V_{dpq}$	Engine displacement per unit heat output	( $cm^3/kW$ )
$V_{d\_sized}$	Sized engine displacement	( $cm^3$ )

$\dot{Q}_{aux\_cap}$

Auxiliary boiler capacity

(kW)

## Chapter 1 Introduction

The welfare of modern societies is dependent on the abundance of energy supply. Fossil fuels are currently the main source for providing the human population with the necessary amount of energy to sustain and/or improve its way of life. As the world population grows and technology advances, more and more energy consuming technologies become part of everyday life and the global energy demand increases as well. The increase in energy demand leads to an increase in fossil fuel consumption and thus in the rate of discharge of greenhouse gasses, toxic combustion products and waste heat, which all have a negative impact on the environment and quality of life in general as the climate is already showing signs of deterioration on a global scale. The effect of the increase in energy consumption has also financial implications since fossil fuel reserves are being depleted at a growing pace leading to an increase in energy prices. In addition, the fact that 60% of the world's known oil reserves are located in areas of high political turmoil causes a high volatility in fossil fuel prices [1].

The dramatic rise and unpredictability in energy prices and the adverse impact of human activities on the environment have generated a worldwide interest in products and processes characterized by a low lifecycle energy consumption and carbon footprint. This interest has driven several countries to develop and put into place legislation that contains guidelines and specifications mandating the industry and the end users to reduce their power consumption and their respective emissions. One such piece of legislation is the Kyoto protocol, a multinational treaty agreed in 1997 that binds the signing parties in reducing their CO<sub>2</sub> emissions [2].

Currently, 40% of all energy consumed in the US is used in the building sector with thermal loads accounting for 20% of all US energy consumption [3], and according to L. M. Chamra et al. [4], the residential sector comprises the largest energy consumption of all US sectors, and exhibits a fast growth

(expected to increase by 25% in the 2001-2025 period). Similarly, in the EU, approximately 1/3<sup>rd</sup> of the total produced energy is consumed in the building sector with the largest portion of this energy being used for space heating. From the above, it can be seen that the building sector comprises a very large portion of the total energy consumption and for this reason, reducing the energy consumption of this sector can have a very strong impact on the reduction of the total carbon emissions and save capital that could be funnelled towards useful purposes.

A reduction in energy usage in the domestic sector may be achieved by either making buildings more energy efficient or by making power supply more efficient [5]. One technological branch that makes power supply in the residential sector more efficient is that of the micro-cogeneration or micro-combined heat and power ( $\mu$ CHP) which is viewed as a potential replacement over the traditional boiler. In the European level, 7 million boilers are sold every year [6] and according to B. Sicre et al. [5], up to 40 million EU dwellings exhibit load characteristics that are suitable for micro-CHP applications with a prospective market of 800,000 micro-CHP system installations per annum. One of the targets of the EU is the gradual increase of the collective capacity of micro-CHP units to 18% of the total European electrical capacity [2].

In the case of the United Kingdom, approximately 80% of dwellings are using a central heating system and thus can accommodate a micro-CHP unit. With 1.3 million boiler replacements per year, it is estimated that by 2020, 5.6 million UK households could be using a micro-CHP system [7]. UK government has set a target to have reduced national CO<sub>2</sub> emissions by 80% by the year 2050 with respect to 1990s emission levels. With the domestic sector being responsible for 30% of the country's total CO<sub>2</sub> emissions [8], low carbon producing technologies such as micro-CHP are considered essential for meeting this target, and the favourable policy of UK Government towards Micro-CHP system proliferation is reflected on existing government funded incentives such as the feed-in tariff (FIT) scheme that rewards users with revenues not only for exporting but also for producing electricity for their own needs [9],[10].

The increase in fuel prices and in domestic energy consumption, combined with government incentives often provided to promote carbon reducing technologies as mentioned above, has made the residential application of distributed energy systems (DES) such as Micro-CHP an attractive alternative to the conventional boiler & grid heat and power supply configuration, thus leading to a market opening in this technological area. Another driving force behind the recent interest of consumers in Micro-CHP technology is the need of autonomy in power supply [5].

The opening of the micro-Cogeneration system market has in turn generated great incentives for engineers and researchers to thoroughly investigate the impact of this technology on energy consumption, CO<sub>2</sub> emissions, and operating costs, and improve the energetic performance and cost effectiveness of the technology by defining sets of design specifications that ensure as close to an optimal operation as possible.

### **1.1. Model based energy analysis and design**

The design and feasibility study of a multi-parameter power system such as a residential cogeneration unit by means of experimental work alone can be inefficient from a technical and financial standpoint [11]. The integration of computers in engineering design processes provides the researcher with the ability to simulate physical systems and acquire data that would otherwise be impossible to obtain experimentally at a reasonable time and cost. For the above reasons, system modelling and simulation can be a valuable tool in the hands of engineers and researchers.

Since a dwelling fitted with a micro-CHP unit combines a very diverse set of functions such as power generation, import, and export, heat recovery and rejection, as well as complex usage patterns characterized by time intervals of heat and power shortage and surplus, and the technical and financial viability of the application depends on the proper component selection and sizing, it can be considered to be a well suited technology to serve as a basis of, and benefit from the development of a dedicated distributed energy simulation and software package as an alternative to existing building energy simulation software.

For the above reasons, in the current PhD project, as part of an energetic and economic feasibility study on the application Micro-Cogeneration technology in the residential sector of the United Kingdom, and the search for micro-CHP design characteristics that enhance system performance, a thermo-economic model of a micro – CHP will be developed on Matlab and Simulink environments, and operated by means of a graphical user interface (GUI). The combination of the model, the GUI, the library, as well as the supporting code, will comprise an integrated distributed energy simulation tool. The model will be simulated under a multitude of different parameter combinations, and the results will then be used for the performance evaluation of these combinations with respect to the performance of the conventional setup of boiler and grid, which is the technology most likely to be replaced by micro-cogeneration.

## **1.2. Power generation and waste heat**

The Second Law of Thermodynamics states that a heat engine, being a cyclic device, cannot convert 100% of the heat inlet to work due to the necessity to complete its thermodynamic cycle by means of rejecting part of the heat inlet in the low temperature reservoir (environment) [12]. This characteristic of heat engines places certain thermodynamic limits on their conversion efficiency. These limits are expressed by the Carnot ideal heat engine cycle composed of reversible thermodynamic processes [13] being characterized by the maximum theoretical efficiency a heat engine may achieve under certain initial and final conditions of the working medium. In reality, no natural process is reversible. Energy conversion, transfer and storage all lead to a loss of work potential and the more frequent and intense these processes are, the greater the losses [4]. For this reason Carnot Cycle efficiency cannot be attained in real life but is only used as a measure of how well a certain system performs compared to this ideal model.

Since heat engine based power generation used to supply the biggest portion of consumed electricity involves numerous thermodynamic and mechanical processes, degradation of energy and loss of work potential are

inevitable, as the theoretical and practical thermodynamic limitations and irreversibilities present during the energy conversion stages from chemical (if applicable) to thermal and from thermal to mechanical do not allow for the conversion efficiency to exceed a certain limit [12], [14], [15]. These irreversible processes lead to the generation and rejection of large amounts of waste heat by the prime mover. Depending on the operating conditions, waste heat may reach (or exceed) 75% of the chemical power that enters a heat engine [16], [17] which translates to relatively poor fuel conversion efficiency (approx. 30 – 35% HHV for conventional and up to 55% HHV in the case of a combined cycle) [18], [19], [20].

### **1.3. Waste heat recovery in combustion engines**

Waste heat generated as a by-product of power production may be recovered and used either as it is, or converted (part of it) into mechanical power by a bottoming cycle [21], [15], and the remaining low grade thermal energy be used for heating applications [22]. In the first case, the overall efficiency of the system is increased compared to the separate production of heat and power. In the second case, both the overall and the electrical efficiency of the unit exhibit a considerable increase. Any remaining heat from the exhaust may be utilized, resulting in a further increase in the system fuel utilization efficiency.

### **1.4. Definition of cogeneration**

Cogeneration is defined as the simultaneous/sequential production of useful work or electricity and heat from a single fuel source/energy stream [18], [19], [23], [24], [25]. As in the case of conventional power producing systems, fuel is supplied to a power generator of a CHP unit to generate electricity as its main product, and waste heat as a by-product. Rather than rejecting this waste heat as would normally happen in conventional power generation, the cogeneration system recovers it by means of dedicated heat exchangers,

and makes it available to the user, thus reducing, or in some cases even eliminating the need to operate a separate heat generating system that would require additional fuel for heating. Therefore, provided there is a demand for both heat and power [25], the negative impact of the inevitable generation of waste heat in the work producing cycle of a heat engine could be alleviated.

Applications of the concept were first encountered in the 1880s in steam (produced onsite) powered industrial plants as means to increase their overall fuel utilization efficiency [4], [18] but for a long period of time, the low fuel prices did not make for a fertile ground for the further proliferation of the technology. The increasing energy consumption in the residential sector, the recent interest of many households for power independence, quality and security [4], and the recent advances in technology that have resulted in more efficient and reliable CHP systems have all led to the resurgence of interest in cogeneration [22].

### **1.5. Micro Cogeneration**

Technology advances such as the development of efficient small scale heat recovery equipment, thermally activated components [24] as well as suitable power generation equipment have allowed for medium and small scale cogeneration units to be economically viable [4]. Micro CHP generators are classified as small scale cogeneration units with a rated electrical power output of  $10kW$  or less [18].

They belong to the greater family of distributed energy systems (DES) and usually find application in the residential sector and more specifically in single family (average four members) dwellings, apartment complexes, and in some cases in small businesses where electrical and thermal power is generated onsite [11]. With the first units for residential applications appearing in the 1980s [26], [27], they are currently available in many types and makes as a viable, environmentally friendly alternative to the conventional burner/boiler [18], and are being fitted as replacement to the



traditional boiler making use of the same heat delivery circuit [20], while also giving the user independence in power supply [28]. Thus their application is more cost effective if a house already has the infrastructure to accommodate a CHP (a house originally heated by electricity is not equipped with the necessary piping and radiators and would be more costly to install a  $\mu$ CHP unit). A schematic of the general layout of a micro-CHP system installed in a dwelling to meet the heat and power demand is shown in Figure 1.1.

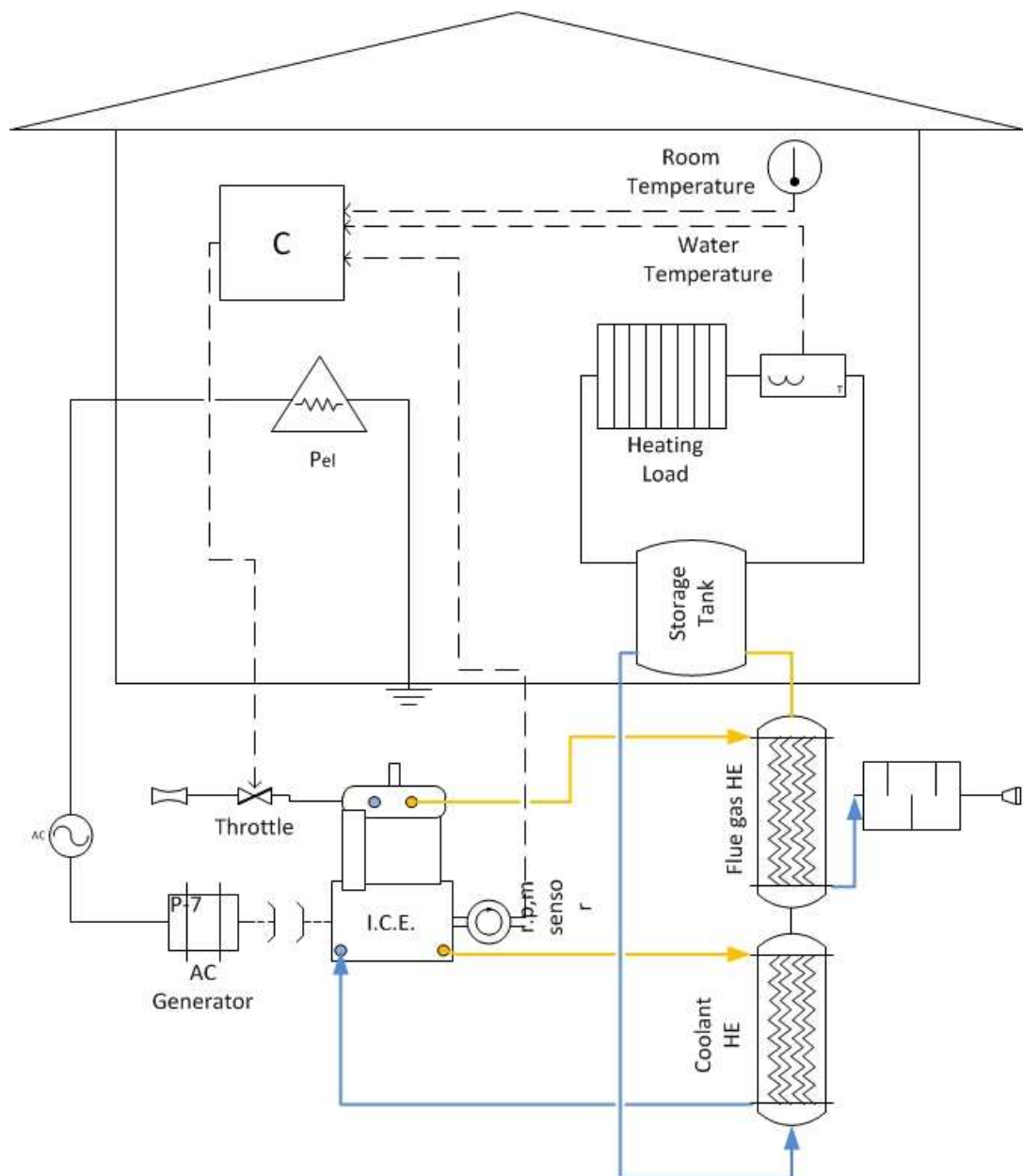


Figure 1.1 Schematic of an I.C.E. based Micro-CHP system

Micro-cogeneration systems have been found to exhibit a tendency for greatly increased overall fuel utilization efficiency when compared to conventional (separate) supply of heat and power [2], [19], [23], [28] which in the case of  $\mu$ CHP can exceed 80% LHV [18] and in some cases reach 90% LHV [19] resulting to a substantial emission and cost reduction [28]. M. Badami et al. [22] observed that for small scale CHP systems, primary energy savings (PES) ranged between 10% and 30% with a respective reduction in CO<sub>2</sub> emissions.

Besides generating savings due to recovering waste heat, another components of CHP generated energy usage reduction is the elimination of the conversion and transmission losses [29] which account for 6% of all transmitted power in the EU [5], [20]. The cost of imported electricity from the utility grid is also reduced due to the reduction in the investment costs of the utility company, as the required capacity and therefore the equipment costs are reduced as well [3], [4], [5], [20].

Pay Back Period (PBP) of the average m-CHP system is considerably shorter than that of competing distributed generation systems such as Photovoltaic Cells or wind turbines [30].

Due to the fact that warmer months of the year are associated with a sharp reduction in thermal demand, a CHP system with a heat following control strategy will only operate for very brief intervals during summer months. On the other hand, an electrical load following strategy will produce heat regardless of the thermal demand leading to heat rejection and poor system performance. A type of cogeneration capable of producing heat, power and cooling is called trigeneration [24] or combined cooling, heating, and power (CCHP). Such a practice may increase the duration of profitable operation of the system well into the warmer months of the year. Cooling may be generated by either using waste heat to drive an adsorption heat pump [15], [24], [31], or by utilizing a traditional cooling cycle. Thermally activated heat pumps tend to exhibit a low efficiency in small scale systems, and traditional cooling cycles generally outperform them [24]. G. Angrisani et al. [24], simulated a  $\mu$ CCHP system for different combinations of heating/cooling

operating duration per year and found a combination that maximized primary energy savings (*PES*) and CO<sub>2</sub> savings. *PES* of up to 28% and CO<sub>2</sub> emission reduction of up to 36% were observed. In terms of the payback period (PBP), values as short as 2.97 years have been calculated by Y. Huangfu et al. [31] for such systems.

### **1.6. An overview of existing $\mu$ CHP types**

Currently, researchers in the field are working on a diverse spectrum of micro-CHP technologies in an effort to define which technology type is most suitable for a given application, as well as to improve their technical and financial viability.

The characteristics of the cogeneration technologies encountered in literature and further discussed in Appendix 1 are summed up in Table 1.1. Due to the inherently favourable characteristics of the ICE based systems such as technical maturity, low cost, combined with good fuel conversion efficiency and a fast electrical and thermal response, this technology is the most popular platform among the competition, and for this reason the main area of focus of the current thesis will be micro-cogeneration systems powered by natural gas (NG) fuelled spark ignited (SI) internal combustion engines (ICE). While Natural Gas SI based systems may exhibit the best performance compared to competing technologies, still financial feasibility is achieved provided the operating and financial conditions are favourable [32] and this highlights the need for carrying out thorough country specific investigation on system characteristics that give optimal performance.

### **1.7. Obstacles to the proliferation of $\mu$ CHP systems**

While micro-CHP systems have certain attributes that favour their recent rise in popularity as alternative means of heat and power supply for residential applications, the special nature of the domestic sector defines divergent design considerations compared to those of larger scale CHP systems [33]. While the technical and economical aspects of large and medium scale cogeneration have been thoroughly explored; small scale cogeneration has not been studied to such a great extent due to the fact that it is a relatively

recent application of cogeneration technology [23]. A number of associated problems as will be analysed below act as obstacles to the marketability of the technology and as a result, they attract a large volume of research.

As mentioned above, the typical ICE based micro-CHP system full load electrical efficiency is higher than of competing systems but still typically remains below 30% [34]. For this reason, the high heat recovery efficiency and low amounts of surplus heat rejection are both very important in the system financial and environmental viability. The heat recovery efficiency depends on the proper system design, and a significant amount of research is dedicated on designing an effective and low cost heat recovery system. On the other hand, the amount of surplus heat that may be produced when a micro-CHP unit is operated in electrical load following mode and rejected unutilized to the environment must be minimized. In order to achieve minimum levels of heat rejection with electricity led systems, it is rather important for the system sizing to be appropriate for the specific dwelling type, size and age as well as the geographical location. The distinction between viable and non viable  $\mu$ CHP applications is another important field of research.

Fuel utilization efficiency of CHP units may exceed 70% LHV [35], but modern separate production of heat and power can be very competitive in that respect due to the high fuel conversion efficiency of combined cycles commonly encountered in large scale power plants. Under these circumstances, modern centralized power supply exhibits a better electrical efficiency than most modern distributed energy systems that operate under the same or similar technology [24]. For the above reasons, the need to increase the fuel conversion efficiency of micro-CHP systems to compete with modern power plants is being addressed by researchers by experimenting with prime movers and electric machines of a higher than usual efficiency, variable speed systems, combined cycles, and thermo-photovoltaic cells as will be discussed in sections 3.1.5 and 3.2.

The non coincidence of residential heating and electricity loads is another important issue associated with micro-CHP [34] and numerous researchers

are working in the design of systems that solve this problem by utilizing optimally sized prime movers as well as thermal and electrical storage devices.

In addition, the current initial capital investment for a micro-CHP unit is relatively high [24]. Therefore, the increased competitiveness of conventional heat and power supply dictates not only an increase in the fuel utilization efficiency and fuel conversion efficiency but also a reduction in the initial system costs.

While considerable energy savings and carbon emission reductions under  $\mu$ CHP heat and power supply are more common than not, the installation of a micro-CHP system does not automatically guarantee savings the degree of which is heavily dependent on factors [36] such as the usage pattern which in turn depends on the application type [34].

Table 1.1 Comparison of existing  $\mu$ CHP technologies

Type		Power range ( <i>kWe</i> )	Purch. Cost	Maint. Cost	Reliability	Maturity Level
ICE	SI	<10	Low	Low	High	Commercialized Widely spread
	CI	<10	Low (but higher than S.I. systems)	Low	High	Commercialized Widely spread
	MT	>25	High	Low (But specialized personnel required)	Very High	Experimental
ECE	StC	<10	High	Low	High	Commercialized But less common than ICE based systems
	RC	<10	Low	Low	High	Commercialized But less common than ICE based systems
FC		<10	Very High	Low	Very High	Experimental/ Field trial
TPV		<10	High	Low	Very High	Experimental
Sources: [2], [3], [4], [18], [19], [23], [26], [32], [33], [35], [37]						

## **1.8. Contribution of the Thesis**

While a fair number of studies on micro-CHP performance in the residential sector exist, based either on field trials or on simulated models, the generated volume of data is still not sufficient to be considered conclusive of the extent to which micro-CHP systems offer a technical and economic advantage over the traditional boiler & grid, under different control strategies, dwelling types and locations, and system electrical efficiencies, for a wide range of system and heat storage tank sizes, and the effect these parameters have on system performance. In addition, while system operating patterns play an important role in emissions, as well as component durability, the availability of studies on this aspect of CHP operation are extremely limited. Considering the fact that United Kingdom comprises only a fraction of the geographical spectrum of existing studies, combined with the interest of UK government in the promotion of micro-Cogeneration technology on a national level, the expansion of the knowledge on micro-CHP performance in the geographical area of UK is rather important for the compilation of case specific sets of micro-CHP system design specifications that would ensure the superiority of the technology in terms of energetic, environmental, and economic performance compared to the traditional method of heat and power supply, as well as for the formulation of future policies to enforce these specifications and further promote micro-cogeneration in the UK residential sector.

Existing studies that involve the use of data generated through simulation have been found to make use of highly sophisticated building simulation software that have been developed focusing on the energetic performance of the building envelope, and usually employ complex 3-dimensional building models [4], [8], [11], [19], [20], [32], [36]. While these software packages generate very accurate simulation results, the nature of expertise they require, results to a long learning curve to be effectively operated. In addition, they place a high computational load and are characterized by long simulation times. Current simulation tools are designed for civil engineering

purposes to evaluate and optimise the materials, layout, and structure of the buildings. These modelling tools and simulation environments are not designed for distributed energy generation sizing and selection from the ground up. The DES modelling method introduced in this thesis is suitable for the design and real time control of  $\mu$ CHP systems.

The main aims of the current PhD project are:

- The construction and presentation of a simulation software environment that specializes on the study of distributed energy systems (DES). The model will be developed using a multiphysics modelling methodology. The algorithm developed for the analysis of DES results in a simulation software package centred on ICE based micro-CHP systems for residential applications. The methodology is capable of calculating the energy exchange taking place through the system boundaries of a dwelling, resulting performance indicators, and component operating patterns.
- The expansion of the existing knowledge on the energetic, environmental, and financial implications of the use of ICE based micro-CHP systems under thermal and electrical load profiles commonly encountered in the residential sector of the United Kingdom.

The objectives of the project are:

- The development of an energy based system modelling method that will enable the modeller to easily connect model components of different energy domains and levels of sophistication.
- The construction of scalable ICE models that describe not only the mechanical power component but also the distribution and the behaviour of the main waste heat components thus being suitable for waste heat recovery modelling.

- The construction of heat transfer component models (heat exchangers, radiators) that accurately describe the non linear behaviour of the actual components.
- The generation of a database of representative dwelling thermal characteristics which, combined with readily available weather data and electricity and domestic hot water (DHW) usage profiles, will be necessary for the relevance of the simulation results.
- The combination of the above component models and libraries along with a developed graphical user interface (GUI) supported by the necessary Matlab code into one integrated distributed energy system (DES) simulation software package.
- The simulation of different CHP design combinations using the developed software package, and the investigation of the behaviour of the main performance indicators and component operating patterns.
- The definition of a set of micro-CHP system design characteristics that yield maximum energetic, environmental, and economic performance for a given application.
- The suggestion of possible amendments in governmental subsidy schemes that would further incentivise the operators to select systems that lead to maximum possible reduction in carbon emissions.

### **1.9. Structure of Report**

The report began with the current chapter which comprised a general introduction discussing the reasons behind the need for the development and application of carbon saving technologies, especially in the residential sector. The importance of the availability of general and specialized energy simulation software for the efficient and optimal design and assessment of energy systems was then discussed. Then, basic information on the operating principle of cogeneration was provided, and a further discussion on cogeneration on the micro scale followed, with a comparison on existing technologies, and an analysis on the technical and financial obstacles present in the push towards the proliferation of micro-CHP systems. The



chapter closed with the project contribution section in which the identified areas of interest of this thesis were discussed, and the project aims and objectives were listed and analysed.

Chapter 2 contains fundamental background knowledge on the flow of energy taking place during power generation as well as the performance indicators used to evaluate a DES. The difference between the energy flow path encountered in conventional generation and supply of heat and power and the energy flow path encountered in cogeneration applications is analysed. A distinction is then made between the CHP device efficiency, and the overall efficiency of the application. The calculation procedure of all the main performance indicators used in Chapter 8, Chapter 9 and Chapter 10 to evaluate the simulated systems is shown.

Chapter 3 comprises the literature review of the project. It is a summary of the most recent research work relative to this project and includes information on the main factors influencing micro-CHP system performance, methods and peripheral equipment enhancing system performance, and modelling techniques used in literature.

Chapter 4 describes the development procedure of the natural gas fuelled spark ignition internal combustion engine based generator set model. The modelling procedure of the heat exchangers used in the heat recovery system, the heating radiators as well as the coil of the heat storage tank is the subject of Chapter 5.

Due to a lack of encountered models of representative UK dwelling models in existing literature, Chapter 6 is dedicated on the development of a number of models/curves that describe the thermal characteristics of typically encountered UK dwellings as a function of the dwelling total floor area.

In Chapter 7, the complete CHP/dwelling model layout is analysed in detail. In addition, the final form, capabilities, and features of the developed software package are presented.

Chapter 8, 9 and 10 contain the simulation results and investigate the effect of varying parameters such as engine grade, dwelling type and age,

geographical location, and operating strategies. The main performance indicators such as CO<sub>2</sub> emissions, primary energy savings, cost savings, as well as component operating patterns of each combination are recorded, and the effects of the variation of each application parameter are discussed.

Finally, this PhD report closes with Chapter 11 which contains the conclusions drawn on the project contributions as well as recommendations regarding potential improvements and additions to the existing work.

## Chapter 2 Background Knowledge

The current chapter provides the reader with background knowledge on the energy flow taking place in the conventional method heat and power supply of boiler & grid, and on cogeneration systems. The procedures of calculation of energetic, environmental, and economic performance indicators are analysed, and a distinction is made between the device efficiency of the DES, and the overall efficiency of the DES application.

### 2.1. Heat and power supply

Energy demand in the residential sector is most commonly comprised of electrical and thermal components. In the conventional layout of heat and power supply, these demands are met by separate equipment with each piece of equipment dedicated to its respective energy domain.

Electrical demand is most commonly met by means of importing electricity generated on a centralized power station and delivered to the end user via the grid. In the UK, approximately 65% of centrally produced power is fossil fuel based [38] and generated in power stations equipped with large scale generator sets powered by Internal or external combustion engines whose operation relies on the conversion of heat released from the combustion of fossil fuel to mechanical power, which is then converted to electricity by means of an electric machine. At the same time, the generated waste heat is rejected in the environment unutilized. An additional amount of fossil fuel respective to the thermal demand is consumed in a domestic boiler to meet any need for heat.

A schematic of the conventional layout of heat and power supply can be seen in Figure 2.1. All power components in this chapter will be in  $kW$  unless stated otherwise. As the user places an electricity demand of  $P_{load\_el}$  to the grid, and since electricity is most likely to be produced at a remote location and transmitted through long distances via the grid to meet the user electrical demand, a fraction of the initial electrical power generated by the centralized

power plant is lost as transmission waste heat  $\dot{Q}_{tran}$  in the environment. Therefore, in order for the electrical demand of the user to be met, the centralized power station must generate electrical power of:

$$P_{el\_cent} = \dot{Q}_{tran} + P_{load\_el} \quad (2.1)$$

If transmission efficiency  $\eta_{tran}$  is known, one may calculate the required electrical power to be generated on the central station from:

$$P_{el\_cent} = P_{load\_el}/\eta_{tran} \quad (2.2)$$

While the transmission losses are calculated from:

$$\dot{Q}_{tran} = P_{load\_el}(1 - \eta_{tran}) \quad (2.3)$$

The power station requires a certain chemical power inlet to generate this electrical output. Depending on the fuel conversion efficiency of the plant  $\eta_{gen}$ , the required amount of fuel power inlet is calculated from:

$$\dot{Q}_{in\_plant} = P_{el\_cent}/\eta_{gen} \quad (2.4)$$

By combining equations (2.2) and (2.4) one gets:

$$\dot{Q}_{in\_plant} = \frac{P_{load\_el}}{\eta_{gen}\eta_{tran}} \quad (2.5)$$

The waste heat rejected by the plant is then calculated from:

$$\dot{Q}_{w\_plant} = \dot{Q}_{in\_plant} - P_{el\_cent} \quad (2.6)$$

When there is a demand for heat, it is generated by purpose built equipment such as boilers fed with a fuel inlet rate proportional to the heat demand. Since not all heat inlet rate to the boiler  $\dot{Q}_{in\_b}$  is available to the user due to a fraction of  $\dot{Q}_{in\_b}$  being rejected to the atmosphere unutilized, the necessary rate of heat to be supplied to the boiler to meet the thermal demand  $\dot{Q}_{load}$  is:

$$\dot{Q}_{in\_b} = \dot{Q}_{load} + \dot{Q}_{w\_b} \quad (2.7)$$

Where  $\dot{Q}_{w\_boil}$  is the rate of heat rejected through the boiler exhaust unutilized.

If the boiler efficiency  $\eta_b$  is known, the required rate of heat inlet for a given thermal load if calculated from:

$$\dot{Q}_{in\_b} = \dot{Q}_{load} / \eta_b \quad (2.8)$$

Fuel utilization efficiency or overall efficiency is defined to be the ratio of total useable power of any form over the expended amount of primary energy:

$$\eta_{oal} = \frac{\sum \dot{Q}_{use} + \sum P_{out}}{\sum \dot{Q}_{in}} \quad (2.9)$$

Where  $\sum \dot{Q}_{use}$  is the total usable heat per unit time,  $\sum P_{out}$  the total usable power, and  $\sum \dot{Q}_{in}$  the total amount of primary energy per unit time used for the generation of the above.

Then, for the conventional solution of heat and power supply of boiler and grid the overall efficiency becomes:

$$\eta_{oal\_conv} = \frac{\dot{Q}_{load} + P_{load\_el}}{\dot{Q}_{in\_b} + \dot{Q}_{in\_plant}} \quad (2.10)$$

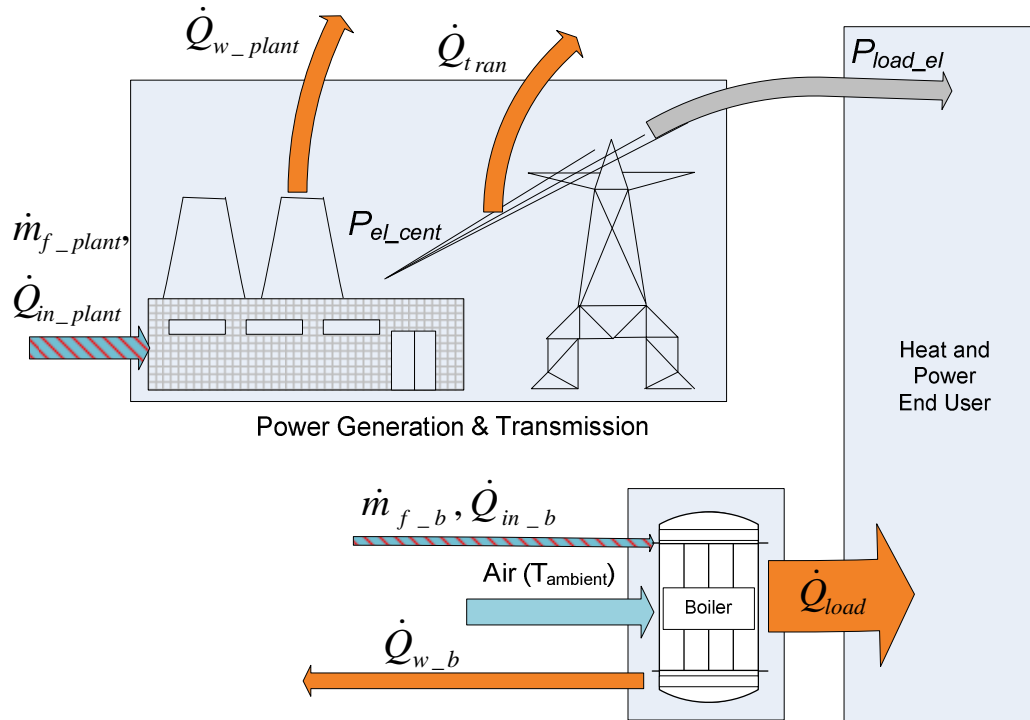


Figure 2.1 Energy flow under conventional supply of heat and power

## 2.2. Combined Heat and Power

A schematic showing the flow of energy taking place between a cogeneration system and the heat and power end user can be seen in Figure 2.2. Due to the fact that for the majority of CHP systems, heat and power are produced and consumed on site, transmission losses are negligible, and the electrical power consumed by the user will be considered to be equal to the load placed on the CHP unit.

If the fuel conversion efficiency of the generator set  $\eta_{gen}$  is known, the required chemical power input to meet the electricity demand of the user is calculated from:

$$\dot{Q}_{in\_CHP} = P_{load\_el}/\eta_{gen} \quad (2.11)$$

And the rate of total waste heat generated by the generator set is calculated from:

$$\dot{Q}_{w\_gen} = P_{load\_el}/(1 - \eta_{gen}) \quad (2.12)$$

$\dot{Q}_{w\_Gen}$  is not recoverable to its entirety due to heat being lost through the generator set surfaces by means of radiation and convection heat transfer mechanisms. The recoverable heat per unit time entering the heat recovery system will then be:

$$\dot{Q}_{w\_R} = \dot{Q}_{w\_Gen} - \dot{Q}_{w\_NR} \quad (2.13)$$

Where  $\dot{Q}_{w\_NR}$  is the rate of non – recoverable heat leaving the generator set unutilized.

Similarly, not all the recoverable heat that enters the heat recovery system is recovered due to technical and financial constraints on heat exchanger size and materials, and this results to exhaust gasses being rejected in the atmosphere at a temperature above ambient. Thus, an additional amount of heat leaves the CHP system without being utilized at a rate  $\dot{Q}_{w\_CHP}$ . The waste heat equilibrium will then be:

$$\dot{Q}_{w\_Gen} = \dot{Q}_{load} + \dot{Q}_{w\_CHP} + \dot{Q}_{w\_NR} \quad (2.14)$$

Assuming the thermal load equals the rate of heat recovery, the heat recovery efficiency of the system is:

$$\eta_{HR} = \dot{Q}_{load}/\dot{Q}_{w\_Gen} \quad (2.15)$$

In terms of energy balance, a combustion based CHP system can be analysed as a control volume. When all components of the system have reached steady state, the rate of energy that enters the system boundaries

must equal the energy rate that leaves them [12]. Applying the above statement one gets [17]:

$$\dot{m}_{f\_CHP}LHV_f + \dot{m}_a \cdot h_a = P_{load\_el} + \dot{Q}_{w\_NR} + \dot{Q}_{load} + \dot{m}_{exh}h_{exh} \quad (2.16)$$

Where:

$\dot{m}_f$ ,  $\dot{m}_a$  and  $\dot{m}_{exh}$  the fuel, air and exhaust mass flow rates respectively in  $kg/s$

$h_a$ , and  $h_{exh}$  the specific enthalpies of air, and exhaust in  $kJ/kg$

$T_{a\_in}$ , intake temperature and  $T_{exh\_o}$  exhaust outlet temperature in  $^{\circ}K$ .

$LHV_f$  is the fuel Lower Heating Value in  $kJ/kg$

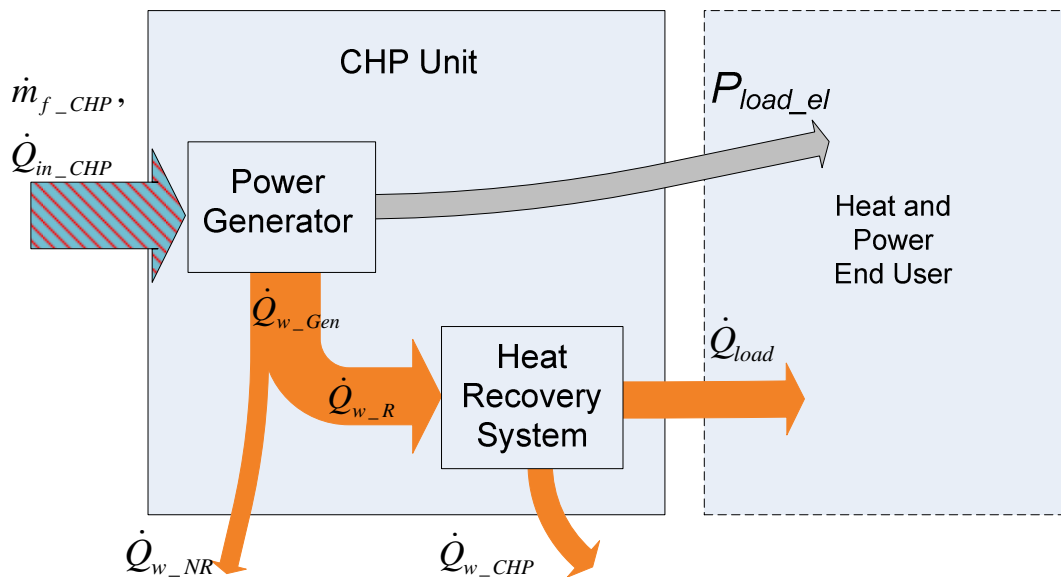


Figure 2.2 Schematic of a basic cogeneration layout



If the temperature of the intake  $T_{a\_in}$  is equal to the ambient temperature  $T_{amb}$ , equation (2.16) becomes:

$$\dot{Q}_{in\_CHP} = \dot{m}_f_{CHP} LHV_f = P_{load\_el} + \dot{Q}_{w\_NR} + \dot{Q}_{load} + \dot{m}_{exh} h_{exh} \quad (2.17)$$

Since in the case of CHP systems, intake temperature is usually equal or almost equal to  $T_{amb}$ , system energy flow rate balance in the current study will be assumed to follow equation (2.17).

In order for a cogeneration system to be economically and environmentally viable, system losses  $\dot{Q}_{w\_NR} + \dot{m}_{exh} h_{exh}$  must be brought to the minimum level possible given existing technical and financial constraints.

### 2.3. Energetic, environmental, and economic performance (EEEP)

To show the effects of the concept of heat recovery, the fuel conversion efficiency will be assumed to be equal for both small and large scale power generators. Then, for the same amount of electrical power reaching the end user, while a CHP system requires an inlet chemical power of  $\dot{Q}_{in\_CHP}$ , the centralized plant must consume  $\dot{Q}_{in\_plant} = \dot{Q}_{in\_CHP} / \eta_{tran}$  due to associated transmission losses. Furthermore, the user of the separate heat and power generation must consume additional boiler inlet heat at a rate  $\dot{Q}_{in\_boil}$  as calculated in equation (2.8) to meet the thermal demand  $\dot{Q}_{load}$ . Therefore, the total heat inlet rate for the separate supply of heat and power will be:

$$\dot{Q}_{in\_sep\_t} = \dot{Q}_{in\_plant} + \dot{Q}_{in\_boil} = \frac{\dot{Q}_{in\_CHP}}{\eta_{tran}} + \frac{\dot{Q}_{load}}{\eta_{boil}} \quad (2.18)$$

Since

$$\frac{\dot{Q}_{in\_CHP}}{\eta_{tran}} \geq \dot{Q}_{in\_CHP} \quad (2.19)$$

And

$$\frac{\dot{Q}_{load}}{\eta_{boil}} \geq 0 \quad (2.20)$$

It can be seen that:

$$\dot{Q}_{in\_sep\_t} \geq \dot{Q}_{in\_CHP} \quad (2.21)$$

Expression (2.26) shows that for a given generator efficiency, a cogeneration system will exhibit equal or lower fuel consumption for the supply of a given amount of heat and power than their separate production. The above observation translates to a reduction in energy consumption, operating costs and carbon emissions associated with CHP operation.

### 2.3.1. Device efficiency vs. overall efficiency

Static energetic comparison may give a general perspective on how a CHP system would ideally perform under conditions of stationary operation but it does not give realistic estimates of system performance [39]. In order to avoid oversimplifying the problem of estimating the performance of DES, it is important to distinguish the device efficiency as described above from the overall energy efficiency. Due to the fact that the magnitudes of heat and power generated by a CHP system rarely match both heat and power demand, micro-CHP system operation is almost always supplemented with heat from an auxiliary boiler and electricity provided by the utility grid [40]. These supplementary sources are not operated simultaneously but their use varies with time [20].

From Figure 2.2 the device efficiency is calculated by:

$$\eta_{dev} = \frac{P_{el\_CHP} + \dot{Q}_{rec\_CHP}}{\dot{Q}_{in\_PM}} \quad (2.22)$$

The overall efficiency of the micro-CHP application of Figure 2.3 is calculated from:

$$\eta_{oal\_CHP} = \frac{P_{el\_CHP} + P_{el\_imp} + \dot{Q}_{rec\_CHP} + \dot{Q}_{rec\_b} - \dot{Q}_{rej}}{\dot{Q}_{in\_PM} + \dot{Q}_{in\_imp} + \dot{Q}_{in\_b}} \quad (2.23)$$

For the above reason, the overall efficiency of the application is not identical to the fuel utilization efficiency of the device which is highly subject to a large array of parameters discussed in section 3.1. In addition, when calculating the overall fuel utilization efficiency and other performance indicators as shown below, the heat and power supplementation and rejection must be taken into account. For this study, device efficiency is viewed as a system characteristic, while the overall efficiency is viewed as a performance indicator. The following section presents the power interactions that take place between a dwelling operating an ICE based  $\mu$ CHP unit, and the environment.

### 2.3.2. Energy stream in ICE based systems

The majority of studies on ICE based micro-CHP systems involve waste heat recovery from two main sources. The exhaust gas waste heat and the jacket water waste heat. In the case of C. D. Aussant [20], a waste heat component recovered from the engine lubricant is added to the above.

Chemical power in the form of fuel enters the cogeneration system prime mover and is converted to mechanical work and thermal energy. Thermal energy ends up in the flue exhaust gasses in the form of enthalpy, in the engine coolant and lubricant, and in the engine and generator components as sensible heat, and can flow away from the system by means of conduction, convection, and radiation [3], [16], [17], [21].

The energy flow rate diagram of an ICE based CHP system is shown in Figure 2.3. Fuel chemical power or heat inlet is supplied to the internal combustion engine at a rate  $\dot{Q}_{in\_PM}$  and part of it is converted into mechanical power  $P_{mech}$ . The remaining amount flows away from the engine as waste

heat via a number of different routes such as the coolant at a rate  $\dot{Q}_{cool}$ , the exhaust gas at a rate  $\dot{Q}_{exh\_in}$ , and the engine surface via radiation and convection at rates  $\dot{Q}_{Rad}$  and  $\dot{Q}_{conv}$  respectively. Electric machine waste heat is generated at a rate  $\dot{Q}_{w\_EM}$  in the conversion phase of mechanical power  $P_{mech}$  to electrical power  $P_{el\_CHP}$  in the electric machine due to resistive as well as frictional losses [41]. In order to generate onsite electrical power of  $P_{el\_CHP}$ , the prime mover must supply the electric machine with a mechanical power output equal to:

$$P_{mech} = \dot{Q}_{w\_EM} + P_{el\_CHP} \quad (2.24)$$

The heat inlet rate to the engine must then be equal to the sum of all energy rate components of the last considered stages.

$$\dot{Q}_{in\_PM} = \dot{Q}_{Rad} + \dot{Q}_{conv} + \dot{Q}_{exh\_in} + \dot{Q}_{cool} + P_{mech} \quad (2.25)$$

Depending on system load  $P_{el\_CHP}$ ,  $\dot{Q}_{w\_EM}$  can vary from 5% to 25% of  $P_{mech}$ . The generated electricity, as well as the rate of total recovered heat from the CHP  $\dot{Q}_{rec\_CHP}$  are supplied to the end user. Any potential rate of surplus heat  $\dot{Q}_{rej}$  is rejected into the atmosphere. Surplus electrical power  $P_{el\_exp}$  is exported to the utility grid. Power deficiency is met by importing electricity  $P_{el\_imp}$  from the utility grid. Any deficiency in heat supply is supplemented with heat from the auxiliary boiler at a rate  $\dot{Q}_{rec\_b}$ . The boiler in turn is supplied with chemical power  $\dot{Q}_{in\_b}$ . Non recoverable waste heat components such as the exhaust heat at the heat exchanger outlet, the radiation heat, the convected heat, the auxiliary boiler waste heat, and the waste heat generated in the electric machine, all flow out of the system at rates  $\dot{Q}_{exh\_out}$ ,  $\dot{Q}_{Rad}$ ,  $\dot{Q}_{conv}$ ,  $\dot{Q}_{w\_b}$ , and  $\dot{Q}_{w\_EM}$  respectively unutilized.

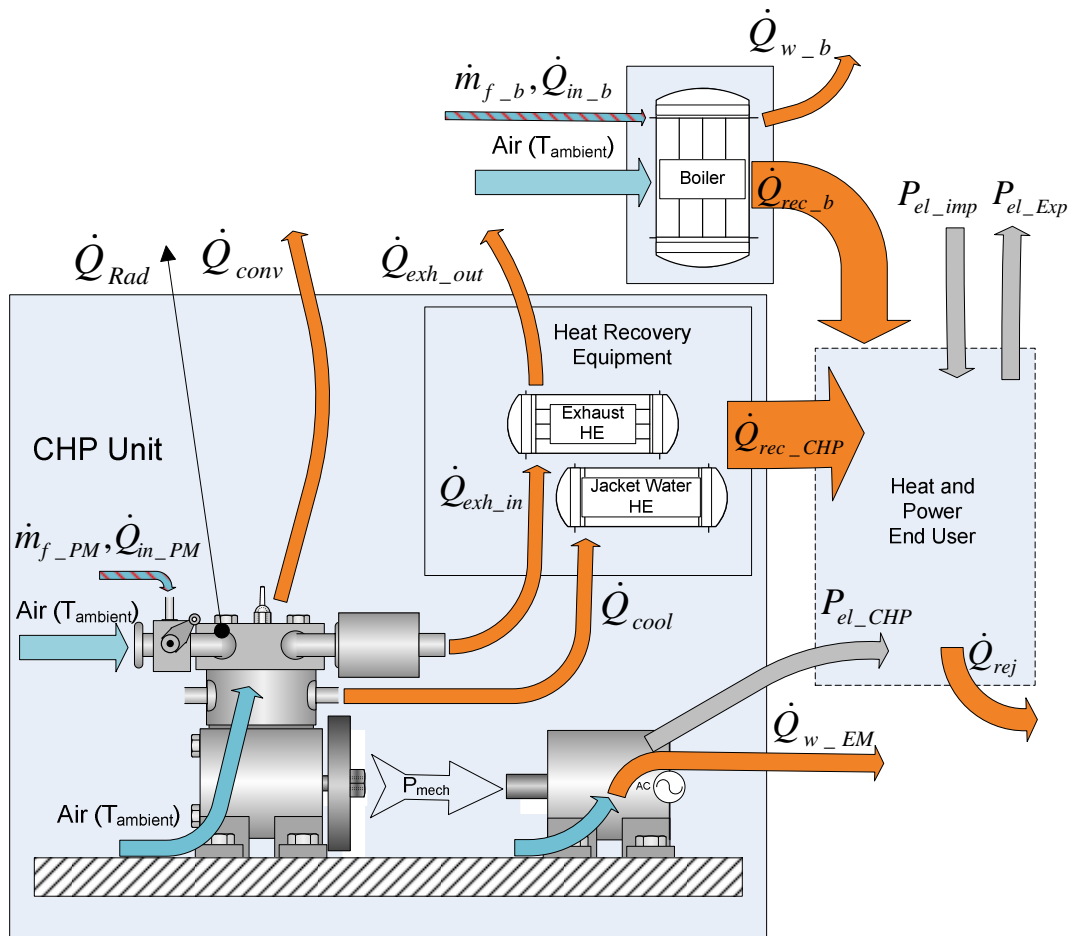


Figure 2.3 Energy flow rate between the CHP, the environment and the user

### 2.3.3. EEEP Indicators

Since significant effort and resources are funnelled towards the reduction of greenhouse gas emissions, a measure of the extent to which a proposed solution increases or decreases CO<sub>2</sub> emissions compared to the existing methods must be used. For this study, this measure will be the percentage of CO<sub>2</sub> difference observed between micro-CHP system and conventional heat and power supply of boiler & grid.

While the amount of CO<sub>2</sub> emitted in the environment to meet the energy demand of a given dwelling is counted as additional emissions, any amount of exported electricity displaces amounts of centrally generated electricity that would have otherwise been produced by a conventional power plant. Thus, when calculating the specific CO<sub>2</sub> emissions, CO<sub>2</sub> savings, and

primary energy savings (*PES*), not only the consumed but all the produced electricity including the exported amount are all taken into account since the exported electricity is a readily useable form of energy to be imported by another user connected to the grid. Therefore, the specific emissions of a CHP system is the emitted mass of CO<sub>2</sub> per *kWh* of useful energy – be it electricity or heat – and they are calculated from:

$$\epsilon_{CO_2\_CHP} = \frac{M_{CO_2\_CHP} + M_{CO_2\_Aux\_b} + M_{CO_2\_el\_imp}}{Q_{space\_total} + Q_{DHW\_total} + E_{el\_CHP\_total} + E_{el\_imp\_total}} \quad (2.26)$$

In the case of the conventional boiler and grid solution, the specific emissions are calculated from:

$$\epsilon_{CO_2\_conv} = \frac{M_{CO_2\_boiler} + M_{CO_2\_el\_imp}}{Q_{space\_total} + Q_{DHW\_total} + E_{el\_imp\_total}} \quad (2.27)$$

Where:

$M_{CO_2\_CHP}$  the mass of emitted CO<sub>2</sub> from the CHP in *kg*

$M_{CO_2\_Aux\_b}$  the mass of emitted CO<sub>2</sub> from the auxiliary boiler in *kg*

$M_{CO_2\_el\_imp}$  the mass of emitted CO<sub>2</sub> for the imported electricity in *kg*

$M_{CO_2\_boiler}$  the mass of emitted CO<sub>2</sub> from the standalone boiler in *kg*

$Q_{space\_total}$  the total amount of used space heat in *kWh*

$Q_{DHW\_total}$  the total amount of used DHW heat in *kWh*

$E_{el\_CHP\_total}$  the total amount of produced electricity in *kWh*

$E_{el\_imp\_total}$  the total amount of imported electricity in *kWh*

The percent reduction in CO<sub>2</sub> emissions is then calculated from:

$$\Delta_{CO_2} = 100 \frac{\epsilon_{CO_2_{conv}} - \epsilon_{CO_2_{CHP}}}{\epsilon_{CO_2_{conv}}} \quad (2.28)$$

Primary energy savings (*PES*) is a performance indicator that contains information on the energetic performance of the micro-CHP unit compared to that of the conventional heat and power supply. As found in [24] [39], primary energy savings are calculated by:

$$PES = 100 \frac{Q_{in_{conv}} - Q_{in_{oal\_CHP}}}{Q_{in_{conv}}} \quad (2.29)$$

Then total heat inlet for the CHP application in *kWh* is calculated from:

$$Q_{in_{oal\_CHP}} = Q_{in_{PM}} + Q_{in_b} + Q_{in_{imp}} \quad (2.30)$$

In the case of the conventional supply of heat and power, the total heat inlet in *kWh* is calculated from:

$$Q_{in_{conv}} = Q_{in_b} + Q_{in_{imp}} \quad (2.31)$$

While technical criteria may provide information on the extent to which a system performs adequately from an engineering point of view, the ability to decide whether an investment is economically viable can be attained only when economic criteria are also considered. Beside the positive environmental implications of generating electricity and heat with a reduced carbon footprint, the main motivation for a household to invest on a micro CHP unit is the capability of such a unit to generate monetary savings with respect to the traditional boiler and utility grid option.

In the case of a power producing system with exporting (net metering) capabilities such as heat led micro-CHP units, certain revenues arise from the sale of surplus power to the utility company as well as various types of financial incentives (feed in tariff scheme for the UK) offered by the government to boost the proliferation of environmentally friendly technologies.

Monetary savings can be defined as the difference between the costs of the conventional heat and power supply and the micro-CHP operation. The percentage cost savings are calculated from:

$$\Delta C_{sys} = 100 \frac{C_{conv} - C_{CHP}}{C_{conv}} \quad (2.32)$$

Where  $C_{conv}$  the operating costs of the conventional supply of heat and power, and  $C_{CHP}$  the operating costs of a solution involving a CHP, both in £

The operating costs of domestic heat and power supply using micro-generation at time  $t$  in hours can be calculated from:

$$\begin{aligned} C_{CHP}(t) &= C_{p_{el\_imp}}(t) + C_{NG}(t) - R_{FIT}(t) - R_{exp}(t) = \\ &= \int_0^t P_{el\_imp}(t) c_{el}(t) dt + \\ &+ c_{NG} \int_0^t (\dot{m}_{NG\_CHP}(t) + \dot{m}_{NG\_boiler}(t)) dt - \\ &- GT \int_0^t P_{el\_CHP}(t) \cdot dt - r_{ex} \int_0^t P_{el\_exp}(t) dt \end{aligned} \quad (2.33)$$



For the case of the conventional supply of heat and power, the operating costs at time  $t$  will be:

$$\begin{aligned}
 C_{conv}(t) &= C_{p_{el\_imp}}(t) + C_{NG}(t) = \\
 &= \int_0^t P_{el\_imp}(t)c_{el}(t) dt + c_{NG} \int_0^t \dot{m}_{NG\_Boiler}(t)dt
 \end{aligned} \tag{2.34}$$

Where  $C_{p_{el\_imp}}(t)$  and  $C_{NG}(t)$  the costs of imported electricity and consumed natural gas respectively,  $R_{FIT}(t)$  the revenues generated by the feed in tariff scheme,  $R_{exp}(t)$  the revenues generated by the electricity export all in (£),  $P_{el\_imp}(t)$ , the imported electrical power,  $c_{el}(t)$  the electricity price in all in (£/kWh),  $\dot{m}_{NG\_CHP}(t)$  and  $\dot{m}_{NG\_Boiler}(t)$  the mass flow rates of natural gas to the CHP and the boiler respectively in kg/s,  $P_{el\_prod}(t)$  the produced power,  $P_{el\_exp}(t)$  the exported electrical power, all at time  $t$  in hours, and  $c_{NG}$  the price of natural gas,  $r_{ex}$  is the export price of electricity, and  $GT$  is the generation tariff (only for FIT eligible systems) all in (£/kWh).

The marginal cost of an investment is the maximum capital cost for which the payback period ( $PBP$ ) will remain within the specified limit (usually 10 years for a micro-CHP unit). If the installation of a micro-CHP unit as a replacement to a conventional boiler is viewed as an investment expected to return the capital cost within the maximum  $PBP$ , it is easy to see the applicability of this economic viability criterion on micro-cogeneration systems for domestic applications. The marginal cost of a CHP investment is calculated from:

$$C_{marg} = (C_{conv\_1y} - C_{CHP\_1y})PBP \tag{2.35}$$

Where  $C_{conv\_1y}$  and  $C_{CHP\_1y}$  are the total annual energy costs of a dwelling equipped with conventional heat and power supply systems and with a CHP respectively.

## **2.4. Summary**

This chapter was dedicated on the background knowledge behind the energy flow taking place in the two methods of heat and power supply compared in the current thesis. The first was the conventional boiler & grid solution, and the second was the ICE based micro – cogeneration unit. The distinction between device static performance and the overall performance of the application is made, and the importance of the use of the latter in the evaluation of micro-CHP performance is highlighted. The chapter ends with an analysis of the relationships used to calculate the necessary energetic, environmental, and economic performance (EEEP) that will be used in Chapter 8, Chapter 9, and Chapter 10 for system evaluation.

## Chapter 3 Literature Review

This chapter contains a review on the existing research work on micro-CHP and is divided in five main sections. In section 3.1, the main factors that influence micro-CHP system viability are analysed. Section 3.2 describes the most popular encountered methods used for the improvement of the fuel conversion efficiency of the ICE based generator set, while the main methods of managing heat and power surpluses and deficiencies is analysed in section 3.3. Current methods for modelling and simulating micro-cogeneration systems are analysed in section 3.4. Literature review closes with a discussion on available weather, electrical demand, and hot water consumption for use in building simulation applications.

### **3.1. System viability and factors that affect it**

Experience has shown that installing a micro-CHP system may not necessarily generate energetic, emission, or monetary savings if it is not well suited to the nature of the application [34], and that the optimal solution can vary significantly from one load combination to another [20]. Factors such as system size, operating strategy, energy prices [42], the combined effect of thermal and electrical loads [36], [43], as well as the characteristics of the reference case of conventional production of heat and power, all have a very strong influence on the viability of a given micro-cogeneration system design.

The following sections contain an analysis of the main factors that influence the financial and environmental viability of micro-CHP systems as encountered in the reviewed literature.

#### **3.1.1. Geographical location**

The development and selection of micro-CHP technologies is influenced to a great extent by the geographical location of the user [4], [20]. Different technological variations of micro-CHP can be expected to be successful in different geographical areas such as Europe and America [11] and this can be the case even between different provinces of the same country [20]. As

can be observed in Figure 3.1, the difference in dry bulb outdoor temperature between different locations within the UK can be substantial [44].

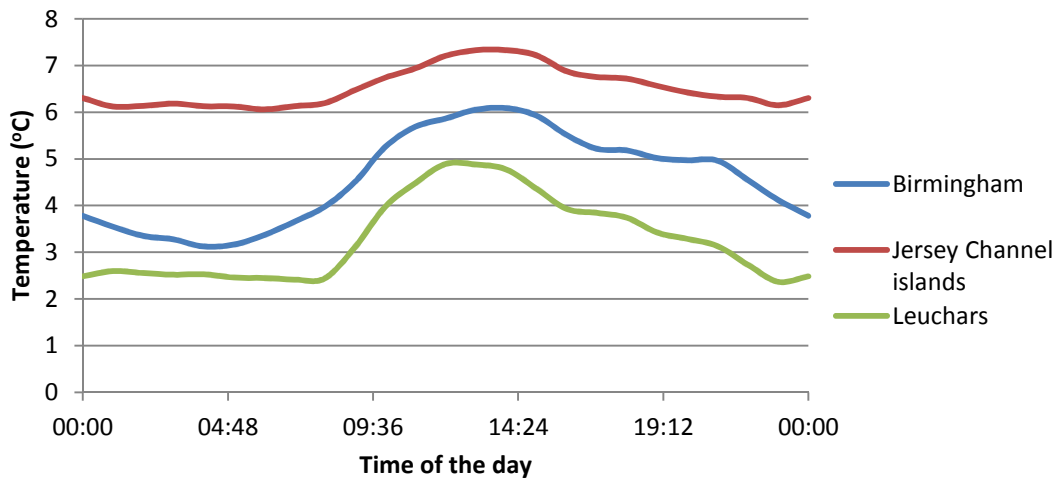


Figure 3.1 Dry bulb outdoor temperature vs. time of a day in January

### 3.1.2. Season of the year

Residential electricity and heat demands vary from one season to another [27]. CHP systems generate savings when both produced heat and power can be utilized. When a micro-CHP unit is controlled to meet the dwelling electrical load, its overall fuel utilization efficiency during the warmer months of the year deteriorates due to a reduction or absence in thermal demand, leading to the generation of surplus heat that must eventually be rejected into the atmosphere unutilized [20]. Thus, during summer, the operation of the electricity priority controller is non profitable and for this reason, F. Caresana et al. [2], suggests turning electricity led micro-CHP systems off during warmer months of the year.

On the other hand, the monthly operating hours of a heat priority, constant output controlled unit depend on the thermal demand and, during warmer months, the unit operates for a limited amount of time [11] and this increases the payback period of the system.

### **3.1.3. Building type and construction method**

Since building type is directly related not only to the geometrical characteristics of its fabric but also to its construction method and used materials, it is expected that it is one of the main factors that define the thermal loads placed on a heating system. Since a better system design is achievable when the building characteristics are taken into account [4], a large number of existing studies on micro-cogeneration have shown special interest on the connection between dwelling type and micro-CHP system performance [2], [5], [20], [26], [27], [32], [36], [45], [46].

Insulation grade is the most important characteristic of a dwelling as it defines the rate at which heat is lost from the indoor space to the outdoors [47]. Thermal mass is another important characteristic of the dwelling fabric as it acts as a thermal buffer, storing large amounts of heat, thus preventing the rapid fluctuations of indoor temperature. J. Abedin et al. [8] observed that during a non heating period, under a UK weather profile, the indoor temperature of a low thermal mass dwelling dropped below 12°C, while for a high thermal mass dwelling, indoor temperature dropped to 17°C. In addition, they found that a high thermal mass allows for a significant shift to the heating period which in turn allows for the CHP system to be operated when the grid can accommodate surplus power export.

Dwelling type is connected not only to the magnitude of the thermal but also the electrical load [48]. Electrical load profiles may vary significantly in terms of both shape and magnitude between dwellings of a different type as shown in Figure 3.2 as generated by the 24 Hour Profile Chooser [49].

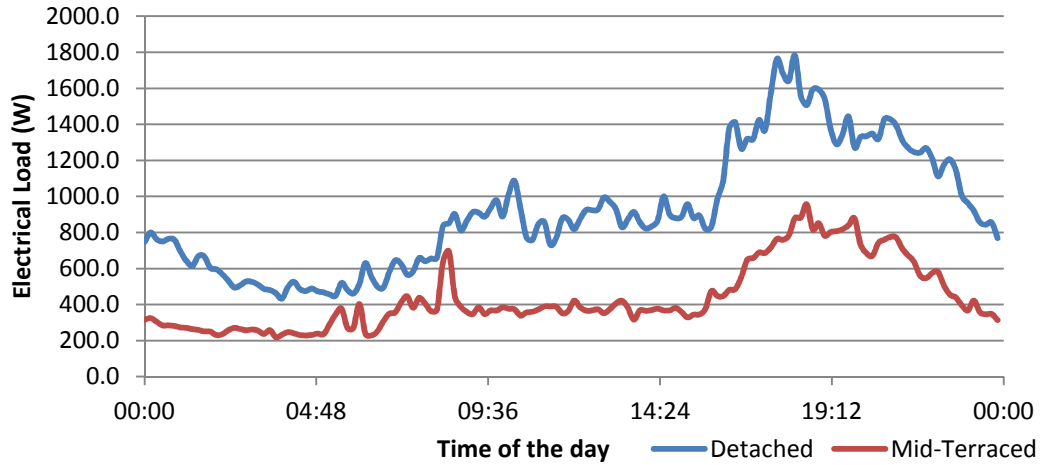


Figure 3.2 Averaged load profiles of a detached and a mid - terraced house

#### 3.1.4. Heat to Power Ratio (*HPR*)

For a CHP system, this is the ratio of the rate of recovered heat  $\dot{Q}_{rec\_CHP}$  over the produced electrical power  $P_{el\_CHP}$ :

$$HPR = \dot{Q}_{rec\_CHP} / P_{el\_CHP} \quad (3.1)$$

The inverse of the *HPR* is the electric to thermal power ratio:

$$C_{CHP} = HPR^{-1} = P_{el\_CHP} / \dot{Q}_{rec\_CHP} \quad (3.2)$$

For the heat and power end user, *HPR* is the ratio of the rate of the used heat over the used power [18]. The *HPR* of the user is strongly related to the type/area of application, and is one of the deciding factors for the selection of a CHP prime mover and operating strategy [11].

The degree of proximity between the *HPR* of a CHP system and the end user is a reliable criterion used to estimate whether a particular cogeneration system type is suitable for a specific sector [18], [19], [50], as it has a strong effect on system financial and environmental feasibility [26].

An example of the negative effects of the difference between the *HPR* of the system and the user can be found in De Paepe et al. [32] where the tested heat priority controlled system produced excessive amounts of electricity. In particular, only 10% to 15% of the generated electricity was used on site while the largest part was exported to the grid which in most cases is undesirable as the low export rates the utility companies often pay to the decentralized producer reduce the system financial viability. In the case where the *HPR* of a heat led controlled system and the user are matched, most, if not all produced electricity is consumed on site and therefore electricity export which usually does not generate savings due to low export prices is avoided.

For electricity priority controlled systems, a similarity between the user and the system *HPR*, translates to smaller amounts of surplus heat rejected into the atmosphere, and this results, to a better overall system efficiency. Since the user *HPR* varies considerably throughout the year while the system *HPR* range does not change, the overall annual efficiency of the CHP unit increases when the average *HPR* of the user increases. Generally, an electricity led system with a high electricity to heat ratio results in higher yearly energy savings [20] while at the same time, high thermal demands result in an increased system profitability [26].

The fuel conversion efficiency of internal combustion engines drops significantly as load is reduced and thus, the percentage of inlet fuel energy that ends up as waste heat increases. As a result, the *HPR* of variable output ICE based cogeneration systems is not constant throughout their operating envelope, and is being reported to range from 8.6 for low loads (low thermal efficiency/high Specific Fuel Consumption) to 2.8 for high loads (high thermal efficiency/low Specific Fuel Consumption) [19].

When comparing SI to CI engines, the former exhibit lower conversion efficiency than the latter leading to higher amounts of generated waste heat and a higher *HPR* for SI ICE based CHP systems [11].

### 3.1.5. System electrical efficiency

This performance indicator evaluates the system in terms of its power generation characteristics [18]. Essentially, it is the conversion efficiency from chemical power input  $\dot{Q}_{in\_CHP}$  to electrical power  $P_{el\_CHP}$ :

$$\eta_{el\_CHP} = P_{el\_CHP} / \dot{Q}_{in\_CHP} \quad (3.3)$$

Where:

$$\dot{Q}_{in\_CHP} = \dot{m}_{f\_CHP} LHV \quad (3.4)$$

Electrical Efficiency for a natural gas fuelled reciprocating ICE based generator set at rated power has been reported by A. Martens et al. [34] to range between 30% and 40% for medium/larger scale engines while for smaller scale engines, it usually falls below 30% *LHV*. In some cases though, small scale system electrical efficiency can reach 30% *LHV* [20] or even exceed this performance, such as in the case of Badami et. al [22] who reported a system electrical efficiency of 32.5% *LHV*. Similar electrical efficiency values for small scale units of 24% – 34% are reported by G. Angrisani et al. [24].

The conversion efficiency of ICE based systems exhibits a considerable decline as the load is reduced [22] due to the deterioration of both the engine and the electric machine performance. Especially in the constant speed, variable output controller configuration, the reduction is more substantial [2]. The plots of Figure 3.3 and Figure 3.4 show the general trends of the variability of the conversion efficiencies of an SI internal combustion engine at 3000rpm and an electric machine at synchronous speed respectively, as functions of the fraction of maximum load  $P/P_{max}$ . It can be observed that for both the prime mover and the electric machine, fuel conversion efficiency suffers at low loads.



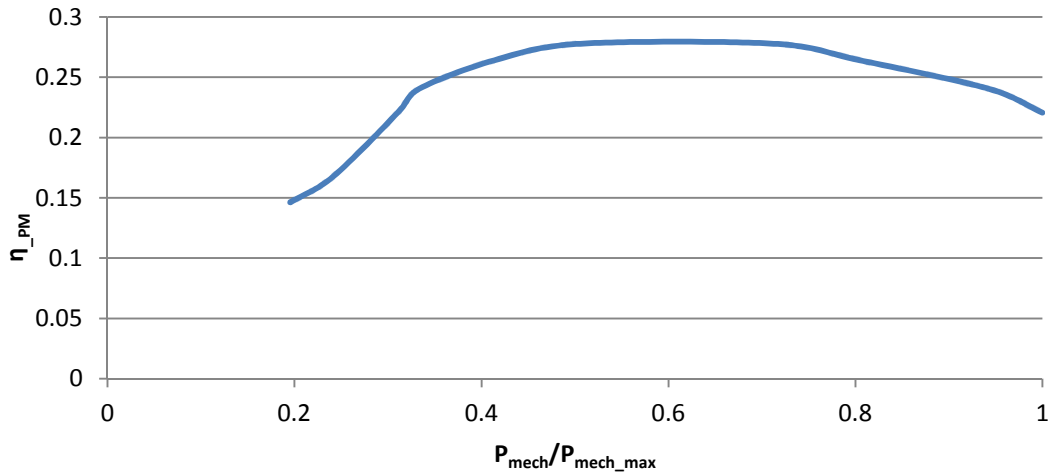


Figure 3.3 Engine conversion efficiency vs. fraction of max. power [17]

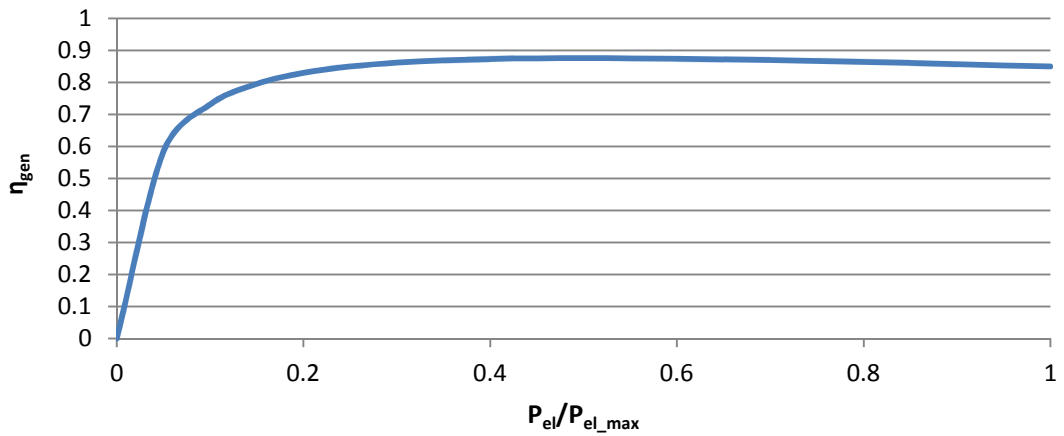


Figure 3.4 Electric machine efficiency vs. fraction of maximum power

In order to achieve high primary energy savings with an electricity led micro-CHP, it is important for the system to operate as close as possible to the point of maximum electrical efficiency as it allows for smaller amounts of rejected heat during the warmer months of the year and a low conversion efficiency would translate to large amounts of rejected heat and thus reduced savings [34]. For the above reasons, M. De Paepe et al. [32] restricted the minimum electrical load placed on the alternator to 50% of the maximum electrical power output. If electrical load drops below the set lower boundary,

the generator was turned off and the load was met exclusively by the utility grid. This practice is also recommended by Y. Huangfu et al. [31]

While in all cases, the system performs better for the more efficient prime movers [24], [31], at the same time, the fact that high conversion efficiency systems are associated with a reduction in available waste heat [29], must be taken into consideration when selecting a system for a particular application.

### **3.1.6. Morphology of load patterns**

While the larger scale cogeneration units (used in blocks of apartments) are subject to electrical and thermal demands that are predictable and relatively uniformly distributed in time, the demand placed on small scale units fitted in single family dwellings exhibits considerable fluctuations during a day and behaves in an unpredictable manner [26], [27], [40], [42]. There are certain times within a day when the thermal and electrical demands of a dwelling reach peak values but these peaks rarely coincide in time [25], [32]. As a result, a dwelling may have a demand for heat but no demand for electrical power and vice versa.

During a peak electrical demand, combined with a low heat demand, a system operating under an electrical priority regime will generate heat that will eventually have to be rejected in the atmosphere [19]. Rejected heat translates to higher fuel cost/unit of useful energy [20] and should be kept at minimum levels. In the case where there is a peak of heat demand combined with a low electrical load, an electrical priority controlled system will meet the electrical demand but generate insufficient heat, making the presence of a form of auxiliary heat supply necessary.

On the other hand, a heat priority controlled unit operating during time intervals of low thermal demand, will produce no power at all, thus increasing the payback period of the investment and necessitating the use of a supplementary power source [19], [20].

This difference in the morphology between load profiles encountered in small scale, and those of larger scale applications, translates into different system

design requirements between larger cogeneration systems and micro-CHP [4].

### **3.1.7. Device fuel utilization efficiency**

Having discussed its method of calculation, as well as the difference between device and overall application efficiency in section 2.3.1, device efficiency depends on parameters such as the type of the prime mover (motor), the type of fuel used, the temperature at which the waste heat is recovered, the condition of the equipment, and the heat recovery system technology/configuration [18], [21].

A. Moran et al. [11] modelled an SI and a CI engine based micro-CHP system and calculated for both systems values of device efficiency located in the region of 80%. Similar but slightly higher values of device efficiency of an SI ICE based cogeneration unit recovering heat from the exhaust and the coolant circuit has been found by H.I. Onovwiona et al [19], Heejin Cho et al. [28] and A. A. Aliabadi et al. [23] where it has been reported to be approximately 85% LHV.

### **3.1.8. Performance of the conventional heat and power supply**

Due to the fact that micro-CHP as an investment is evaluated in terms of the savings in consumed energy, operating costs and CO<sub>2</sub> emissions it may generate with respect to the conventional combination of a boiler and the utility grid, the knowledge of the environmental and financial performance of the conventional solution is necessary.

The environmental performance of electricity plants can vary significantly depending on the applied technology. For example, in the case of Belgium, the fuel conversion efficiency of combined cycle equipped plants ranges from 53% to 56% LHV, but the average Belgian conventional fossil fuel based plant has a fuel conversion efficiency of 42% LHV [32]. Similarly, power production in the United Kingdom, is characterized by an average fuel conversion efficiency of approximately 40%, and transmission losses of approximately 7.5% of demand [38]. In terms of CO<sub>2</sub> emissions, UK

centralized power supply at the time of this writing generates  $0.4903kg$  of  $CO_2$  for every  $kWh$  of delivered (average transmission losses included) electricity [51].

Condensing boilers which is the most modern domestic boiler variant have a very high energy performance being able in some cases to utilize more than 90% of the fuel inlet heating value [34].

From the above, one may observe the high performance of modern centralized power production and domestic boilers. The energy savings and emission reductions a micro-CHP system may generate are not guaranteed but depend on the type of power plant it is competing against [20].

### **3.1.9. Control strategy**

The operating strategy of a cogeneration system is defined by the objective of the system controller. Two main system operating strategies currently dominate the micro-CHP market. Heat priority control (HPC) mode in which the controller manages the system resources in a way that the thermal demand of the dwelling is met, and electricity priority control (EPC) mode, in which the controller adjusts system operation aiming to satisfy the electrical demands of the user [2], [11], [18], [19], [20], [27], [42].

For the average residential application, the electricity priority controller was observed by C. D. Aussant et al. [20] to be less suitable than the heat priority controller due to the nature of the load profiles being characterized by low thermal demand and considerable electrical load fluctuations. For the above reason, only very small (undersized) engines were found to be viable for the electricity priority control mode. They suggested the fitting of an adsorption heat pump (AHP) to the CHP unit to alleviate the heat surplus problem during summer by utilizing surplus heat to meet potential cooling demands. On the other hand, they found the thermal priority system during the warmer months to be characterized by long periods of non operation leading to a long payback period (PBP).

H.I. Onovwiona et al [19] observed that when the electricity priority controller was chosen in oversized systems, the engine operated on average at part

load leading to a low system electrical efficiency, and while the electricity load remained relatively constant throughout a year, the heating demand during summer was only that of the domestic hot water (DHW). They found heat priority controller to be a more fuel efficient solution than the electricity priority controller mainly in the case of oversized systems. When undersized systems were considered, the electricity priority controller was found to be the more efficient solution, and the above observations led the authors to conclude that the optimal strategy is case sensitive and depends mainly on system size and configuration, and conversely, that the optimal strategy depends on the sizing of the system relative to the thermal load demand.

The application of CHP as a central heating and power supply unit meeting the demand of multiple users has been investigated by F. Caresana et al [2]. In this case, a battery was used to store the generated electricity. The results of their simulations showed that the most economically viable application of micro-CHP technology is in the residential sector which in their study was a 10-flat apartment building. A novel variable speed heat priority controller was found to generate maximum savings (10% more than the constant speed, heat priority controller). Savings of similar levels were observed for electrically led systems of both constant and variable speed modes. In all simulated cases, the greatest savings were observed in the winter months.

In cases where energy prices vary within the duration of a day, it is not uncommon to encounter control strategies that schedule the operation to minimize operating costs. One such system was studied by E.S. Barbieri et al. [26] who simulated a micro-CHP model for two different dwelling types. On/off type control with thermal storage was used in all cases. The unit was switched on during periods of high revenues even when there was no direct heat demand to generate profit from net metering. Another study where a cost optimal operating strategy was investigated is found in the article of A. Canova et al. [25] who modelled a micro-trigeneration unit operating under a control scheme capable of managing the activation and deactivation times of the system assets with the purpose of achieving operation at a minimum cost. A similar linear programming based cost optimal strategy concept was also developed by Heejin Cho et al. [28].

### **3.1.10. System size**

The proper sizing of a micro CHP system and its components is an essential part of its design process as it affects the system economic and environmental performance with payback period (PBP) being directly dependent on the unit size [37]. In addition, system size has been found to also affect the thermal cycling patterns and the usage time per year of a CHP system [39]. The main sizing criteria of a micro-CHP unit are the expected load profiles, the prices of fuel and electricity, and the associated investment costs [20].

Over sizing a micro CHP unit has been found to cause more problems than under sizing it. On a financial standpoint, an oversized CHP unit may lead to no improvement over a conventional heat and power supply configuration of boiler and grid [52] and in all cases, properly sized or undersized systems operate more efficiently than oversized ones [19]. Therefore, micro-CHP systems should not be sized to cover peak loads as it is more profitable to involve storage equipment, an auxiliary boiler and the grid to supplement any deficiencies and meet peak demand [40].

A heat priority controlled system sized to cover the complete heat demand of the dwelling without the help of an auxiliary heat source will produce surplus electricity that must either be stored and used when the electrical load is increased or be sold for revenue to a user who is in need for this electricity [19], [20]. The application of an oversized unit operated under heat priority control makes sense only when the electricity export prices are high. For low export prices (as is more commonly encountered), the system sizing should minimize the generation of surplus electricity [11].

Systems that operate under electricity priority control should be sized to operate closest to the point of maximum fuel conversion efficiency for as long as possible. The higher system efficiency observed for smaller systems for given load profiles can be attributed to the reduced amounts of surplus heat generated when the engine operates at a point of high fuel conversion efficiency [20].

Typical micro-CHP units encountered in the UK have an electrical capacity of  $1kW$  on average for free standing houses and about  $5kW$  on average for medium density housing with central heating [5]. Besides system capacity, proper sizing of heat activated equipment such as the heat exchangers and adsorption heat pumps are of great importance for system performance [53].

A system may be designed in a way as to meet a given electrical power demand at the torque speed combination of maximum efficiency [16], [17], [54]. For a system with a variable power output, a variable speed control strategy that meets a given demand at optimal points at all times minimizes break specific fuel consumption (*bsfc*) for all loads. Due to this advantage, variable speed micro-CHP systems have been found to exhibit an improved electrical efficiency, especially at low loads, increased savings by 10% on average [2], and reduced harmful emissions such as  $NO_x$  [22] when compared to their constant speed counterparts .

When a driven component must be operated at speed range about which the engine would not normally operate efficiently, using a gearbox may provide a solution. As seen in Y. Li et al [54], a prime mover connected to a gearbox with carefully selected transmission ratios may ensure the operation within a specified economical zone, while an optimal torque curve described by a polynomial function of speed crossing the zone provides the torque for which the fuel conversion efficiency is maximized at a given speed.

### **3.1.11. Energy prices**

The prices of electricity and fuel are among the key factors in the economic feasibility of micro-CHP systems [6], [20], [37] and this technology tends to be viable for high and low electricity and natural gas prices respectively [55].

As fuel price increases, monthly savings decline until the point where the system starts operating at a loss. Since energy prices have a strong effect on the monetary savings, and since PBP depends on the monthly savings it generates compared to the separate production of heat and power, PBP is dependent on energy prices as well [11]. Plots of monthly generated monetary savings (or losses for negative values) for three different price

rates of natural gas sourced from A. Moran et al [11]. can be seen in Figure 3.5.

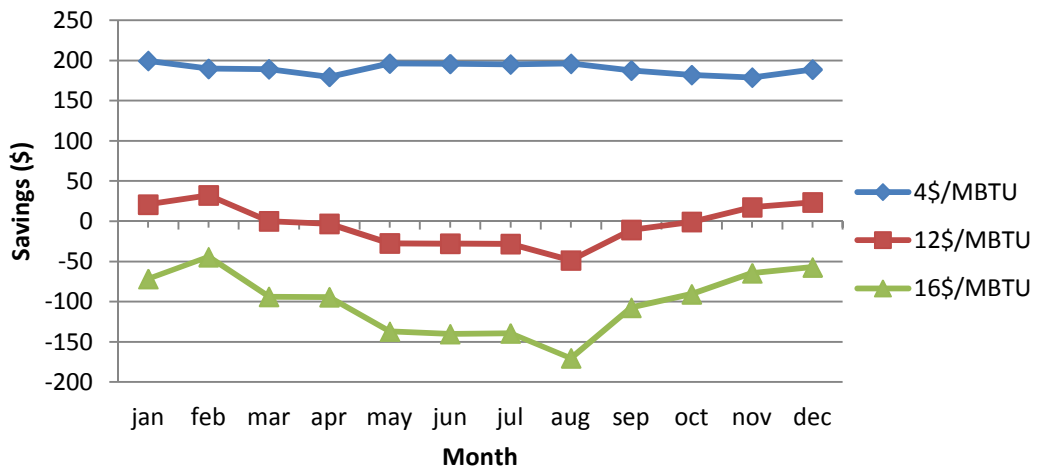


Figure 3.5 Monthly cost savings for three different fuel prices

### 3.1.12. Electricity export prices

Electricity export price is one of the more important parameters in the financial viability of a heat priority controlled micro-CHP unit as it directly affects the electricity export generated revenues [32].

### 3.1.13. Government subsidies

Government funded monetary incentives are in many cases offered to operators of low carbon footprint technology such as micro-cogeneration [20], [26], [37]. These incentives artificially alleviate the usually high initial cost of the equipment [39], and therefore enhance the economic performance indexes of such investments.

The form and degree of interference of these incentives vary significantly from one country to another [6]. Government monetary incentives on distributed energy systems in the United Kingdom are covered under the UK Feed In Tariff (FIT) Scheme which was put in place in 2010 [10]. Any micro-CHP unit that falls under the specifications of the UK government (one of which being that the electrical output of the unit be  $2kW_e$  or less) is eligible for one of 30,000 available grants. FIT Scheme grantee operators receive



Generation Tariff revenue of  $GT = 13.24 \text{ p/kWh}$  of generated electricity [56]. In addition, export revenues are paid to the operator at an export rate of  $r_{ex} = 4.77 \text{ p}$  for every  $kWh$  of exported electricity. Units ineligible for the scheme may still provide revenues for exported electricity which in the current project will be  $r_{ex} = 3.0 \text{ p}$  per  $kWh$  of exported electricity as found in [9].

While the intent of these government subsidies is the promotion of carbon saving technologies, the installation of a micro-CHP does not necessarily guarantee energy and carbon savings but its success is rather depended on numerous factors as pointed out in [20]. For this reason, is important to investigate the extent to which government subsidies are restricted to environmentally friendly applications of the technology as also studied by K. Voorspools et al. [39].

#### **3.1.14. Loads and system inertia**

One of the conclusions of the field trials on different micro-CHP technologies carried out by the UK Carbon Trust was that micro level scale system performance differs from that encountered in medium scale systems. The tested micro-CHP systems underperformed when compared to simulation results due their thermal inertia being excessively higher than that of the conventional boiler. This characteristic of micro-CHP systems translates to a limited load following capability [33].

In the case of ICE based systems, the electrical response is fast but the heating response - especially during start up - is relatively slow [22], [39]. Every time a system is stopped, cooled down and started again, a considerable amount of fuel must be expended before the system is reheated and rated thermal output is reached. In addition, warm up periods are characterized by a lower fuel conversion efficiency that reduce the overall efficiency of the unit [33], [57], [58], [59], cause increased engine wear [36], [39], [58], and generate the majority of HC emissions [60].

K. Voorspools et al. [39], analysed experimental data and observed that after 30 minutes of operation from cold start, only 65% of the system maximum

thermal output was available. As can be seen in the plots based on data from L. Fu et al [61] in Figure 3.6, the thermal response of the system varies depending on the time elapsed from the last stop, and while it took approximately 25 minutes for heat output to reach steady state when started 1h after stop, in the case of cold start it required approximately 50 minutes of engine operation.

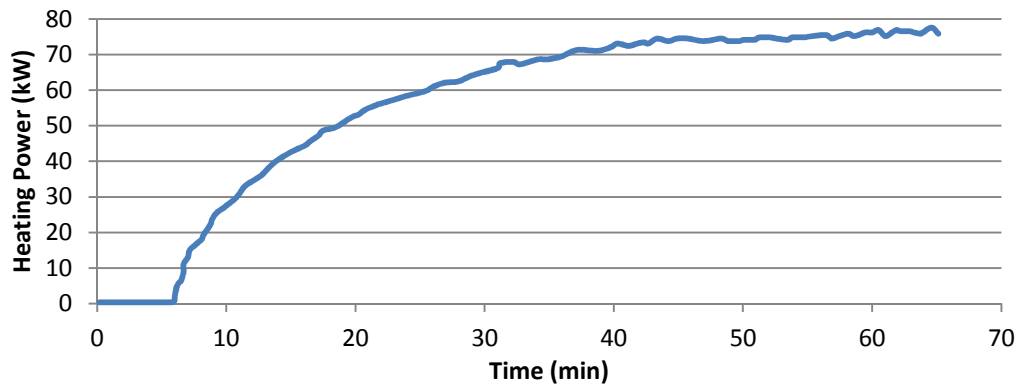


Figure 3.6 Response of the heat recovery system start up

In the system tested by L. Fu et al. [61], additional amounts of fuel consumed during start ups not directly associated to the system warm up were reported with approximately 1 minute of system operation required before the system could be connected to the grid, and a further 3 to 5 minutes of engine operation necessary before power output stabilized to the rated level. During shut down, the engine load had to be gradually reduced (took 30 seconds to 1 minute) due to the inertia of the moving parts. In addition, natural gas remaining in the cylinder and vent pipe after fuel supply was cut off, was sufficient to run the system for a further 5 to 6 minutes while being drawn at a flow rate of 35% of the maximum value.

From the above, it can be seen that turning on and off the system increases the operating costs and emissions, and causes excessive system wear. For these reasons, A.D Peacock et al. [59] suggest a minimum operating period of 30' in order to reduce the number of start-ups. In addition, the incorporation of the thermal inertia of the CHP system in the model is important for the generation of relevant simulation data.

N. J. Kelly et al. [36] found a strong dependence of micro-CHP cycling frequency on season, grade of dwelling insulation, selected control strategy as well as occupancy patterns. In general, heavy thermal loads tended to lead to a reduction in system cycling frequency. The colder the weather and the lower the insulation grade of the host dwelling were, the lower the observed cycling frequency.

### **3.1.15. Useful operating life**

In order for an investment to be viable, its useful operating life must be at least equal or greater than its payback period. According to F. Caresana et al [2], service life is an aspect in which small scale ICE based CHP systems underperform compared to larger scale units and considered a useful operating life of ICE based micro-CHP of 25,000*h*. On the other hand, G. Angrisani et. al. [24] proposed an engine life of 80,000*h* for the system to be viable.

## **3.2. Improving $\mu$ CHP fuel conversion efficiency**

The importance of high fuel conversion efficiency as discussed in section 3.1.5 creates grounds for research and development that has resulted in a number of different technical routes used to increase the electrical efficiency of ICE based micro-CHP systems as discussed below.

### **3.2.1. High performing internal combustion engines**

Since the greatest portion of waste heat during the conversion of chemical power to electricity is generated in the ICE, the improvement of the fuel conversion efficiency of internal combustion engines is a very common research field. Engine efficiency is benefitted by high compression ratios [16], [17], lean burn operation, and exhaust gas recirculation (EGR), while homogenous charge compression ignition (HCCI) engines and premixed charge compression ignition (PCCI) engines are some of the directions towards increased ICE efficiency [62].

In addition, engines operating on novel thermodynamic cycles in which the expansion ratio is higher than the compression ratio, offer another alternative

to the low efficiency problem of ordinary small engines. Y. Takita et al. [29] tested a novel micro-CHP system equipped with an Extended Expansion Linkage Engine built by Honda, and marketed as the Honda EXLink. This engine type operates on the Atkinson thermodynamic cycle [17], and its efficiency was observed to surpass that of a conventional Otto cycle by 3.8 percentage points.

### 3.2.2. Combined cycles

Another means of increasing system fuel conversion efficiency is the use of a form of a combined cycle [22]. This concept consists of a prime mover whose generated waste heat is recovered and fed into a second prime mover of a design capable of converting it to mechanical power. As a result, fuel utilization efficiency, fuel conversion efficiency as well as exergy efficiency may be increased considerably. The work producing cycle whose waste heat is supplied to another cycle is called a Topping cycle. The work producing cycle operating on recovered heat from the topping cycle is called a bottoming cycle [21].

The combined mechanical break specific fuel consumption in  $kg/kWh$  is calculated from:

$$BSFC_{Mech} = \frac{\dot{m}_{f\_PM}}{P_{bottom} + P_{PM}} \quad (3.5)$$

Where  $\dot{m}_{f\_PM}$  is the fuel inlet rate to the prime mover in  $kg/s$ ,  $P_{PM}$  is the prime mover power output in  $kW$ , and  $P_{bottom}$  the bottoming cycle power output in  $kW$ .

The combined electrical break specific fuel consumption is calculated from:

$$BSFC_{El} = \frac{\dot{m}_{f\_PM}}{P_{bottom}\eta_{bottom\_gen} + P_{PM}\eta_{gen}} \quad (3.6)$$

Where  $\eta_{bottom\_gen}$  is the conversion efficiency of the bottoming cycle electric machine.

There are still some disadvantages associated with combined cycles which in large scale systems may not constitute important barriers, but can be detrimental for micro-cogeneration applications. These include a high initial cost, increased complexity, specialized technology, and long warm-up times needed for the bottoming cycles to reach rated power – a non favourable characteristic when interrupted system operation such as in the case of a micro-CHP [26], [40] is considered. In addition, while a bottoming cycle increases system fuel conversion efficiency, at the same time it reduces the available usable heat and thus, system Heat to Power Ratio is also reduced [22] and this must be taken into consideration during system selection for a given application. A more detailed discussion on existing bottoming cycle technologies can be found in Appendix 2.

Due to the advantages of conventional ICE based technology, combined with the current disadvantages of combined cycles, the current thesis will focus on conventional ICE based systems. For the performance comparison between the low and high fuel conversion efficiency systems, a low, and a high compression ratio engine of conventional technology will be simulated.

### **3.3. Managing heat and power surplus and deficiency**

Since it is quite unlikely that the HPR of the user exactly matches the HPR of the micro-CHP at any given time, it is expected that depending on the selected control strategy, surpluses and deficiencies in heat and power cannot be avoided without the help of certain peripheral components as well as a dedicated segment of code in the control software [2], [18], [19], [20]. The possible types of heat and power surpluses and deficiencies, along with the different components and techniques used for this purpose are described in the following subsections.

#### **3.3.1. Electricity surplus**

A surplus amount of electricity is generated when a cogeneration system is operated under a heat priority control at time periods during which a heat demand is present, while at the same time the electrical demand is not

sufficient to consume the complete amount of produced electricity [2], [18], [19], [22].

Net metering is the connection of the unit in parallel to the grid, exporting the excess electricity to the utility company (under certain revenue/kWh rates). [2]. Exported surplus power may reduce operating costs provided the export prices are high [32]. A battery can be a viable alternative to net metering in cases when the unit operates in standalone mode or when the buyback rates of the exported electricity are too low to make such an operation profitable. A battery enables the user to store the produced surplus electricity and use it when there is a respective demand [19], [22].

### **3.3.2. Electricity deficiency and import**

An electrical deficiency occurs when the electrical load is higher than the maximum power output of the unit, either due to being a heat led system turned off in the absence of heat demand, or due to the electrical power output of the unit being insufficient to cover the electrical load at a given time.

If the electrical demand surpasses the maximum output of the system, or when the system is switched off, supplementary electrical power is purchased from the grid at normal rates [18], [19] or drawn from a battery (if applicable).

### **3.3.3. Thermal surplus and heat rejection**

Any amount of generated heat that cannot be readily used due to a lack of an equal or greater thermal demand is considered to be surplus. In order to prevent the system from overheating and to protect its technical integrity while keeping the unit in operation, any surplus amounts of heat are rejected in the environment with the use of a force cooled radiator fitted to the coolant circuit [2]. According to C. D. Aussant et al. [20] the annual amount of rejected heat depends on the length of heating season, the performance characteristics of the ICE, the system demands, and the dwelling characteristics. Rejection of surplus heat is an undesirable occurrence as it reduces the system generated *PES* [42].

The set temperature limits that control heat rejection must always be within the operating limits of the system components. H.I. Onovwiona et al [19] regulated heat rejection switch on and switch off temperatures of the storage water to be triggered at 75°C and 70°C respectively.

#### **3.3.4. Thermal deficiency and the auxiliary burner**

When the heat output of the CHP unit is insufficient to meet the thermal demand, an auxiliary burner fitted on the system is commonly used to cover the thermal deficiency between the demand and CHP thermal output [18], [19], [28], [32]. While the availability of an auxiliary burner is optional for heat led systems, it is necessary when the system operates under an electricity priority control strategy where periods of thermal deficiency are almost certain to occur. The auxiliary burner is usually triggered as a response to thermal loads of a long duration [26] and prevents the water temperature to fall below a specified set point [20]. H.I. Onovwiona et al [19] set the auxiliary burner trigger on and off limits to 50°C and 60°C respectively.

The efficiency of the auxiliary burner may vary from one case to another but will not detract significantly from the value of 90% LHV as provided by M. De Paepe [32].

The auxiliary burner must be sized in a way that ensures that the heat demand is met while at the same time excessive thermal cycling is avoided. O.A. Shaneb et al. [27] used linear programming as well as the maximum rectangle method to size the backup burner in their CHP model for optimal cost performance under UK loads, energy prices and subsidies. It was concluded that cost optimal boiler size depends on factors such as the load type, the initial cost of the CHP system, and the characteristics of the Feed In Tariff scheme.

##### **3.3.4.1. Thermal Storage**

The availability of a thermal storage tank to the circuit of the micro-CHP unit (especially in the electricity priority controlled case) can enhance its environmental and financial performance as a significant amount of surplus

heat that would have otherwise been rejected in the atmosphere, is stored in the tank and then made available during a period of thermal deficiency. Therefore, a CHP unit equipped with a heat storage tank can operate profitably for a longer period of time than one without [30].

In addition, when heat storage is applied in heat led systems, it allows for the heat demand placed on the CHP system to be shifted in relation to the peak space and DHW load and thus, the heating system may follow a different operating schedule than the heating elements. Such a characteristic can be an advantage on the aggregate scale as the simultaneous export or import of power to and from the grid can be avoided by scheduling a network of CHP units to operate at different times. On a financial point of view, the user may purchase electricity from the grid when the price is the lowest, thus allowing for the CHP system to generate higher cost savings [8].

For the above reasons, the use of heat storage to meet both space heat and DHW demands is gaining popularity [63].

The capacity of the heat storage is itself a very important factor in the management of surplus heat and thermal load spikes [6], [26], [30], and its selection directly influences fuel consumption and PES [26]. As heat storage capacity is increased up to a certain point, the duration of profitable operation increases as well [6], [26]. While a large heat storage capacity allows for flexible heat management, it also leads to higher heat losses than a smaller tank. Thus, a further increase of the tank size beyond its optimal value may not affect the savings significantly but the heat losses will increase [30]. Optimal heat storage capacity depends on a large number of parameters [26] and for this reason; the optimal tank size is case specific [30].

The proper selection of the space heating and DHW temperatures may lead to a cost effective and energy efficient boiler or micro-CHP system operation. Liao et al. [64] used a constant water temperature setting of 70°C. H.I. Onovwiona et al. [19] kept water temperature between 70°C and 75°C and the boiler got activated when water temperature dropped below 60°C. C. D. Aussant et al. [20] used a DHW supply temperature of 55°C with set point range of 52°C - 58°C. B. Sicre et al. [5] set the temperature to 45°C and took



into account the seasonal variation of water inlet temperature. A wider temperature range between 50°C and 75°C was used by M. Badami et al. [22].

Another configuration as found in N. J. Kelly et al. [36] uses a 200L buffer tank in the role of heat storage, and a separate DHW only tank. The buffer tank supplied both the radiators and the DHW tank at a temperature of approximately 50°C. The buffer tank temperature dead band was 10°C with lower and upper limits set at 65°C and 75°C respectively.

#### **3.3.4.2. Heat recovery system and fluid temperatures**

Heat recovery in reciprocating ICEs can be achieved through a combination of heat flow routes, each of which characterized by a different heat grade/temperature range. Waste heat from the intercooler is available at 30°C - 80°C. The engine lubricant temperature ranges between 35°C - 95°C, while the engine coolant temperature ranges between 78°C - 120°C. On the other hand, the heat in the exhaust is characterized by the highest grade of all waste heat components, with exhaust temperature ranging from 360°C to 640°C [21].

The exhaust heat exchanger outlet temperature is one of the defining factors in the exhaust heat recovery efficiency and device fuel utilization efficiency of the CHP system. For this reason, the design of the exhaust heat exchanger in particular is very important for the CHP device efficiency [24].

In most non condensing systems, the exhaust outlet temperature does not usually fall below 100°C. H.I. Onovwiona et al [19] report engine exhaust temperatures that ranged from 330°C to 585°C and the exhaust heat exchanger outlet temperature varied from 125°C to 190°C exhibiting an average drop of 315°C. Similar values are found in X.L. Zhao et al [57] where an exhaust outlet temperature is reported to range from 120°C to 170°C.

Since the dew point of the vapour in the exhaust ranges between 45°C and 55°C, the latent heat contained in the exhaust gasses cannot be recovered by using a conventional heat exchanger alone (flue gas thermal recovery is

typically in the order of 20% of the total input energy) and this translates to a loss of approximately 50% of the exhaust available thermal energy. The condensing heat exchange system designed and tested by X.L. Zhao et al [57] leads to a drop in exhaust temperature to well below the dew point of the exhaust (below 30°C in their system) leading to a flue gas thermal recovery efficiency of approximately 30% of the fuel input power.

The engine coolant is another readily available source of waste heat as its main function is to collect heat from the engine and reject it in the environment. Up to 30% of the input fuel power can end up flowing through the circuit [18] and the temperature depending on application, type of fluid and load can range from 80°C to 120°C [34]. X.Q. kong et al. [35] used an outlet temperature of 80°C and in order for the engine to operate efficiently, they proposed an inlet coolant temperature that ranges between 60°C and 85°C.

The engine lubricant may also be used as a waste heat recovery source provided that there is a lubricant cooling circuit present on the engine. Oil temperature ranges between 35°C and 95°C [34].

Dropping the return temperature of the heat recovery fluid below that of the lowest heat grade source to be recovered is essential for the successful recovery and high fuel utilization efficiency [34].

### **3.3.5. Indoor temperature settings**

1997 ASHRAE Fundamentals Handbook (SI) [65] recommends 24°C as a comfortable indoor temperature. On the other hand, UK publications provide lower indoor temperature limits. According to the Energy Saving Trust [66], the room thermostat should be set to the lowest comfortable temperature which ranges from 18°C to 21°C. Ruming Yao et al. [67] used a 19°C set point for an occupied dwelling, while they considered 15°C as the typical temperature of an unoccupied house. Similar values are found in J. Abedin et al. [8], who simulated a UK dwelling with a set indoor temperature of 20°C.

### **3.4. Modelling and Simulation of micro-CHP systems**

When a researcher investigates the performance of a DES such as a micro-CHP unit by means of a computer simulation tool, the use of realistic mathematical models and load profiles is a key factor towards extracting meaningful results. Since there is a fair amount of studies involving the simulation of domestic heat and power consumption, various modelling and simulation approaches have been encountered.

#### **3.4.1. Micro-CHP studies with building simulation packages**

The review on existing studies on micro-CHP systems carried out by means of simulation(s) showed that a considerable number of researchers opt to use a dedicated building simulation program. This category of simulation software makes use of complex, very detailed 3-D discretized building models that are capable of producing very accurate and realistic results.

C. D. Aussant et al. [20], N. J. Kelly et al. [36] and H.I. Onovwiona et al. [19] carried out studies on the performance of micro-CHP systems using ESP-r which is a building energy simulation software package developed by the University of Strathclyde. The libraries of this software contain detailed calendars of occupancy, DHW and electricity consumption patterns for weekdays and weekends, as well as the building characteristics and geographically specific yearly weather profiles (Uses weather data from EnergyPlus simulation software). Another, well known energy simulation software that utilizes extensive libraries, and is encountered on a frequent basis in the industry is DOE 2.0 and its variants such as DOE 2.5 which was used by M. De Paepe et. al. [32] to create load profiles (heat & electricity) for a period of one year. L. M. Chamra et al. [4], J. Abedin et. al. [8], and Heejin Cho [28] used TRNSYS to simulate the micro-CHP operation, while A. Moran et al. [11] used Trace Load 700 software to estimate the average energy load of an office building for each month of the year.

A short trial of the above software by the author revealed that while very accurate and detailed in nature, their complexity requires a deep knowledge of the Civil Engineering discipline, and the building model configuration

procedure takes time and effort that could be funnelled towards the study of the DES itself. The heavy computational load the 3-D building model places leads to long simulation times, which means that the much needed for DES studies large volumes of simulation data are not easily achievable, and this is reflected by the relatively small amount of generated data most encountered studies involved. Following the review of studies involving DES modelling and simulation, the general conclusion is that this software type is targeted more towards the Civil Engineers focusing on the case specific performance of the building fabric or that of the heating, ventilation and air – conditioning (HVAC) systems rather than the performance of the simulated DES. A more simplistic 1-D building model, easy to setup and capable of thermally modelling the most likely to encounter dwelling types in the UK, would be a very desirable tool, that while sacrificing some realism in the building thermal behaviour, it would speed up model configuration and data generation considerably, thus in many cases being a more suitable application for the study of DES than existing simulation software. For this reason, the development of a simulation tool based on a 1-D building model but with DES model components of equal or higher complexity than those encountered in literature, will be pursued in the current thesis in order to facilitate the studies focusing on DES performance investigation.

### **3.4.2. CHP System Modelling**

The development of a mathematical model that describes the CHP system behaviour accurately throughout its complete operating envelope can be essential when variable output operation is simulated.

#### **3.4.2.1. Constant coefficient models**

This is the simplest form of CHP model as the performance is described by constant coefficients. While this model type is simple to construct and use and suitable for modelling constant output systems, it is not suitable when variable output systems are considered.

### 3.4.2.2. Quasi-stationary CHP models

Since CHP system performance parameters are functions of system load and engine speed [32], and since system load (and speed in the case of variable speed systems) may vary considerably throughout a day in the case of an electricity following strategy, a model capable of describing the performance of the CHP throughout its operating range is necessary for the simulation of a variable output operation. The most common model type used in CHP simulation applications is Quasi-stationary.

One method to construct this model type is the fitting curves/surfaces on experimental data (or data generated by a physical, crank angle based model when modelling the engine as a standalone model [68]). H.I. Onowwiona et al [19], N. J. Kelly et al [36] and C. D. Aussant et al. [20] simulated a complete micro-CHP unit based on manufacturer provided data on ESP-r. The CHP system in this case was modelled as one single unit (no separate analysis of the engine, the electric machine, and the heat exchangers). The model dependent variables such as the Break Specific Fuel Consumption, the Electrical Efficiency and the Heat to Power Ratio are calculated as polynomial functions of part load ratio. A correction function is integrated in this model to take into account performance deviation caused by deviations in altitude and temperature from the reference conditions. The thermal transient behaviour of the engine is described by means of polynomial functions of time elapsed after shut down.

A similar polynomial model was used by Heejin Cho et al. [28] who simulated an ICE based micro CHP model following a cost optimal strategy on TRNSYS. The system electrical efficiency in this case was calculated from:

$$\alpha_1 = -0.0011x_5^2 + 0.0287x_5 + 0.0699 \quad (3.7)$$

where  $x_5$  the electrical output of the generator set. Coolant and exhaust heat in this model were assumed to be constant fractions of the chemical power inlet (0.3 for each component).

Another commonly used method of constructing quasi-stationary CHP models is the use of lookup tables. Under this modelling layout, experimental data may be used to populate matrixes that utilize interpolation techniques to return the model dependent variables for given values of the independent variables. F. Caresana et al. [2] used one lookup table that returned fuel flow for given combinations of engine torque and speed, and one that returned the exhaust heat as fraction of chemical power inlet for these same inputs. The complete engine model was controlled by a proportional – integral gain (PI controller). A saturation filter cleared the control signal from a potential demand for negative torque (e.g. during engine load reduction) or torque out of the engine specifications.

#### **3.4.2.3. Thermodynamic ICE model**

A thermodynamic engine model is constructed using ideal engine thermodynamic cycles. Spark ignited and compression ignited engines are modelled by their respective ideal Otto and Diesel cycles, and depending on the engine compression ratio and the heat input, the engine output and the exhaust temperature can be calculated as shown in A. Moran et al [11] who used this engine modelling layout to model a CHP system using separate component models.

#### **3.4.2.4. Transient ICE behaviour and micro-CHP engine modelling.**

As discussed above, due to the nature of the residential loads, the use of a micro-CHP model that incorporates the transient behaviour of the system can be highly beneficial for the generation of reliable data. As shown by Tobias Heß et al. [69], the maximum power output and fuel conversion efficiency of an ICE do exhibit a transient behaviour, and when the engine is cold, a higher fuel power input is required to produce a given amount of power than when the engine warms up, but according to K. Voorspools et al. [39], this transient behaviour is small enough to be neglected in micro-CHP simulations.

On the other hand, as discussed in section 3.1.14, the engine transient thermal response is much slower and for this reason, it is often included in

engine models used in simulations of cogeneration systems with intermittent operation. N. J. Kelly [36] used a parametric engine model whose thermal behaviour was described by a lumped capacitance transient thermal model with one node representing the engine and the heat exchanger masses, and another node representing the water mass. In terms of the transient behaviours of the exhaust temperature and the HC emissions J. C. Zavala et al. [60], found in their experimental data that they can be adequately described by 1<sup>st</sup> order linear transfer functions, with AFR, spark timing and engine speed as their main model inputs. They also observed that the engine speed has a stronger influence than the air mass inlet rate on exhaust temperature and HC emissions.

The parametric engine model as found in Tobias Heß et al. [69], described the transient nature of ICE torque during warm up. Engine torque was calculated by subtracting the product of three main parametric loss components from a calculated internal torque proportional to fuel inlet rate. Each heat loss component was a function of one of three main model inputs: internal torque, engine speed, and engine block temperature. The parameters of the model were calibrated using actual engine data.

#### 3.4.2.5. Generator shaft dynamics

In cases where a variable speed system is to be simulated, the inclusion of the engine shaft dynamics component can be a useful addition in a model as it can realistically describe the load ramp limitations of a system. F. Caresana et al. [2] included rotating shaft dynamics in their model using the following torque balance equation for the model of their generator:

$$M_{t\_ICE} - M_{t\_gen} - M_{t\_Fr} - M_{t\_acc} = 0 \quad (3.8)$$

Where:

$M_{t\_ICE} = \frac{P_{mech}}{\omega}$  is the engine torque, with  $P_{mech}$  the mechanical power output of the engine and  $\omega$  the shaft angular velocity,

$M_{t\_gen} = \frac{P_{el}}{\eta_{gen}\omega}$  is the generator torque, winding resistance losses included, with  $P_{el}$  the electrical load placed on the generator, and  $\eta_{gen}$  the generator conversion efficiency,

$M_{t\_Fr} = (\alpha_1 + \alpha_2\omega_e + \alpha_3\omega_e^2)$  is the friction/aerodynamic loss torque with  $\alpha_1$ ,  $\alpha_2$ , and  $\alpha_3$  being fitted coefficients based on experimental data,

$M_{t\_acc} = J \frac{d\omega_e}{dt}$  is the torque due to rotational inertia with  $J$  being the total moment of inertia of the engine and the generator.

### 3.4.2.6. ICE Exhaust Temperature calculation

When modelling the CHP system using separate component models, exhaust temperature is one of the main ICE model outputs. The exhaust temperature of an internal combustion engine plays an important role in the sizing of the exhaust gas heat exchanger as well as the heat recovery efficiency of a CHP system at a given operating point. Experience has shown that the exhaust temperature may vary significantly throughout the operating range of an internal combustion engine. In the case of spark ignited (SI) engines, exhaust temperature for higher loads lies in the region of 600°C [70] and in some cases may even reach 900°C while exhaust temperatures at idle lie in the region of 300°C [50], [70]. For this reason, several micro-CHP models encountered in literature feature a means of calculating the exhaust temperature at a given operating point.

As discussed above, the engine model of F. Caresana et al. [2] includes a lookup table that returns the exhaust heat fraction  $X_{exh}(M_{t\_ICE}, \omega_e)$  and from this ratio their model calculated the rate of exhaust heat rejection from:

$$\dot{Q}_{exh}(M_{t\_ICE}, \omega_e) = \dot{Q}_{in}(M_{t\_ICE}, \omega_e)X_{exh}(M_{t\_ICE}, \omega_e) \quad (3.9)$$

And the exhaust temperature at the engine outlet  $T_{exh}$  was calculated by solving iteratively for  $T_{exh}$  the following equation:



$$T_{exh} = \frac{\dot{Q}_{exh} + \dot{m}_{air}c_{p,air}T_{amb} + \dot{m}_f c_{p,f}T_{amb}}{(\dot{m}_{air} + \dot{m}_f)c_{p,exh}} \quad (3.10)$$

Where the specific heat of the exhaust was calculated from:

$$c_{p,exh} = n_{N_2}c_{p,N_2} + n_{CO_2}c_{p,CO_2} + n_{H_2O}c_{p,H_2O} \quad (3.11)$$

They modelled natural gas after methane and the mass fractions for stoichiometric combustion of NG used in their simulation were:

$$n_{N_2} \cong 0.725, n_{CO_2} \cong 0.151, n_{H_2O} \cong 0.124$$

The rate of release of recoverable heat from the ICE engine at a given engine torque  $M_{t\_ICE}$  and angular speed  $\omega_e$  was then calculated from:

$$\dot{Q}_{rec\_CHP} = \dot{Q}_{in\_CHP} - X_{disp}\dot{Q}_{in\_CHP} - \omega_e M_{t\_ICE} \quad (3.12)$$

Where  $X_{disp}$  is the fraction of input power lost in the environment due to incomplete heat recovery of the total waste heat and was assumed to be constant at 0.05 throughout the system operating range.

On the other hand, K. Gluesenkamp et al [3] calculated the exhaust temperature from:

$$T_{exh} \cong T_{amb} \left( \frac{1}{1 + AFR} \right) (LHV)(X_{exh})(1 - \eta_{el}) \times \left( \frac{1}{c_{p,exh}} \right) \quad (3.13)$$

Where  $c_{p,exh}$  and  $X_{exh}$  were assumed constant with  $X_{exh} = 0.35$ .  $AFR$  is the air/fuel ratio of the mixture.

M. S. Rocha et al. [53] calculated  $T_{exh}$  using the specific heat of Nitrogen  $c_{p,N_2}$  to approximate the specific heat of the exhaust  $c_{p,exh}$ .

### 3.4.2.7. Waste heat in the engine coolant

Another important output that must be included in an ICE model built for the simulation of micro-CHP is the rate of waste heat released in the engine coolant. F. Caresana et al. [2] calculated the recoverable thermal power that ends up in the engine coolant from:

$$\dot{Q}_{coolant} = \dot{Q}_{rec\_CHP}(1 - X_{exh}(M_e, \omega_e)) \quad (3.14)$$

With a coolant temperature at the engine outlet:

$$T_{cool\_out} = \frac{\dot{m}_{cool}c_{p\_cool}T_{cool\_in} + \dot{Q}_{coolant}}{\dot{m}_{cool}c_{p\_cool}} \quad (3.15)$$

Where  $\dot{m}_{cool}$  the coolant mass flow rate,  $c_{p\_cool}$  the coolant specific heat (assumed constant), and  $T_{cool\_in}$  the coolant temperature at the engine inlet.

### 3.4.3. Heat exchanger modelling

Due to their inherent simplicity, constant coefficient HE models are not uncommon. One such case has been encountered in the article of Heejin Cho et al. [28] who used a constant heat exchanger efficiency value of 0.85 as found in ASHRAE HVAC handbook [71]. While being simple, this model type will not describe the heat exchanger behaviour accurately when variable output systems or transient operation are considered.

While a significant volume of existing studies that involves micro-CHP modelling was reviewed, the information on viable heat exchanger models that predict the component behaviour through a wide range of input values has been limited.

F. Caresana et al [2] who built a complete ICE based micro-CHP model in Matlab/Simulink using separate component models followed a hybrid modelling method which allowed the transient characteristics of the heat exchanger to be taken into account but with a main focus on the steady state

results. The Logarithmic Mean Temperature Difference (LMTD) was used to model the Heat Exchanger static performance, and a first order transfer function was used to describe the transient characteristics of the HE. The fluid specific time constant was calculated by dividing the fluid mass contained in the Heat Exchanger by its mass flow rate. In order to take the thermal contribution of the Heat Exchanger mass into account, a fluid mass thermally equivalent to the HE was added thus giving a better approximation of the transient thermal characteristics of the system. In order to use the LMTD method, a trial and error algorithm must be employed to calculate the HE outlet temperatures.

#### **3.4.4. Heat Storage Tank Models**

There are two main storage tank model categories: Stratified models capable of calculating the temperature distribution in one [72], [73] or two dimensions [74], and fully mixed models (or capacity models) in which the temperature is assumed to be constant throughout the complete water mass, and thus its behaviour approaches that of a continuously mixed tank [63], [75], [76], [77]. Stratified models are particularly useful when solar water heating systems are being modelled [63], [74] due to the sensitivity of the panel performance on inlet conditions. In the case of cogeneration though, the performance of the system is less sensitive to the temperature distribution in the tank and this, combined with the inherent simplicity of a zero dimensional model, makes it the most attractive option [63].

Weimin Wang et al. [63], built and validated a model of a gas fired thermal storage tank based on the fully mixed model configuration with cogeneration system simulation in mind and used three separate control volumes to describe the different heat capacitance elements within the system. The first node represented the water content and the casing. The second node represented the combustion chamber. The third node represented the flue gas where the enthalpy of the exhaust was calculated by taking into consideration the mass fraction of the flue gasses.

### 3.5. Load profiles

A number of researchers who developed their own models had to resort in finding or generating load profiles without the use of energy simulation software such as M. Bianchi et al. [45] who generated electricity demand profiles using data provided by the Odyssee project. B. Sicre et al. [5] obtained thermal loads for DHW by using statistical methods.

#### 3.5.1. Energy demand in single family dwellings

System loads are heavily dependent on the behavioural characteristics of a given household and the environment under which the household exists [67]. Electrical load profiles depend on social and economic factors as well as the habits of the dwellers. The seasonal variation of electrical load profiles is rather small [2] but it does depend on whether a weekday or a holiday is considered [20], [27], [42]. As can be seen from the averaged electrical load profiles of a detached dwelling of Figure 3.7 as generated by the 24 Hour profile chooser [49], the electrical demand on holidays tends to be higher than of workdays for most of the day.

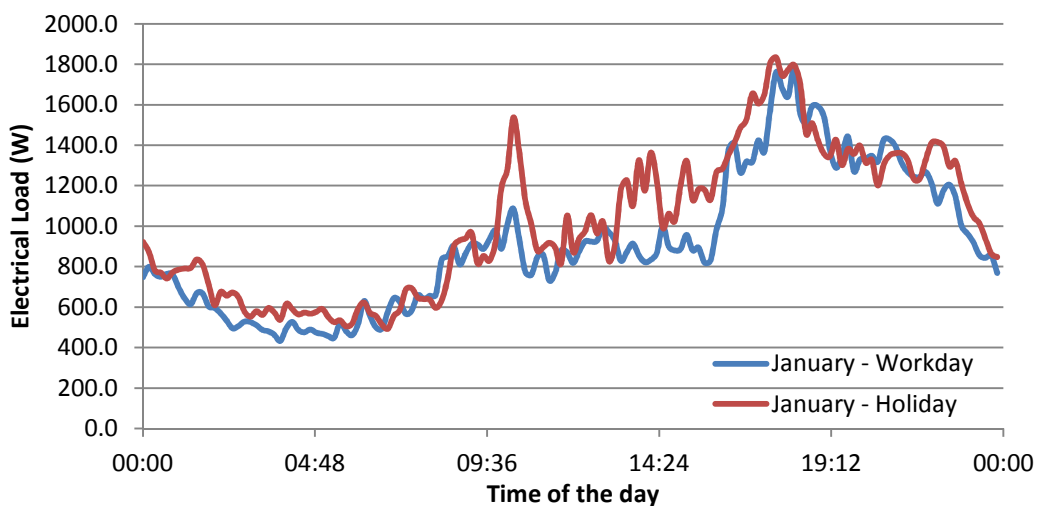


Figure 3.7 Electrical load profiles during a workday and a holiday

### 3.5.2. Representative electrical load profiles and their usage

There are two types of domestic usage profiles encountered in literature useful for the simulation of Distributed Energy Systems:

#### 3.5.2.1. Experimentally based aggregated profiles

Profiles of this type are based on data acquired by means of collecting multiple successive measurements of electricity consumption through the duration of a day. Depending on the level of detail, separate profiles for work days and weekends may be compiled. This process may be repeated for different months of the year and for different household sizes as encountered in the Household Electricity Survey [48].

The results of the Household Electricity Study were compiled into a Microsoft Excel file, forming an interactive electricity profile generator tool named “24-Hour Profile Chooser” by Cambridge Architectural Research Ltd and is being offered free of charge on the company website [49]. The profiles use 10 minute time increments through the duration of a day for workdays and holidays. As shown on the sample plot of Figure 3.8, the electrical load is composed of the various individual load components.

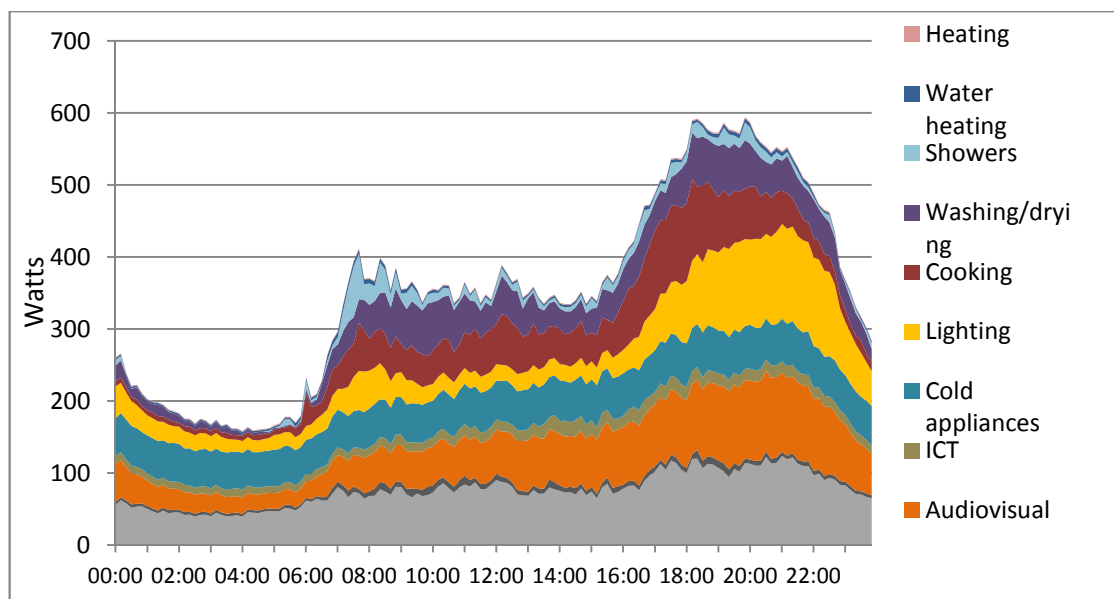


Figure 3.8 Averaged electricity profile of mid terraced dwellings

### 3.5.2.2. Synthetic Profiles

Currently, the most detailed synthetic electricity profile model available for the UK is the Domestic Electricity Demand Model with a resolution of 1 minute. It was built by I. Richardson et al. [78], and is based on occupancy survey data from TUS 2000 [79] and appliance usage data collected by the authors. An excel tool that generates electricity profiles based on this model is available [80]. The user can generate a profile as shown in Figure 3.9 by entering the number of active occupants, the month of the year, and the type of the day.

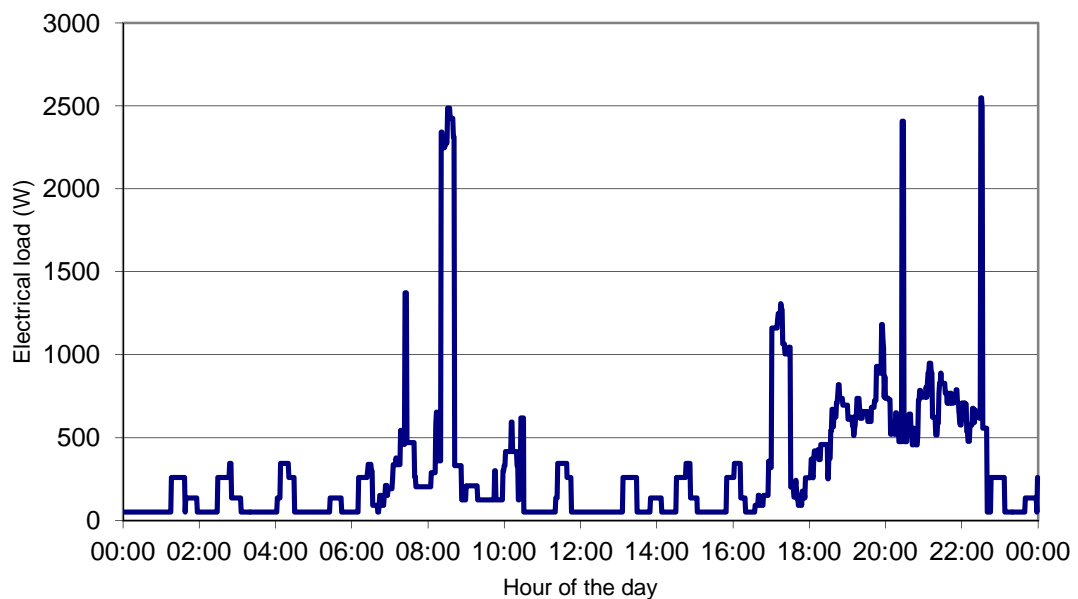


Figure 3.9 Electrical profile generated by the Domestic Electricity Demand Model [78]

A similar method was followed by Ruming Yao et al. [67] who constructed electrical load profiles based on appliance loads, statistical data on the appliance usage as well as associated occupancy patterns.

While the usage profiles encountered in the Household Electricity Survey [48] are averaged from a large number of dwellings and their contour

represents aggregated rather than individual energy consumption, the synthetic electricity profile model of I. Richardson et al. [78], gives usage profiles whose general form represent actual profiles encountered in single homes. Energy wise, the two profile types are not expected to be very different. There may be some cases though where the synthetic profile be superior such as when estimating electricity purchased from the grid. On the other hand, the fact that the model of the Household Electricity Survey [48] offers dwelling type specific profiles, and since the performance of micro-CHP systems in different dwelling types is to be investigated, it is considered to be a more suitable candidate for the current project.

### **3.5.3. IWECC weather data**

International Weather for Energy Calculations (IWECC) files are detailed hourly weather data files of numerous geographical locations compiled by ASHRAE. These include multiple UK locations. Each of the files represents a typical year at the given location and includes a large number of variables. IWECC data files are quite popular among researchers due to their good resolution and high volume of information and are used by well known building energy simulation software such as EnergyPlus. UK IWECC files for 10 different UK locations have been found on the website of the US Department of Energy [44].

### **3.5.4. Domestic Hot Water (DHW) Profiles**

According to Ruming Yao et al. [67], domestic hot water accounts for 20% of total residential energy production and on average, it is supplied at 40°C. In their article, they presented a method to generate synthetic DHW load profiles based on data on DHW usage.

The most detailed work on DHW profiles has been carried out as a part of subtask A of Annex 42 [81] of the International Energy Agency's Energy Conservation in Buildings and Community Systems (ECBCS) programme titled "The Simulation of Building-Integrated Fuel Cell and Other Cogeneration Systems (COGEN-SIM)" [82] is dedicated on the study of

domestic electrical and DHW profiles. At the time of this writing, the resulting profiles are available for free on ECBCS website [83].

### **3.5.5. Occupancy Pattern and heating period**

The occupancy pattern provides information on the time periods during which the occupants are in the dwelling and are not asleep (active occupants). Occupancy pattern drives the heat and electricity demand to a great extent, and for this reason, it is essential for domestic energy simulation software to include a basic form of occupancy pattern in its libraries.

J. Abedin et. al. [8] used a heating schedule that consisted of one morning heating period that lasted from 7am to 9am, and of one evening heating period that lasted from 4pm to 11pm.

O.A. Shaneb et al. [27] concluded that using one representative day per month may not be enough as it may not describe peak loads adequately, and suggested the use of a representative week.

A number of UK occupancy studies have emerged being either the product of detailed surveying or synthesized from survey data with the purpose of generating representative occupancy profiles. In the former group, one finds the Time Use Survey 2000 (TUS 2000) [79] which includes survey based 24 hour occupancy profiles with a 10 minute resolution. In the latter category, one finds the synthetic occupancy profiles as generated by I. Richardson et al. [84], who used stochastic methods and data from TUS 2000 survey to create representative active occupancy profiles for weekdays and weekends with a 10' resolution. Another piece of work involving the use of occupancy patterns in the UK may be found in Ruming Yao et al. [67] who provided six common occupancy patterns to be met in UK households. Out of the six profiles, two have been identified as most useful for use in the current project. A profile for a typical workday, for which it is considered that during a period from 9am to 6pm all occupants are away, and a weekend profile, for which the dwelling was assumed to be occupied during the whole length of the day.



### **3.6. Summary**

The current chapter reviewed existing literature most relevant to this thesis. Among the identified parameters that influence system performance, building type, geographical location, electrical efficiency, control strategy, system size, the system financial regime, storage tank size and operating temperatures have been found to be of most interest for the project, due to the fact that they are subject to a small or large extent to the decisions of the designer and the customer. Since currently the amount of existing studies and relevant results have been found to be too limited to be conclusive with regards to micro-CHP system design for sustainable operation, the effect of the above parameters on system performance will be thoroughly investigated. The most common methods to increase system electrical efficiency have been discussed and the high performing, high compression ratio engine has been found to be the most promising of the competing solutions. For this reason, it has been decided to focus on conventional ICE technology, and the effect of system electrical efficiency will be studied by constructing a low and a high compression ratio engine models. The main methods of managing heat and power surpluses and deficiencies have also been further discussed.

Certain characteristics of dedicated building simulation software constitute disadvantages when the main area of focus is the performance investigation of the DES, and for this reason, a DES oriented energy simulation tool will be developed in Chapter 4 to Chapter 7. In addition, most encountered quasi-stationary CHP models in literature were modelled as a single component and return the system electrical and thermal output without consisting of component sub-models. While this makes for a simple, easy to use model, such layout does not allow for the independent variation of component performance characteristics unless a complete unit with the desired characteristics is tested, thus being characterized by a lack of flexibility and a high development cost when many different systems are to be modelled. Another disadvantage of these models is the fact that they consider heat recovery efficiency to be only a function of the system operating point, while in reality, heat recovery efficiency also depends on the inlet conditions of the

secondary heat exchanger circuit. For these reasons, it has been decided to use a CHP model consisting of the main system sub-models. A micro-CHP model making use of separate heat exchanger and electric machine models has been encountered and discussed in section 3.4.3 but it is felt that a model more suitable for the current application can be developed. In the process of developing the tool, the shortcomings in encountered existing engine, heat exchanger, and dwelling models will be addressed, and contributions in these areas will be made.

## Chapter 4 Modelling the ICE based generator set

ICE models used in cogeneration applications, must have certain attributes which may not be of great importance in applications that do not involve heat recovery operations, but can be essential for the successful integration of the engine model to the main CHP model. Scalability that facilitates optimization processes, ease in connection to other sub models of the main CHP model, and the description of waste heat component behaviour in detail are all important characteristics in order to ensure realistic simulation results and versatility.

The majority of ICE related studies tend to focus on the mechanical aspect of ICE performance and for this reason, the availability of research work on the generated waste heat and especially on the behaviour of the exhaust temperature is limited. While some of the encountered engine modelling layouts being discussed in section 3.4.1 may give good results for the particular applications, a readily available scalable model layout, easy to calibrate and connect to other components that operate in different energy domains, and well suited to be used in tandem with waste heat recovery system models due to having the capability to predict the associated waste heat components in detail can be a useful addition to the virtual toolbox of a CHP modeller. A comparative schematic that describes the main differences between the inputs and outputs of engine models for non cogenerating applications and the model developed in the current chapter for use in CHP modelling can be seen in Figure 4.1.

The main aim of this chapter is the development of a quasi-stationary SI ICE based generator set model layout that incorporates the behaviour of all the necessary power components, temperatures and flow rates for use in CHP system simulation, being characterized by an increased scalability, simplicity and a low computational load. In order to achieve the above, the behaviour of all power components of spark ignited internal combustion engines, will be investigated.

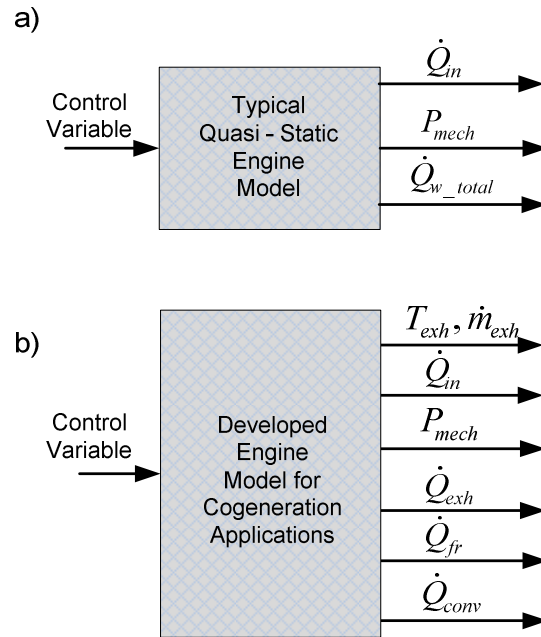


Figure 4.1 Comparison between the input and outputs of a) a typical engine model (for non cogenerating applications), and b) the developed engine model

The development of the model begins in section 4.1 where the quasi stationary energy based, waste heat driven model layout is presented, followed by the “Parameter Identification” of section 4.2 in which the experimental procedure for collecting engine performance data necessary for the generation of the lookup tables used in the model is described. The procedure of calculating the specific enthalpy of the stoichiometric combustion products of hydrocarbons is presented in section 4.3. Section 4.4 describes the modelling procedure of an energy based quasi-stationary electric machine model. The developed generator set model is then simulated and validated in section 4.5, and the results are discussed in section 4.6. In section 4.7 an equation that approximates the rate of waste heat that ends up in the engine coolant is presented. The implications of using natural gas as a fuel in SI engines, existing NG engine types and fuel specific performance curve adjustment are discussed in sections 4.8, 4.9, and 4.10, while in section 4.11 the performance curve scaling procedure that resulted in the two natural gas engine model variations to be used in the simulations is presented.

#### 4.1. System Model

Initially, the main components of power and mass flowing into and out of an internal combustion engine must be identified. As shown in Figure 4.2, when an I.C.E. operates, heat inlet from the fuel is released in the combustion chamber at a rate  $\dot{Q}_{in}$  and flows through three main different routes. Exhaust heat is carried by the high temperature exhaust gasses at a rate  $\dot{Q}_{Exh}$ . Convection heat flows at a rate  $\dot{Q}_{conv}$  from the hot combustion gasses in the combustion chamber into the cylinder walls and into the engine coolant and the engine surroundings in the form of convection and radiation heat. Heat generated by friction at a rate  $\dot{Q}_{fr}$  is the result of the relative motion of contacting surfaces, and is dissipated by the engine oil, the engine coolant or is added up to the total radiated heat from the engine surface to its surroundings [16], [17].

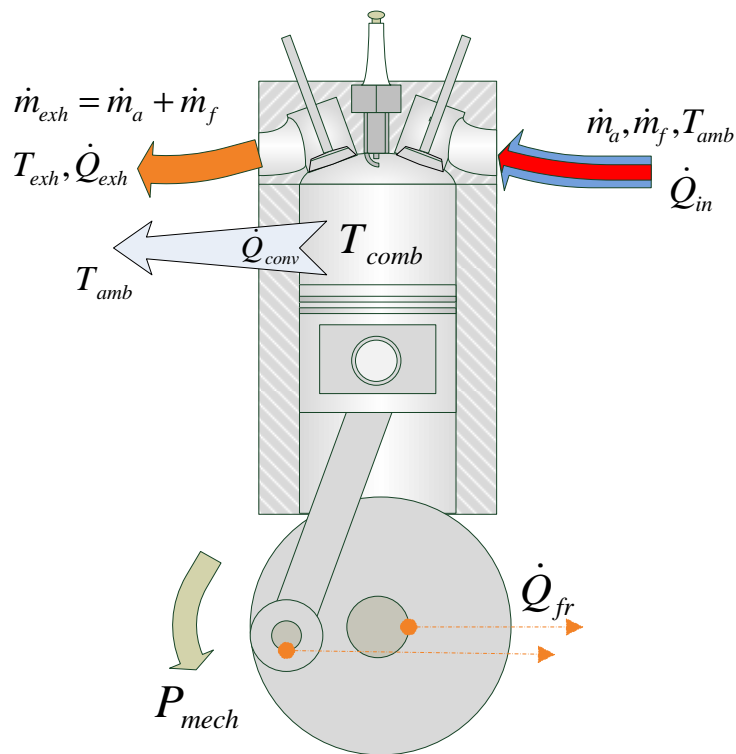


Figure 4.2 Diagram of the main routes of energy flow

Due to the fact that the operation of CHP systems involves multiple stages of energy transfer and conversion between different energy domains (as shown

in Figure 2.3), and since model simplicity and low associated development time and computational load are highly desired model characteristics, the development of a model layout that offers as much of universal component connectivity and versatility as possible will be pursued. This layout, rather than using the well established effort and flow configuration [85], [86], [87], it will be energy based as in such configuration; power can be used to easily connect individual subsystems and phenomena that handle energy on multiple domains.

In addition, contrary to most existing lookup table based engine models whose main maps include parameters directly linked to mechanical power and fuel consumption, the current model follows a reverse logic by means of which, specific sub-models and their respective lookup tables provide the generated waste heat generation rate components whose values are then subtracted from the energy input rate  $\dot{Q}_{in}$  to provide the mechanical power output  $P_{mech}$  - not unlike the general layout found in Tobias Heß et al. [69]. This configuration gives the modeller not only the ability to model the behaviour of all waste heat components, but also to calibrate an existing model by tuning the three different waste heat sub models to better approximate the performance characteristics of a given engine model. Furthermore, although being quasi-stationary in principle, the developed model if necessary, allows the incorporation of dynamic behaviour to some extent into the various power components by means of using transfer functions dedicated to a respective power component, with each transfer function having appropriately selected terms. In the current project, the model will incorporate the engine transient thermal characteristics by lumping the engine mass thermal capacitance with the thermal capacitance of the control volume of a pipe as described in Chapter 7.

A more detailed schematic of the developed model of Figure 4.1b analysing its layout and main constituent subsystems is shown in Figure 4.3.

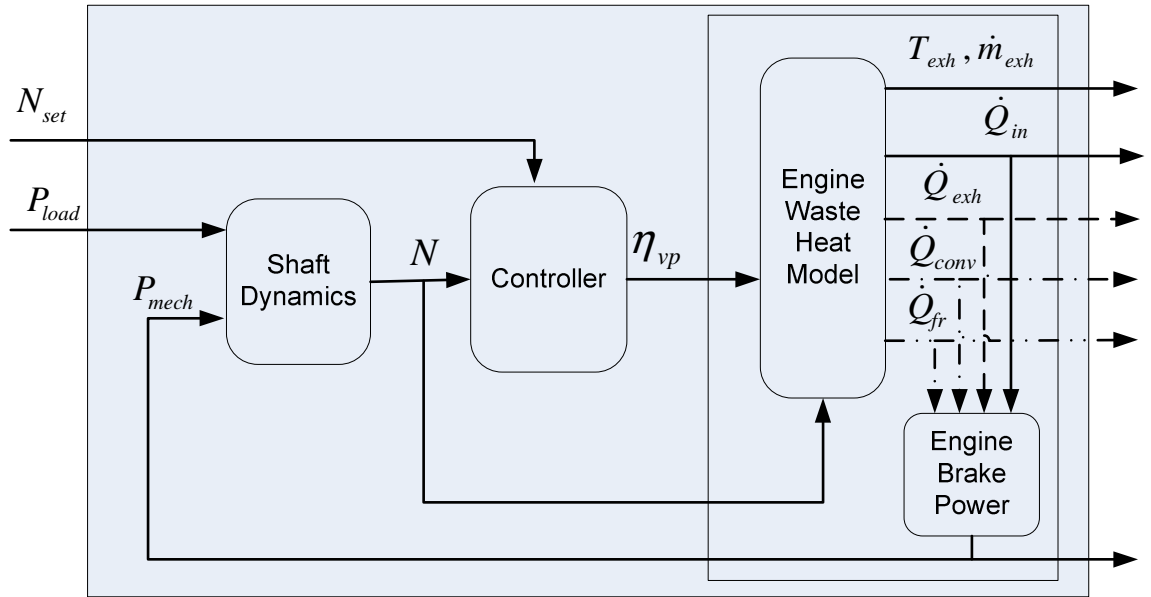


Figure 4.3 Block diagram of the proposed engine model

Engine breathing efficiency is the most important variable used to control the power output of SI engines, as power input is varied by varying the mixture inlet rate. The degree to which the full theoretical swept volume is utilized in the developed model will be represented by the engine volumetric efficiency  $\eta_{vp}$  at a given operating point. This representation of load ensures the scalability of the model as the maps are the same for any engine of the same type. A proportional controller uses the set speed value and the actual speed  $N$  to calculate and communicate the necessary value of  $\eta_{vp}$  to the power component sub-system contained in Figure 4.3. The physical operating limits of the system are defined by a saturation filter whose limits are set by two lookup tables that return the maximum and minimum feasible values of  $\eta_{vp}$  for a given engine speed  $N$ . The  $\eta_{vp}$  values that populate the upper and lower limit tables are obtained experimentally.

The following procedure is used for the calculation of the volumetric efficiency  $\eta_{vp}$  of an engine at any given test point. It must be followed for the generation of data points with the purpose of either populating the model lookup tables, or alternatively being used for the development of a surface fitted polynomial model.

In all calculations, fluid densities and specific volumes for atmospheric pressure  $P_{amb} = 1atm$  rather than for the manifold pressure are used due to the fact that the pressure characteristics of the manifold may vary significantly throughout the engine operating range and from one engine type to another, and in order for a universal, easy to calibrate engine model to be feasible, it must be delinked from these variables by using an independent pressure reference point.

If no values of fuel mass flow rate  $\dot{m}_f$  are available but fuel consumption is rather given in the form of break specific fuel consumption (*bsfc*) in  $g/kWh$ ,  $\dot{m}_f$  must first be calculated from:

$$\dot{m}_f = \frac{P_{mech}bsfc}{3.6 \times 10^6} \left( \frac{kg}{s} \right) \quad (4.1)$$

Once the measured or derived  $\dot{m}_f$  data are available, one may begin calculations with the mass flow rate of the induced air:

$$\dot{m}_a = \dot{m}_f AFR_{st} \left( \frac{kg}{s} \right) \quad (4.2)$$

In the case of petrol, the stoichiometric Air Fuel Ratio of petrol  $AFR_{st}$  is 14.7:1 [17].

The amount of fuel present in the charge is assumed to have completely evaporated before it enters the cylinder and under this assumption, the volumetric flow rate of vaporized fuel is calculated from:

$$\dot{V}_{f\_vap} = v_{f\_vap} \dot{m}_f \quad (4.3)$$

Where  $v_{f\_vap}$  the specific volume of the vaporized fuel in ambient conditions.

The specific volume of the vapour of any petrol type as a mixture of different hydrocarbon molecules has not been encountered in literature, and for this reason, and due to the prevalence of n-Octane as a representative of petrol



mixtures, it has been decided to use the specific volume of the gaseous phase of n-Octane under room conditions as found in [88] to be:

$$v_{f\_vap} = v_{ptr\_vap} = 0.213 \text{ m}^3/\text{kg}$$

The volumetric flow rate of intake air is

$$\dot{V}_a = v_a \dot{m}_a \quad (4.4)$$

Air specific volume at room conditions is sourced from [12]:

$$v_a = 0.831 \text{ m}^3/\text{kg}$$

In the case of port injected engines, part of the charge volume is comprised of fuel and must be taken into account in order to avoid overestimating the maximum air quantity and thus chemical power input for a given engine speed. Therefore, charge volumetric flow rate is the sum of the volumetric flows of the intake air and the evaporated fuel:

$$\dot{V}_{ch} = \dot{V}_{f\_vap} + \dot{V}_a \quad (4.5)$$

The theoretical swept volumetric rate is calculated from:

$$\dot{V}_{sw} = \frac{V_d N}{1.2 \times 10^8} \quad (4.6)$$

Where  $V_d$  the engine displacement in  $\text{cm}^3$ , and  $N$  the engine speed in  $\text{rpm}$ .

Then the volumetric efficiency is calculated from:

$$\eta_{vp} = \frac{\dot{V}_{ch}}{\dot{V}_{sw}} \quad (4.7)$$

The rate of exhaust heat rejection  $\dot{Q}_{exh}$  is a function of the exhaust temperature  $T_{exh}$  and the exhaust mass flow rate  $\dot{m}_{exh}$ , and thus the calculation of the exhaust mass flow rate is an important element of the

model operation. Since the model input is the volumetric efficiency  $\eta_{vp}$ , the model must be capable to translate this input into fuel and charge mass flow rates for a given engine speed and engine size. The following assumptions can be made in the model and these are generally true for commercially available, calibrated, healthy running SI engines:

- The charge air fuel ratio ( $AFR$ ) is assumed to always be stoichiometric.
- Spark timing is assumed to occur at maximum brake torque (MBT) for all operating points.

Under the above assumptions, the following steps result in a relationship for calculating the mass flow rate of an air-fuel mixture of a known ratio.

A given mass of charge of stoichiometric  $AFR_{st}$ , can be analysed as:

$$m_{ch} = m_f + m_a = m_f + AFR_{st}m_f \quad (4.8)$$

The volume of the above amount of charge is analysed as:

$$V_{ch} = V_f + V_a = m_f v_{f\_vap} + m_a v_a \quad (4.9)$$

Therefore the charge density is:

$$\rho_{ch\_atm} = \frac{m_{ch}}{V_{ch}} = \frac{m_f + AFR_{st}m_f}{m_f v_{f\_vap} + m_a v_a} = \frac{1 + AFR_{st}}{v_f + AFR_{st}v_a} \quad (4.10)$$

The charge mass flow rate which equals the exhaust mass flow rate is given by:

$$\begin{aligned} \dot{m}_{ch} = \dot{m}_{exh} &= \dot{V}_{sw} \eta_{vp} \rho_{ch\_atm} = \\ &= N \frac{V_d}{1.2 \times 10^8} \eta_{vp} \rho_{ch\_atm} \end{aligned} \quad (4.11)$$

Using the charge density of equation ( 4.10 ) on equation ( 4.11 ), the equation that will be used in the model to calculate the charge (and exhaust) mass flow rate for a given engine displacement  $V_d$ , engine speed  $N$ , and volumetric efficiency  $\eta_{vp}$  will be:

$$\dot{m}_{ch} = N \frac{V_d}{1.2 \times 10^8} \eta_{vp} \frac{1 + AFR_{st}}{v_f + AFR_{st} v_a} \quad (4.12)$$

For the calculation of  $\dot{m}_{ch}$ , the specific volumes of n-Octane in the case of petrol fuelled operation, and Methane in the case of natural gas fuelled operation at normal conditions as found in [88] and [89] respectively are used. Using equation ( 4.10 ), charge density for a stoichiometric petrol-air mixture is calculated to be  $\rho_{ch\_ptr} = 1.242 \text{ kg/m}^3$  while for a stoichiometric NG-air mixture,  $\rho_{ch\_NG} = 1.126 \text{ kg/m}^3$ .

The calculation of the charge (or exhaust) mass flow rate enables the calculation of the exhaust heat rejection rate  $\dot{Q}_{exh}$  which in turn is used to calculate the rate of heat convected through the cylinder walls  $\dot{Q}_{conv}$  both of which are the dominant modes of loss of work potential at high loads.

Exhaust heat is rejected at rate  $\dot{Q}_{exh}$  from the engine stored as enthalpy in the hot exhaust gas mass leaving the engine at a temperature  $T_{exh}$  (given by a lookup table) and a mass flow rate  $\dot{m}_{exh} = \dot{m}_{ch}$ , where  $\dot{m}_{ch}$  is the charge mass flow rate calculated using equation ( 4.12 ). At the time of this writing, the most relevant study on the behaviour of the exhaust temperature of SI engines has been found to have been conducted by Lars Erikson [90] who based on results from crank angle based combustion models assumed a linear dependence of the exhaust temperature on the exhaust mass flow rate. In this thesis, exhaust temperature will be modelled as a function of engine speed  $N$  and volumetric efficiency  $\eta_{vp}$  as experiments showed a dependence on both variables.

Using the method analysed in section 4.2, the specific enthalpy of the exhaust gas is calculated for the exhaust outlet temperature

$h_{exh}(T_{exh}(N, \eta_{vp}))$  and the ambient temperature  $h_{exh}(T_{amb})$ . For known  $h_{exh}(T_{exh}(N, \eta_{vp}))$ ,  $h_{exh}(T_{amb})$ , and  $\dot{m}_{ch}$ , the exhaust heat rejection rate  $\dot{Q}_{exh}$  can now be calculated in the model from:

$$\dot{Q}_{exh} = \left( h_{exh}(T_{exh}(N, \eta_{vp})) - h_{exh}(T_{amb}) \right) \dot{m}_{ch} \quad (4.13)$$

The second component of waste heat in internal combustion engines is the rate of convected heat  $\dot{Q}_{conv}(N, \eta_{vp})$ . This heat component flows through the cylinder walls to the engine block mass as a result of the temperature differential between the hot and turbulent combustion products present in the combustion chamber and the colder engine mass. As shown in the block diagram of Figure 4.4, in the developed model, convection heat is defined by the rate of exhaust heat rejection  $\dot{Q}_{exh}(N, \eta_{vp})$  and the heat ratio – a non engine size dependent representation of convection heat rejection rate – at a given operating point  $Q.R.$  In order to generate data to populate the  $Q.R.$  lookup table from experimental data, each element is calculated from:

$$Q.R.(N, \eta_{vp}) = \dot{Q}_{conv}(N, \eta_{vp}) / \dot{Q}_{Exh}(N, \eta_{vp}) \quad (4.14)$$

Once the  $Q.R.$  table is populated, model calculates the rate of heat loss through convection from:

$$\dot{Q}_{conv}(N, \eta_{vp}) = Q.R.(N, \eta_{vp}) \dot{Q}_{Exh}(N, \eta_{vp}) \quad (4.15)$$

$Q.R.$  links  $\dot{Q}_{conv}$  to  $\dot{Q}_{exh}$  and makes model scaling a simple task since engine displacement defines the rate of exhaust heat rejection  $\dot{Q}_{exh}$ , the heat inlet rate  $\dot{Q}_{in}$ , and the rate of heat generation by friction  $\dot{Q}_{fr}$  (discussed below). In turn,  $\dot{Q}_{exh}$  defines  $\dot{Q}_{conv}$  for a given operating point. In order to construct the  $Q.R.$  map, the availability of data on engine performance throughout the engine operating envelope will be necessary.

The third waste heat component encountered during engine operation is heat generated by friction. In ICEs, the totality of frictional forces and torques that act on its moving parts including hydraulic and aerodynamic components is summed up in the frictional mean effective pressure ( $f_{mep}$ ). Colin R. Ferguson et al [16], tested a large number of different S.I. Engines and created a representative mathematical model of  $f_{mep}$  as a quadratic function of engine speed  $N$ :

$$f_{mep}(N) = 94.8 + 2.3 \left( \frac{N}{1000} \right) + 4 \left( \frac{N}{1000} \right)^2 \quad (kpa) \quad (4.16)$$

The rate of heat generated from friction  $\dot{Q}_{fr}$  is then calculated from:

$$\dot{Q}_{fr}(N) = \frac{NV_d f_{mep}(N)}{1.2 \times 10^8} \quad (kW) \quad (4.17)$$

( $V_d$  in  $cm^3$ )

Equation ( 4.17 ) is used both in the model as well as the procedure for the population of the  $Q. R.$  map.

Heat inlet rate  $\dot{Q}_{in}$  is the rate at which energy enters the engine in the form of fuel chemical power

$$\dot{Q}_{in} = \dot{m}_f LHV_f \quad (4.18)$$

Where  $LHV_f$  is the lower heating value of the fuel in  $kJ/kg$ .

Once the main waste heat flow rate components and the respective heat inlet rate have been calculated by following the procedure presented above, the engine mechanical power output is calculated by the model from:

$$P_{mech}(N, \eta_{vp}) = \dot{Q}_{in}(N, \eta_{vp}) - \dot{Q}_{Exh}(N, \eta_{vp}) - \dot{Q}_{conv}(N, \eta_{vp}) - \dot{Q}_{fr}(N) \quad (4.19)$$

Following the analysis of the different power components, a block diagram illustrating the sequence of calculations that take place in the power component calculator subsystem can be seen in Figure 4.4.

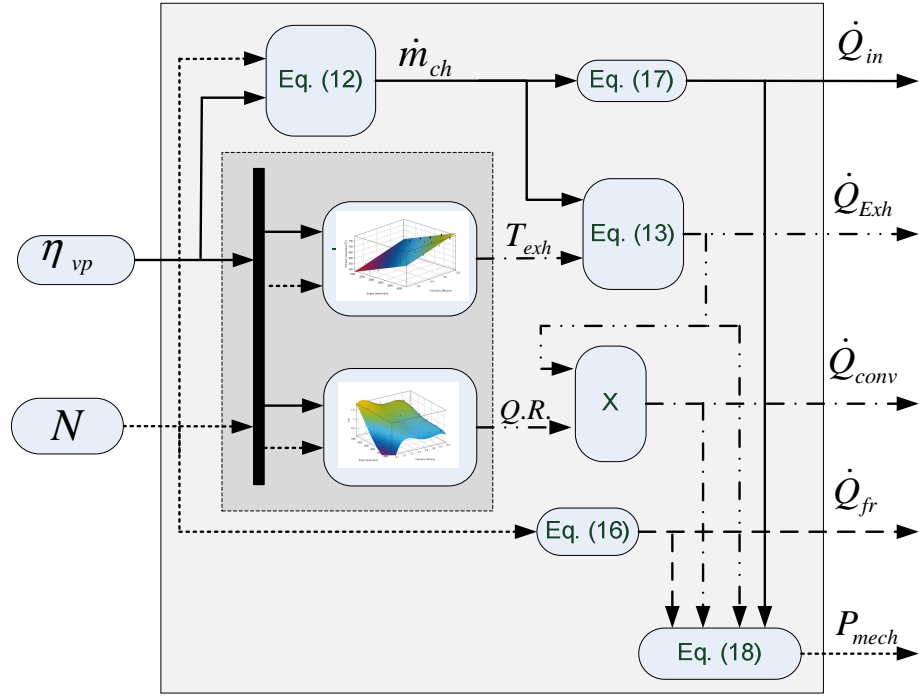


Figure 4.4 Block diagram of the power component calculator subsystem

The energy based approach discussed above, extends to the rotating parts as well. The net power  $P_{net}$  (kW) that enters or leaves the rotating parts of the engine is the difference between the mechanical power input from the engine  $P_{mech}$  (kW) to the rotating parts and the engine load  $P_{load}$  (kW) (electric machine):

$$P_{net} = P_{mech} - P_{load} \quad (4.20)$$

This net power is then integrated in order to calculate the stored rotational kinetic energy in the rotating parts  $E_{rot}$  (kJ) at time  $t$ :

$$E_{rot} = \int_0^t P_{net}(t) dt \quad (4.21)$$

Since the rotational kinetic energy in  $kJ$  is calculated from:

$$E_{rot} = \frac{J_{eq}(2\pi N/60)^2}{2000} \quad (4.22)$$

Where  $J_{eq}$  the equivalent moment of inertia of the engine and the electric machine rotating parts. Then the engine speed is calculated from:

$$N = \frac{60 \sqrt{\frac{2000 E_{rot}}{J_{eq}}}}{2\pi} \quad (4.23)$$

In the case of a generator set with a 1:1 transmission ratio, the equivalent moment of inertia is:

$$J_{eq} = J_{eng} + J_{EM} \quad (4.24)$$

Where  $J_{eng}$  and  $J_{EM}$  are the moment of inertia of the engine and the electric machine respectively, both in  $(kgm^2)$ .

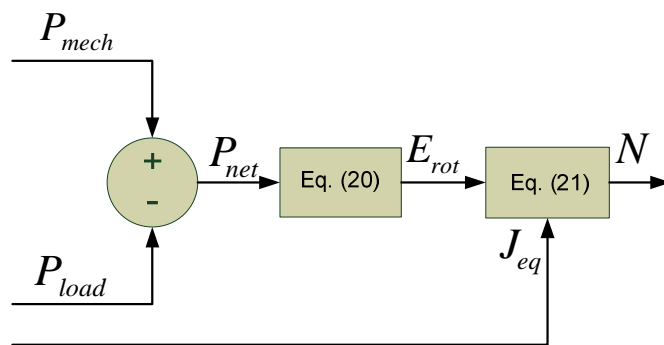


Figure 4.5 Layout of the shaft dynamics subsystem

## 4.2. The stoichiometric combustion of fuels

The fuel type and in particular the number of carbon atoms per fuel molecule play a decisive role in the environmental performance of a thermal engine [12] and for this reason the, composition of the combustion products of a given fuel must be taken into consideration for the environmental evaluation of the system to be relevant [34].

When a stoichiometric fuel/air charge burns, complete oxidization takes place and the products of this reaction include CO<sub>2</sub> (when the fuel contains carbon), H<sub>2</sub>O (in the case of hydrocarbons) and N<sub>2</sub> which ideally does not react with oxygen but it is contained in the atmospheric air, and as a result it is part of the charge.

The exhaust gas enthalpy can be calculated with the application of the first thermodynamic law for a Control Volume system as found in Yunus A. Cengel et al. [12]:

$$\begin{aligned} q - W - \bar{h}_c^o + \sum n_r (\bar{h} - \bar{h}^o)_r &= \\ &= \sum n_p (\bar{h} - \bar{h}^o)_p = q_{exh} \end{aligned} \quad (4.25)$$

$$\bar{h}^o = h(298^{\circ}K) = 0$$

Reactants enter the engine at 298°K. Thus:

$$\sum n_r (\bar{h} - \bar{h}^o)_r = 0 \quad (4.26)$$

$$q_{exh} = \sum n_{p,i} (\bar{h}(T))_{p,i} \quad (4.27)$$

Where  $n_{p,i}$  is the number of moles of each product per mole of burned fuel, and  $(\bar{h})_{p,i}$  is the specific molar enthalpy of each product.



The specific molar enthalpy of the exhaust gas mixture in  $kJ/Kmol\ fuel$  is then calculated from:

$$q_{exh} = n_{CO_2} \bar{h}_{CO_2}(T) + n_{H_2O} \bar{h}_{H_2O}(T) + n_{N_2} \bar{h}_{N_2}(T) \quad (4.28)$$

The graphs of Figure A.3.1, Figure A.3.2, and Figure A.3.3 in Appendix 3, show  $\bar{h}$  plotted against temperature for each product, based on data found in Yunus A. Cengel et al. [12].

The fitted 4<sup>th</sup> order polynomials as functions of temperature for each product are:

$$\bar{h}_{CO_2}(T) = 7 \times 10^{-10}T^4 - 6 \times 10^{-6}T^3 + 0.021T^2 + 28.027T - 10189 \quad (4.29)$$

$$\bar{h}_{H_2O}(T) = -10^{-10}T^4 + 7 \times 10^{-8}T^3 + 0.0066T^2 + 28.489T - 9002.7 \quad (4.30)$$

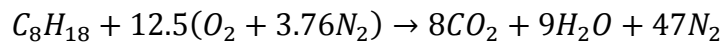
$$\bar{h}_{N_2}(T) = 6 \times 10^{-11}T^4 - 10^{-6}T^3 + 0.0051T^2 + 25.159T - 7854.9 \quad (4.31)$$

By substituting equations ( 4.29 ), ( 4.30 ), and ( 4.31 ) to equation ( 4.28 ) we have:

$$\begin{aligned} & [n_{CO_2}(7 \times 10^{-10}) + n_{H_2O}(-10^{-10}) + n_{N_2}(6 \times 10^{-11})]T^4 + \\ & [n_{CO_2}(-6 \times 10^{-6}) + n_{H_2O}(7 \times 10^{-8}) + n_{N_2}(-10^{-6})]T^3 + \\ & [n_{CO_2}(0.021) + n_{H_2O}(0.0066) + n_{N_2}(0.0051)]T^2 + \\ & [n_{CO_2}(28.027) + n_{H_2O}(28.489) + n_{N_2}(25.159)]T + \\ & (n_{CO_2}(-10189)) + (n_{H_2O}(-9002.7)) + (n_{N_2}(-7854.9)) = \\ & = q_{exh} \left( \frac{kJ}{kmol\ fuel} \right) \end{aligned} \quad (4.32)$$

#### 4.2.1. Stoichiometric Combustion of n-Octane

Petrol composition may vary significantly between samples produced by different companies, and a theoretical equivalent molecule like in the case of natural gas has not been found in literature. In addition, since petrol is mostly octane with the addition of a small percentage of other hydrocarbons, octane is most commonly used in combustion calculations. The combustion reaction of octane is readily found in Y. A. Cengel et al [12]:



This means that for 1 *kmol* of stoichiometrically burned octane, the following are produced:

$$n_{CO_2} = 8 \text{ kmol}, \quad n_{H_2O} = 9 \text{ kmol}, \quad n_{N_2} = 47 \text{ kmol}$$

#### 4.2.2. Stoichiometric Combustion of Natural Gas

Natural gas is a fossil fuel comprised mainly of methane. Other components often found in natural gas are Ethane, Nitrogen and CO<sub>2</sub>. Y. A. Cengel et al [12] listed the typical chemical proportions of natural gas:



The chemical type ( 4.33 ) is not an actual chemical formation since it represents a mixture of different molecules, and fractions of atoms do not exist, but is rather an indicator of the proportionality of atoms per atoms of carbon in the mixture.

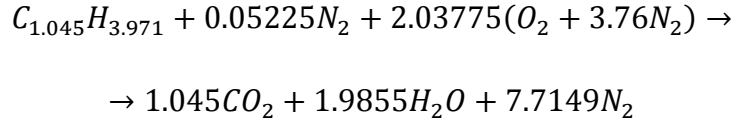
The average molecular weight of natural gas is 18. In order to find *n*, we solve the following equation:

$$12.011n + 3.8 \times 1.00794n + 0.1 \times 14.0067n = 18 \leftrightarrow$$

$$\leftrightarrow 17.2319n = 18 \leftrightarrow n = 1.045$$

$C_{1.045}H_{3.971}$  is still not an actual chemical formation but a hypothetical average composition of hydrocarbons contained in the typical Natural Gas specimen that will serve as an basis for the combustion equation.

Thus, the reaction of stoichiometric combustion (air assumed to be dry in the calculations) becomes:



This means that for 1 *kmol* of stoichiometrically combusted natural gas, 1.045 *kmol* of CO<sub>2</sub>, 1.9855 *kmol* of H<sub>2</sub>O and 7.7149 *kmol* of N<sub>2</sub> are produced, and we have:

$$n_{CO_2} = 1.045 \text{ kmol}, \quad n_{H_2O} = 1.9855 \text{ kmol}, \quad n_{N_2} = 7.7149 \text{ kmol}$$

### 4.3. Parameter Identification

In the current section, the two main maps of the model, one that calculates the exhaust temperature  $T_{exh}$ , and one that calculates the heat ratio  $Q.R.$ , both as functions of the engine speed  $N$  and the engine load (represented in the model by  $\eta_{vp}$ ) will be constructed. In order to obtain the necessary information on how the distribution of the different power components varies throughout the operating envelope of spark ignited internal combustion engines, a series of tests have been conducted on a transient engine test cell. The engine characteristics, as well as the settings used for the collection of data, are presented in Table 4.1.

Heat inlet rate to the tested engine is controlled by varying  $\alpha$  which is the percentage of maximum throttle angle. The rate of air and fuel (charge) that enters the combustion chamber corresponds to the value of  $\alpha$ . The desired engine speed is set and communicated to the controller of the dynamometer. Speed measurements are used as feedback to the controller which adjusts the electric current flowing through the dynamometer windings to control the

load placed on the engine shaft and maintain the engine speed as close and about the set speed value as possible.

Table 4.1 Characteristics and settings of the tested engine

<b>Engine type</b>	SI, Naturally Aspirated, direct injection
<b>Displacement</b>	1.6L
<b>ECU settings</b>	Constant stoichiometric AFR Spark timing at maximum break torque (MBT)

The tests were conducted for a range of engine speeds and values of  $\alpha$ . Set speed was varied from 1500 rpm to 4000 rpm in 500 rpm increments. For each set speed value,  $\alpha$  was varied from 20% to 100% of maximum throttle angle in increments of 10%. The exhaust temperature, the fuel mass flow rate, and the engine torque were directly measured. The dynamometer controller was programmed to use the above three variables in conjunction with Equations ( 4.2 ) to ( 4.19 ) to obtain the maps of Figure 4.6 and Figure 4.7 that are necessary for the model to operate. All tests were carried out on the same day to ensure as much of relevance in results as possible.

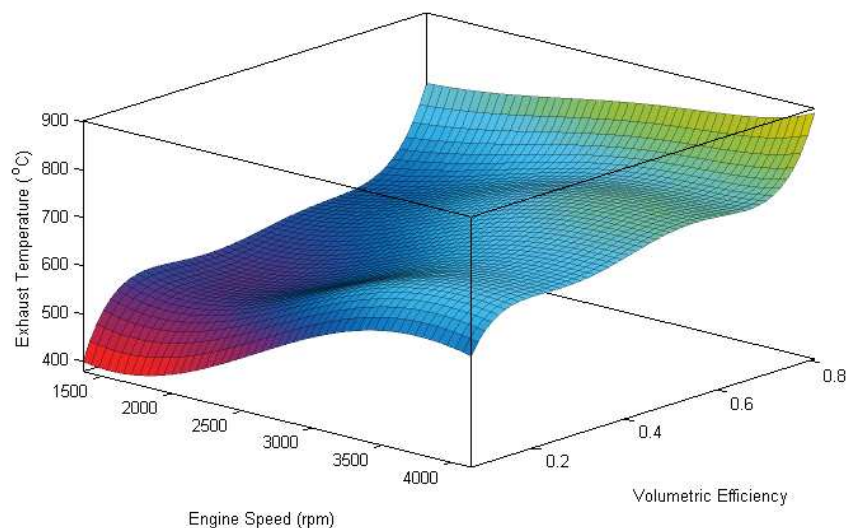


Figure 4.6 Exhaust temperature vs. engine speed and volumetric efficiency

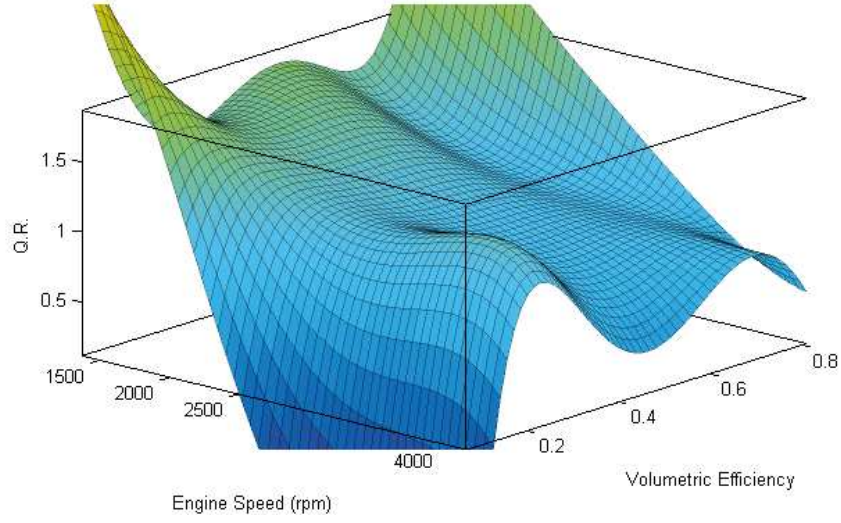


Figure 4.7 Q.R. vs. engine speed and volumetric efficiency

Since ready to use equations of the two main model maps may be desirable by the reader, the coefficients of 5<sup>th</sup> order polynomial fits performed on the acquired datasets of  $T_{exh}(N, \eta_{vp})$  and  $Q.R.(N, \eta_{vp})$  are provided in Table 4.2 to be used in a polynomial of the general form shown in equation ( 4.34 )

$$\begin{aligned}
 f(N, \eta_{vp}) = & p_{00} + p_{10}N + p_{01}\eta_{vp} + p_{20}N^2 + p_{11}N\eta_{vp} + \\
 & + p_{02}\eta_{vp}^2 + p_{30}N^3 + p_{21}N^2\eta_{vp} + p_{12}N\eta_{vp}^2 + \\
 & + p_{03}\eta_{vp}^3 + p_{40}N^4 + p_{31}N^3\eta_{vp} + p_{22}N^2\eta_{vp}^2 + \\
 & + p_{13}N\eta_{vp}^3 + p_{04}\eta_{vp}^4 + p_{50}N^5 + p_{41}N^4\eta_{vp} + \\
 & + p_{32}N^3\eta_{vp}^2 + p_{23}N^2\eta_{vp}^3 + p_{14}N\eta_{vp}^4 + p_{05}\eta_{vp}^5
 \end{aligned} \tag{ 4.34 }$$

Table 4.2 Coefficients of the 5th order polynomial surface fits on  $T_{exh}$ , and  $Q.R.$

	$T_{exh}$	$Q.R.$
$p_{00}$	181	-15.26
$p_{10}$	-0.01864	0.03765
$p_{01}$	9717	-62.01
$p_{20}$	-0.0002382	-2.308e-05
$p_{11}$	-2.664	-0.01654
$p_{02}$	-4.732e+04	359.6
$p_{30}$	2.091e-07	4.749e-09
$p_{21}$	0.0004299	4.275e-05
$p_{12}$	9.603	-0.2169
$p_{03}$	1.034e+05	-396.1
$p_{40}$	-5.329e-11	-1.954e-13
$p_{31}$	-4.319e-08	-1.029e-08
$p_{22}$	-0.001427	1.043e-06
$p_{13}$	-8.814	0.3173
$p_{04}$	-1.131e+05	-19.82
$p_{50}$	4.266e-15	-2.644e-17
$p_{41}$	6.416e-12	7.893e-13
$p_{32}$	3.797e-08	1.077e-09
$p_{23}$	0.0008733	-5.83e-06
$p_{14}$	2.013	-0.1529
$p_{05}$	4.992e+04	176
$R^2$	0.9959	0.9881

#### 4.4. Energy based model of the electric generator

The conversion efficiency of an electric machine is not constant but rather varies throughout its operating range with low conversion efficiency levels for low loads and peak efficiency when operated close to the maximum load. The reason for such variation in conversion efficiency being the fact that for a given voltage, resistive losses are proportional to the electric current

squared. For this reason, the inclusion of the variation of conversion efficiency with a varying electrical load can be an important factor in the accurate simulation of variable output cogeneration systems. Rather than using a constant coefficient model, it is decided to build a variable output alternator model based on relevant circuit analyses encountered in [46] that includes the resistive, as well as windage and bearing friction loss components present during the electric machine operation.

As shown in Figure 4.8, a typical synchronous machine consists of two separate windings. The armature winding on which  $EMF$  is generated, resulting in the flow of AC current to the end user, and the field winding which serves as a means to generate the necessary magnetic field flux  $\Phi_p$  ( $Wb$ ) to excite the armature and regulate the output voltage to the desired level ( $230V$ ).

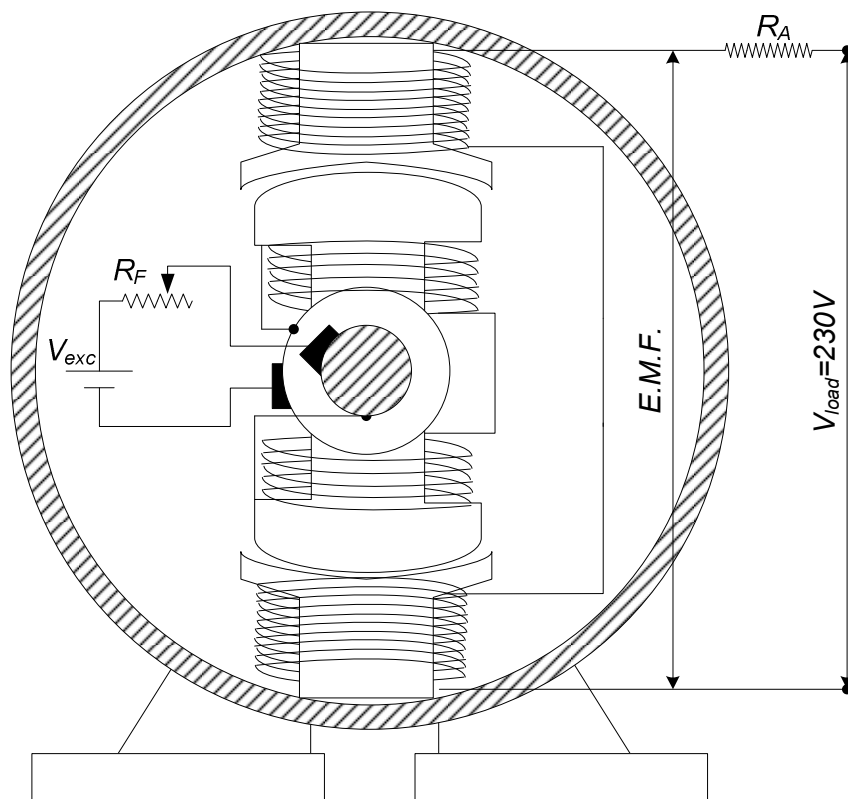


Figure 4.8 Schematic of a voltage regulated synchronous electric machine

As seen in [91], the electromotive force developed between the poles of the alternator is a function of the engine speed  $f_{me}$  in  $Hz$  (rotational frequency), the field winding factor  $K_w$  which in the current study will be considered to equal 1, the number of pole pairs  $N_{pp}$  (or number of phases  $N_{ph}$  when AC generators are considered) and the net air magnetic flux  $\Phi_p$ . The rms electromotive force is given from:

$$E.M.F. = \sqrt{2}\pi f_{me} K_w N_{pp} \Phi_p \quad (4.35)$$

When a synchronous generator is considered, it is rather important for the output voltage to remain at a constant specified value. In UK, and most EU countries the standard is 220-230V.

In order to adjust the generated  $EMF$  to account for a drop in voltage caused by the armature resistance  $R_A$ , field current is varied with load to control the magnetic field flux  $\Phi_p$ . The resulting regulated voltage of 230V at the poles of the electric machine is the value of the  $EMF$  minus the voltage drop.

In a constant voltage supply electrical system, power is varied by varying the supplied electrical current. The generator load may be represented by a variable resistor connected in parallel to the generator. As the resistance of the load decreases, load increases and vice versa.

Since both armature and field windings are characterized by their respective internal resistance values, it is expected that as current flows through them, a drop in voltage takes place and part of the generated electricity is converted into heat inside the machine, thus reducing the system conversion efficiency.

Due to the fact that the excitation field losses are relatively small compared to the armature losses, and since field current increases with the increase in armature current (in addition, the power factor curve tends to follow the conversion efficiency curve), for the sake of simplicity field excitation losses in this model will be lumped with armature losses. Using the armature current (load), and the sum of the resistive losses, an equivalent armature resistance



is calculated in order to approximate the system using a simplified equivalent circuit similar to that of a permanent magnet machine as shown in Figure 4.9.

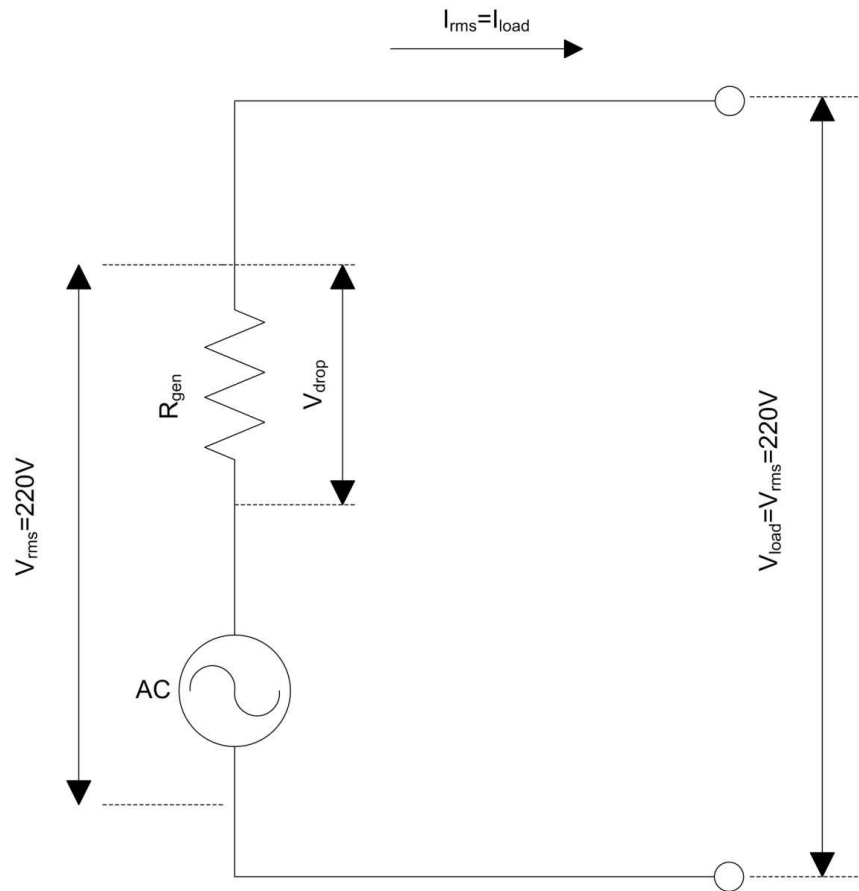


Figure 4.9 The simplified diagram of the generator/load circuit

For the creation of the alternator performance curve, the equivalent internal resistance  $R_i$  and the windage and friction loss rate  $\dot{Q}_{gen\_fr\_d}$  at a known design operating point must be obtained. Thus, the knowledge of the main operating generator parameters at a given design point of operation is necessary. In most cases, the manufacturer provides the value of the alternator conversion efficiency  $\eta_{gen\_d}$  at the maximum power output (electrical load)  $P_{L\_d}$ . Knowing that:

$$\eta_{gen\_d} = \frac{P_{L\_d}}{P_{mech\_d}} \quad (4.36)$$

The design mechanical power input  $P_{mech\_d}$  is obtained from:

$$P_{mech\_d} = \frac{P_{L\_d}}{\eta_{gen\_d}} \quad (4.37)$$

And the rate of total design power losses  $\dot{Q}_{Loss\_gen\_t\_d}$  can be calculated from:

$$\begin{aligned} \dot{Q}_{Loss\_gen\_t\_d} &= P_{mech\_d} - P_{L\_d} = \frac{P_{L\_d}}{\eta_{gen\_d}} - P_{L\_d} = \\ &= \frac{P_{L\_d}(1 - \eta_{gen\_d})}{\eta_{gen\_d}} \end{aligned} \quad (4.38)$$

Assuming that the ratio of the design windage and friction power losses over the total design power losses is:

$$r_{fr\_d} = \frac{\dot{Q}_{gen\_fr\_d}}{\dot{Q}_{Loss\_gen\_t\_d}} \quad (4.39)$$

and is known to be approximately 5-15%,  $\dot{Q}_{gen\_fr\_d}$  can be calculated from:

$$\dot{Q}_{gen\_fr\_d} = r_{fr\_d} \dot{Q}_{Loss\_gen\_t\_d} = r_{fr\_d} \frac{P_{L\_d}(1 - \eta_{gen\_d})}{\eta_{gen\_d}} \quad (4.40)$$

With  $\dot{Q}_{gen\_fr\_d}$  known, one can now calculate the design power loss across the equivalent resistance:

$$\begin{aligned} \dot{Q}_{Ri\_d} &= \dot{Q}_{Loss\_gen\_t\_d} - \dot{Q}_{gen\_fr\_d} = \\ &= (1 - r_{fr\_d}) \frac{P_{L\_d}(1 - \eta_{gen\_d})}{\eta_{gen\_d}} \end{aligned} \quad (4.41)$$

Since the load voltage  $V_{Load}$  is specified and constant (at 230V for UK), the design current  $I_{L\_d}$  can now be calculated from:

$$I_{L_d} = \frac{10^3 P_{L_d}}{V_{Load}} \quad (4.42)$$

Given that  $I_{L_d}$  passes through the internal resistance  $R_i$ , the internal resistance can be calculated from:

$$\begin{aligned} R_i &= \frac{10^3 Q_{Ri_d}}{I_{L_d}^2} = \frac{10^3 \dot{Q}_{Ri_d}}{\left(\frac{10^3 P_{L_d}}{V_{Load}}\right)^2} = \frac{\dot{Q}_{Ri_d} V_{Load}^2}{10^3 P_{L_d}^2} = \\ &= (1 - r_{fr_d}) P_{L_d} \frac{1 - \eta_{gen_d}}{\eta_{gen_d}} \frac{V_{Load}^2}{10^3 P_{L_d}^2} = \\ &= \frac{(1 - r_{fr_d})(1 - \eta_{gen_d}) V_{Load}^2}{10^3 \eta_{gen_d} P_{L_d}} \end{aligned} \quad (4.43)$$

Having calculated the main model parameters  $R_i$  and  $\dot{Q}_{gen\_fr\_d}$  which are assumed to remain constant throughout the complete machine operating range, a complete performance map can now be generated.

For a given generator load  $P_L$ , the voltage drop across the internal resistance  $R_i$  can be calculated from:

$$V_{Ri} = I_L R_i = \frac{P_L (1 - r_{fr_d})(1 - \eta_{gen_d}) V_{Load}}{\eta_{gen_d} P_{L_d}} \quad (4.44)$$

With the knowledge of the voltage drop  $V_{Ri}$  and the standard load voltage, the necessary electromotive force  $EMF$  for a given operating point is calculated from:

$$\begin{aligned} EMF &= V_{Load} + V_{Ri} = V_{Load} + I_{L_d} R_i = \\ &= V_{Load} + \frac{P_L (1 - r_{fr_d})(1 - \eta_{gen_d}) V_{Load}}{\eta_{gen_d} P_{L_d}} \end{aligned} \quad (4.45)$$

The mechanical power input for any operating point may now be found from:

$$\begin{aligned}
 P_{mech} &= 10^{-3} I_L EMF + \dot{Q}_{gen\_fr\_d} = \\
 &= \frac{P_L}{V_{Load}} \left( V_{Load} + \frac{P_L(1 - r_{fr\_d})(1 - \eta_{gen\_d})V_{Load}}{\eta_{gen\_d}P_{L\_d}} \right) + \\
 &\quad + r_{fr\_d} \frac{P_{L\_d}(1 - \eta_{gen\_d})}{\eta_{gen\_d}} = \\
 &= P_L + \frac{P_L^2(1 - r_{fr\_d})(1 - \eta_{gen\_d})}{\eta_{gen\_d}P_{L\_d}} + \\
 &\quad + r_{fr\_d} \frac{P_{L\_d}(1 - \eta_{gen\_d})}{\eta_{gen\_d}}
 \end{aligned} \tag{4.46}$$

The plot of Figure 4.10 illustrates the power output  $P_L$  as a function of the mechanical power input  $P_{mech}$  for a maximum (design) power output of  $P_{L\_d} = 2.8kW$  and a design conversion efficiency  $\eta_{gen\_d} = 0.85$ .

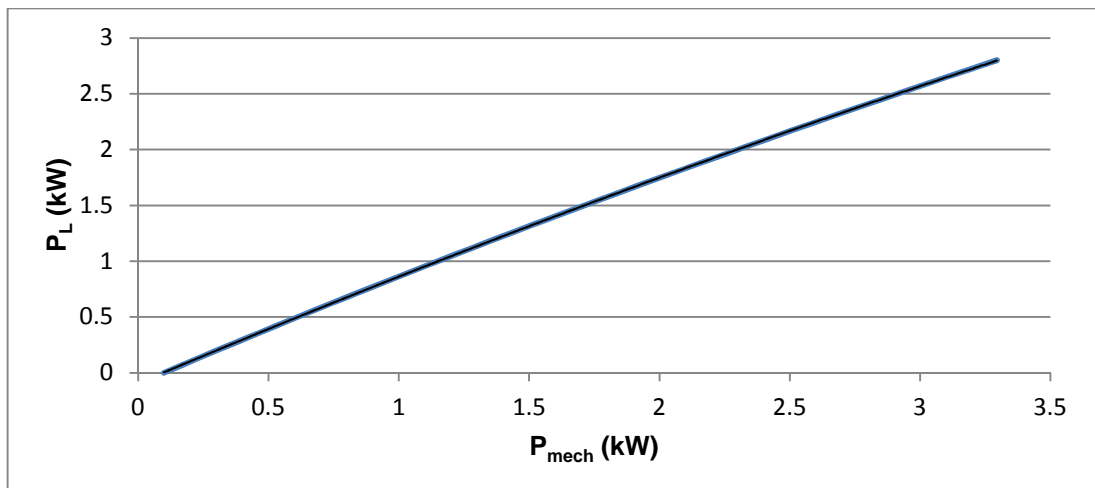


Figure 4.10 The electrical load placed on a 2.8kW alternator vs. the required mechanical power input

Figure 4.11 contains the plot of the alternator conversion efficiency  $\eta_{gen}$  against percentage of maximum power output  $P_{out}$ .

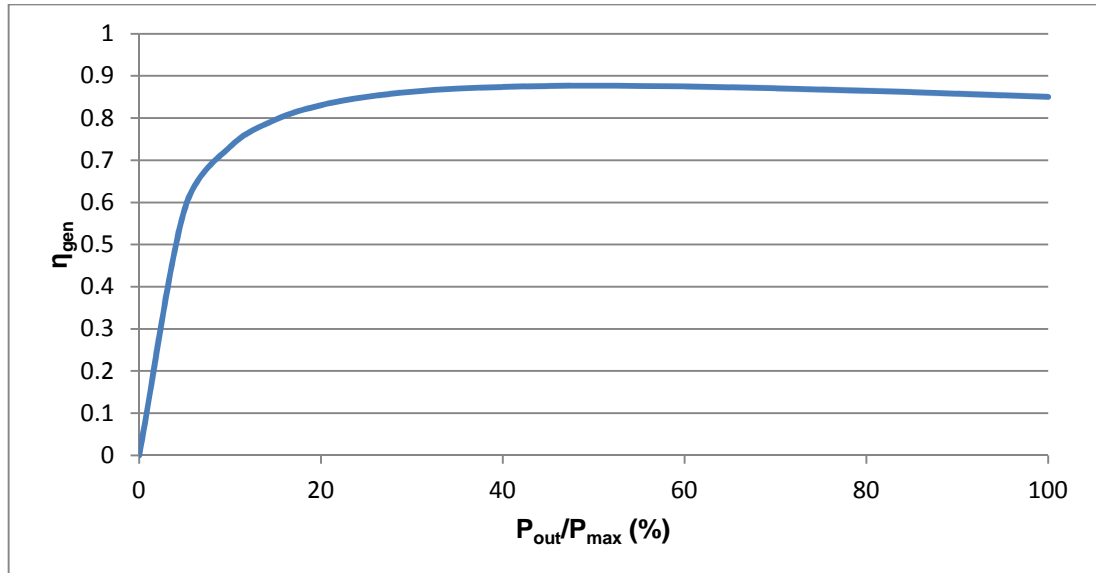


Figure 4.11 Alternator conversion efficiency vs. the percentage of maximum power output

#### 4.5. Simulation and Validation

In order to verify the developed engine model and prove the concept functionality, Matlab/Simulink environment was used to construct and simulate the engine model in the role of a component of a higher level micro-generation model. A constant speed, electricity priority control strategy was followed, and the duration of the simulation was 1 day in 1 second increments. For the current procedure, the engine model has been scaled to a displacement of  $80cm^3$  (micro-CHP category) and the electrical load profile of a mid-terraced house during a January work day as found in [49] is used as the system electrical load.

Following the simulation, the plots of the different estimated power components flowing through the engine model and the system electrical load profile can be seen in Figure 4.12. The time intervals during which all

components are equal to 0, are when the system is switched off due to load being too low for a profitable operation. The power distribution between the modelled energy components can be observed to vary with load as the distance between each curve is not proportional to the magnitude of the heat input rate curve. This behaviour is particularly observable when the mechanical power and the exhaust heat rate plots are compared. While the rate of exhaust heat rejection for low loads has a noticeably higher magnitude than the produced mechanical power, for higher loads, the rate of rejected exhaust heat and power output magnitudes are similar in value. This behaviour is expected as it reflects the higher engine conversion efficiency usually observed at higher engine loads. Due to a constant speed operation, the rate of heat generated from friction remains nearly constant.

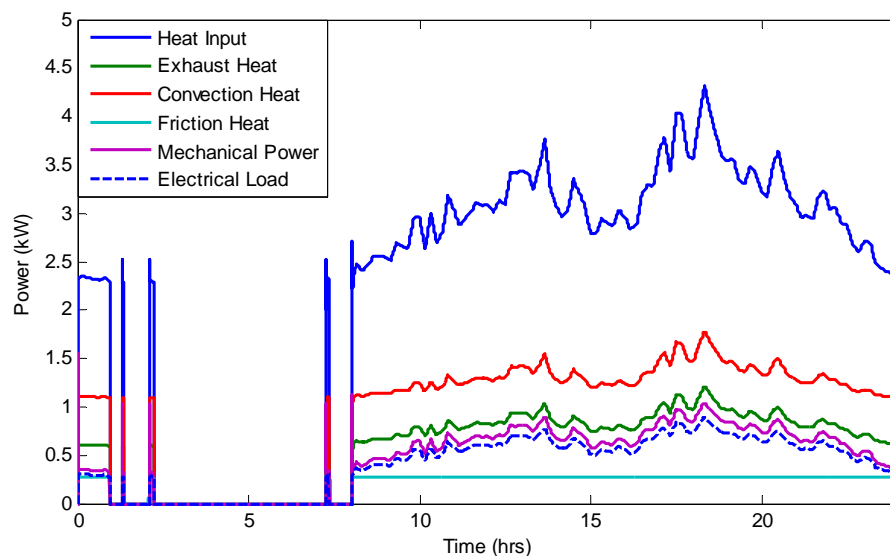


Figure 4.12 Power component distribution vs. time

Similarly, the effects of load fluctuation on the predicted exhaust temperature can be observed on the plot of Figure 4.13 where the simulated exhaust temperature is plotted against time with the electrical load on the same graph scaled by the right y-axis. Again, the model is found to calculate exhaust temperature values that come to a general agreement with the measured values and whose behaviour follows the observations made on the

experimental data where higher loads lead to higher predicted temperatures and vice versa.

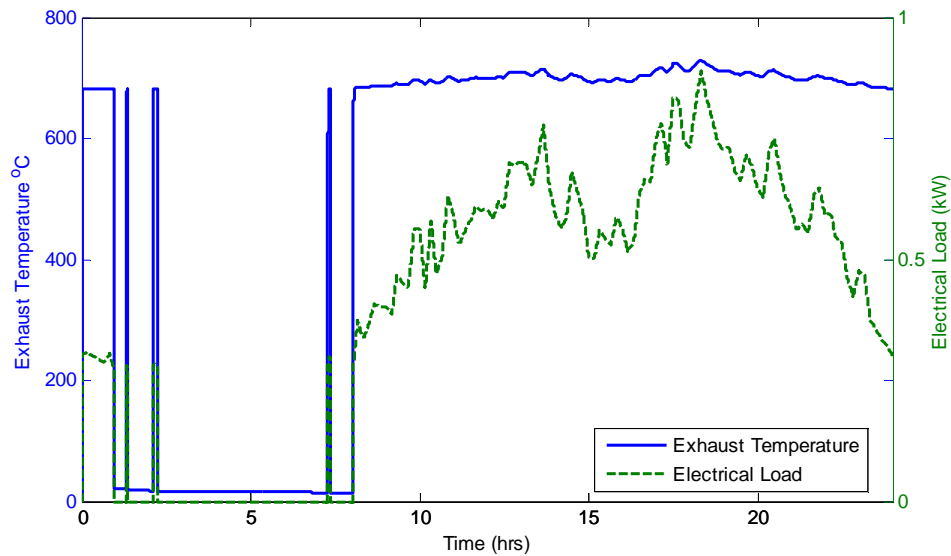


Figure 4.13 Electrical load and engine exhaust temperature vs. time

In order to validate the model, the engine testing procedure described in section 4.3 was succeeded by a second testing session. A segment of the load profile (from 12:00 to 18:00 hours) placed on the simulated engine (purple line in Figure 4.12) was scaled up to be in proportion with the 1.6L test engine displacement, and the dynamometer controller was programmed to emulate this scaled load profile for a constant synchronous speed of 3000 *rpm*. The main model attributes to be validated are the prediction of the consumed chemical power, as well as the predicted exhaust temperature for a given engine load profile.

As can be observed in Figure 4.14, the plotted line of the simulated chemical power inlet rate exhibits a shape and magnitude very similar to the experimentally obtained line (scaled down to 80cc). The plot of the simulated chemical power inlet rate remains below the experimental curve for the complete duration of the test. One may observe in Figure 4.15 that the relative error of the model is rather small ranging between  $-0.8\%$  and  $-1.4\%$  with the contour of the line corresponding to changes in engine load.

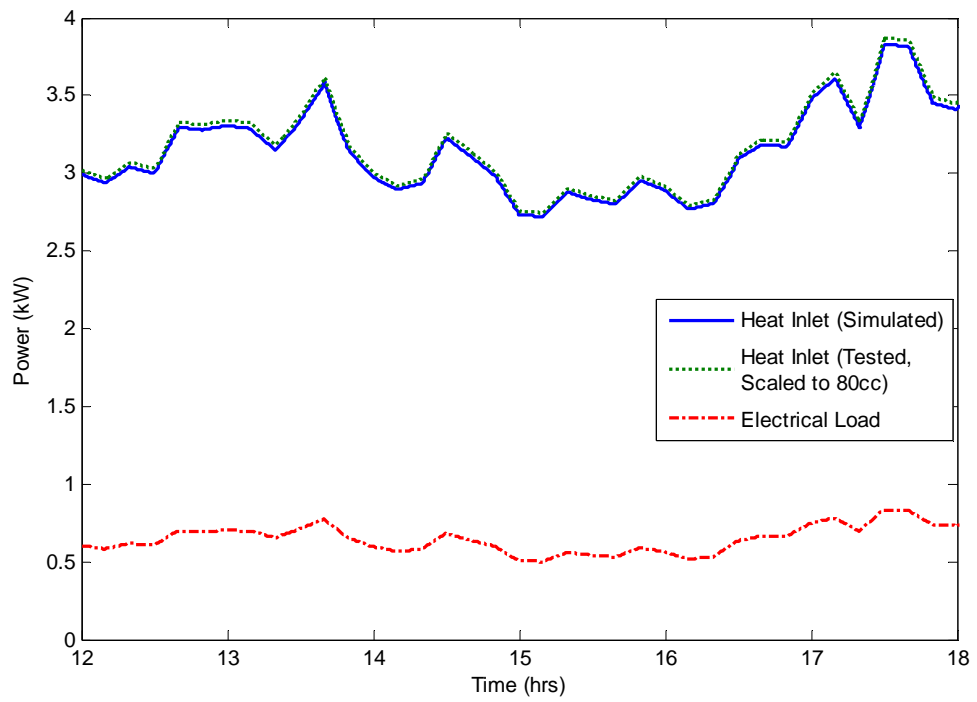


Figure 4.14 Simulated and tested heat inlet rate and electrical load vs. time

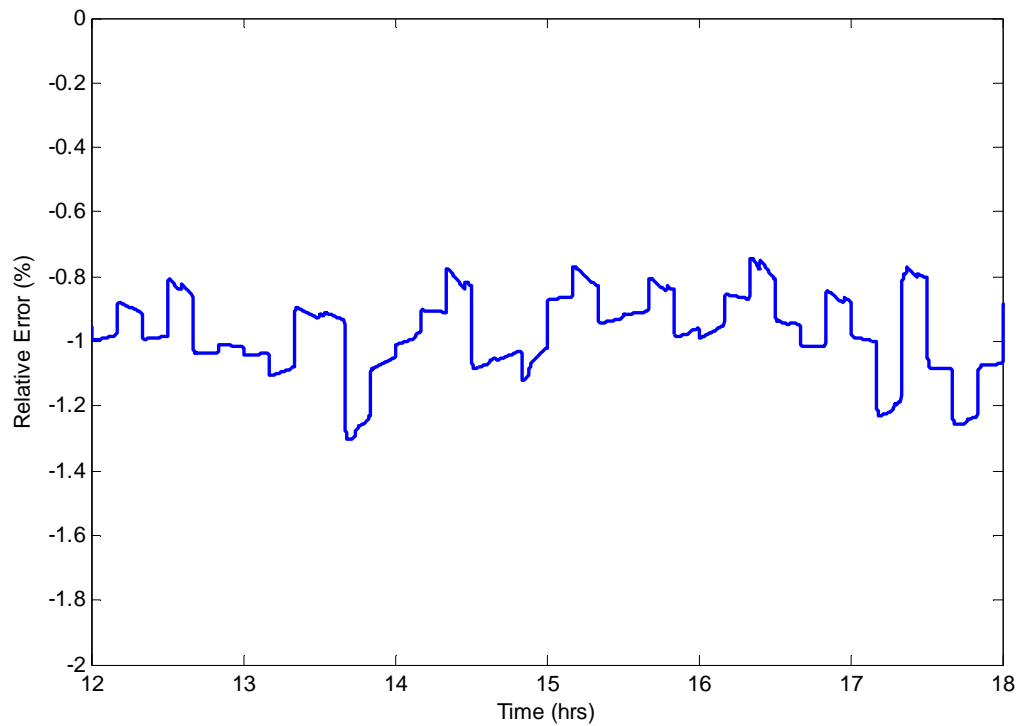


Figure 4.15 Relative error of the estimated fuel input rate by the model vs. time



Similarly, the degree to which the developed model predicts the exhaust temperature may be observed in Figure 4.16 where the exhaust temperature profile recorded during the drive cycle phase of the engine test and the exhaust temperature predicted by the model for the same load are plotted against time. The difference between the two lines ranges between 3°C and 5°C with the simulated line being above the measured temperature curve throughout the duration of the test. A difference of 5°C for temperatures positioned about the 700°C mark translates to a relative error of less than 1% when a reference point of 25°C is considered.

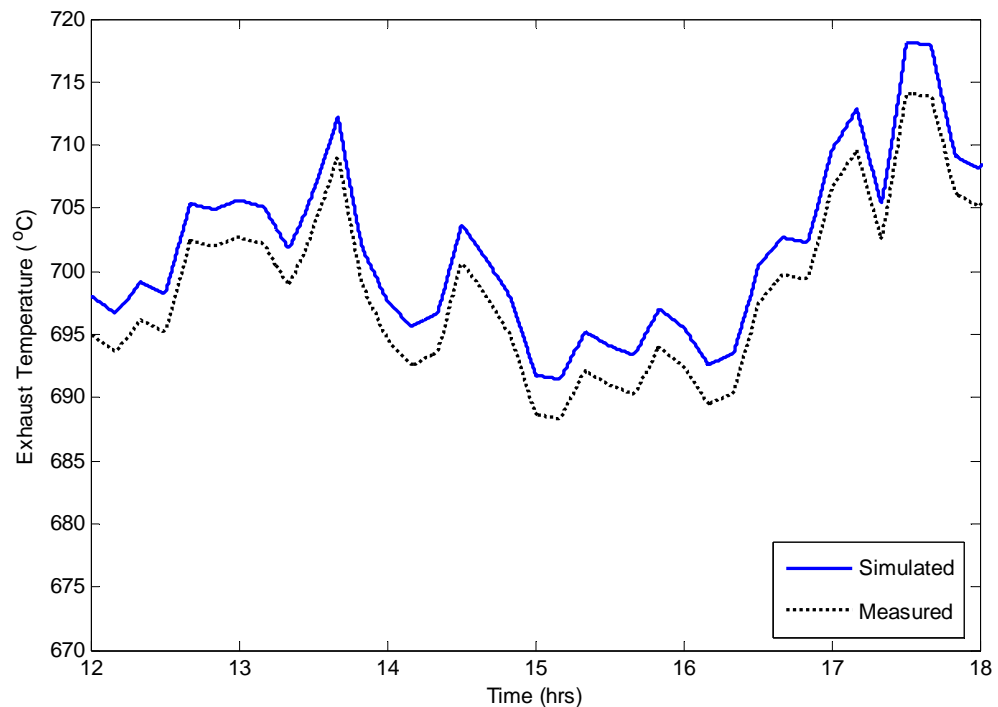


Figure 4.16 Simulated and measured exhaust temperatures vs time

The plots of Figure 4.16 come to agreement with Figure 4.17 where the relative error of the predicted exhaust temperature is plotted against engine speed and volumetric efficiency. It can be observed that the relative exhaust temperature error ranges between  $-2\%$  and  $+2\%$  throughout the complete operating range of the engine. Since the engine speed was held at a constant synchronous speed of 3000 *rpm* for both the case of the drive cycle

phase of the engine test, as well as the CHP simulation, and minimum electrical output of the generator was restricted to 40% of its maximum electrical output to ensure a fuel efficient operation, the relative error of the simulation remained positive and below 1% throughout the whole duration of the tests due to the engine model being simulated over a map region that is characterized by a low and positive relative exhaust temperature error.

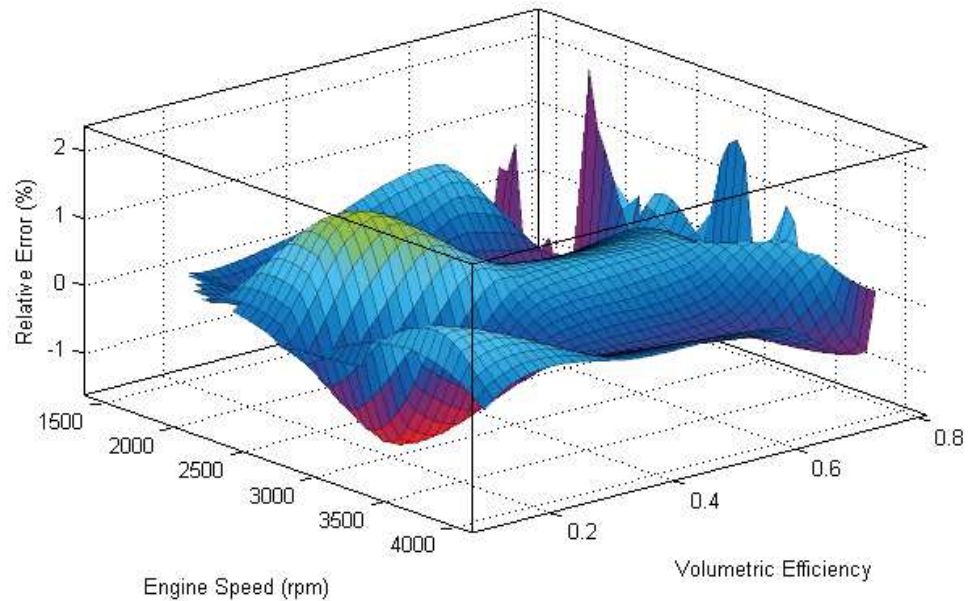


Figure 4.17 Relative error of the exhaust temperature predicted by the model vs. engine speed and volumetric efficiency

#### 4.6. Design and Analysis

As shown in the simulation phase of section 4.5, the observations made on the behaviour of the developed engine model come to agreement with generally established knowledge on the behaviour of spark ignited internal combustion engines, as well as the engine behaviour recorded in the collected engine data, the collection procedure of which is described in section 4.3.

The distribution of the different power components flowing through the engine model exhibits a behaviour that is quantitatively and qualitatively very similar to that encountered in the tested engine. As expected, the fraction of

the inlet chemical power  $\dot{Q}_{in}$  that is converted to mechanical power output (fuel conversion efficiency) at lower loads is low compared to the fractions of  $\dot{Q}_{in}$  that end up to become the engine main waste heat components. At higher loads, mechanical power output accounts for a greater proportion of the inlet chemical power than in the case of low loads, and this translates to an increase in fuel conversion efficiency. In addition, the proportion each waste heat rate component accounts relative to the chemical power inlet changes with load as well, and depending on the waste heat recovery configuration this may cause a variation in the system overall fuel utilization efficiency as engine speed and load is varied.

The predicted exhaust temperature exhibits behaviour very close to the recorded profile. As in the case of the tested engine, the predicted exhaust temperature is affected by both engine speed and load with speed having a considerably stronger influence on the exhaust temperature magnitude than engine load.

In terms of the degree to which the fitted model of Table 4.2 predicts the magnitude of measured engine outputs accurately, the model validation phase of section 4.5 showed a high proximity of the simulation results to the measured data. The relative error of the exhaust temperature fit prediction has been found to be less than 1% for the engine drive cycle tests. For the same tests, the relative error of the required chemical power inlet for the same load profile remained between  $-0.7\%$  and  $1.4\%$  throughout the whole simulated period. The good accuracy of the predicted values of  $T_{exh}$  and  $Q.R.$  is reflected in the high coefficients of covariance  $r^2$  which were calculated by the surface fitting tool of Matlab to be 0.9959 and 0.9881 respectively, and this can be attributed to the high order of the surface fits. Another potential factor that may have contributed to low relative errors is the fact that all tests were carried out on the same day, which assured that the testing conditions were kept as constant and controlled as possible. While a test performed during a different day of the year may give relative errors of a higher magnitude, the low errors encountered under optimal testing indicate that the fitted model is adequate for the purpose of modelling and simulating ICE

based cogeneration systems, provided that no dramatic changes are made in the engine running conditions such as in the case of operating under a very low barometric pressure due to high altitude.

#### 4.7. Thermal load on the cooling system of SI ICEs

Since the percentage of heat input rate that ends up being lost by means of radiation on a liquid cooled SI ICE engine does not vary significantly throughout the engine operating range as shown from data sourced from [17] and plotted in Figure 4.18. Therefore, for a petrol fuelled automotive engine, a value of constant 9% of the rate of heat input for the rate of radiated heat would be a relatively safe assumption to make for the synchronous speed of 3000 rpm.

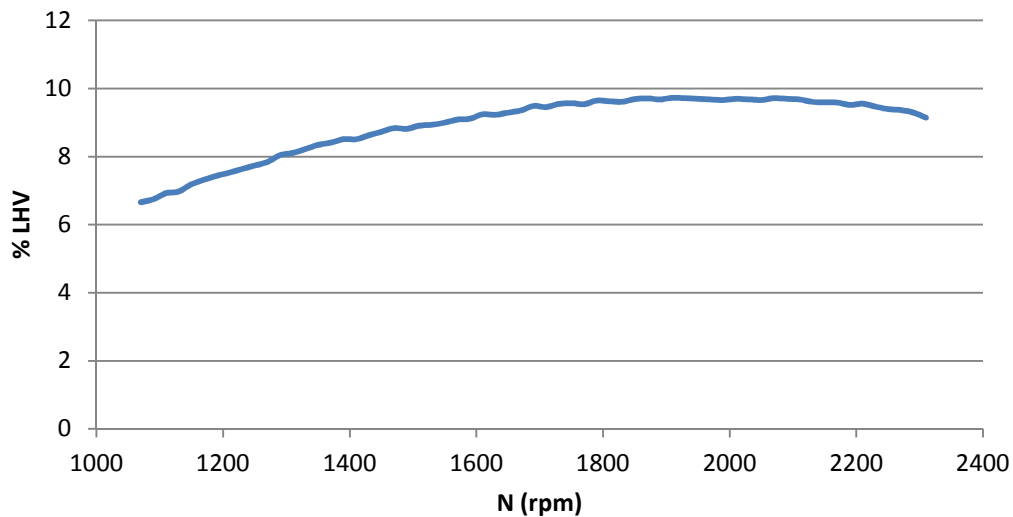


Figure 4.18 Percentage of fuel input that enters the cooling system vs. engine speed

Based on the above, one may calculate the load placed on the cooling system by subtracting the rate of radiated heat component from the sum of the rates of convected and friction generated heat components as shown below.

$$\begin{aligned}\dot{Q}_{coolant} &= \dot{Q}_{conv} + \dot{Q}_{friction} - \dot{Q}_{radiant} = \\ &= \dot{Q}_{conv} + \dot{Q}_{friction} - 0.09\dot{Q}_{fuel\_in}\end{aligned}\tag{ 4.47 }$$

#### 4.8. Natural Gas as an ICE fuel

While petrol operation still dominates the SI ICE market, natural gas (NG) is an attractive alternative option – especially for stationary engines - due to advantages analysed below.

As it consists mostly of methane which is characterized by the lowest carbon content of all hydrocarbons, CO<sub>2</sub> emissions are reduced when compared to other carbon based fuels [92], [93]. In addition, as it enters the cylinder in a completely gaseous form, a more complete combustion takes place leading to reduced levels of HC [94], [95] and CO emissions [92], [93].

The significantly higher research octane number (RON) of NG (approx. 130), allows for dedicated NG engines to operate on high compression ratios leading to a significant improvement in fuel conversion efficiency and to a further reduction in CO<sub>2</sub> and CO emissions [94], [96].

*BSFC* of NG fuelled engines was observed by Aslam et al. [92] to minimize at 65% of maximum load, and in addition to be reduced by 17.3% on average compared to the *BSFC* of the same engine fuelled by petrol. Similarly, Mohamad et al. [93] observed an average reduction of 22%.

While the advantages of NG analysed above show the potential of NG as a fuel for stationary SI engines, there is a number of drawbacks analysed below that must be taken into consideration

The lower density and higher stoichiometric AFR of Natural Gas compared to petrol, and the absence of latent cooling of the charge when gaseous fuels are used, all reduce the maximum amount of air that enters the cylinder by 10% – 12% compared to petrol fuelled operation [97], [98], [99]. As a result

of the above, power output is negatively affected. Geok et al. [99] observed a reduction in torque and brake horse power by 10% on average. An even greater reduction was recorded by M.U. Aslam et al. [92] and A. Das et al [100], who found power output for NG operation to be reduced by 16% on average with respect to petrol fuelled operation. A similar level of reduction of 15.5% was predicted by K. Resapour et al. [97]. BMEP is expected to follow this reduction in power output as engine speed, brake power and BMEP are interdependent [93], [96]. Maximum power output may also vary as a function of charge temperature as seen in M. A. Sera et al. [94].

In addition, the longer combustion curve of Natural Gas leads to an increase in the percentage of waste heat diffusing in the engine block by means of convection resulting in an increase in the load placed on the cooling system as well as the coolant and oil temperatures [100].

While NG generally produces emissions that have a smaller environmental impact than that of petrol, NO<sub>x</sub> levels tend to increase due to the higher combustion temperatures present under NG fuelled operation. M.U. Aslam et al. [92] reported 33% higher NO<sub>x</sub> levels on average than petrol fuelled operation.

#### **4.9. Categories of Natural Gas fuelled ICEs**

A literature review on the available NG fuelled SI ICE technology revealed two main types of this engine group, each representing different design and production strategies and result in different associated costs, performance and emission characteristics.

In the first group belong SI engines originally designed and built as petrol fuelled units and converted to run on natural gas. They are of a lower cost than purpose built CNG engines, but the converted unit lacks in performance and fuel conversion efficiency when compared to the latter type [92]. The reviewed studies [92], [97], [101] seem to give inconclusive results as to whether converting an originally low compression ratio petrol engine to operate on NG results to a noticeable and consistent change in fuel conversion efficiency. Due to the above, it could be safe to assume that fuel

conversion efficiency (FCE) remains the same for engines of the same compression ratio having been converted from petrol to NG if stoichiometric mixtures are used and suitable spark timing is applied for both cases.

The second engine category includes engines designed with dedicated NG operation in mind. As a result, the high compression ratio NG may operate under can achieve FCE levels not possible in a petrol fuelled engine or a modified bi-fuel converted engine.

In all cases, existing investigations on the effect of the increase in compression ratio have showed considerable improvements in fuel conversion efficiency for the high CR engines over their low CR counterparts. A fuel conversion efficiency of up to 40% LHV was achieved by A. Das et al. [100] which is a 35% improvement on the fuel conversion efficiency of the stock, low CR engine.

#### 4.10. Fuel modified performance surfaces

While at the time of this writing, no engine data on natural gas fuelled engine operation was available for the generation of an NG specific model, the fact that power curves of petrol and natural gas follow the same trend if the engines are operated under the same conditions [100] allows for existing petrol based performance maps to be modified to approximate NG fuelled engine behaviour, provided that general observations on the performance of NG engines are taken into consideration.

For this purpose, it will be assumed that the ratio of break specific consumption of the fuel modified engine  $BSFC_{model\_s\_new\_f}(N, \eta_{vol\_pump})$  over the break specific consumption of the original fuel engine  $BSFC_{map\_orig\_f}(N, \eta_{vol\_pump})$  remains constant throughout the complete operating range of the engines:

$$\frac{BSFC_{model\_s\_new\_f}(N, \eta_{vol\_pump})}{BSFC_{map\_orig\_f}(N, \eta_{vol\_pump})} = C \quad (4.48)$$

When one modifies  $BSFC_{map\_orig\_f}(N, \eta_{vol\_pump})$  for a different fuel, the map is expected to change due to the different  $LHV$  of different fuels. If  $LHV_{orig\_f}$  and  $LHV_{new\_f}$  are the lower heating values of the original and the new fuel respectively, and assuming that the performance map for the original fuel has already been scaled in terms of FCE, the break specific fuel consumption surface for the new fuel is calculated as follows:

Since:

$$\frac{BSFC_{model\_s\_new\_f}}{BSFC_{map\_orig\_f}} = \frac{\frac{3600}{LHV_{new\_f} \eta_{FC\_map}}}{\frac{3600}{LHV_{orig\_f} \eta_{FC\_map}}} = \frac{LHV_{orig\_f}}{LHV_{new\_f}} \quad (4.49)$$

Equation ( 4.49 ) rearranges to:

$$\begin{aligned} BSFC_{model\_s\_new\_f}(N, \eta_{vol\_pump}) &= \\ &= BSFC_{map\_orig\_f}(N, \eta_{vol\_pump}) \frac{LHV_{orig\_f}}{LHV_{new\_f}} \end{aligned} \quad (4.50)$$

As seen in section 4.1, there is a strong dependence between fuel density, stoichiometric AFR, LHV and engine maximum power output. In order to produce a model that describes the modelled engine behaviour accurately, the change in maximum power output must be taken into account.

In the current study, petrol stoichiometric AFR is sourced from J.Heywood [17] to be 14.7:1 while the stoichiometric AFR of NG is calculated using the NG typical composition as found in Y. A Cenzel et al. [12] to be 15.6:1 as presented in section 4.2.

As an example, at 3000rpm wide open throttle (W.O.T.), the energy content of one 200cc cylinder charge in the case of petrol is approximately 0.62kJ while for NG fuelled operation the charge energy content is approximately



0.59kJ. This means that for the given fuel properties, the maximum cylinder charge energy content is reduced by 4.8% and heat input for the NG fuelled model at the same volumetric efficiency will be:

$$\dot{Q}_{fuel\_in\_max\_NG}(N) = 0.952\dot{Q}_{fuel\_in\_max\_petrol} \quad (4.51)$$

#### 4.11. Proposed engine model variations

Following the review of section 4.9 on the types and performance characteristics of SI NG fuelled ICEs, it is decided to create two derivative models based on the model layout developed in section 4.3 to represent the two main SI NG fuelled engine subcategories that may be encountered in micro-cogeneration applications. For all cases it is assumed that the air – fuel equivalence ratio  $\lambda = 1$ . The main performance maps that were obtained experimentally will be modified in the following two subsections. Then the procedure of sections 4.1 and 4.2 will be repeated for each NG engine variant model.

##### 4.11.1. Low CR Petrol engine converted to NG

According to Aslam et al. [92], for  $\lambda < 1.3$ , NG and petrol operation of the same compression ratios exhibit very similar values of FCE. Therefore, the modelled NG engine for this study will make use of the calculated FCE values of the petrol based data with modified values of *BSFC* for NG for the same calculated FCE values.

$$\begin{aligned} BSFC_{model\_new\_f}(N, BMEP) &= \\ &= BSFC_{map\_orig\_f}(N, BMEP) \frac{LHV_{petrol}}{LHV_{NG}} = \\ &= BSFC_{map\_orig\_f}(N, BMEP) \frac{44.7}{50.02} = \\ &= 0.89BSFC_{map\_orig\_f}(N, BMEP) \end{aligned} \quad (4.52)$$

In terms of exhaust temperature, a positive offset of 160°C will be applied equal to the average difference encountered by P. M. Darade et al. [95] for low CR NG engine operation.

#### 4.11.2. High CR purpose designed NG exclusive engine

This engine type exhibits a considerable improvement compared to the low CR counterparts. For the scaling of the existing performance map, the observations of A. Das et al. [100] will be used. They observed that a purpose built NG engine with a CR of 15:1 exhibited an improved FCE by 35% on average over that of a low CR petrol engine of the same displacement. Taking this into consideration:

$$BSFC_{model\_s}(N, BMEP) = BSFC_{map\_orig}(N, BMEP) \frac{100}{100 + 35} \quad (4.53)$$

And the final fuel modified map will now be:

$$\begin{aligned} BSFC_{model\_new\_f}(N, BMEP) &= \\ &= BSFC_{model\_s}(N, BMEP) \cdot \frac{LHV_{petrol}}{LHV_{NG}} = \quad (4.54) \\ &= 0.89BSFC_{model\_s}(N, BMEP) \end{aligned}$$

In terms of the exhaust temperature, while a conversion from petrol to NG operation may lead to an increase by approximately 160°C when an engine of the same compression ratio is involved [95], in this case, the considerably higher compression ratio, increases the thermal efficiency of the thermodynamic cycle, hence converting a larger fraction of the fuel energy input into work. This reduces the contribution of combustion related waste heat components such as the exhaust and convection heat to the total waste

heat. The dependence of exhaust temperature on compression ratio has been investigated among other performance indicators by E. Tribbett et al. [102] where exhaust temperature has been observed to fall from  $1120^{\circ}K$  for a CR of 5:1, to  $1050^{\circ}K$  for a 7:1 CR and to  $1025^{\circ}K$  for CR=9:1. Using a curve fit as found in E. Tribbett et al. [102], it is estimated that for a NG fuelled engine, the transition from a CR of 9:1 to that of 15:1, will reduce the exhaust temperature by approximately  $65^{\circ}K$ . Therefore, for the purpose built high CR NG fuelled engine, the exhaust temperature is assumed to be on average approximately  $100^{\circ}K$  higher than that of the low CR petrol engine. Thus, during the exhaust temperature modelling, the exhaust temperature values will have a  $100^{\circ}K$  offset over the those of the petrol fuelled model.

#### **4.12. Summary**

In this chapter, the model of an SI ICE based generator has been developed. The quasi - stationary engine modelling layout has been developed with micro-CHP applications in mind and emphasizes in the description of all waste heat components and mass flows for the complete engine operating range, while being easy to scale and to connect with components operating at different energy domains. It is also capable of describing the dynamic behaviour of moving parts.

In order to generate the model maps, a series of engine tests have been conducted and a two variable exhaust temperature model as a function of engine speed and engine load has been developed.

The model of the electric machine is quasi-stationary in nature and is based on the analysis of a simplified equivalent circuit of a synchronous machine. The characteristics of an existing generator were used as design conditions to calculate the internal resistance and windage losses which allowed for the generation of performance curves.

## Chapter 5 Heat Exchanging Systems

As discussed in section 3.4.3, while there is a need for simple and computationally light heat exchanger models that predict the outlet conditions of a heat exchanger for the inputted inlet temperatures and mass flow rates, their availability is next to nonexistent due to the complex nature of the modelled system. The current chapter is a response to this requirement, by developing lookup table based models for the heat exchanging components of the modelled system. These are the two shell & tube heat exchangers used for waste heat recovery, the coil heat exchangers used to transfer heat from and to the heat storage tank, and the heating radiators. In order to populate the lookup tables, standalone software that controls discretised versions of the aforementioned component models is developed and used.

### 5.1. Flow circuit types

The two main flow stream route categories distinguished in the heat recovery system of a typical cogeneration unit are the primary and the secondary circuits. A primary heat exchanger circuit is the heat exchanger side which carries heat of a higher grade than the other. As a result of the temperature gradient, this high grade heat flows through the walls of the heat transfer surface and is made available to the lower heat grade secondary circuit. In the case of an ICE based cogeneration system, one can classify the exhaust gas side and the jacket water side as the primary circuits of the two heat exchangers. The secondary circuits involve the fluid path through which the generally colder heat recovery fluid (water in the present study) flows, gaining heat from the primary stream and delivering it to either the end user or to a heat storage unit. In Figure 5.1, the secondary circuit is represented by the interrupted line of the form “---”. As in F. Caresana et al [2], both the jacket water and flue gas heat exchangers are operated in a counter flow configuration, but in this case, the secondary circuits of the two heat

exchangers are connected in parallel rather than in series, thus facilitating heat exchanger sizing and ensuring that the secondary circuit of both heat exchangers has the same low inlet temperature.

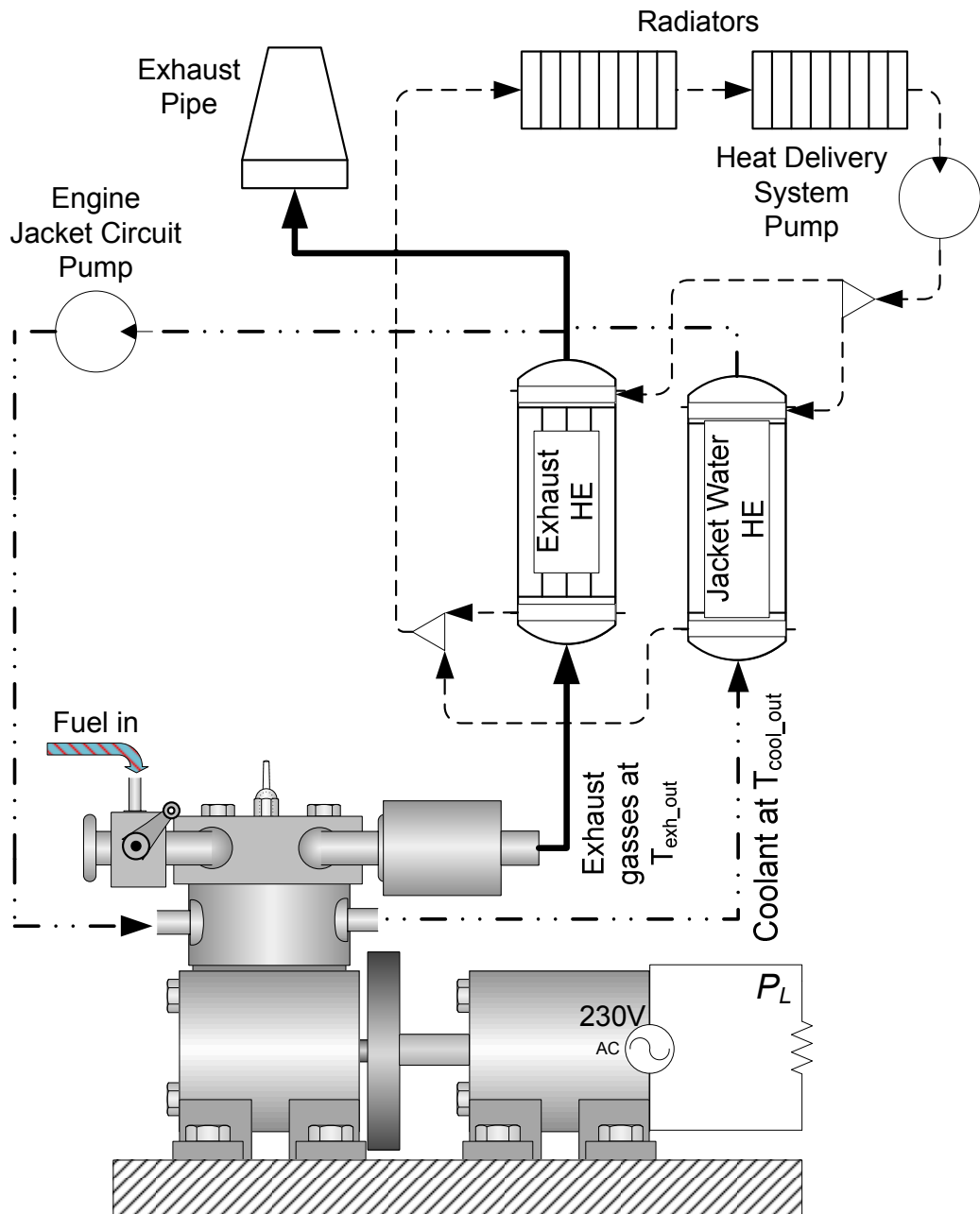


Figure 5.1 Schematic of a basic micro - CHP layout

When heat storage is employed, heat is usually transferred from the CHP to the tank and from the tank to the load by means of two different water loops [31].

## 5.2. Heat Exchanger Modelling

The concept of cogeneration involves complex, non linear energy conversion and transmission processes which result to a system behaviour characterized by considerable performance variations throughout its operating envelope. As in the case of the prime mover, models of the heat exchange devices, such as those of heat exchangers, must be capable of realistically describing the component behaviour throughout their intended operating range.

As can be shown in Figure 5.2, a basic heat exchanger model can be analysed as a system with four different main inputs and one output. The inputs are the mass flow rates and the inlet temperatures of the two streams while the output is the heat transfer for a given operating point. Therefore, the developed heat exchanger model must use the above inputs and return either one of the outlet temperatures or the transferred amount of heat.

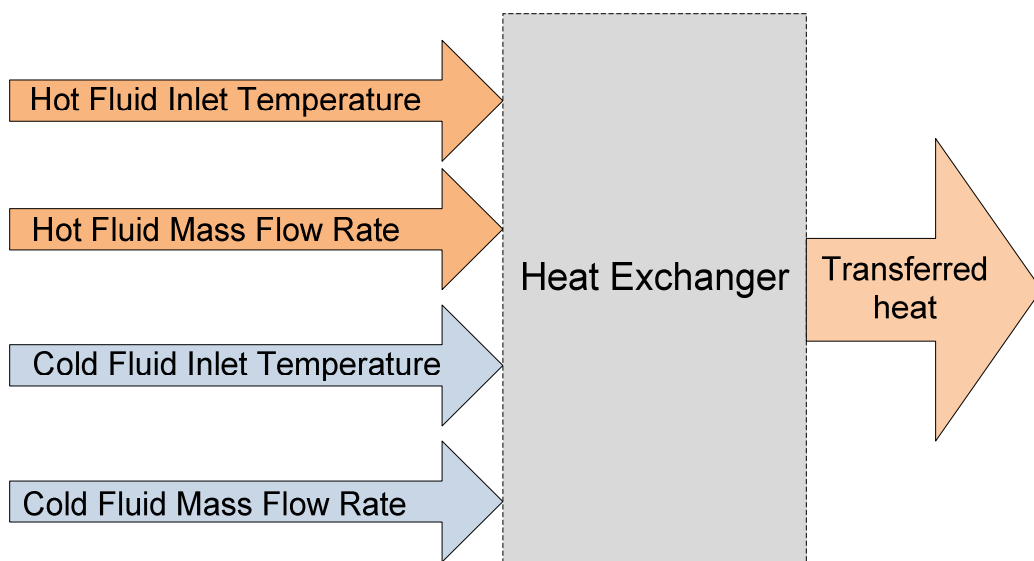


Figure 5.2 Input/Output diagram of a basic heat exchanger model

The complex flow and heat transfer phenomena present under convective heat transfer, pose great obstacles in the development of a general purpose heat exchanger model via analytical methods. The well proven heat exchanger preliminary calculation and rating methods found in [103], [104], [105], and [106] and incorporated as separate subroutines in the heat exchanger design and simulation software developed in the current chapter and presented in section 5.7, are all very useful as means to design or select heat exchanger characteristics, but are based on trial and error techniques, and therefore they cannot serve as a basis of a heat exchanger model since by definition, the main purpose of a mathematical model of a physical system is the capability to predict the system output/s for given input/s. Thus, the use of some form of numerical method or experimental modelling technique will be necessary.

By examining the available solutions, it should be obvious that an experimental model can provide the most accurate representation of the system, but due to the fact that the heat exchanger is a four input system, several thousands of data points must be collected. As a result, the necessary duration of the testing procedure, is estimated at several months. At the same time, the obtained experimental data is only valid for a particular heat exchanger tube length, thus limiting the versatility of such a model type considerably.

While the heavy computational load associated with a discretised heat exchanger model being used as a component of the main CHP model leads to an excessively high simulation duration, its use as a data generator for a lookup table based quasi-stationary model can nevertheless be a very time and cost effective way to build a heat exchanger model of a light computational load.

For the above reasons, it has been decided to develop a discretised shell and tube heat exchanger model on Simulink of which the simulation will be controlled via the user interface presented in section 5.7. The resulting data of all simulated operating points will then be used to populate lookup table

based HE models, which in turn will serve as the actual heat exchanger components of the main cogeneration model described in Chapter 7.

### 5.3. Shell & tube heat exchanger

Due to the lack of knowledge on the temperature distribution as well as the heat transfer coefficient distribution along the heat exchanger tube, a heat exchanger model discretised along the direction of the flow will be developed, in which the inlet temperature of a cell is the outlet temperature of the preceding cell. As shown in Figure 5.3, the tube is longitudinally divided to  $n$  cells. At any given time, the main variables along each cell (flow rates, temperatures of both fluids and heat transfer coefficients) are assumed to be constant and equal to their inlet values.

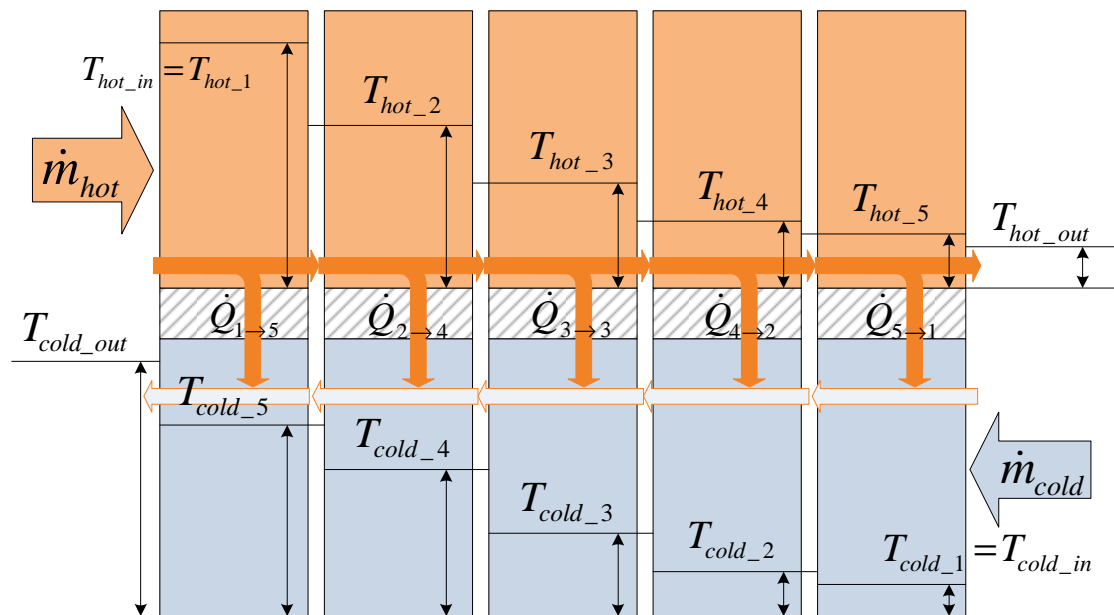


Figure 5.3 Schematic of the discretised counter flow heat exchanger model

#### 5.3.1. Forced convection and heat transfer

The basic element of the discretised shell and tube heat exchanger consists of a tube of standard inner and outer diameter  $d_i$  and  $d_o$  respectively with a



thermal conductivity  $k_{tube}$  ( $W/m \cdot ^\circ K$ ) as shown Figure 5.4. The heat conduction characteristics of the inner and outer boundary layer are represented by their respective heat transfer coefficients  $h_i$  and  $h_o$  in ( $W/m^2 \cdot ^\circ K$ ).

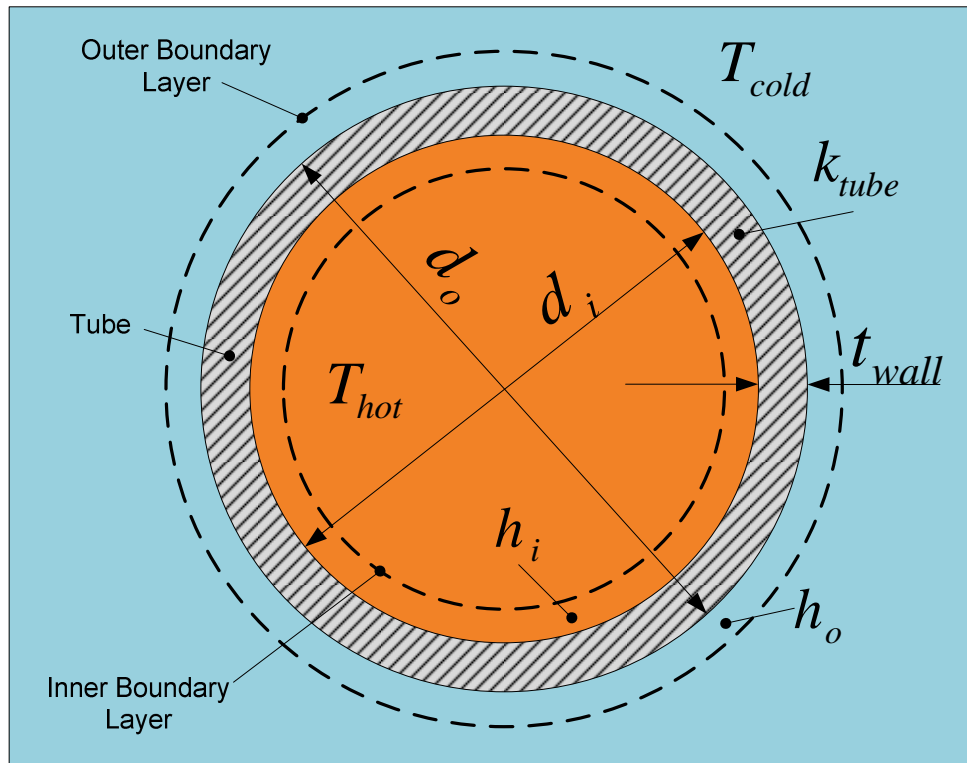


Figure 5.4 Section of the heat exchanger tube profile

The hot fluid enters one side of the incremental heat exchanger cell  $j$  at a mass flow rate  $\dot{m}_{hot}$  and an inlet temperature  $T_{hot,j}$ . If the heat inlet rate via mass inflow in the hot side control volume is  $\dot{Q}_{hot\_in\_j} = \dot{m}_{hot}h(T_{hot,j})$ , where  $h(T_{hot,j})$  the specific enthalpy of the hot fluid for  $T_{hot,j}$ , the heat flow balance will be:

$$\begin{aligned} \dot{Q}_{hot\_out\_j} &= \dot{m}_{hot}h(T_{hot,j}) - \dot{Q}_{incr\_j} = \\ &= \dot{Q}_{hot\_in\_j+1} = \dot{m}_{hot}h(T_{hot,j+1}) \end{aligned} \quad (5.1)$$

Where  $\dot{Q}_{incr\_j}$  is the incremental heat transfer rate component (as discussed below).

In the developed Simulink model, the hot fluid cell outlet temperature  $T_{hot\_j+1}$  is provided by lookup tables as a function of the remaining fluid specific enthalpy.

The cold fluid flows along the opposite side of the tube wall (shell side), entering at an inlet temperature  $T_{cold\_j}$  in a parallel flow and  $T_{cold\_n-j}$  in the case of a counterflow heat exchanger as in our case. The heat input rate in the cold side control volume will be:

$$\dot{Q}_{cold\_in\_j} = \dot{m}_{cold} h(T_{cold\_N-j}) \quad (5.2)$$

The temperature difference between the hot and cold streams causes a portion of the hot fluid inlet enthalpy to flow towards the cold fluid with the form of an incremental heat transfer rate component  $\dot{Q}_{incr}$ . The length of each cell  $L_{incr}$  is assumed to be small enough to allow for the temperature difference along the cell  $\Delta T_{in-out}$  to be negligible. This allows for the cell hot and cold temperatures and heat transfer coefficients to be taken as constant in the cell heat transfer calculations. Given the above assumptions, the heat transfer rate in the incremental tube segment  $j$  of a counter flow heat exchanger is calculated from:

$$\begin{aligned} \dot{Q}_{incr\_j} &= U_{incr\_j} A_{incr} \Delta T_{incr\_j} = \\ &= U_{incr\_j} \pi d_o L_{incr} (T_{hot\_j} - T_{cold\_N-j}) \end{aligned} \quad (5.3)$$

The combined heat transfer coefficient of multiple cylindrical layers can be calculated by means of following the relevant procedure as found in F. Kreith et al.[107]. Based on the schematic of Figure 5.4, the overall heat transfer coefficient of the tube and the two boundary layers can be calculated from:

$$U_{oal\_j} = \frac{1}{\frac{d_o}{d_i} \frac{1}{h_{i\_j}} + \frac{d_o}{2k_{tube}} \ln(d_o/d_i) + \frac{1}{h_{o\_j}}} \quad (5.4)$$

Where :

$$h_{i\_j} = h(T_{hot\_i}, \dot{m}_{hot}) \quad (5.5)$$

And:

$$h_{o\_j} = h(T_{cold\_N-j}, \dot{m}_{cold}) \quad (5.6)$$

In order to allow for the transient effects of the tube mass to be included in the model behaviour, rather than using equation ( 5.4 ), it is decided to model two separate heat transfer coefficients that will describe the heat exchange between the tube incremental mass  $M_{tube\_incr}$  and the two fluids, and whose steady state result equals that of equation ( 5.4 ).

The heat transfer coefficient of the inner boundary layer and the material within half the tube thickness is:

$$U_{incr\_i\_j} = \frac{1}{\frac{d_o}{d_i} \frac{1}{h_{i\_j}} + \frac{d_m}{2k_{tube}} \ln(d_m/d_i)} = \frac{1}{R_{incr\_i\_j}} \quad (5.7)$$

The heat transfer coefficient of the half tube thickness and the outer boundary layer is:

$$U_{incr\_o\_j} = \frac{1}{\frac{d_o}{2k_{tube}} \ln(d_o/d_m) + \frac{1}{h_{o\_j}}} = \frac{1}{R_{incr\_o\_j}} \quad (5.8)$$

Where  $R_{incr\_i\_j}$  and  $R_{incr\_o\_j}$  the inner and outer thermal resistance of cell  $j$ .

The schematic of Figure 5.5 illustrates the heat transfer relationship between the hot fluid, the tube incremental mass  $M_{tube\_incr}$  and the cold fluid.

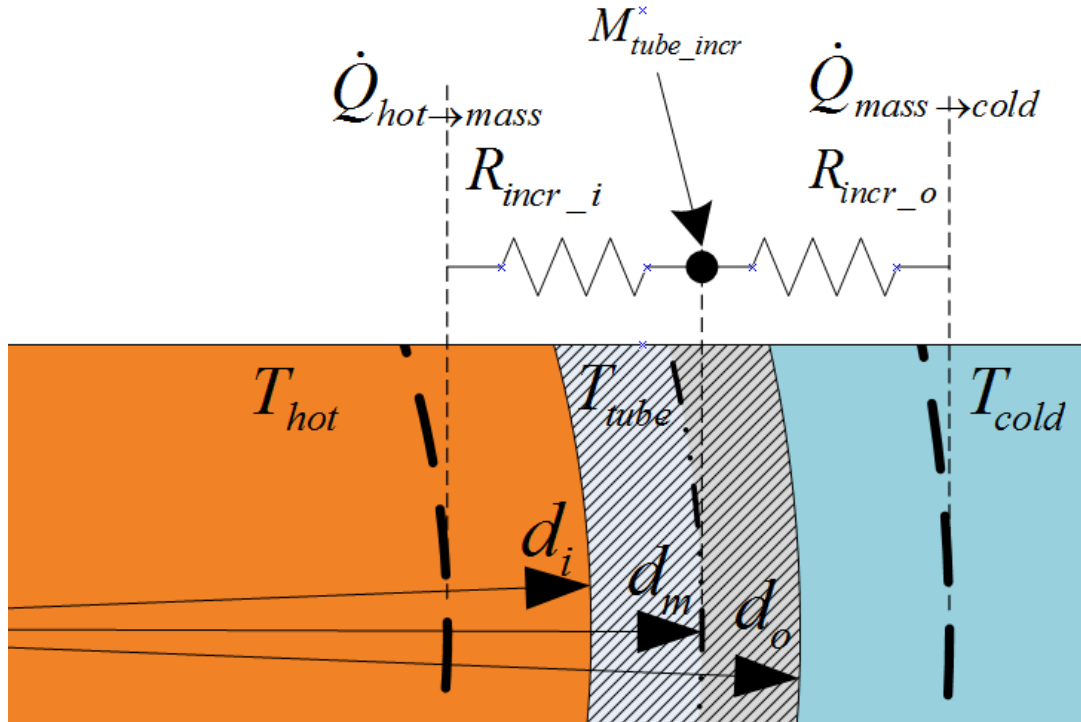


Figure 5.5 Schematic of the heat transfer relationship between the incremental mass node and the fluid streams

Heat transfer takes place between the mass of the tube wall and the two fluids. The rate of heat that enters the incremental tube mass element  $j$  is a function of the hot side heat transfer coefficient  $U_{incr\_i\_j}$  as well as the difference between the inlet temperature of the hot fluid  $T_{hot\_j}$  and the temperature  $T_{tube\_j}$  of the incremental mass of the same element:

$$\dot{Q}_{tube\_in\_j} = U_{incr\_i\_j} A_{incr} (T_{hot\_j} - T_{tube\_j}) \quad (5.9)$$

Similarly, the rate of heat that leaves the incremental tube mass  $M_{tube\_incr\_j}$  is a function of the cold side heat transfer coefficient and the difference between the tube mass temperature and the inlet temperature of the cold stream  $T_{cold\_N-j}$ .

$$\dot{Q}_{tube\_out\_j} = U_{incr\_o\_j} A_{incr} (T_{tube\_j} - T_{cold\_N-j}) \quad (5.10)$$

The incremental heat transfer rate between the flow streams of each cell depends on the difference between the rate of heat entering the incremental tube mass from the hot stream and the rate of heat flowing out of the incremental tube mass and into the cold stream. The net rate of heat that enters the incremental tube mass  $M_{tube\_incr\_j}$  is:

$$\dot{Q}_{net\_j} = \dot{Q}_{tube\_in\_j} - \dot{Q}_{tube\_out\_j} \quad (5.11)$$

When  $\dot{Q}_{net\_j} = 0$ , the cell can be considered to have reached steady state, and under steady state, heat transfer rate is only a function of the cell inlet conditions. The heat absorbed or released by the incremental mass  $M_{tube\_incr\_j}$  at time  $k$  is given from:

$$Q_{M\_incr\_j} = \int_0^k \dot{Q}_{net}(t) dt \quad (5.12)$$

The tube temperature  $T_{tube\_j}$  of cell  $j$  at any given time is calculated from:

$$T_{tube} = \frac{Q_{M\_incr}}{M_{tube\_incr} cp_{tube}} \quad (5.13)$$

Where  $cp_{tube}$  is the specific heat capacity of the tube material.

### 5.3.2. Heat transfer coefficients

The heat transfer coefficient of a boundary layer of a fluid flowing along the inner or outer surface of a circular section of diameter  $d$  can be found from:

$$h = Nu \frac{k}{d} \quad (5.14)$$

Where  $Nu$  is the Nusselt number,  $k$  the thermal conductivity of the boundary layer, and  $d$  in  $m$  the characteristic length (tube diameter in this case). Nusselt number represents the ratio of the convective heat transfer over the conductive heat transfer.

### 5.3.3. Flow conditions and heat transfer

It is common knowledge that flow conditions severely affect convection heat transfer processes. Numerous empirical relationships have been developed to approximate the value of  $Nu$  for known flow conditions, thus allowing for the accurate estimation of the heat transfer. For the above reasons, a brief analysis of flow regimes and their respective mathematical correlations of the Nusselt number will be necessary.

Fluid flow can be distinguished by the form it takes inside the shell or tube. Experience has shown that Reynolds number is a reliable criterion of distinguishing between different flow types. Reynolds number of flow in a section of any shape is calculated from:

$$Re = \frac{D_H \dot{m}_{flow}}{\mu A_{flow}} \quad (5.15)$$

Where  $D_H$  the hydraulic diameter of the flow in  $m$ ,  $\dot{m}_{flow}$  the mass flow rate in  $kg/s$ ,  $\mu$  the dynamic viscosity in  $Ns/m^2$  and  $A_{flow}$  the flow area in  $m^2$ .

### 5.3.4. Laminar flow

For low fluid speeds, the motion through the tube takes place in an organized manner mainly in parallel to the bulk velocity axis resulting in laminar flow. The following equations are valid only for laminar flow which takes place when  $Re \leq 2300$

Graetz number  $Gz$  describes the thermal development of the laminar flow and is calculated from:

$$Gz = \frac{D_H Re Pr}{L} \quad (5.16)$$

Where  $L$  the distance from the flow entrance in  $m$ , and  $Pr$  the Prandtl number whose value is a function of the fluid temperature.

A series of different Nusselt number relationships corresponding to different Graetz number regions as found in John H. Lienhard [105] is given below:

For  $2 \times 10^4 \leq Gz$

$$Nu = 1.302Gz^{1/3} - 1 \quad (5.17)$$

For  $667 \leq Gz \leq 2 \times 10^4$

$$Nu = 1.302Gz^{1/3} - 0.5 \quad (5.18)$$

And for  $Gz \leq 667$

$$Nu = 4.364 + 0.263Gz^{0.506}e^{-41/Gz} \quad (5.19)$$

### 5.3.5. Turbulent flow

Higher flow speeds force the bulk molecules to move not only in the direction of the bulk fluid velocity but rather in all possible directions leading to a turbulent flow. Due to the discontinuity on the flow behaviour between the laminar and the turbulent flow regions, relationships used for the estimation of the Nusselt number of laminar flows cannot be used on turbulent flows ( $Re > 2300$ ) [104].

A number of studies on turbulent flow heat transfer characteristics have resulted to empirical relationships which are valid for  $Re > 2300$  as shown below. The most commonly encountered Nusselt number relationship in heat transfer studies involving turbulent flow is the Colburn correlation [108]:

$$Nu = 0.023Re^{0.8}Pr^{0.33} \quad (5.20)$$

A more modern empirical relationship such as the Petukhov-Kyrillov equation may give a better estimation of Nusselt number for a wider range of Reynolds values ( $10^4 < Re < 5 \times 10^6$ ):

$$Nu = \frac{(f/8)RePr}{1.07 + 12.7\sqrt{f/8}(Pr^{2/3} - 1)} \quad (5.21)$$

Based on the Petukhov-Kyrillov equation, Grielski formulated an improved version which yields a reliable estimation of the Nusselt number for  $2300 \leq Re \leq 5 \times 10^6$  [105]:

$$Nu = \frac{(f/8)(Re - 1000)Pr}{1 + 12.7\sqrt{f/8}(Pr^{2/3} - 1)} \quad (5.22)$$

Where  $f$  is the Darcy-Weisbach friction factor and may be calculated from:

$$f = \frac{1}{(1.82 \log_{10} Re - 1.64)^2} \quad (5.23)$$

The above equation is valid for smooth tubes. In the current study, the tubes will be assumed to be smooth with no fouling. Since Grielski equation is reported to exhibit a better correlation to real data compared to similar relationships for a wider range of Reynolds numbers, it is selected to be used for the calculation of Nusselt number in the turbulent flow region.

### 5.3.6. Exhaust gas side - pulsated flow

While the use of the idealised (time averaged) gas flow method can predict the rate of heat rejected from the engine exhaust very accurately (as is also being done in the current study), it has been found that in the case of convective heat transfer, flow pulsations result in heat transfer characteristics that deviate from those of a constant flow considerably with the value of the Nusselt number of the pulsated flow being in some cases quite higher than that of the constant flow as seen in Ngy Srun AP [109] and C. Depcik et al. [108].



Since the equations of sections 5.3.4, and 5.3.5 have been formulated based on experimental data recorded under continuous flow conditions, their application in heat transfer calculations under pulsated flow conditions gives relative errors that may reach up to 50% [109] and are therefore inherently unsuitable to be used for the calculation of the heat transfer coefficient of the exhaust gas side.

As a result of the inability of constant flow derived heat transfer equations to describe pulsated flow heat transfer phenomena, a number of studies have been conducted based on data obtained through measurements of heat transfer between the exhaust streams of 4 and 6 cylinder automotive engines and a heat recovery medium.

Ngy Srun AP [109] conducted a series of experiments for the purpose of calculating the heat transfer coefficient of the exhaust pipe of an automotive ICE. Data was collected for various loads and engine speeds and a  $Nu - Re, Pr$  correlation was developed for the pulsated exhaust flow similar in form to that of the Colburn correlation but with different coefficients to account for the effects of the pulsating flow:

$$Nu = 0.33581Pr^{0.33}Re^{0.52376} \quad (5.24)$$

The results of his derived equation were then compared to those of the Colburn equation and it was observed that for low Reynolds numbers ( $Re \leq 2000$ ), Nusselt number for pulsated flow can be almost twice the magnitude of that of constant gas flow, while this ratio is reduced to 1.1 for  $Re \approx 12000$ . Thus, this difference is expected to be more pronounced for idle rather than in the case of high speed operation [106].

Another relevant study was carried out by C. Depcik et al. [108] who used model generated rather than experimental data to end up with a universal relationship applicable to both the intake and the exhaust of the form:

$$Nu = 0.07Re^{0.75} \quad (5.25)$$

#### 5.4. The discretised heat exchanger model on Simulink

The block diagram of a counter flow heat exchanger developed on Simulink can be seen in Figure 5.6. Each subsystem on this figure models one heat exchanger cell. The inputs of each cell are the outputs of the preceding cell. Due to being a counter flow configuration, the shell cell temperature input/output direction is the reverse of the tube cell temperature.

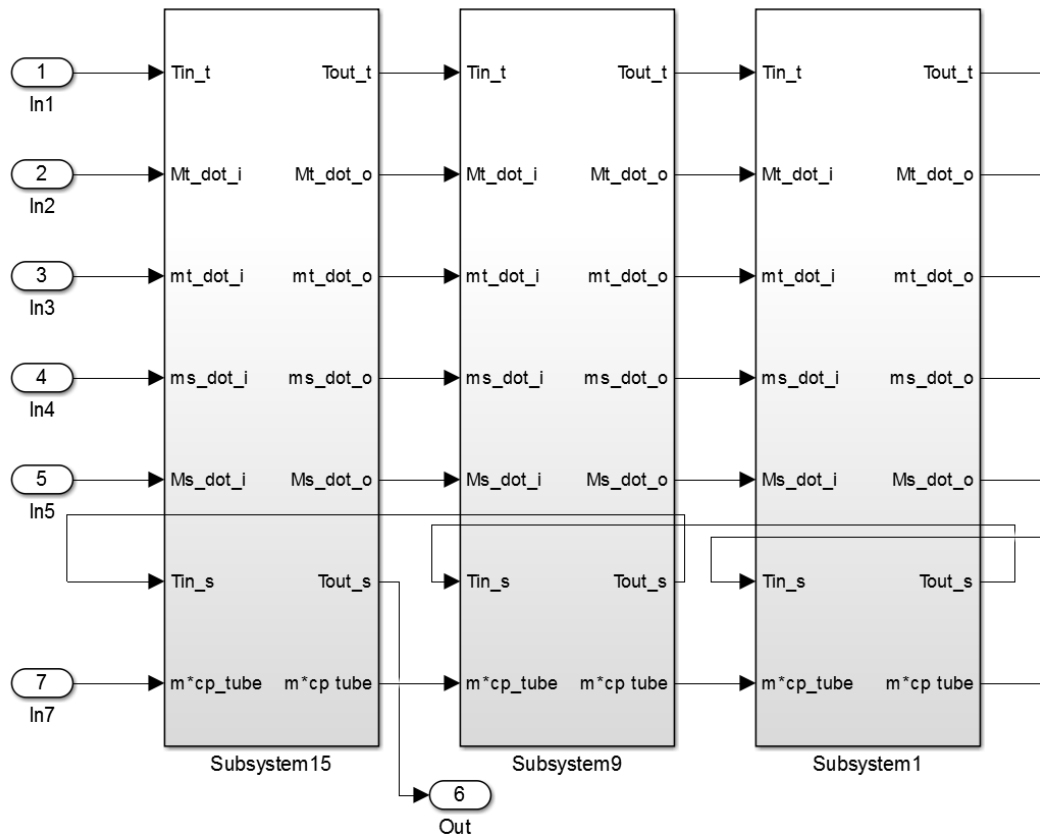


Figure 5.6 Simulink block diagram of the discretised exchanger model

The block diagram of each cell can be seen in Figure 5.7. Sensible energy in the tube material is accumulated in the “integrator 1” block. The block “tube side” calculates the heat transfer rate between the mass of the tube and the bulk of the fluid flowing through the tube side and the tube cell outlet temperature. Similarly, the block “shell side” calculates the heat transfer rate between the mass of the tube and the bulk of the fluid flowing through the shell side and the shell cell outlet temperature.

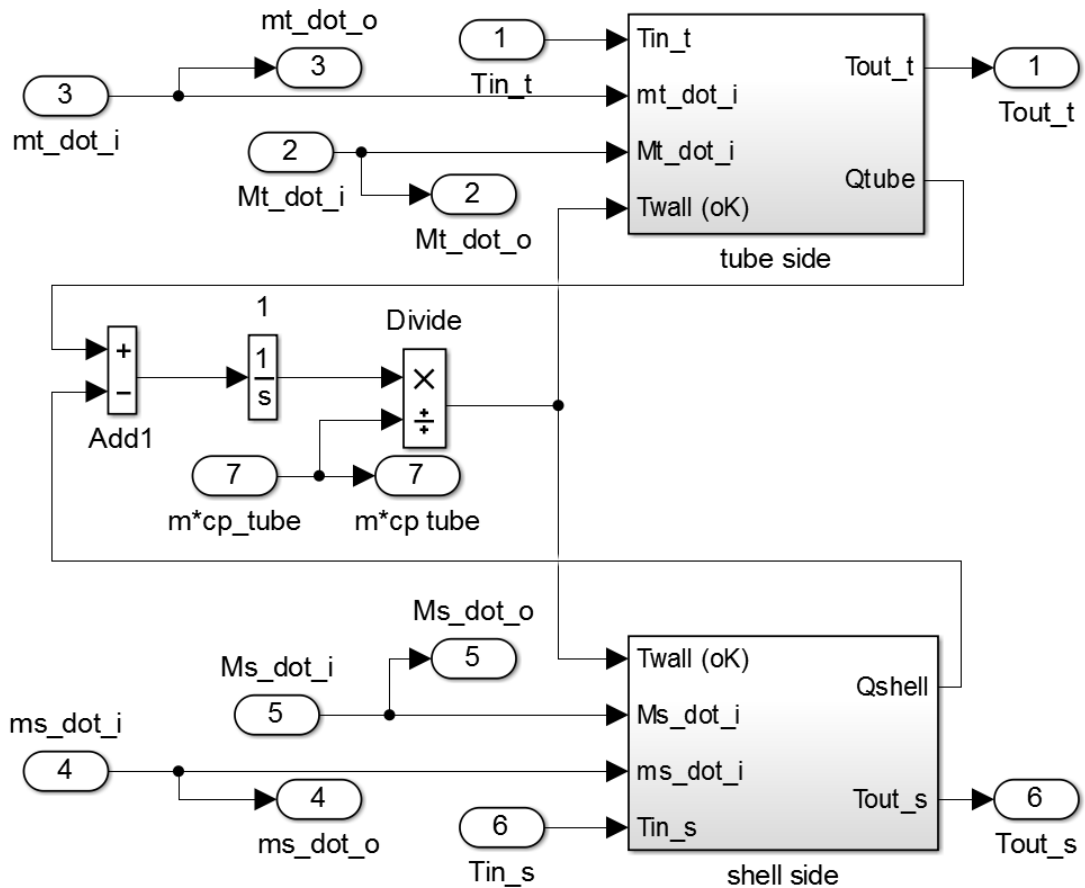


Figure 5.7 Simulink block diagram of each heat exchanger cell

The block diagrams of blocks “tube side” and “shell side” can be seen in Figure 5.8 and Figure 5.9 respectively. Each block consists of a thermodynamic table block that calculates the fluid properties at the average boundary layer temperature. A respective embedded Matlab function uses the calculated fluid properties, the fluid mass flow rate and the geometrical characteristics of the flow cross section to calculate the heat transfer coefficient of the tube side and the shell side. The calculated heat transfer coefficient is then used in conjunction with the bulk temperatures of the two flow streams and the incremental mass to calculate the heat exchange rates between the two fluid streams and the tube wall. The outlet temperature of each stream is calculated by means of using the heat transferred to or from the tube wall and the stream mass flow rate. After the specific enthalpy of the outlet is calculated, it is used as input to a lookup table that returns the respective outlet temperature.

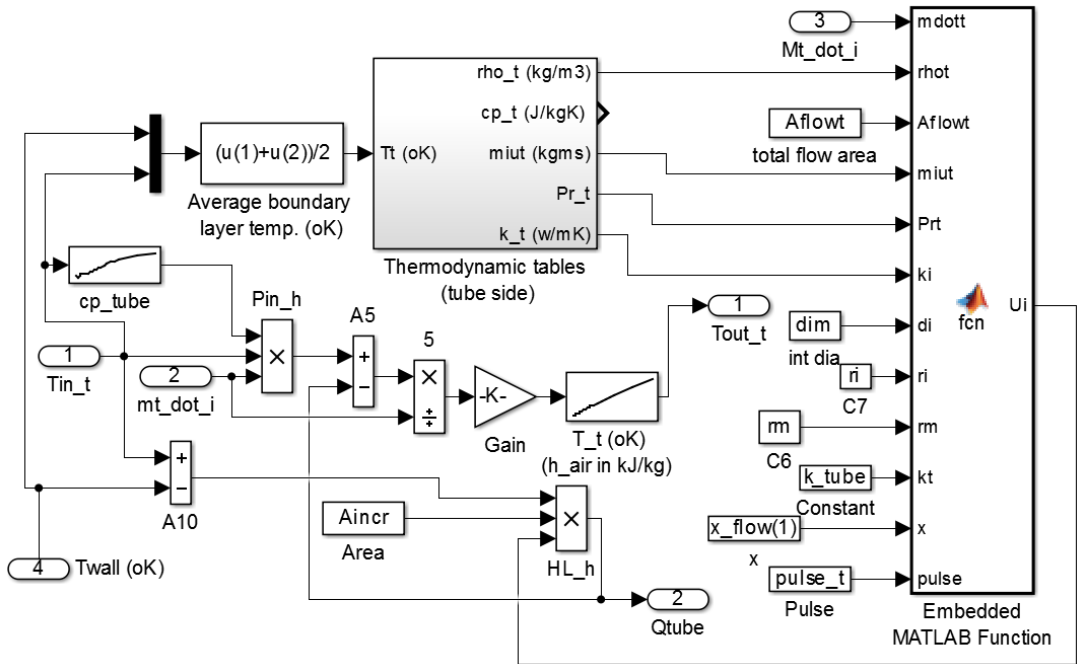


Figure 5.8 Simulink block diagram of the "tube side" block

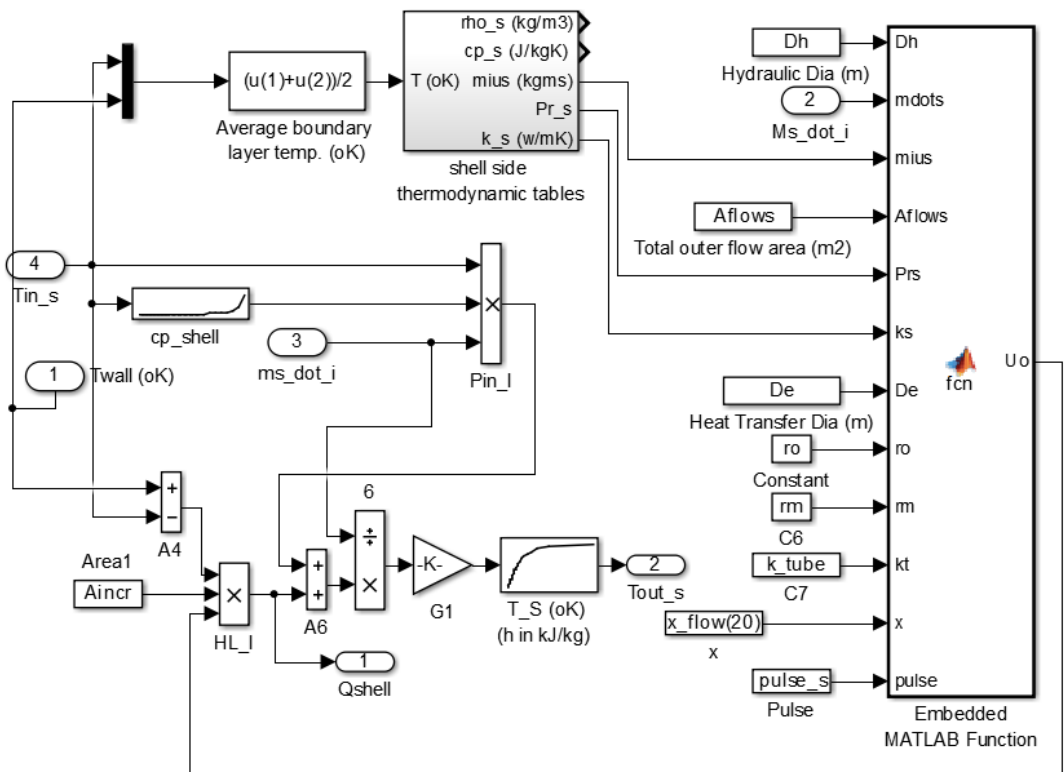


Figure 5.9 Simulink block diagram of the "shell side" block

### 5.5. Coil type heat exchanger

The coil type heat exchanger consists of a coil commonly made of copper tube that exchanges heat from and to a thermal storage tank. A 3d CAD model of the general shape of the coil is shown in Figure 5.10. Since a fully mixed heat storage tank model will be used, and for the sake of simplicity, the modelling problem is handled as a straight single tube water to water heat exchanger with all the shell side cells sharing the same storage tank temperature, and the same heat transfer mechanism of natural convection. Thus, the model of the storage tank coil will use a variation of the shell and tube model structure as presented in section 5.3.

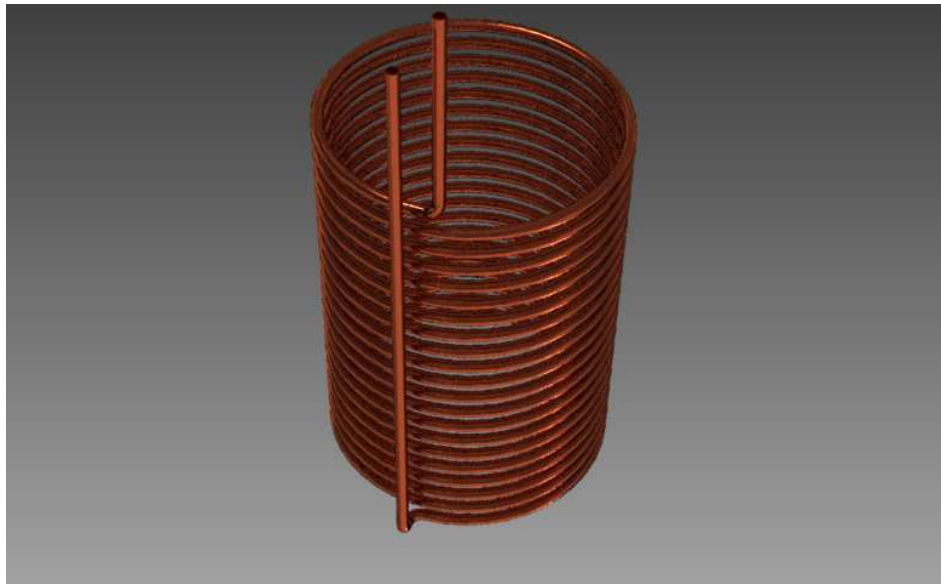


Figure 5.10 3d CAD model of a coil type heat exchanger

The heat transfer mechanism on the outer tube surface is considered to be free convection and will be modelled as a horizontal tube of the same total unwound length. For this reason, mass flow rate is not used in the heat transfer calculations of the outer tube surface. Nusselt number for the outer tube side is calculated using the methodology as found in F.P. Incropera et al. [106] and analysed below.

Grashof number  $Gr$  is defined as the ratio of the buoyant over the frictional forces acting upon the heated fluid and is calculated from:

$$Gr = \frac{d_o^3 \rho^2 g \Delta T \beta}{\mu^2} \quad (5.26)$$

Where  $d_o$  the outer tube diameter in  $m$ ,  $\rho$  the density of the surrounding fluid in  $kg/m^3$ ,  $\Delta T$  the temperature difference between the surface of the solid and the bulk of the fluid in  $^{\circ}C$ , and  $\beta$  the coefficient of volume expansion of the surrounding fluid in  $1/^{\circ}C$ .

In the case of ideal gasses such as Air:

$$\beta = \frac{1}{T(^{\circ}K)} \quad (5.27)$$

Rayleigh number  $Ra$  describes the principal mode of heat transfer in non forced convection conditions and is calculated from:

$$Ra = GrPr \quad (5.28)$$

Where  $Pr$  is the Prandtl number of the surrounding fluid.

The Nusselt number of naturally convected heat transfer between a horizontal cylinder and the surrounding fluid is calculated from:

$$Nu = \left\{ 0.60 + \frac{0.387Ra^{1/6}}{(1 + (0.559/Pr)^{9/16})^{8/27}} \right\}^2 \quad (5.29)$$

The discretised coil model layout is based on the shell and tube HE model as shown in Figure 5.11 with the tube side being unchanged. The main difference lies in the outer tube surface submodel where the bulk temperature for all cells is assumed to be kept constant throughout the coil length as can be seen in Figure 5.11 as well as the Simulink model block diagram of Figure 5.12.

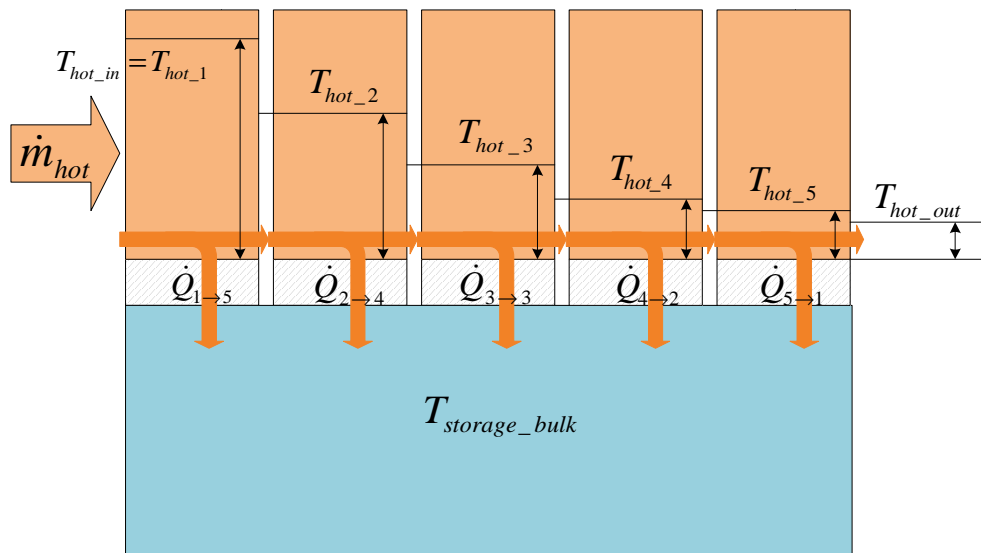


Figure 5.11 Schematic of the discretised coil type heat exchanger model

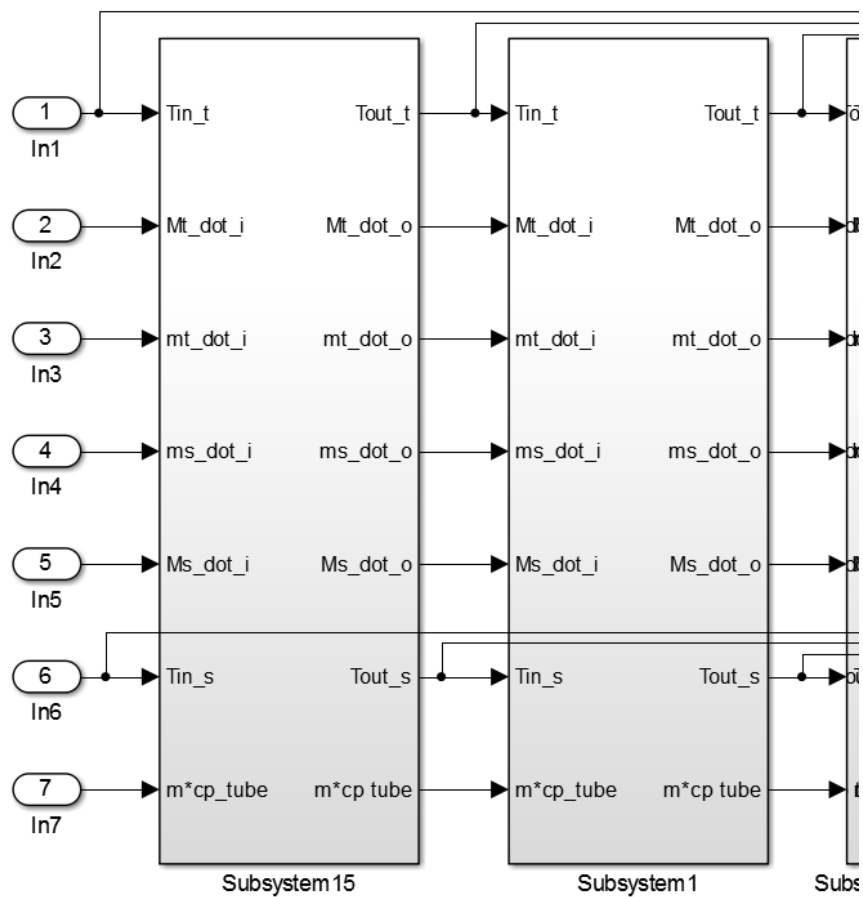


Figure 5.12 Segment of the discretised coil type heat exchanger model on Simulink

Again, in the Simulink block diagram, each block is a single cell as can be seen in Figure 5.13.

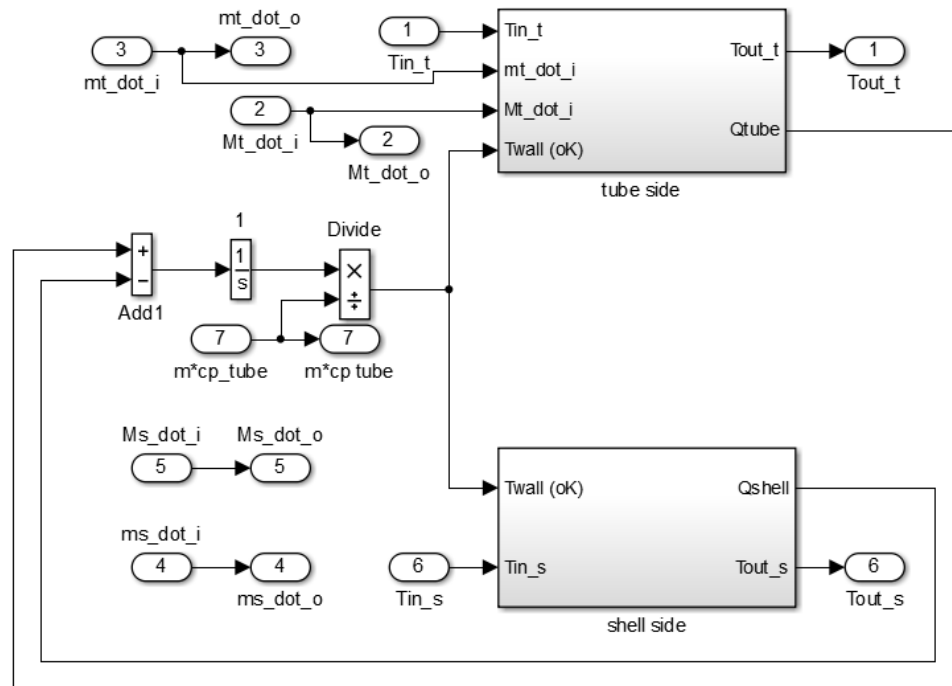


Figure 5.13 Simulink block diagram of a coil type heat exchanger cell

The “tube side” block is the same as in the case of the shell and tube heat exchanger. The “shell side” block whose Simulink block diagram is shown in Figure 5.14, is separately developed to calculate the natural convection heat transfer coefficient and the transferred heat of a horizontal pipe. The embedded Matlab function contains code using equations ( 5.26 ) to ( 5.29 ).





The main heat transfer mechanisms present during its operation are forced convection for the internal surface (water side) and natural convection for the external surface (air side). The modelling procedure of the radiators will be similar to that of the heating coil but in this model, only one cell is used due to the inability for the adjacent air temperature distribution to be calculated along the direction of the water flow, unless the model is of two or three dimensions. A schematic of the general model layout can be seen in Figure 5.16.

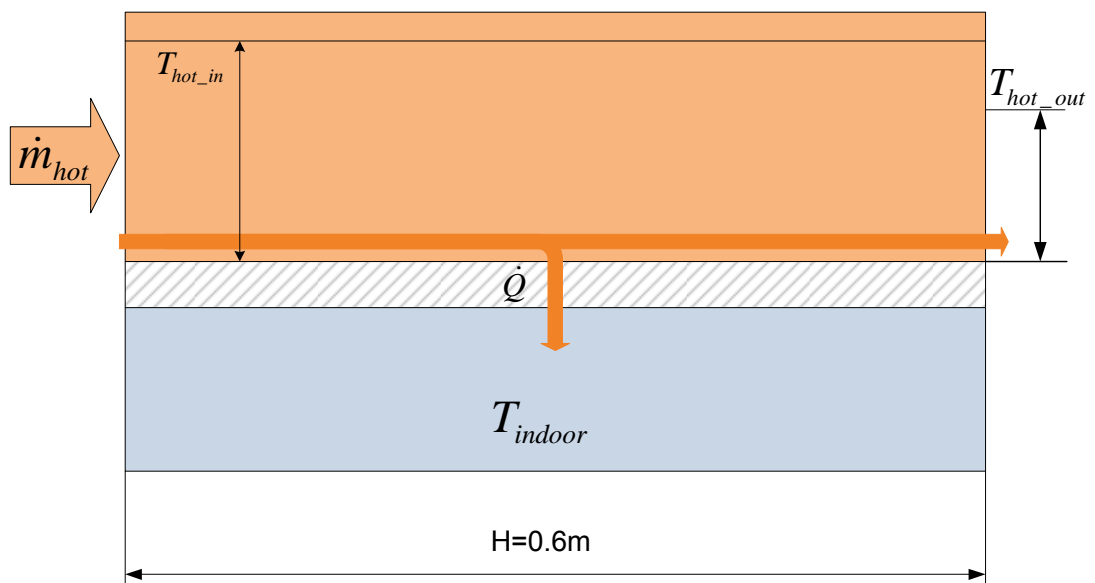


Figure 5.16 Schematic of the of the radiator model rectangular element

Again, an elemental section will be modelled and simulated by the developed interface to obtain a lookup table model which will be used in the main CHP models of Chapter 7. The heat transfer on the external surface of the elemental radiator is treated as a natural convection on a vertical plate.

For  $Ra \leq 10^9$ , Nusselt number is calculated from:

$$Nu = 0.68 + \frac{0.670Ra^{1/4}}{(1 + (0.492/Pr)^{9/16})^{4/9}} \quad (5.30)$$

And for  $Ra > 10^9$

$$Nu = \left\{ 0.825 + \frac{0.387Ra^{1/6}}{(1 + (0.492/Pr)^{9/16})^{8/27}} \right\}^2 \quad (5.31)$$

A 2-pipe system will be considered in the current study. In such configuration, all radiator elements in the dwelling are connected in parallel leading to a very uniform temperature distribution and performance in all areas of the house, provided that each radiator is regulated to ensure that all elements have almost identical inlet conditions regardless of any differences in size between the connected radiators. Therefore, the radiators in the CHP main model may be represented by a single properly sized lumped radiator model which for given inlet conditions results in the specified heat transfer rate.

### **5.7. Heat Exchanger Simulation and Mapping Tool**

The developed graphical user interface shown in Figure 5.17 and Figure 5.18, is supported by relevant code that allows the user to configure the heat exchanger main geometrical characteristics as entered in panel "Input Data", and the desired inlet and outlet conditions to perform preliminary heat exchanger sizing. The function of preliminary heat exchanger sizing returns a rough estimate of the necessary number of tubes and shell diameter of a shell and tube type heat exchanger. One of the most important functions of the tool is the control of the simulation of the discretised Simulink models, and the calculation of the outlet temperature time constant, the steady state outlet temperatures, and the steady state transferred heat. All sides of the heat exchanger model can be simulated for either constant or pulsating flow.

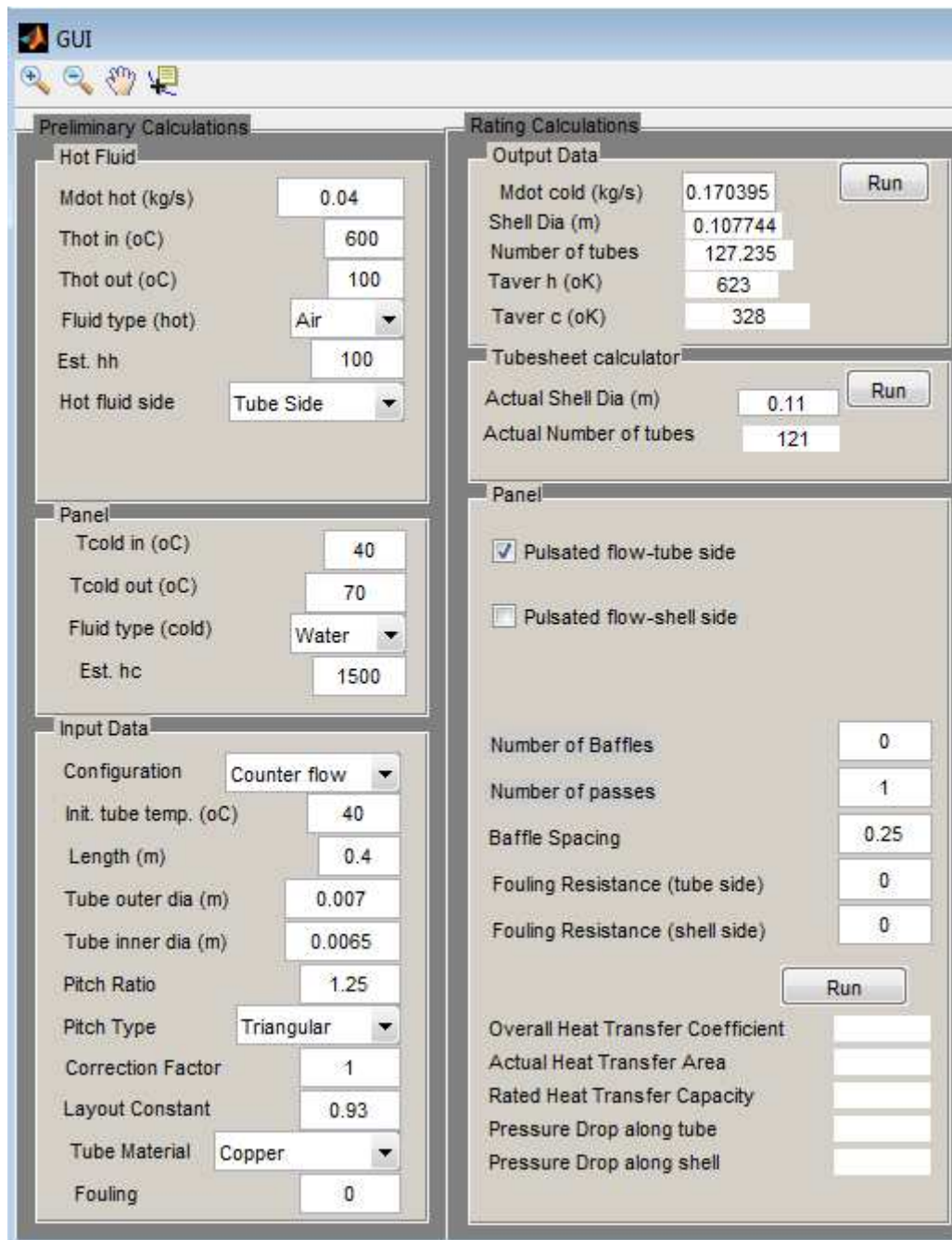


Figure 5.17 Parameter input panel

When the simulation is complete, graphs of the time response of the two heat exchanger outlets are plotted as shown in Figure 5.18. An animation of the temperature distribution along both sides of the heat exchanger may also be played by pressing the button “Play Animation”. The function of the tool that is essential for the development of lookup table based models is the map generation controlled by the button “Generate Map” as can be seen in

Figure 5.18. The minimum and maximum values of the inlet conditions and the number of samples of each variable are set on the panel. Once the simulation process is complete, the software generates maps that contain the steady state outlet temperatures and steady state heat transfer rate, and the time constants of each heat exchanger outlet stream. In order for the resulting maps to be scalable, the mass flow rate breakpoints and heat transfer rate are recorded in a per tube format. Therefore, it is just a matter of using a scalar multiplier to generate a case specific, sized lookup table based heat exchanger or radiator model.

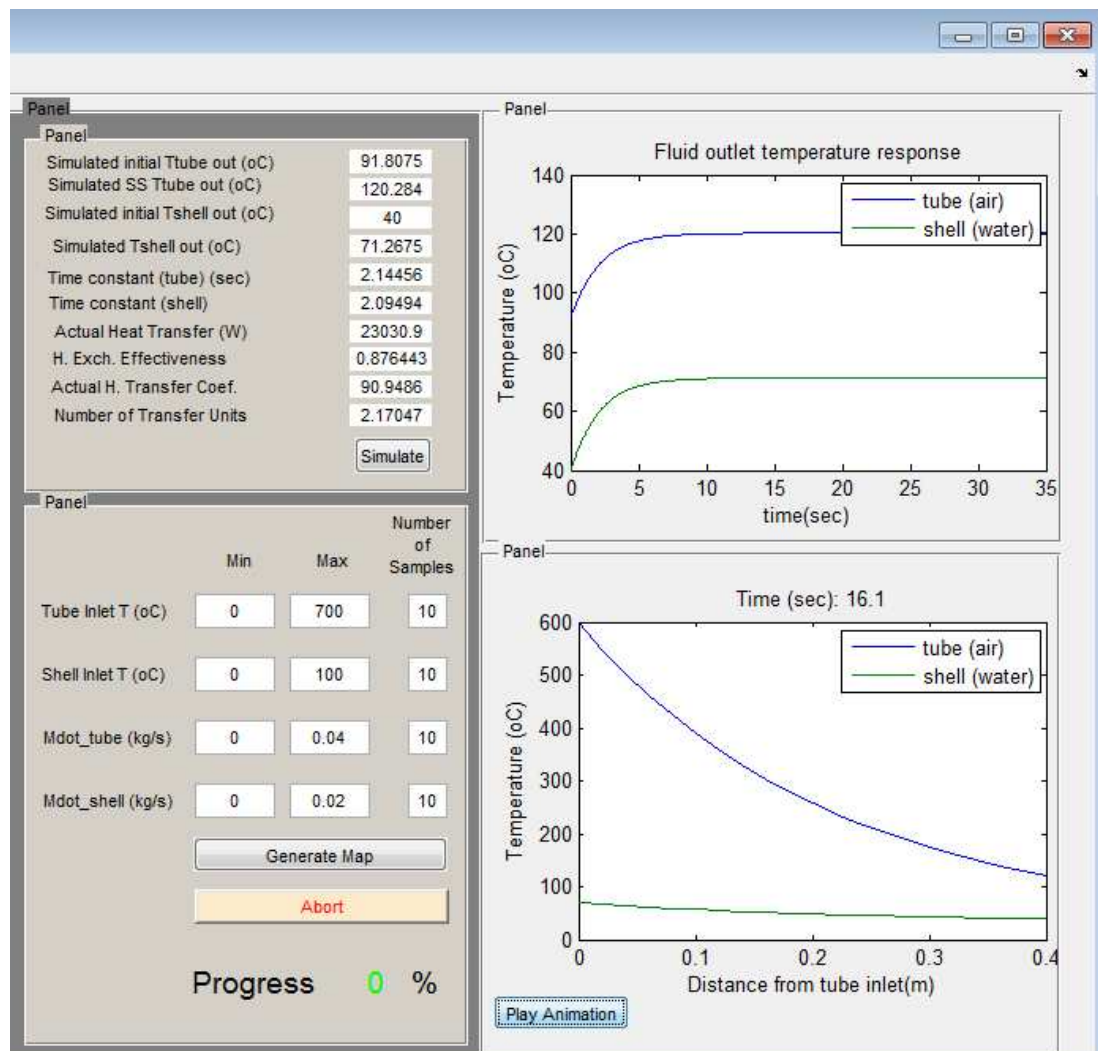


Figure 5.18 Results display and mapping panel

## 5.8. Lookup table based quasi - stationary models

Following the generation of the necessary heat exchange performance maps, the lookup table based models that will be used in the general micro-CHP model as presented in Chapter 7 are developed in the following sections.

### 5.8.1. The shell and tube heat exchangers

The Simulink block diagram of the quasi - stationary exhaust heat exchanger model is shown in Figure 5.19. Fluid inputs and outputs are data structures that consist of the mass flow rate and the temperature of the fluid. The core of the exhaust heat exchanger model is the 4 – D lookup table titled “T\_tube out (oC)” which returns the tube outlet temperature for given tube and shell inlet mass flow rates and temperatures. The tube outlet rate of sensible heat is then calculated in the block “exhaust heat” and is subtracted from the tube inlet rate of sensible heat in the subtraction block “A3” to calculate the rate of heat loss or gain between the tube inlet and outlet. This rate of heat is added to the shell side by means of addition block “A6” to calculate the shell outlet specific enthalpy. The outlet specific enthalpy is then used as an input to the lookup table “T\_W” that calculates the shell outlet temperature for the given specific enthalpy. The saturation block prevents the division block “6” from dividing the heat output rate of block “G3” by 0.

A similar but slightly modified structure is used by the jacket water heat exchanger model of which the block diagram is shown in Figure 5.20. In this case, the enthalpy entering the tube side is calculated inside the block through the product block “Pin\_I1”. Product block “Pin\_I2” calculates the enthalpy of the tube outlet. The heat transfer rate is calculated in the product block “Pin\_I3”.

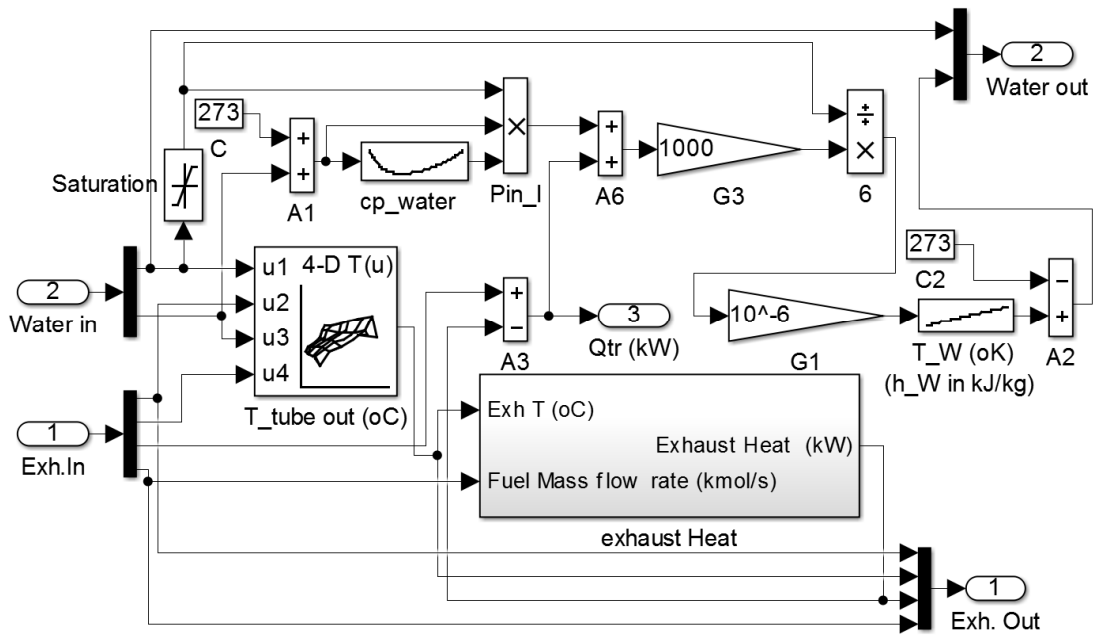


Figure 5.19 Block diagram of the lookup table based exhaust gas heat exchanger model

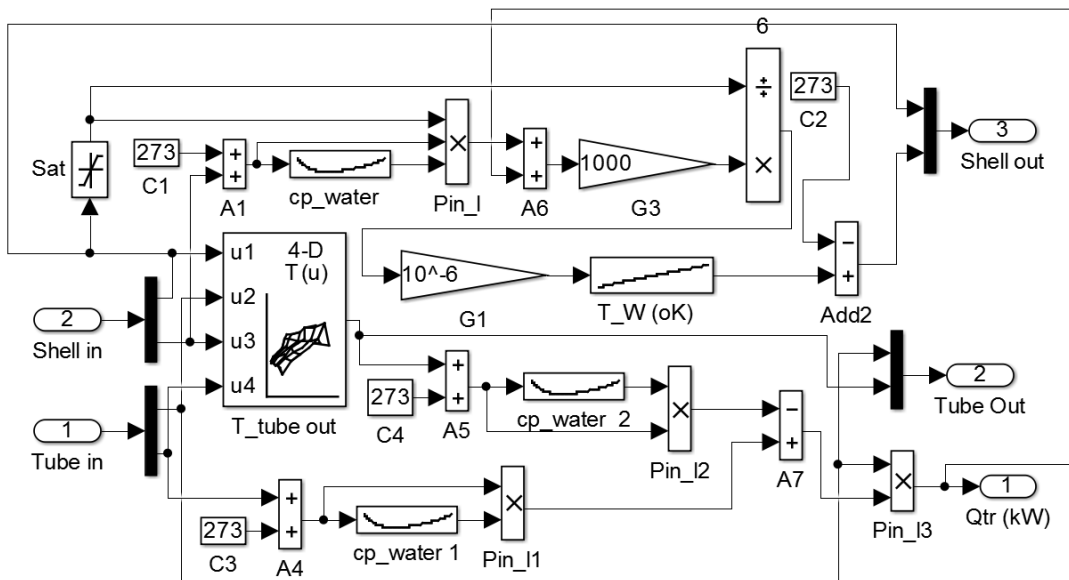


Figure 5.20 Block diagram of the lookup table based jacket water heat exchanger model

### 5.8.2. The storage tank coils

As in the case of the shell and tube heat exchangers, the quasi-stationary tank coil models shown in Figure 5.21 and Figure 5.22 are based around a lookup table that returns the tube outlet temperature, but instead of using 4 inputs, the coil lookup tables use a 3D map. The tube inlet temperature and mass flow rate, and the tank water temperature.

The outputs of the coil HE blocks are the water outlet and the rate of heat transfer. Transferred heat for both the coil to radiators model of Figure 5.22, and the coil to CHP model of Figure 5.21, is either added or subtracted to the stored heat depending on the involved temperatures as may also be observed in Figure 7.11.

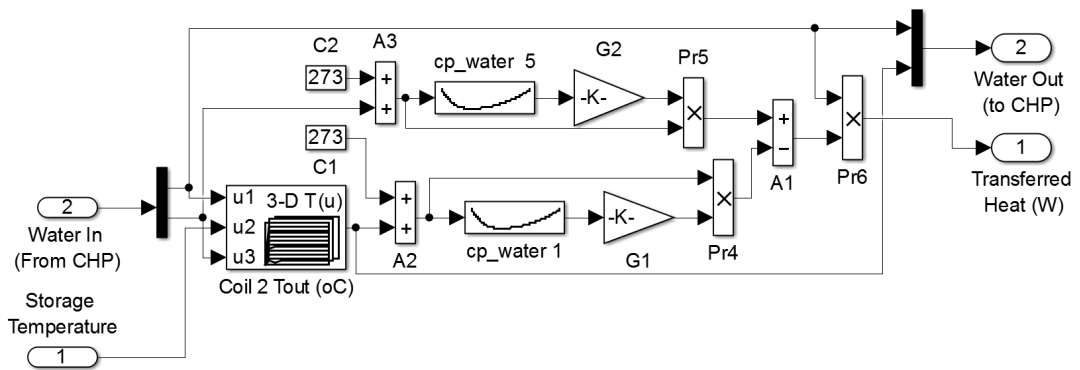


Figure 5.21 Block diagram of the primary circuit coil type heat exchanger model

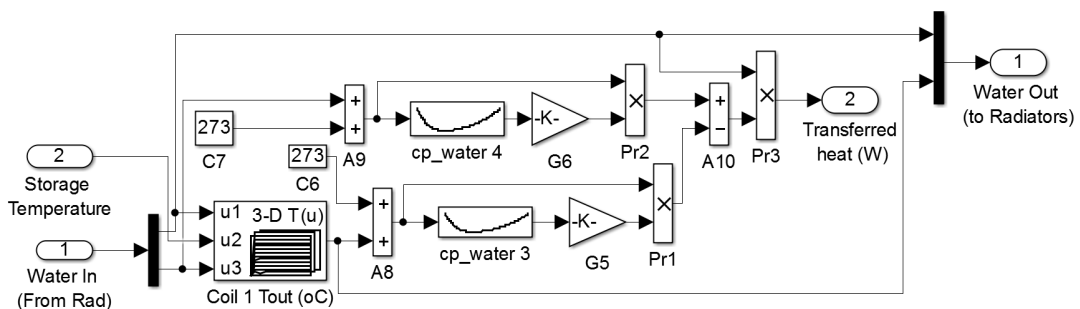


Figure 5.22 Block diagram of the secondary circuit coil type heat exchanger model





of all heat exchange devices were generated and used to populate the lookup tables of the quasi-stationary models. The resulting component models have been found to work as intended predicting outlet conditions while placing a low computational load on the computing system. It is concluded that the combination of the developed simulation software package, along with the quasi-stationary models are a cost effective and time saving proposal for modelling applications where the inlet conditions do not remain constant.

## Chapter 6 UK Dwelling Models

The use of realistic heat and power demand profiles is of great significance for the collection of meaningful simulation results. While as discussed in section 3.5, representative usage profiles of electricity and hot water consumption do exist in literature, no profiles of space heating demand have been found, mainly due to the fact that heat demand may be met by using numerous strategies and rated heat outputs. For this reason, a basic building thermal model combined with weather data will be necessary in order to simulate thermal demand. Since average values of dwelling thermal characteristics encountered in literature were not accompanied by the dwelling geometrical characteristics which can be important when dwelling and indoor air thermal masses are considered, and when the modelling of two or more dwelling construction methods is desired, the thermal characteristics of UK dwellings will be modelled using dwelling representative geometrical characteristics and material properties as found in literature. Curves of representative dwelling thermal characteristics as a function of floor area for each dwelling type and for two construction periods will be generated and integrated in the libraries of the energy simulation software presented in section 7.2.

### 6.1. Dwelling models for simulation

While dedicated building simulation software do exist and produce very accurate case specific results, by taking into account a very large number of parameters and using computationally intensive 3-Dimensional CFD algorithms, at the same time they are highly sophisticated and require long learning curves as well as model development times which might not be practical for modellers with no architectural/civil engineering background and whose study mainly focuses on the DES performance. In addition, the long simulation time they require makes them impractical in applications where a large volume of results is necessary in a short period of time such as in sensitivity analyses and optimization applications. Thus, the existence of

simple, easy to use representative UK 1-D dwelling models can be useful for certain applications.

A literature review carried out prior to this study did not yield any appreciable results regarding existing easy to use representative UK dwelling models. The aim of the current chapter is the development of a series of 1-D dwelling models which cover the small residential UK sector, and will serve as a basis for the evaluation of DES such as micro-CHP in terms of their performance and suitability for a particular application.

## **6.2. The importance of dwelling model diversity**

As discussed in section 3.1.3, a number of researchers including C. D. Aussant [20], M. De Paepe et al. [32] and M. Bianchi et al. [43] reported that the optimal selection of the type and size of a micro-CHP system is case specific. This means that for a different application, a different heating system type/size combination might give best technical and economical results. Dwelling size, type, and age are the most important factors on heat losses, and thus they define the technical and economic viability of a heating system to a great extent. For this reason, a model of a single type and age may not be sufficient to cover studies on the totality of the small residential sector in the UK, and for this reason, it has been decided to build representative models of all relevant dwelling types for two different construction periods. A series of dwelling model types will represent modern standards of construction (post-1967), and another series of house models that exhibit considerably higher losses and will represent older/obsolete standards of construction (pre-1967).

## **6.3. Geometrical characteristics of typical UK dwellings**

In order to create typical dwellings geometries, one must first know the average floor area of each dwelling type, and the most commonly encountered relationships/ratios between the basic dimensions/areas for each dwelling type

Peter F. Chapman [110] collected a large volume of geometrical data on dwellings and entered them into classes of age and type. For each class, he performed a quadratic interpolation between the number of rooms and the total dwelling area, as well as a linear interpolation between the total dwelling area and total window area. Additionally, typical ceiling heights and floor aspect ratios are given. By inputting different room numbers for a given combination of dwelling type and dwelling age group, different total house areas and window areas will be calculated. Using ceiling height and the geometrical characteristics of each dwelling type, one can then calculate the exposed wall area, ground floor area and roof area. These models will provide the current study with adequate information through which the typical thermal characteristics of UK homes will be calculated. The input/output diagram of the dwelling geometrical model of Peter F. Chapman [110] is shown in Figure 6.1.

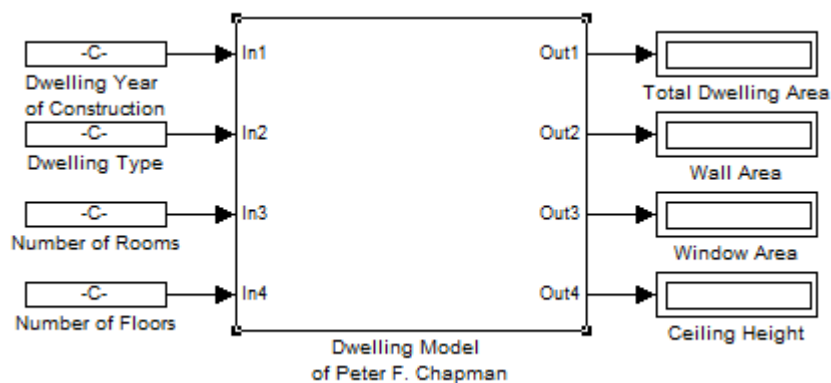


Figure 6.1 I/O Diagram of the building model of Peter F. Chapman [110]

#### 6.4. Statistical data on UK dwellings

The Housing Stock Report 2008 [111] provides statistical information on several dwelling geometries and construction characteristics, elements of which will be used for the development of the dwelling models. One of the defining parameters for the heat losses of a house is its total exposed area  $A_{total}$  ( $m^2$ ). For a given floor area  $A_{floor}$  ( $m^2$ ), the number of storeys  $n_s$

heavily influences the exposed area and as a result, it also defines the Heat Loss Parameter (*HLP*) which is the rate of heat loss per unit of usable floor area  $A_{floor}$  per degrees Kelvin of temperature difference between the indoors and the outdoors ( $kW/m^2 \cdot ^\circ K$ ). A schematic of the position of each dwelling type in relation to neighbouring dwellings is shown in Figure 6.2.

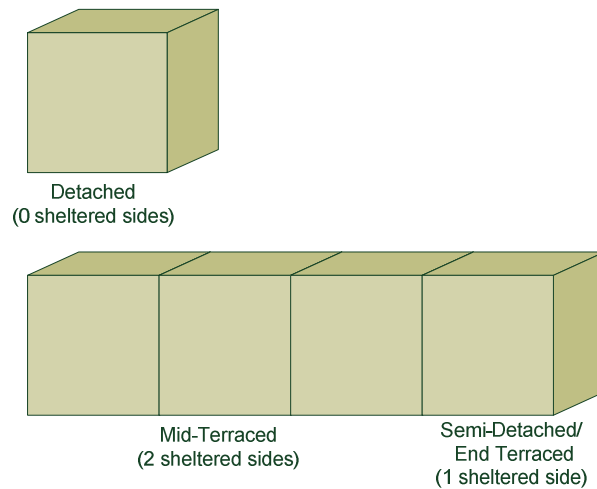


Figure 6.2 Representation of different dwelling layouts in space

The statistical data on the composition of UK dwellings per number of storeys as sourced from Housing stock report 2008 [111] and contained in Table 6.1 shows that 2-storey houses are most frequently encountered of all configurations. Due to the 2-storey houses being almost 8 times more common than the second candidate, and since no statistical data on the number of storeys for each individual dwelling type for a given construction period have been encountered, the 2-storey configuration is selected as default for the calculations of all preliminary models but the bungalows which are by definition of a low rise design and single storey.

Table 6.1 Statistical composition of UK dwellings per number of storeys

Number of Storeys	Percentage of all houses (%)
1 Storey	11.5
2 Storey	79.6
3 Storey	8.6
4 Storey	0.2

Another important geometrical characteristic is the typical floor area for a given house type. The Housing stock report 2008 [111] lists mean floor surface values of each house type. No values separated in terms of different age groups have been found in the researched literature. For this reason, the mean area of each house type as found in [111] and shown in Table 6.2 will be used for both age groups.

Table 6.2 Average Total Dwelling Areas per dwelling type

Dwelling Type	Total Area ( $m^2$ )
Small Terraced	82.3
Medium/Large Terraced	82.3
Semi-Detached	92.5
Detached	147.1
Bungalow	76.0

Since the dwelling geometrical model developed by Peter F. Chapman [110] (whose calculation block diagram is shown in Figure 6.1) does not distinguish between small and medium/large terraced houses, but rather makes a distinction between End-Terraced and Mid-Terraced houses, the values of the typical Small Terraced and Medium Terraced house floor areas are weight averaged in order to obtain a representative area value for all terraced houses using floor area values and percentages of each house type extracted from the Housing stock report 2008 [111].

## 6.5. An overview of heat loss calculations

There are two main mechanisms of heat loss in a building:

a) Transmission losses through the various construction components whose totality constitutes the dwelling fabric. Under this mechanism, a differential between the indoor and the outdoor temperature results in heat transfer by means of conduction and convection from the warm area towards the cold area. In a dwelling, the main construction elements that define the boundaries of the indoor space from the environment are walls, windows, roof and ground floor. The transmission loss rate of any individual construction element subjected to a temperature differential is calculated as follows:

$$\dot{Q}_{i\_fabric} = A_i U_i \Delta T = A_i U_i (T_{indoor} - T_{outdoor}) \quad (6.1)$$

Where  $\dot{Q}_{i\_fabric}$  is the heat loss rate of any individual construction element in  $W$ ,  $A_i$  the surface area in  $m^2$ ,  $U_i$  the heat transfer coefficient in  $W/m^2 \cdot ^\circ K$  of the individual components.

Figure 6.3 shows the direction of transmitted heat through a fabric component when the indoor temperature is higher than the ambient. Heat transfer coefficient is calculated from:

$$U_i = \frac{K_i}{X_i} \quad (6.2)$$

Where  $X_i$  is the component thickness in  $m$ , and  $K_i$  the thermal conductivity of the material in  $W/m \cdot ^\circ K$ . In related literature, the heat transfer coefficients of each material/component type are usually provided and need not be calculated.

In Figure 6.4, a wall with a window in the middle is pictured with their respective areas and heat transfer coefficients.



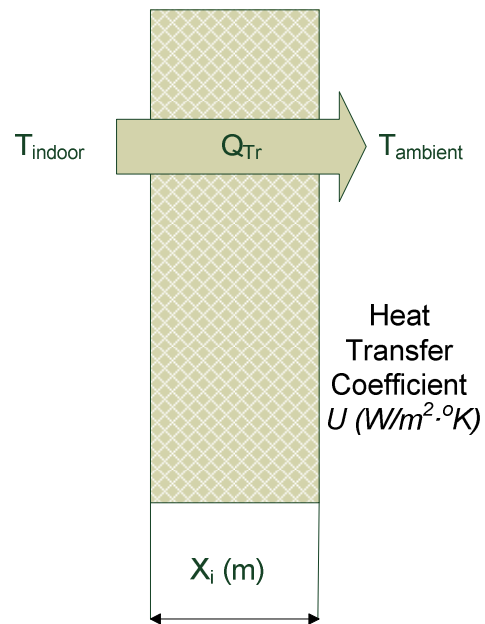


Figure 6.3 Cross section of a heat transfer surface

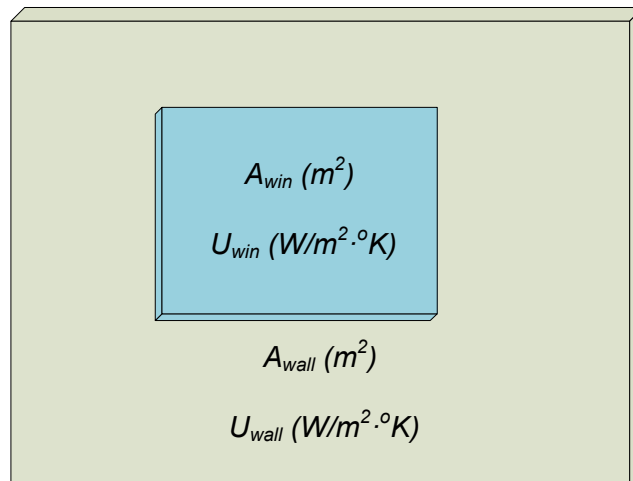


Figure 6.4 Sketch of a wall fitted with a window

The sum of the transmission loss rates of the individual dwelling components constitutes the total dwelling fabric transmission loss rate:

$$\begin{aligned}
 \dot{Q}_{fabric} &= \sum \dot{Q}_{i\_fabric} = \\
 &= \dot{Q}_{win} + \dot{Q}_{wall} + \dot{Q}_{roof} + \dot{Q}_{ground} = \\
 &= (A_{win}U_{win} + A_{wall}U_{wall} + A_{roof}U_{roof} + \\
 &\quad + A_{ground}U_{ground})(T_{indoor} - T_{outdoor})
 \end{aligned} \tag{6.3}$$

Therefore, in order to obtain the total transmission loss rate characteristics of a building, one must calculate:

$$\sum_{i=1}^n (A_i U_i) \quad (W/^{\circ}K) \tag{6.4}$$

b) Air infiltration due to imperfections in the construction as well as purposely built ventilation necessary to keep indoor air quality at healthy levels. According to the 1997 ASHRAE Fundamentals Handbook (SI) [65], a total infiltration rate of more than 0.5 Air Changes per Hour (*APH*) might be necessary for maintaining an acceptable air quality. One *ACH* (Air Change per Hour) is one complete replacement of the indoor air volume in one hour. Thus, for the same value of *ACH*, a house of a greater volume will have a proportionally higher air volume flow rate and infiltration related heat losses. The concept of *ACH* is useful in the implementation of empirical *ACH* values to scale air infiltration effects for any given dwelling size. The heat loss rate due to air infiltration is calculated from:

$$\dot{Q}_{inf} = c_{p\_air} \rho_{air} V_{intern} ACH (T_{indoor} - T_{ambient}) \tag{6.5}$$

Where  $c_{p\_air}$  the specific heat of air in  $W/kg^{\circ}K$  and  $\rho_{air}$  the density of air in  $kg/m^3$ . Therefore, one needs to calculate the internal volume of the building  $V_{intern}$  in  $m^3$  and the Air Change Rate by implementing a standardized procedure such as the ones found in the SAP 2005 [47], ASHRAE Fundamentals Handbook (SI) [65] or other relevant sources.

The sum of the fabric and air infiltration heat loss rates comprises the total heat loss rate of a dwelling:

$$\dot{Q}_{total} = \dot{Q}_{fabric} + \dot{Q}_{inf} \quad (6.6)$$

The thermal characteristics of the dwelling models in the current study will be calculated following The Government's Standard Assessment Procedure for Energy Rating of Dwellings - SAP 2005 V. 9.81/9.83 [47] which is a standardised method for calculating the thermal performance of a given dwelling, and whose input/output diagram is shown in Figure 6.5.

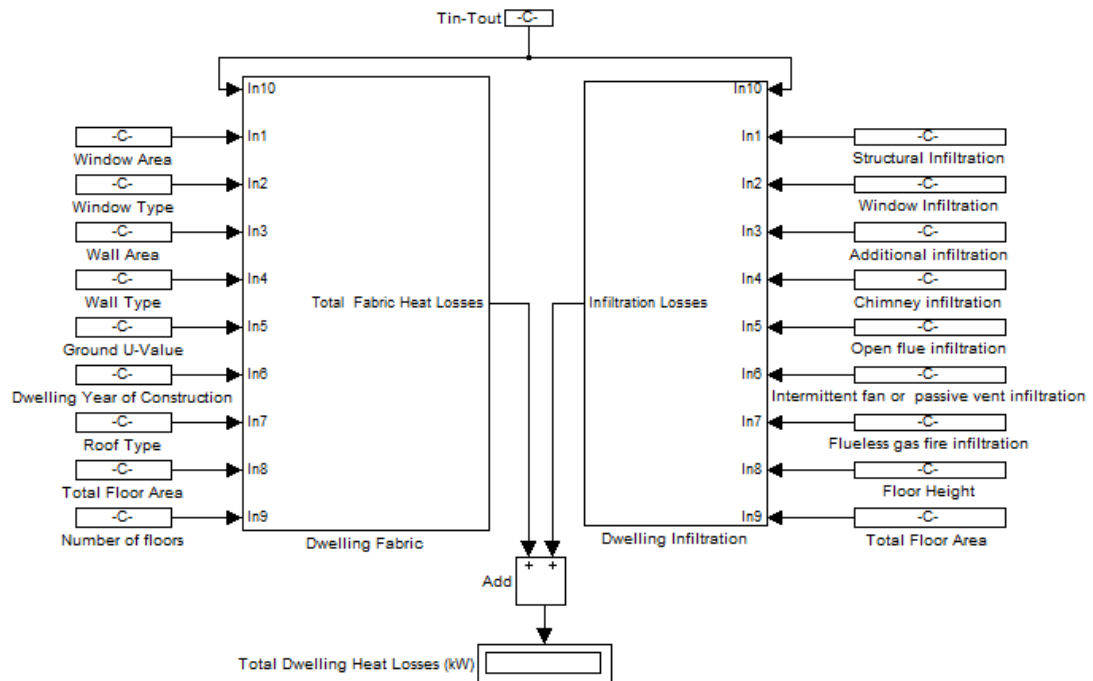


Figure 6.5 I/O block diagram of heat loss calculations

## 6.6. Thermal characteristics of dwelling fabric components

As seen in the section 6.5, the component materials, along with the building geometry, are key factors in the transmission losses of the building. In order to construct thermally representative dwelling models, materials most likely to be encountered under given housing specifications must be selected and their characteristics be used as input. The product of the Heat Loss Parameter and the total floor area gives the dwelling Heat Loss Coefficient:

$$U \times A = HLP \times A_{floor} (W/^{\circ}K) \quad (6.7)$$

The more general form of the Heat Loss Parameter calculation is shown in eq. ( 6.8 )

$$HLP = \frac{\sum_{i=1}^n (A_i U_i) + c_{p\_air} \rho_{air} V_{intern} ACH}{A_{floor}} \quad (6.8)$$

The dwelling configuration specific algebraic manipulations of the above equation as well as the formulas that calculate the exposed area sourced from Peter F. Chapman [110] yield the following relationships of heat loss parameter for different dwelling types.

For detached dwellings:

$$HLP_{det} = \frac{((2 + 2\epsilon)hYn_s - A_{win})U_{wall}}{A_{floor}} + \frac{U_{ground} + U_{roof}}{n_s} + c_{p\_air} \rho_{air} hACH \quad (6.9)$$

For semi-detached dwellings:

$$\begin{aligned}
 HLP_{semi} = & \frac{((2 + \epsilon)hYn_s - A_{win})U_{wall}}{A_{floor}} + \\
 & + \frac{U_{ground} + U_{roof}}{n_s} + c_{p\_air}\rho_{air}hACH
 \end{aligned}
 \tag{6.10}$$

For terraced dwellings:

$$\begin{aligned}
 HLP_{terr} = & \frac{(2hYn_s - A_{win})U_{wall}}{A_{floor}} + \\
 & + \frac{U_{ground} + U_{roof}}{n_s} + c_{p\_air}\rho_{air}hACH
 \end{aligned}
 \tag{6.11}$$

Where  $Y$  the length of the long side of the house in  $m$ ,  $\epsilon$  the aspect ratio of the dwelling floor,  $h$  the dwelling height in  $m$ .

## 6.7. Dwelling age groups

From building component thermal characteristic data tables found in SAP 2005 V. 9.81/9.83 [47], it has been observed that for most wall types, age group E (1967-1976) was the period during which a notable reduction in U-values began to occur, while for pre 1967 houses, U-values were considerably higher and did not change between age groups. This indicates a change in building practices during that period in an effort to achieve more economically favourable building thermal characteristics.

In order to create models that represent commonly encountered building geometries in the UK and also to account for the differences between

thermal performance of older and more modern buildings, the current chapter, will distinguish models based on their thermal characteristics in two main groups: A series of typical low performance pre-1967 houses and a series of typical post-1967 houses.

## **6.8. Dwelling Fabric**

Two main sources of building component properties have been chosen for the construction of the building models.

The first source of component properties as well as of the methodology of heat loss calculations is SAP 2005 V. 9.81/9.83 [47]. It has been selected over SAP 2012 [112] (the latest SAP version at the time of this writing) due the lack of component property data as well as the fact that the heat loss calculation procedure encountered in the latest version is too case specific for the current application.

The second source used is Y. McNally et al. [113] which contains tables of heat transfer coefficients of dwelling components for different age groups and dwelling types encountered in Northern Ireland. While Northern Ireland is just a fraction of the UK market, a look in SAP 2005 [47], shows that within the UK, building practices between all areas exhibit differences small enough to be neglected. Therefore, some building component data from [113] may be used to adequately represent dwelling characteristics throughout the UK.

### **6.8.1. Walls**

The majority of dwellings in all post-1919 groups make use of cavity masonry. For pre-1919 groups, solid masonry is the mostly used type of construction. In addition, houses built between 1919 and 1965 comprise 36.7% of all existing dwellings compared to pre-1919 houses comprising 21.5% of total [47]. This observation makes the cavity masonry a more logical selection for representing pre-1965 houses.

According to the Housing Stock Report 2009 [114], 50% of all existing dwellings with cavity walls were by that time insulated while in 1996 this percentage was just 22%, indicating that this percentage is most likely to

increase with time. Wall insulation is a relatively recent practice and would not be representative of pre-1967 dwellings mostly using cavity walls. Therefore, cases of non insulated cavity masonry and filled cavity masonry will be used for pre-1967 and post-1967 houses respectively. In the case of cavity masonry, all 1919-1967 age group entries have a  $U = 1.6W/m^2\text{°K}$ . For post-1967 dwellings, the U-value for filled cavity walls is found in SAP 2005 [47] to be  $U = 0.35 W/m^2\text{°K}$ .

### **6.8.2. Roof**

Roof construction may vary significantly from one dwelling type to another, and for this reason, the roof U-values as listed in Y. McNally et al. [113] will be used for the current model due to being published for different house types and ages.

### **6.8.3. Ground Floor**

As soil type is a significant factor, and depends on building location, it has been decided to adopt the reference floor U-value provided by SAP 2005 [47], as  $U = 0.25W/m^2\text{°K}$

### **6.8.4. Windows**

The most common type of windows encountered in all age groups is the double glazed PVC . SAP 2005 [47] provides a reference U-value for double glazed windows of  $U = 2.0W/m^2\text{°K}$ .

## **6.9. Model Validation**

Since no actual “typical” UK dwellings are currently available for the purpose of measuring their Heat Loss Parameters for the validation of the model results, the validity of the models is investigated by comparing the calculated Heat Loss Parameters (*HLP*) of the modelled dwellings to the Heat Loss Parameter values found in the ECUK: User Guide [115]. No available data have been found that separate the dwellings in each age group and for this reason, the only means to obtain a picture on the validity of the models would be to calculate the weight averaged U-values of the pre-67 and post-

67 U-values shown in Table 6.3 and then compare the results to the data from ECUK: User Guide [115].

As can be seen in Table 6.3, the calculated Heat Loss Parameters exhibit relative errors of 6% or less. While the limited volume of data available for the purpose of model validation does not allow for the most reliable process possible, the low error percentage is nevertheless a good indicator that the models exhibit an adequate degree of realism for the purpose.

Table 6.3 Heat Loss Parameters for different dwelling types

Dwelling Type	Pre-1967 (58.2%)	Post-1967 (41.8%)	Weighted Average	Data from [115]	e%
Detached	4.01	2.32	3.3	3.32	0.7
Semi detached	3.81	2.39	3.22	3.40	5.5
End Terraced	3.95	2.3	3.26	3.47	6
Mid Terraced	4.06	2.01	3.2	3.09	3.6
Detached Bungalow	4.16	2.98	3.67	-	-
Semi detached	3.51	2.81	3.22	-	-
Bungalow (all)	-	-	3.44	3.36	2.4

Table 6.4 contains the basic characteristics of the dwelling models that have been generated based on data from the Housing stock report 2008 [111] and Y. McNally et al [113], the polynomial dwelling model of Peter F. Chapman [110], and the procedure from SAP 2005 [47]. The product of the internal volume and the air density gives the thermal mass of air. The Heat Loss coefficient  $UA$  multiplied to the difference between the internal and outdoor temperatures yields the heat loss rate of the dwelling. The Heat Loss Parameter is a measure of the heat loss rate per usable floor area and is a means of comparing the energy efficiency of different dwellings.



Table 6.4 Representative UK dwelling characteristics

Pre-1967		Post-1967	
Mid Terraced 2 Storeys	Total Area=81.82 m <sup>2</sup> 6 rooms Y=5.22 m Wall Area=41.35 m <sup>2</sup> Window Area=12.96 m <sup>2</sup> Internal Volume=212.72 m <sup>3</sup> UA=332 W/°K HLP=4.06 W/m <sup>2</sup> ·°K	Mid Terraced 2 Storeys	Total Area=83.63m <sup>2</sup> 7 rooms Y=5.28 m Wall Area=34.28 m <sup>2</sup> Window Area=12.38m <sup>2</sup> Internal Volume=200.71 m <sup>3</sup> UA=168 W/°K HLP=2.01 W/m <sup>2</sup> ·°K
End Terraced 2 Storeys	Total Area=82.8m <sup>2</sup> 6 rooms Y=5.25m Wall Area=81.88 m <sup>2</sup> Window Area=13.73 m <sup>2</sup> Internal Volume=215.28 m <sup>3</sup> UA=327 W/°K HLP=3.95 W/m <sup>2</sup> ·°K	End Terraced 2 Storeys	Total Area=81.61m <sup>2</sup> 6 rooms Y=5.21m Wall Area=73.67 m <sup>2</sup> Window Area=13.95 m <sup>2</sup> Internal Volume=187.70 m <sup>3</sup> UA=188 W/°K HLP=2.30 W/m <sup>2</sup> ·°K
Semi-Detached 2 Storeys	Total Area=88.23m <sup>2</sup> 7 rooms Y=5.42m Wall Area=77.13 m <sup>2</sup> Window Area=17.76 m <sup>2</sup> Internal Volume=220.58 m <sup>3</sup> UA=336 W/°K HLP=3.80 W/m <sup>2</sup> ·°K	Semi-Detached 2 Storeys	Total Area=92.73m <sup>2</sup> 7 rooms Y=5.56m Wall Area=73.97 m <sup>2</sup> Window Area=19.43 m <sup>2</sup> Internal Volume=222.55 m <sup>3</sup> UA=222 W/°K HLP=2.39 W/m <sup>2</sup> ·°K
Detached 2 Storeys	Total Area=142.04m <sup>2</sup> 9 rooms Y=6.88m Wall Area=159.51m <sup>2</sup> Window Area=19.39 m <sup>2</sup> Internal Volume=369.30 m <sup>3</sup> UA=569 W/°K HLP=4.01 W/m <sup>2</sup> ·°K	Detached 2 Storeys	Total Area=142.1m <sup>2</sup> 10 rooms Y=6.88m Wall Area=138.73 m <sup>2</sup> Window Area=26.44 m <sup>2</sup> Internal Volume=341.04 m <sup>3</sup> UA=330 W/°K HLP=2.32 W/m <sup>2</sup> ·°K
Detached Bungalow 1 Storey	Total Area=75.75m <sup>2</sup> 6 rooms Y=7.11 Wall Area=74.62 m <sup>2</sup> Window Area=17.76 m <sup>2</sup> Internal Volume=196.95 m <sup>3</sup> UA=315 W/°K HLP=4.16 W/m <sup>2</sup> ·°K	Detached Bungalow 1 Storey	Total Area=78.84m <sup>2</sup> 6 rooms Y=7.25 m Wall Area=70.13 m <sup>2</sup> Window Area=16.87 m <sup>2</sup> Internal Volume=189.22 m <sup>3</sup> UA=235 W/°K HLP=2.98 W/m <sup>2</sup> ·°K
Semi Detached Bungalow 1 Storey	Total Area=78m <sup>2</sup> 7 rooms Y=7.21 m Wall Area=47.64 m <sup>2</sup> Window Area=17.98 m <sup>2</sup> Internal Volume=195.00 m <sup>3</sup> UA=274 W/°K HLP=3.51 W/m <sup>2</sup> ·°K	Semi Detached Bungalow 1 Storey	Total Area=76.2m <sup>2</sup> 7 rooms Y=7.12m Wall Area=43.4 m <sup>2</sup> Window Area=16.47 m <sup>2</sup> Internal Volume=182.88 m <sup>3</sup> UA=214 W/°K HLP=2.81 W/m <sup>2</sup> ·°K

## 6.10. Generated curves

For each building type and age combination, four different series of heat loss parameter vs. total floor area curves (separate series for different numbers of storeys) are generated and plotted against floor area as shown in Figure 6.7 and Figure 6.8. As can be observed, the larger the floor area for a given combination of dwelling type, age and number of storeys, the lower the *HLP*. This translates to higher energy efficiency for larger dwellings. At the same time, the effect of increasing the number of storeys on *HLP* can be observed. The number of exposed walls and the value of the heat loss coefficient  $U \times A$  of the exposed wall area, as well as its ratio over the hear loss coefficient of the roof area define the degree to which a change in the number of storeys results to a change in *HLP*.

The following plots can be used either as a visual means of comparing the energy efficiency of different combinations of dwelling type, age, floor area, and number of storeys, or as tool to calculate the heat loss coefficient  $U \times A$  for a given combination of dwelling type, age, floor area and number of storeys other than the ones shown in

Table 6.4, thus giving the modeller the ability to easily model an infinite number of dwelling combinations that share construction characteristics commonly encountered in the UK. Some geometrical combinations may not be applicable/existing, and it is up to the modeller to either select realistic combinations, or experiment with non existing ones.

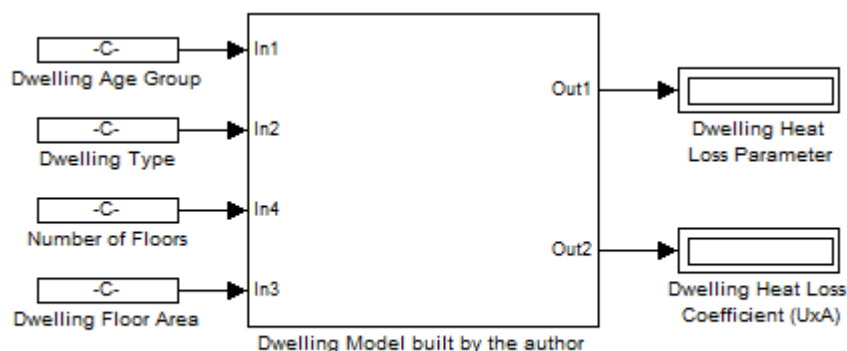


Figure 6.6 I/O block diagram of the developed dwelling model

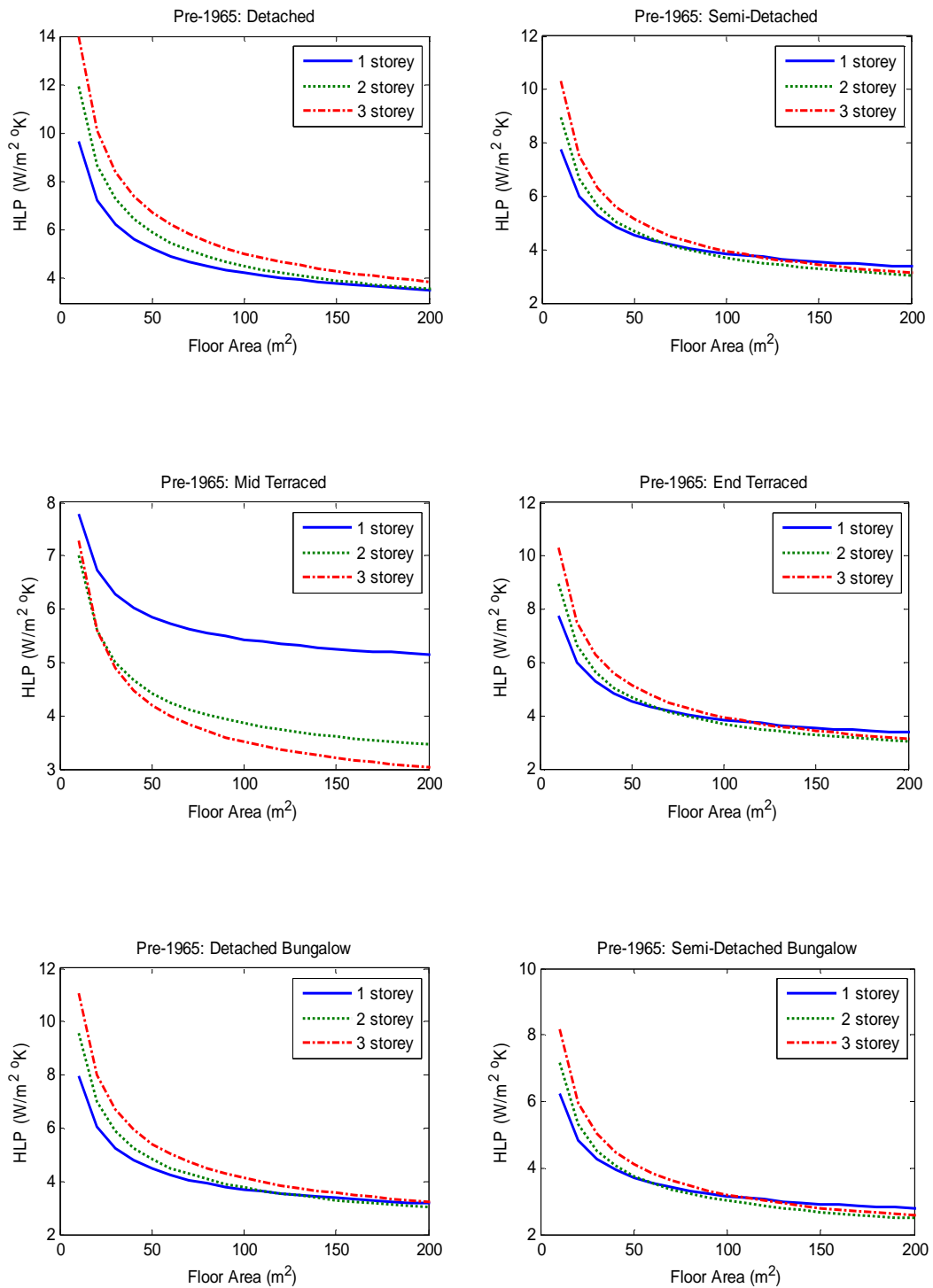


Figure 6.7 HLP vs. Floor Area for Pre 1967 dwellings

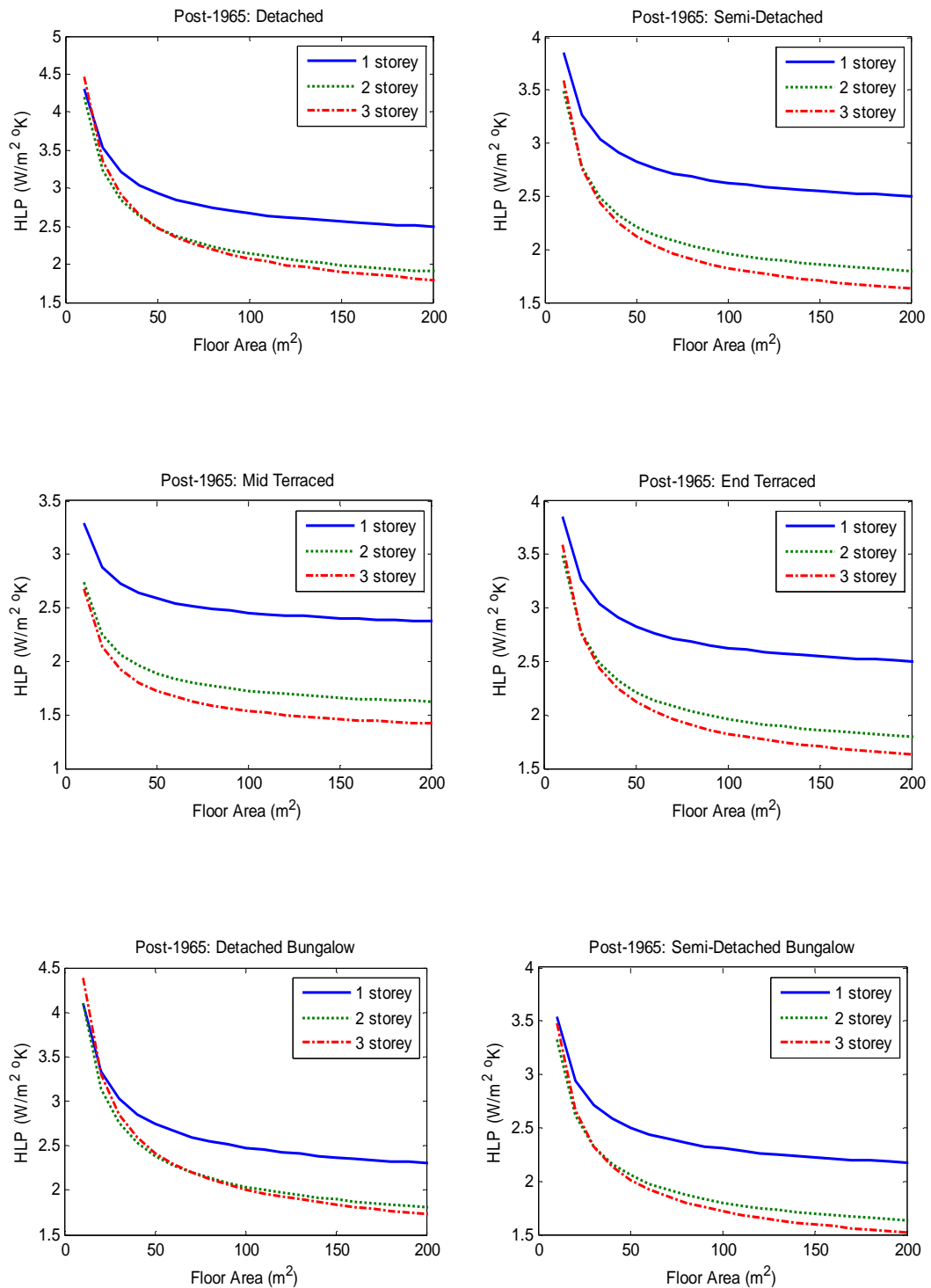


Figure 6.8 HLP vs. Floor Area for Post 1967 dwellings

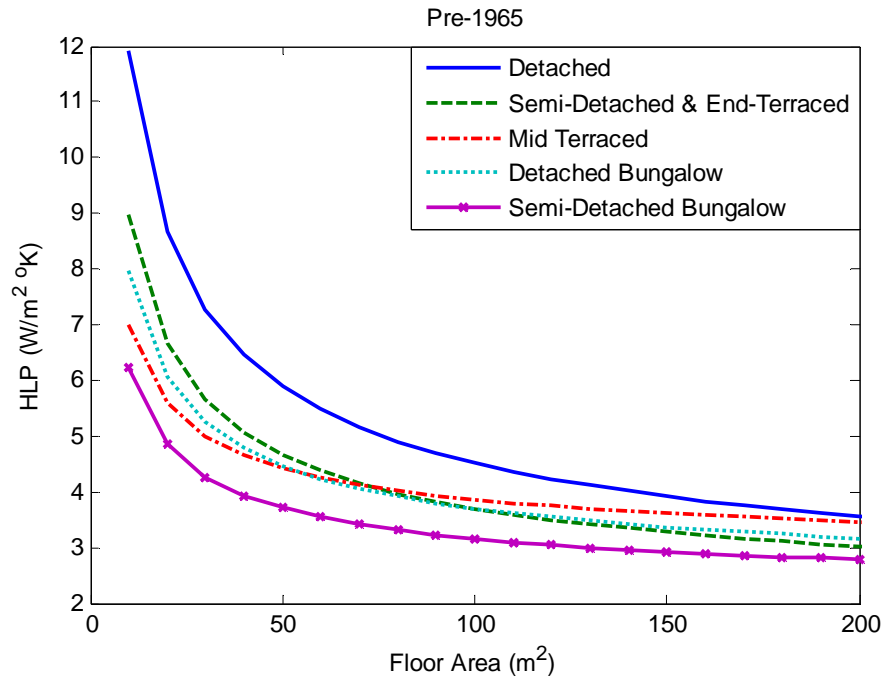


Figure 6.9 *HLP* vs. Floor Area for Pre - 1967 dwellings

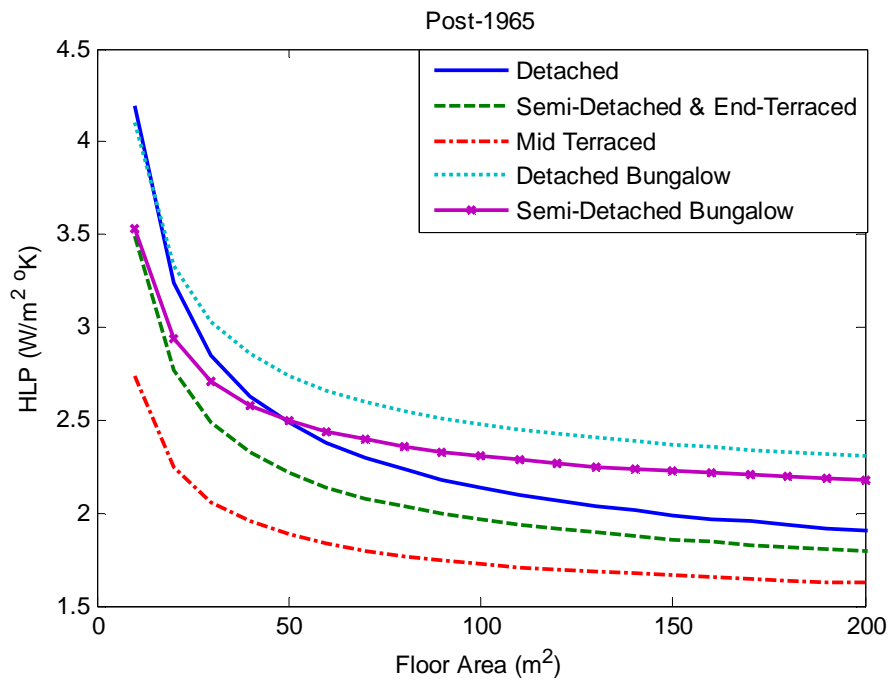


Figure 6.10 *HPL* vs. Floor Area for Post - 1967 dwellings

All curves of Figure 6.7 and Figure 6.8 will become integral part of the library of the DES simulation software package developed in Chapter 7 and used to simulate micro-CHP systems under representative UK dwelling envelopes in Chapter 8, Chapter 9, and Chapter 10. The internal volume can be calculated by multiplying the given total floor area by the ceiling height which is  $2.6m$  and  $2.4m$  for Pre-1967 and for Post-1965 dwellings respectively. The input/output diagram of the developed model is shown in Figure 6.5.

### **6.11. Summary**

In the current chapter, a series of dwelling models of different types, and construction periods were developed. Then, curves of Heat Loss Parameter as a function of total floor area for all dwelling types and three different numbers of storeys were generated based on the model. These plots can be used to calculate the dwelling *HLP* (and from the *HLP* the Heat Loss Coefficient *UA*) for a given total floor area and number of storeys other than the representative models of Table 6.3, thus giving the modeller an infinite array of options.

It is considered safe to conclude that the representative models describe dwellings most likely to be encountered in the UK reasonably well while giving the designer the capability not only to perform tests in old, less energy efficient dwellings but also in houses built on modern specifications. In addition, the developed *HLP*-Floor Area charts come in agreement with the values encountered in literature, and thus they are found to describe the heat loss mechanism adequately well for the purpose, and are suitable to be included in the library of the DES simulation software developed in Chapter 7 and used in the simulations of Chapter 8, Chapter 9, and Chapter 10.

## Chapter 7 Modelling structure

The current chapter is dedicated on the description of the complete residential micro-CHP model, as well as the modular simulation platform developed during the course of the current project which will be used in Chapter 8, Chapter 9, and Chapter 10 for the extraction of information on the environmental and financial feasibility of ICE based micro-CHP systems in the United Kingdom.

In the following paragraphs, the main system model is broken down to its constituent components and the function and structure of each component is analysed. The analysis of the multiphysics software based CHP model is then followed by a description of the developed graphical user interface, used to input the simulation parameters, control the multiphysics software based model, and perform post processing operations on the simulation results.

### 7.1. General layout

As can be seen in Figure 7.1, the main model consists of three blocks. The “Dwelling” block, the “Controller” block and the “Micro-CHP System” block. The “Dwelling” and “Micro-CHP system” blocks are comprised of subsystems, whose structure is based on the work described in the previous chapters, and they respectively model the behaviour of a dwelling and an ICE based Micro-CHP system. The feedback that both of these two blocks provide to the “Controller” block enable the virtual controller of Figure 7.9, to manage the electrical and thermal demands, surpluses and deficiencies encountered during the operation of a micro-CHP system operating under conditions commonly encountered in single family UK homes. Three different binary variables, “Switch”, “Switch\_Rad”, and “Switch\_Rej” switch on and off the engine, the radiators and the heat rejection mechanism respectively.

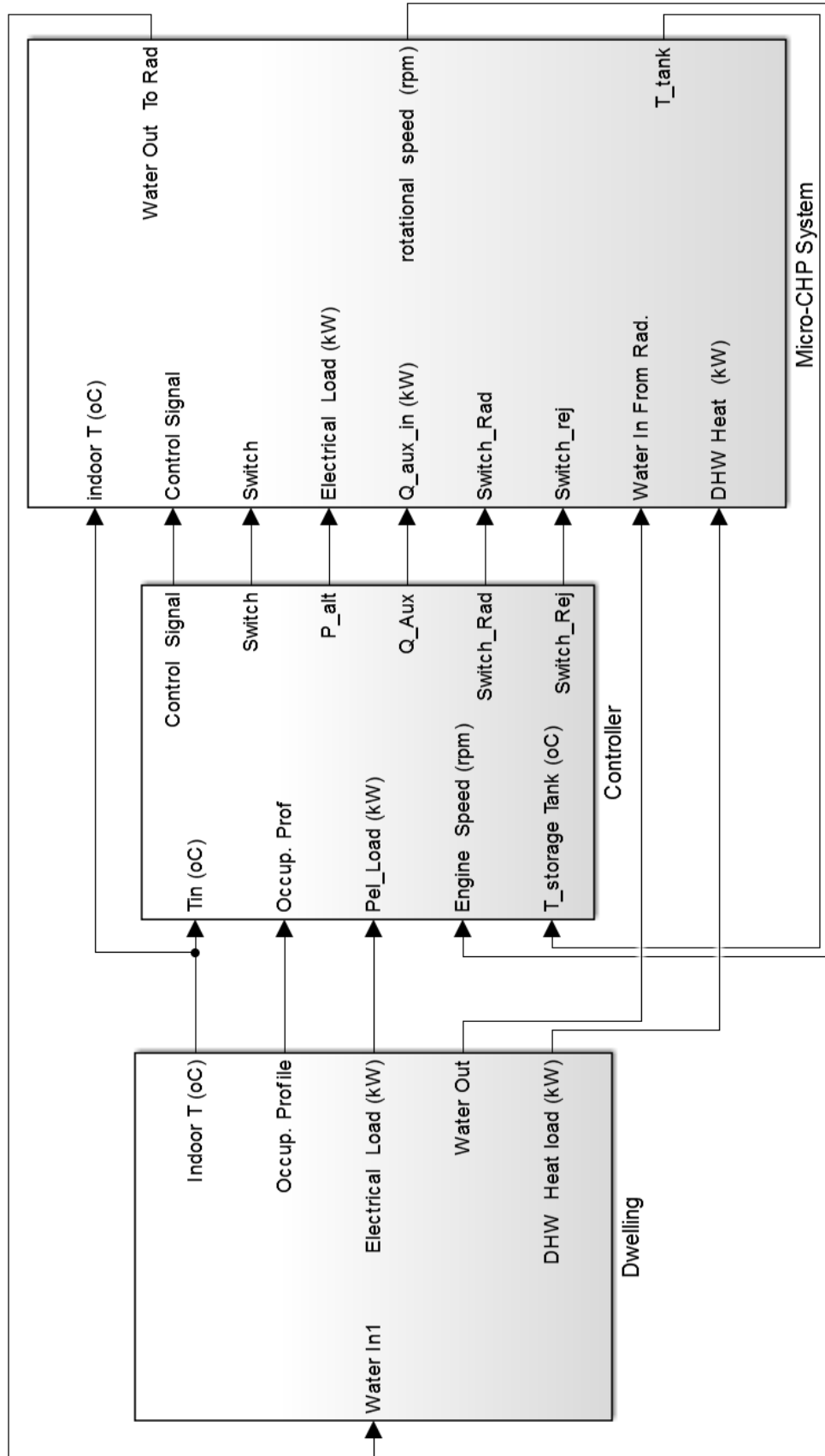


Figure 7.1 Top level of the Simulink based CHP/Dwelling model



### 7.1.1. The Load Block

The “Load block” contained in the “Dwelling” block as shown in Figure 7.2, provides the dwelling model with the outdoor temperature profile, and the controller with the occupancy, electrical load, and Domestic Hot Water consumption profiles by means of respective lookup tables. The data points of each lookup table in the load block, as well as the rest of the model parameters, are set by means of using the developed graphical user interface as presented in section 7.2 of the current chapter.

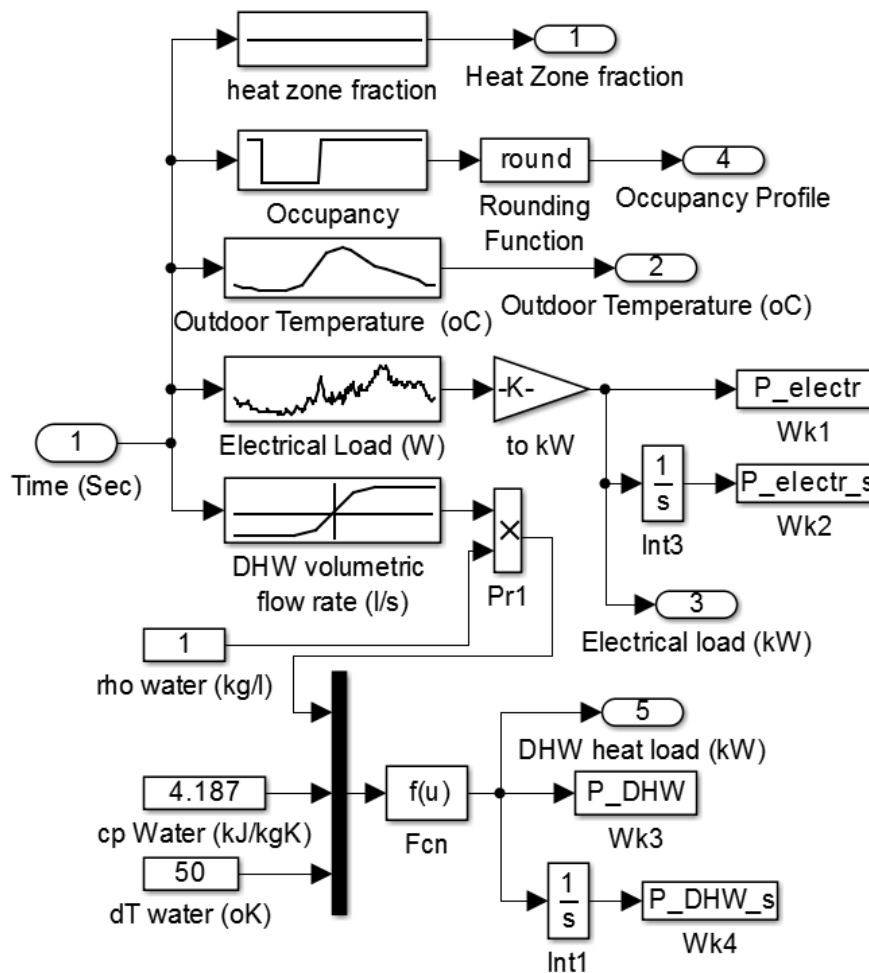


Figure 7.2 Block diagram of the “load block”

### 7.1.2. The dwelling

The “Dwelling” block is comprised of the model of the dwelling fabric whose content is shown in Figure 7.5, the radiator model as developed in section 5.6 and illustrated in Figure 7.11, the water circuit blocks to radiator and to CHP, and the indoor air mass block as shown in Figure 7.5. Heat losses of piping to indoor have been included in the model similarly to A. Moran et al. [4]. In addition, thermal gains due to the electrical appliance usage are taken into account.

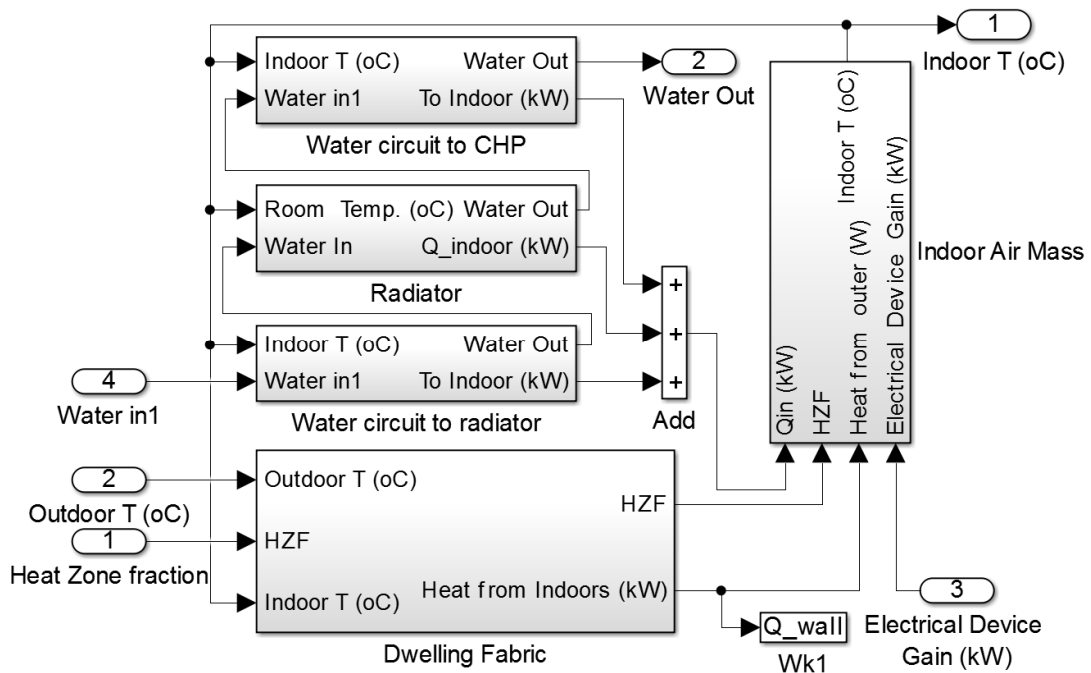


Figure 7.3 Block diagram of the "Dwelling" block

In order for the dwelling model to be characterized by realistic indoor temperature behaviour, the thermal mass of the building as well as the temperature gradient across the building walls must be taken into account. For this purpose, the wall model will be discretised along its thickness with three mass nodes of equal length. For the sake of simplicity, the wall properties are assumed to be uniform along its thickness. Then each layer will have a mass  $M_{layer} = M_{wall}/3$  with a thermal capacity  $K_{layer} = K_{wall}/3$ . A thermal capacity of  $K_{wall} = 150kJ/m^2\text{o}K$  has been selected as a

representative value of masonry cavity walls and therefore  $K_{layer} = K_{wall}/3 = 50kJ/m^2\text{°K}$ .

As shown in equation ( 6.2 ), the thermal resistance of a plate is proportional to the plate thickness. Assuming that each of the three nodes is located in the middle of each respective layer, and considering the fact that the U-values of construction components from [47], and [113] have U-values of the boundary layer and the material lumped together, there are four thermal resistances to analyse in the current model. Two thermal resistances located in the outer sides of the wall have half the length of each layer. Since each layer has a thickness of:

$$X_{layer} = X_{wall}/3 \quad (7.1)$$

The resistance of each layer will have a value of:

$$R_{layer} = R_{wall}/3 \quad (7.2)$$

And the outer resistances will have a value of:

$$R_{layer_o} = \frac{R_{layer}}{2} = \frac{R_{wall}}{6} \quad (7.3)$$

Each of the two resistances inside the wall consists of two half layers and therefore their value will equal the resistance of one layer:

$$R_{layer_i} = R_{layer} = R_{wall}/3 \quad (7.4)$$

Since the heat transfer coefficient is the inverse of the thermal resistance:

$$U = \frac{1}{R} \quad (7.5)$$

The outer resistances translate to a heat transfer coefficient of:

$$U_{layer_o} = \frac{6}{R_{wall}} = 6U_{wall} \quad (7.6)$$

While the inner resistances translate to a heat transfer coefficient of:

$$U_{layer_i} = \frac{3}{R_{wall}} = 3U_{wall} \quad (7.7)$$

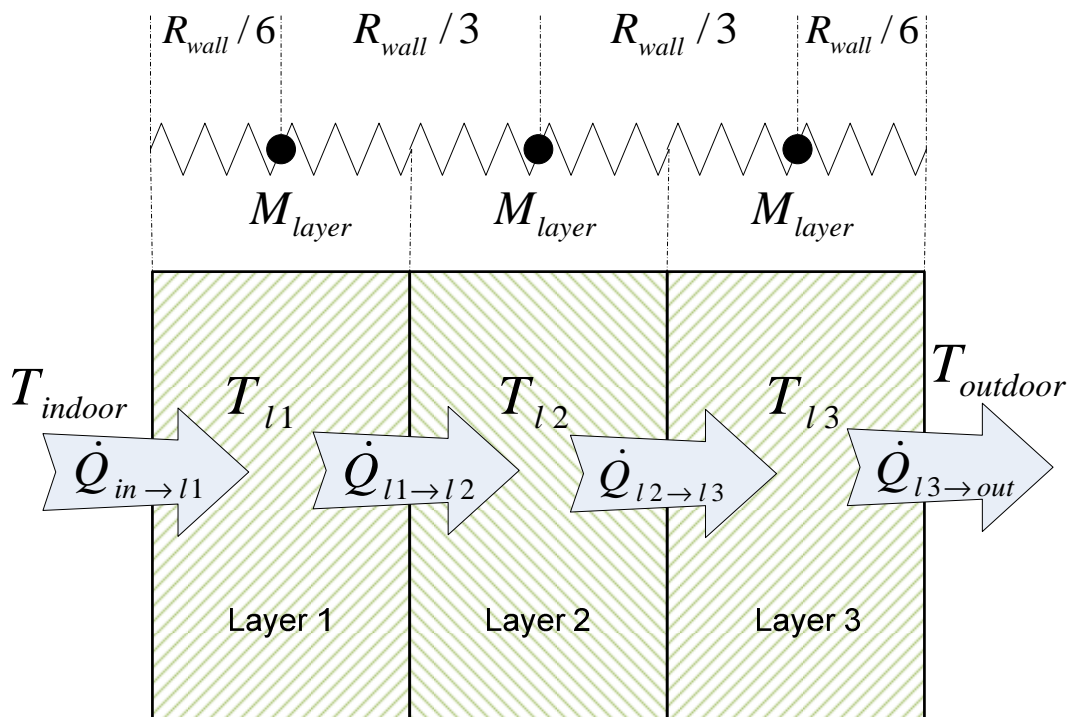


Figure 7.4 Schematic of the 3-node discretised wall model

The above model developed in Simulink can be seen in Figure 7.5 consisting of four thermal conductivity layers and three lumped building sub-masses.

Each of the ‘Layer’ blocks whose structure can be seen in Figure 7.6, calculates the heat transfer that takes place between the indoors and the “Inner Wall Layer Mass” block, between the “Inner Wall Layer Mass” block and the “Mid Wall Layer Mass” block, between the “Mid Wall Layer Mass”

block and the “Outer Wall Layer Mass” block, and Between the “Outer Wall Layer Mass” block and the outdoors.

This structure mimics the way indoor temperature rise and fall is affected by the building thermal mass and in addition the temperature difference between the inner and outer wall layers that forms a temperature damper between the indoors and the outdoors. HZF is the dwelling heat zone fraction and in the case of single family dwellings, it is taken as 1.

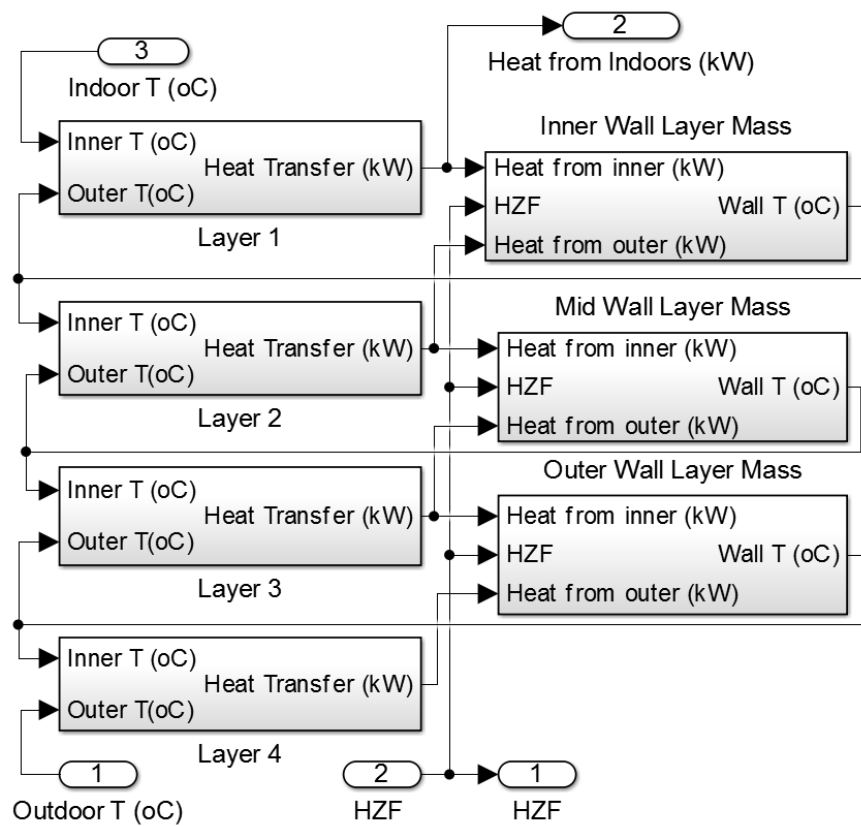


Figure 7.5 Block diagram of the "Dwelling Fabric" block

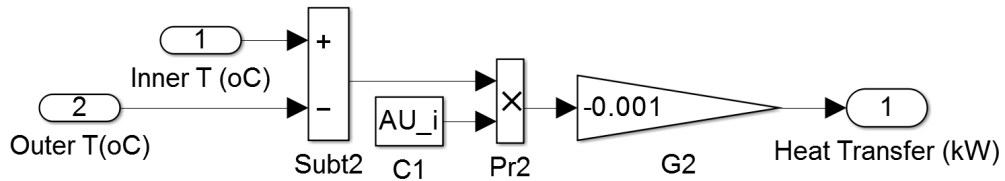


Figure 7.6 Block diagram of heat transfer "Layer" blocks 1 - 4

The structure of the Wall Layer Mass blocks can be seen in Figure 7.7. In this block type, depending on the associated temperature differences between the inner and outer blocks, heat is subtracted or added to the block integrator from both the inner and the outer layers. When the system reaches thermal equilibrium, heat is transferred through each layer at the same rate.

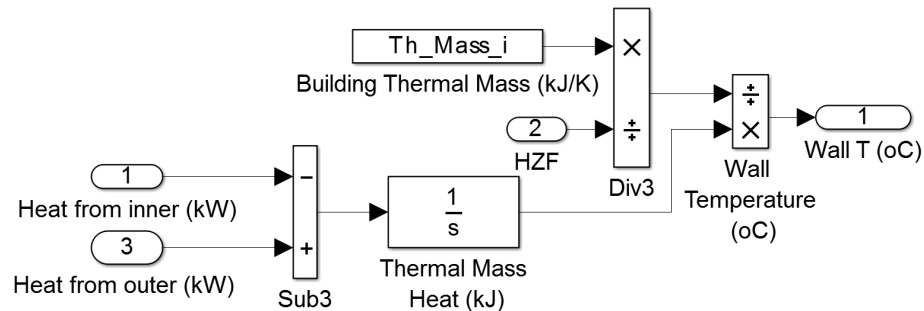


Figure 7.7 Block diagram of the "inner", "mid", and "outer" "Wall Layer Mass" nodes

### 7.1.3. Transient system thermal characteristics

As discussed in section 3.4.2.4, while the response of the mechanical power output is fast enough for the transient part of the mechanical power output to be neglected, the slow thermal response of ICE based micro-CHP systems makes the inclusion of the thermal transient characteristics necessary in order to simulate heating patterns realistically. In the current model, the dynamic thermal behaviour of all components involved in the heating process will be lumped in respective piping models. As shown in Figure 7.8, segments of piping are modelled as fully mixed control volumes where a volume is characterized by an average temperature based on the stored enthalpy.

Enthalpy enters the control volume at temperature  $T_1$  and a mass flow rate of  $\dot{m}_{wat}$  in  $kg/s$ . The dependence of the specific heat of water  $c_{p\_wat}(T)$  with temperature is taken into account and in the model it is given by lookup table “cp\_water 2”.

The heat inlet rate in the control volume is calculated from:

$$\dot{Q}_{wat\_in} = \dot{m}_{wat} c_{p\_wat}(T_1) T_1 \quad (7.8)$$

The enthalpy stored in the mass of the water contained in the control volume  $m_{w\_cv}$  is calculated from:

$$Q_{cv} = m_{w\_cv} c_{p\_wat}(T) T \quad (7.9)$$

The rate of heat leaving the control volume is calculated from:

$$\dot{Q}_{wat\_out} = \dot{m}_{wat} c_{p\_wat}(T) T \quad (7.10)$$

The first derivative of the stored enthalpy is:

$$\frac{dQ_{cv}}{dt} = \dot{Q}_{wat\_in} - \dot{Q}_{wat\_out} = \dot{m}_{wat} (c_{p\_wat}(T_1) T_1 - c_{p\_wat}(T) T) \quad (7.11)$$

And the stored enthalpy in the control volume at time  $w$  will be:

$$Q_{cv} = \int_0^w \dot{m}_{wat}(t) (c_{p\_wat}(T_1(t)) T_1(t) - c_{p\_wat}(T) T) dt \quad (7.12)$$

In all control volumes, it is assumed that the lumped component and the fluid share the same temperature  $T$ :

$$T = \frac{Q_{cv}}{m_{w\_cv} c_{p\_wat}(T) + C_{comp}} \quad (7.13)$$

Where  $C_{comp}$  is the heat capacity of the lumped component in  $kJ/^\circ K$  which is assumed to remain constant for the temperature operating range.

In the control volume of Figure 7.8, the component thermal capacity consists of the thermal capacity of the tube and the radiators. If it is assumed that the radiators are made of steel and the tube is made of copper, then their combined thermal capacity “MxCp\_Mat” will be:

$$C_{comp} = c_{p\_steel}m_{rad} + c_{p\_copper}m_{tube} \quad (kJ/^\circ K) \quad (7.14)$$

Where  $c_{p\_steel}$  and  $c_{p\_copper}$  the specific heat capacities of steel and copper respectively in  $kJ/kg^\circ K$ , and  $m_{rad}$  and  $m_{tube}$  the masses of the radiator and the tube section respectively in  $kg$ .

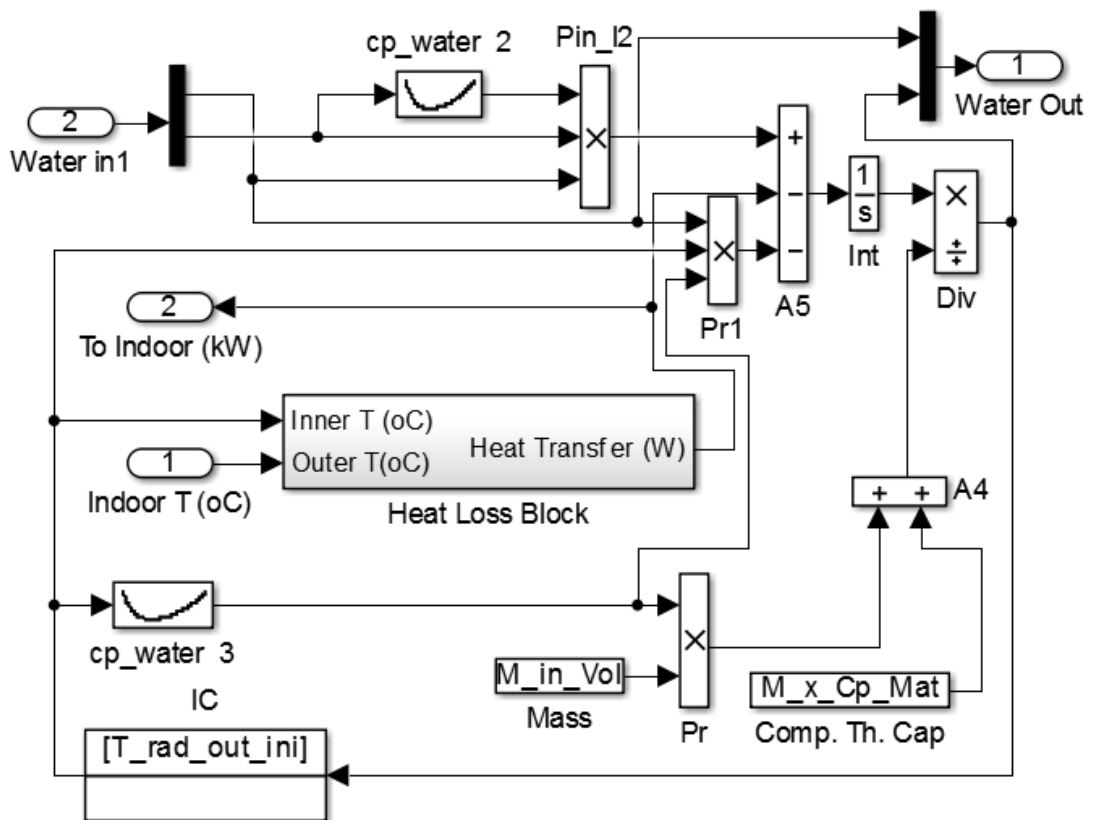


Figure 7.8 Block diagram of the water circuit segment that connects the radiator outlet to the heat storage coil



The same layout is used to incorporate the thermal response of the engine in the model. The engine mass will be lumped in the block diagram of the pipe that supplies heat to the primary coil of the heat storage tank. Assuming that the engine mass is represented by aluminium and the tube is made of copper, the heat capacity of this node is calculated from:

$$C_{comp} = c_{p\_alu}m_{eng} + c_{p\_copper}m_{tube} \quad (7.15)$$

Where  $c_{p\_alu}$  the specific heat capacity of aluminium in  $kJ/kg^{\circ}K$ , and  $m_{eng}$  the engine mass in  $kg$ .

The method described above, is similar in concept to the lumping of the thermal behaviour of the heat exchanger mass into the water circuit mass as found in F. Caresana et al. [2], but makes use of differential equations rather than transfer functions, and the specific heat of the used material rather than of water.

#### 7.1.4. The system Controller

The virtual system controller pictured in Figure 7.9 is based on an embedded Matlab function and runs code for either heat priority or electricity priority controlled systems depending on the mode selection made through the graphical user interface described in section 7.2.

Control signals from the virtual controller are used to manage all system assets. The engine is powered on and off by the “Switch” Boolean variable and its power output is set by the “Control Signal” variable where the objective is to meet the “Electrical Load” demand at the required speed. “Switch\_Rad” turns on and off the flow of water through the radiator circuit and supplies the indoors with heat. “Switch\_rej” controls the rejection of surplus heat from the storage tank. “Q\_aux\_in” is the heat from the auxiliary boiler being added to the existing stored heat and “DHW Heat” is the domestic hot water heat demand being removed by the stored heat.

For the control of the indoor and the heat storage tank temperatures “ $T_{in}$ ” and “ $T_{stor}$ ” respectively, the value of the two temperatures and their first time derivatives are used as controller feedback. Indoor temperature limits set through the graphical user interface and occupancy information provided by the occupancy lookup table in the load block of Figure 7.2 are used by the controller to evaluate whether a need for space heating exists. In all cases, the controller reads the indoor temperature “ $T_{in}$ ” and compares it with the lower and higher indoor temperature limits “ $setT1$ ” and “ $setT2$ ” respectively. If the value of the occupancy profile Boolean variable is 0, the radiators are always deactivated. When the occupancy profile variable value is 1 and “ $T_{in}$ ” < “ $setT1$ ”, the controller sets the value of the Boolean radiator circuit switch “ $Switch\_Rad$ ” to 1 and water flows through the radiators heating the indoor air until “ $T_{in}$ ”  $\geq$  “ $setT2$ ” where the Boolean “ $Switch\_Rad$ ” is set to 0, thus disabling the circulation of water in the radiator circuit until the indoor temperature drops to the lower indoor temperature limit “ $T_{in}$ ”  $\leq$  “ $setT1$ ” where water circulation is again activated.

Similarly, the operation of the engine and the auxiliary boiler in the case of heat priority control, or the operation of the auxiliary boiler and the heat rejection mechanism in the case of an electricity priority control is activated or deactivated when the storage tank temperature “ $T_{stor}$ ” crosses certain operating limits. When heat priority control is implemented, the engine and the auxiliary boiler (when applicable) operate at full power for tank temperatures lower than the lower tank temperature limit “ $T_{st\_lim1}$ ”. When the intermediate tank temperature limit “ $T_{st\_lim2}$ ” is crossed as the tank temperature increases, the auxiliary boiler is shut off and the engine supplies heat on standalone. If the heat demand is lower than the engine heat supply, the tank temperature will rise, eventually crossing “ $T_{st\_lim3}$ ” in which case the engine will be switched off until tank temperature falls and crosses the lower storage temperature limit “ $T_{st\_lim1}$ ” where the engine and the auxiliary boiler are again activated. When the engine is operated, electricity is generated at a rate of maximum power output “ $P_{alt}$ ” = “ $P_{el\_o\_h}$ ”. Surplus electricity (“ $P_{alt}$ ” > “ $P_{el\_load}$ ”) is exported to the grid for revenues (“ $P_{grid}$ ” = “ $P_{el\_load}$ ” – “ $P_{el\_o\_h}$ ” > 0). Power deficiency (When “ $P_{el\_load}$ ” >

“Pel\_o\_h”) on the other hand is remedied by purchasing electricity from the grid (“P\_grid” = “Pel\_o\_h” – “Pel\_load” < 0).

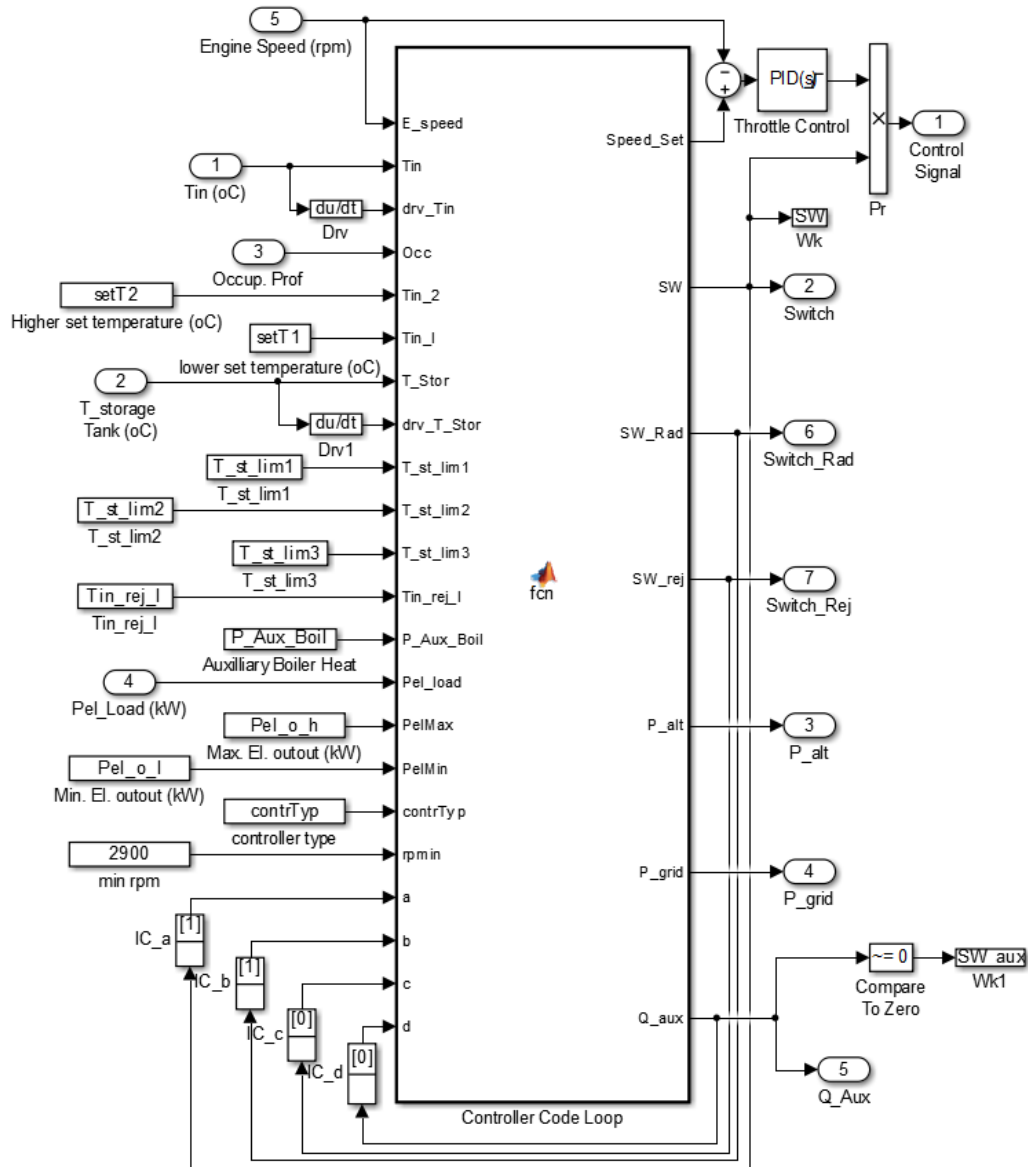


Figure 7.9 Block diagram of the controller block. The controller code is contained in the "Controller Code Loop" Embedded Matlab Function

In the case of the electricity priority mode, while the auxiliary boiler is actuated in the exact same manner as in the case of the heat priority controller, the engine is operated to follow the electrical load “Pel\_load”. When electrical load falls below the lower operating limit (“Pel\_o\_l” >

“Pel\_load”), the engine is switched off to avoid inefficient electricity production, and all the electricity demand is met by the grid. When there is an electricity deficiency (“Pel\_load” > “Pel\_o\_h”), the generator is operated at full load “P\_alt” = “Pel\_o\_h” and the CHP power supply is supplemented by the grid (“P\_grid” = “Pel\_o\_h” – “Pel\_load” < 0). In order to prevent the tank water from overheating, the heat rejection mechanism is activated when “T\_stor” crosses the upper tank temperature limit “T\_st\_lim3” and is deactivated when the heat rejection switch off temperature “Tin\_rej\_l” is crossed.

#### **7.1.5. The $\mu$ CHP System block**

The  $\mu$ CHP System block layout pictured in Figure 7.10 is comprised of the “Cogeneration Unit” block and the “Heat Storage System” block. The cogeneration unit exchanges heat with the heat storage via the water circuit that flows through the secondary heat exchanger sides of the heat recovery system, and “Coil 2” of the heat storage tank whose layout is shown in Figure 7.11. “Water Out1” and “Water Out2” are the outlets of secondary heat exchanger sides of the exhaust and the jacket water heat exchangers respectively, and “Water In” is the combined water return leaving “Coil 2” of the storage tank and being again fed to the heat recovery system to close the cycle. All “Water” inlets and outlets are structures that contain the water mass flow rate and the temperature.

The heat storage system exchanges heat with the heating radiator circuit of the dwelling. The “Water Out to Rad” water outlet shown in the block diagram of Figure 7.10 supplies hot water to the heat delivery water circuit which in turn supplies this heat to the radiator whose block diagram can be seen in Figure 5.23. Piping heat losses for this circuit are taken into account, and lost heat is added to the indoor air mass as shown in Figure 7.3 where the outputs “To Indoor” supply the pipe losses to the indoor space.

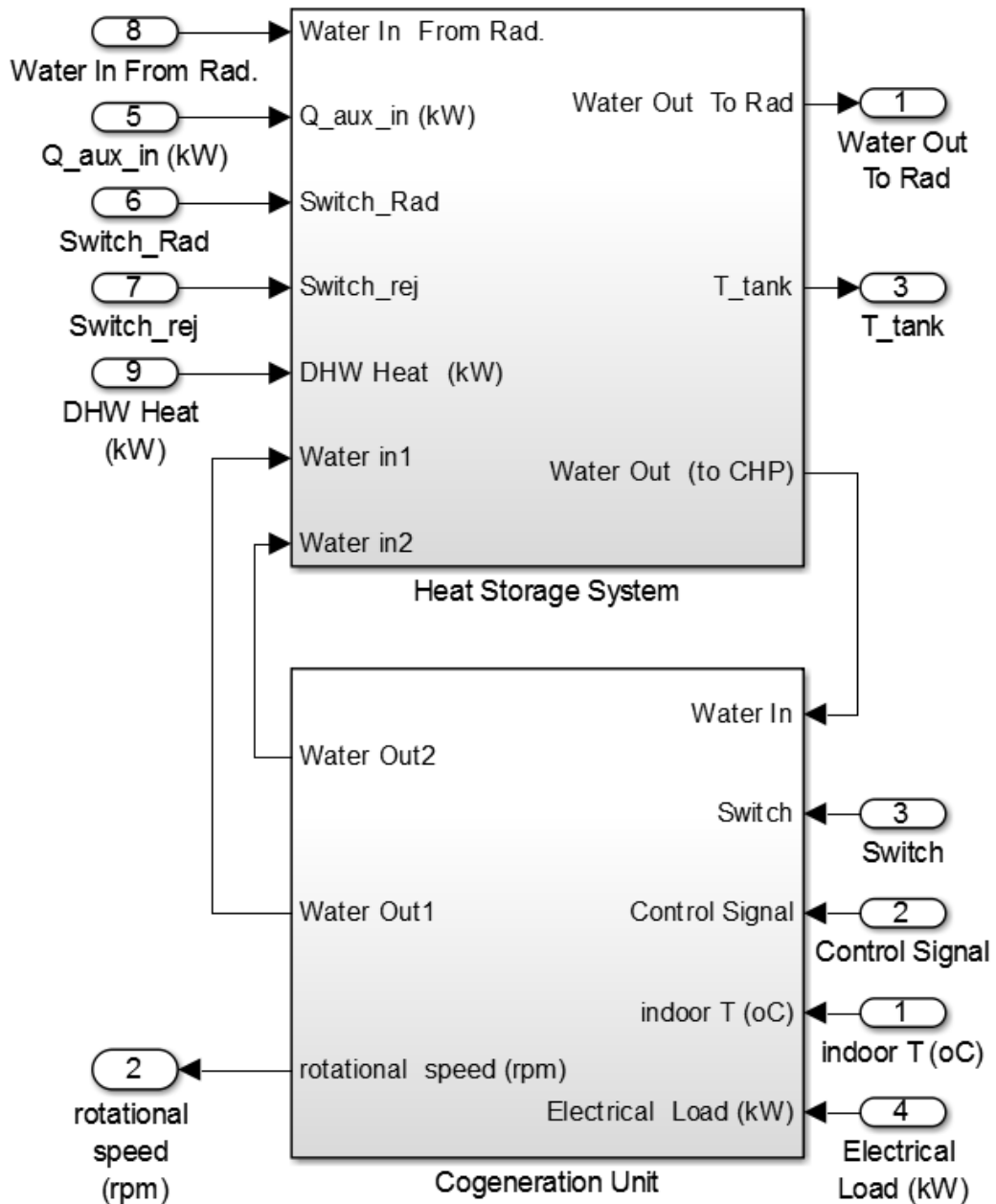


Figure 7.10 Block Diagram of the "Micro – CHP System" block

### 7.1.6. The Heat Storage System block

The "Heat Storage System" block whose structure is shown in Figure 7.11, consists of the "Water Valve" block which depending on the state of the "Switch\_Rad" boolean control variable switches on or off the circulation of water to the radiators, the "Heat Storage" block which contains the model of the heat storage tank including the heating coils, and the "Water circuit to

Heat Storage” block which merges the two inlets from the heat recovery system into one flow used as inlet in Coil 2.

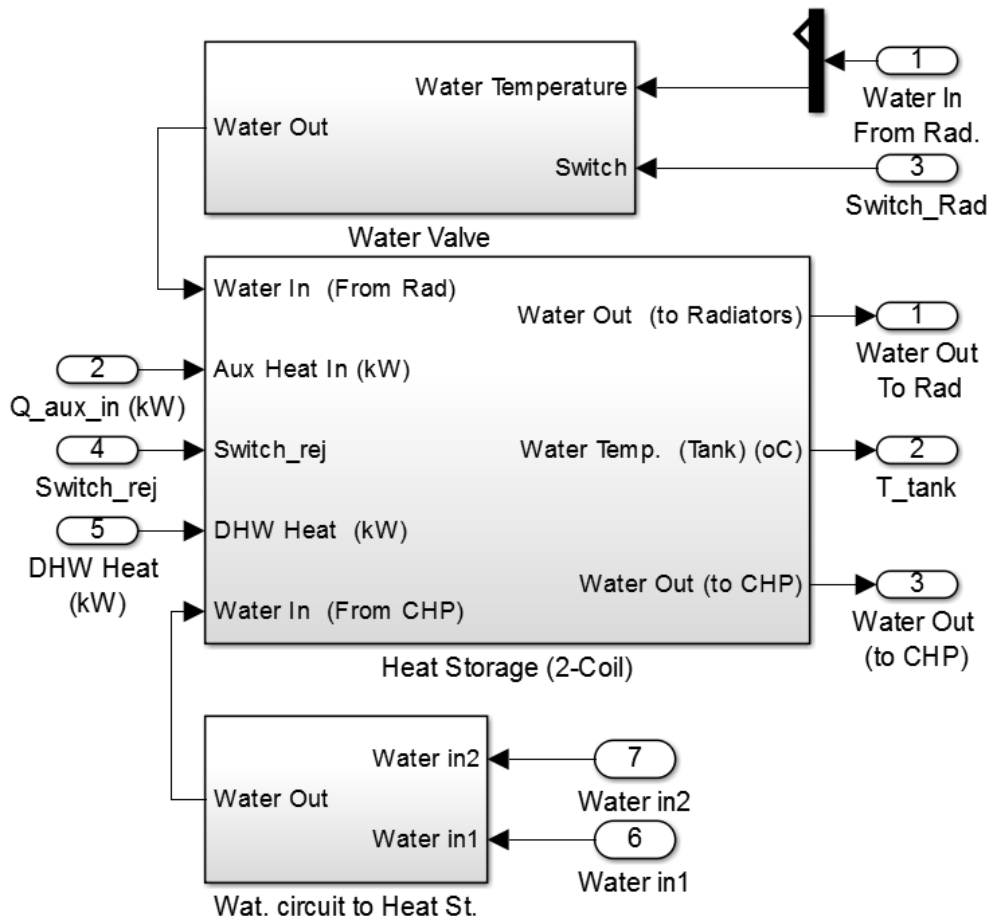


Figure 7.11 Block diagram of the “Heat Storage System”

The structure of the “Heat Storage” block is shown in Figure 7.12. Block inputs “Water In (From Rad)” and “Water In (From CHP)” are fed to Coil 1 and Coil 2 respectively. “Coil 1” output “Transferred Heat” is the heat load placed by the radiator circuit on the heat storage tank. On the other hand, “Coil 2” output “Transferred Heat” is the heat load that the storage tank places on the CHP heat recovery circuit, thus increasing the stored heat of the tank. The development procedure and analyses of the coil model as well as the Coil block layout can be found in section 5.8.2.

Auxiliary heat input “Aux Heat In” is the heat supplied by the auxiliary boiler under conditions discussed above, and it is added to the storage thermal inputs, thus increasing the stored heat in the tank when necessary. Boolean variable “Switch\_rej” activates and deactivates surplus heat rejection at a rate “Q\_rejec” and reduces the stored heat, as does the domestic hot water heat load “DHW Heat”. Storage tank water temperature “Water Temp (Tank)” is communicated as feedback to the virtual controller.

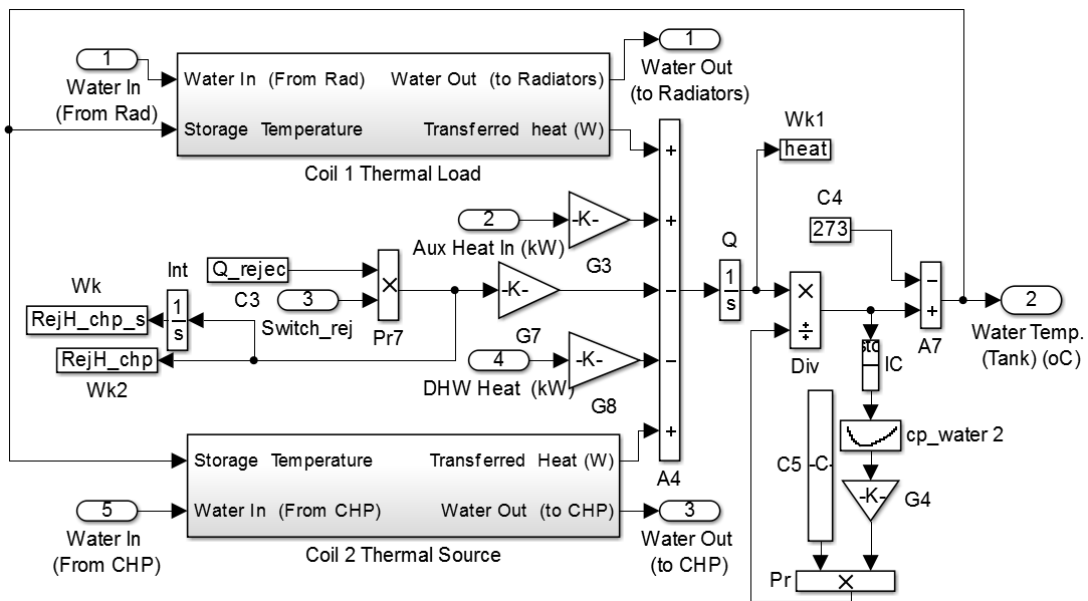


Figure 7.12 Block diagram of the block "Heat Storage (2-Coil)"

### 7.1.7. The “Cogeneration Unit” block

As can be seen in Figure 7.13, the “Cogeneration Unit” block is comprised of the “Generator Set”, the “Heat Recovery System”, the “Water Valve 1”, The “Water circuit to Water to Water Heat Exchanger”, and the “Water circuit to Engine Jacket” blocks.

The “Generator Set” block outputs “Exhaust out” and “Jacket Water out” are connected to the “Heat Recovery System” block inputs “Exh In” and “Tube In” which are the inlets of the primary sides of the exhaust and jacket water heat exchangers respectively. Both exhaust and jacket water heat is recovered in the “Heat Recovery System” block and transferred to the

secondary sides whose outlets are “Water Out1” and “Water Out2” which as pointed out above, are connected to the “Heat Storage” block.

The jacket water circuit is represented by “Water circuit to Water to Water Heat Exchanger”, and the “Water circuit to Engine Jacket” blocks. These two blocks model the temperature response of the jacket water mass that flows from and to the engine jacket respectively and the engine mass.

The block “Water Valve 1” switches on and off jacket water circulation when the engine is turned on and off according to the value of the Boolean variable “Switch”.

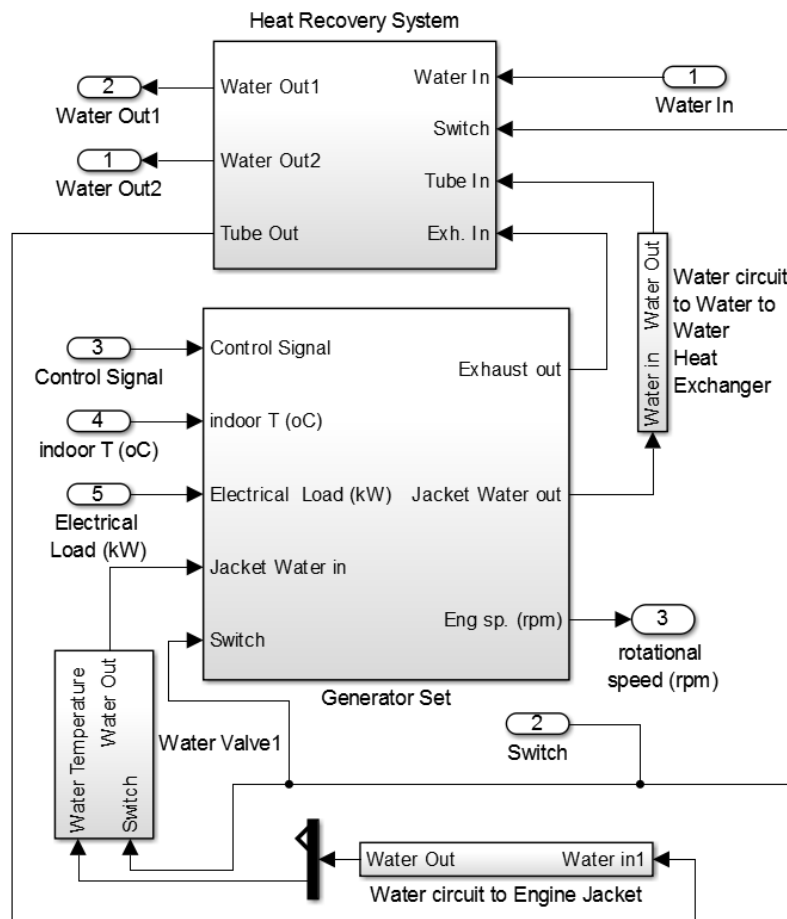


Figure 7.13 Block diagram of the "Cogeneration Unit" block



### 7.1.8. The “Heat Recovery System” block

The “Heat Recovery System” block whose structure is shown in Figure 7.14, is comprised of the “Exhaust Gas Heat Exchanger” model and the “Jacket Water Heat Exchanger” model, both developed in section 5.8.1.

In addition, one “Water Valve” type block for each heat exchanger turns the respective secondary flows of each heat exchanger on and off according to the value of the “Switch” variable.

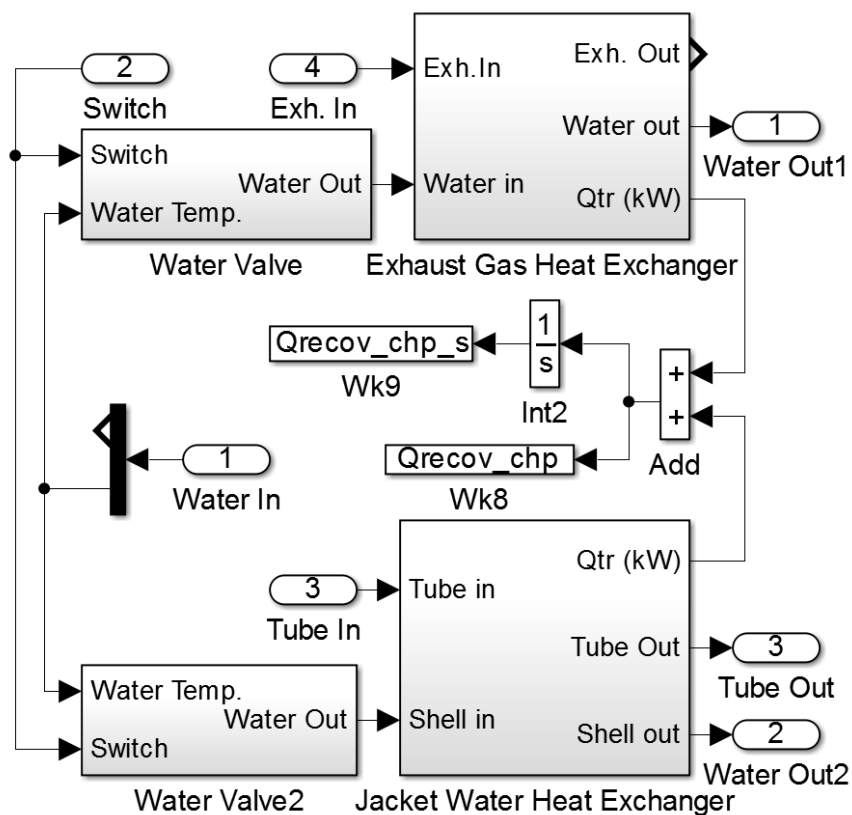


Figure 7.14 Block diagram of the "Heat Recovery System" block

### 7.1.9. The Generator Set block

The “Generator Set” block whose structure can be seen in Figure 7.15, is essentially the model of an ICE based generator set and it is comprised of three main components. The “Combustion Engine” block, the “Shaft Dynamics” block and the “Electric Machine” block.

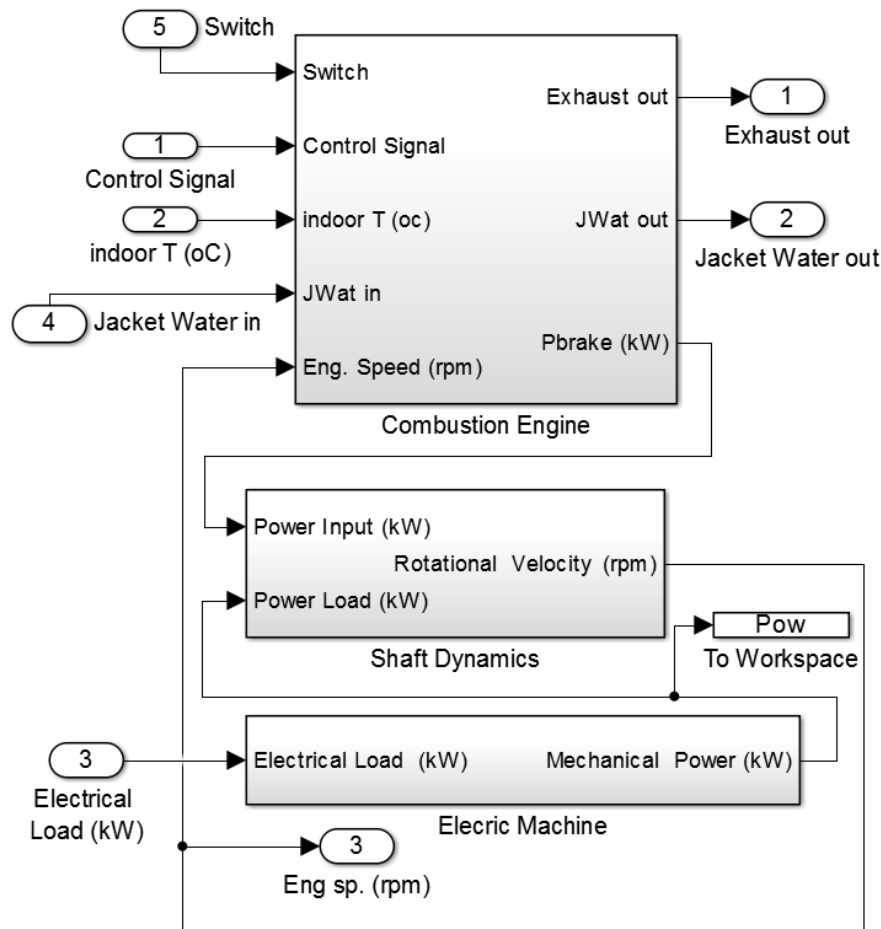


Figure 7.15 Block diagram of the "Generator Set" block

The “Combustion Engine” block is based on the engine model developed in Chapter 4 and its operation and output is controlled by “Switch” and “Control Signal” inputs in order to meet the “Electrical Load” which is the load placed on the electric machine. The “Shaft Dynamics” block models the dynamic behaviour of the engine and generator rotating parts, and its model layout is based on the energy based modelling configuration presented in Chapter 4. The engine power output and the load from the electric machine are directly used as inputs to the “Shaft Dynamics” block. The time integration of the net power acting on the rotating parts results in accumulated rotational energy which in turn translates into a corresponding rotational speed which is used as feedback to the virtual controller. The “Electric Machine” model block

contains a lookup table based block diagram that describes the electric machine model developed in Chapter 4.

## **7.2. Micro-CHP Energy Simulation Tool**

In order to facilitate the system configuration and simulation procedure of the Micro-CHP Simulink model described above, a graphical user interface (GUI), whose main configuration window is shown in Figure 7.16 has been developed. This GUI (supported by relevant Matlab code) is used for the configuration of the main simulation parameters in a straightforward and time conserving manner, enables the sizing of a micro-CHP unit for a given application, controls the simulation of the Simulink model, and provides flexible post processing capabilities of the simulation results.

### **7.2.1. Simulation parameters**

The following paragraphs describe the main model and simulation parameters that are adjustable through the developed GUI.

#### **7.2.1.1. Engine displacement**

The engine displacement represents the size of a power plant and directly affects the system thermal and electrical output. It is adjustable through the GUI and is inputted in cubic centimetres.

#### **7.2.1.2. Engine type**

The user can select between three engine types: a petrol fuelled, a low compression ratio natural gas fuelled, and a high compression ratio natural gas fuelled engine. This allows the researcher to investigate the effect of fuel type and engine conversion efficiency on the main system performance indicators.

#### **7.2.1.3. Electric machine conversion efficiency at maximum load**

Since the efficiency of the electric machine may affect the system feasibility, the conversion efficiency of the electric machine at maximum load is one of the main model parameters. For a given combination of engine size, type,

conversion efficiency at maximum load, and value of rms voltage, a segment of code in the system initialization function generates and assigns a calculated map of thermal losses vs. electrical load to the lookup table of the electric machine Simulink model.

#### **7.2.1.4. CHP system configuration**

In the current developmental stage of this energy simulation tool, two main system configurations are available for selection. The first available option is an SI ICE based micro-CHP system with heat storage. The second available option is an SI ICE based micro-CHP system without heat storage.

#### **7.2.1.5. Design Heat Exchanger temperatures**

The design inlet and outlet temperatures of the heat exchangers play an important role in heat exchanger size and thus the unit cost. In addition, the exhaust outlet temperature defines the heat recovery efficiency of the exhaust enthalpy, and therefore affects the overall fuel utilization efficiency of the system. Different combinations of the exhaust and jacket water heat exchanger inlet and outlet temperatures can be selected from respective popup menus on the developed GUI configuration window.

#### **7.2.1.6. Design radiator temperatures**

The design radiator temperatures define not just the radiator size, but also affect the thermal response of the radiators. Similarly to the heat exchanger temperatures, the design radiator temperatures may be set on the developed GUI.

#### **7.2.1.7. Dwelling Location**

The user may select between ten different UK locations. This selection assigns the respective weather file to the outdoor temperature look up table of the “Load Block” of Figure 7.2.

#### 7.2.1.8. Dwelling configuration

In terms of available settings in dwelling characteristics, the user can adjust the following dwelling parameters:

- Dwelling type – Selection from five different dwelling types
- Dwelling age – Selection from two different dwelling age groups
- Dwelling floor area (m<sup>2</sup>)
- Number of floors – Options between 1 and 4 floors are available

The selected combination of dwelling characteristics is used by the system configuration environment to select the appropriate heat loss parameter (*HLP*) curve as created in Chapter 6 and available in the software library. The curve selection is followed by the calculation of the *HLP* value for the inputted floor area by means of interpolation. The heat loss parameter is then multiplied by the dwelling total floor area resulting in the calculation of the heat loss coefficient  $U \times A$  of the particular dwelling combination.  $U \times A$  is then used by the dwelling model in Simulink as one of the two main parameters that defines its thermal behaviour.

#### 7.2.1.9. Generation of representative dwelling combinations

While the capability to vary the dwelling characteristics to yield a large number of combinations adds to the versatility of the tool, the need to produce results relevant to system loading conditions commonly encountered in the United Kingdom necessitates the specification of representative dwelling configurations as discussed in Chapter 6. For this reason, a subroutine that sets the representative floor area and number of floors for a selected combination of dwelling type and age, based on the values provided in

Table 6.4 has been added in the graphical user interface. This function is called by the virtual button “Generate Representative Dwelling” as shown in Figure 7.16.

#### **7.2.1.10. Dwelling thermal mass**

The second most important parameter defining the thermal behaviour of the building model is the dwelling thermal mass which is also adjustable in the model.

#### **7.2.1.11. System operating mode**

The user may select between electricity or heat priority controlled operating strategies.

In the case of the electricity priority controller, the generator output is controlled to match the electrical load profile, provided the demand is higher than the minimum system load. When the demand is lower than the minimum system load, the system is switched off and the demand is met by the grid. If the demand lies between the minimum and the maximum system operating limits, the demand is met solely by the system. When the demand is greater than the maximum generator output, the controller automatically imports supplementary electricity from the grid. No electricity is exported to the grid under this strategy. Any shortage in available engine waste heat is met by an auxiliary boiler. If the thermal storage tank is saturated, condition taking place when the water in the heat storage tank crosses a predefined temperature upper safety limit, no more heat is storable past this point, but generated waste heat is rather rejected in the environment as surplus heat.

In the case of the constant output heat priority controller, the engine is essentially operated as a boiler, and the electricity load profile does not influence the operation of the engine but rather defines the amount of generated electricity that is consumed on site, exported to the grid as surplus, or imported from the grid. No surplus heat is produced and thus, no heat is rejected to the environment.

#### **7.2.1.12. Indoor temperature limits**

The lower and upper indoor temperature limits define not only the cycling patterns of the radiators and the engine but may also affect the system fuel

consumption. In the developed GUI, these two temperature limits are adjustable.

#### **7.2.1.13. Thermal storage tank size**

As will be shown in Chapter 9, the storage tank size affects not only the cycling patterns of the heat sources such as the boiler and the CHP but also defines the amount of surplus heat that may be stored before heat rejection occurs when the system operates under electricity priority control. The heat storage tank size is adjustable through the GUI panel.

#### **7.2.1.14. Auxiliary burner capacity**

The capacity of the auxiliary burner can be chosen in a way that it supplements that of the CHP unit. In order for a combined thermal capacity to remain the same while varying the CHP electrical and thermal capacity, the auxiliary burner capacity must be varied to address this change. For a given total thermal capacity, a reduction in the CHP size will translate to an increase in the auxiliary burner size and vice versa. For the above reasons, the auxiliary burner capacity can be adjusted via the developed GUI.

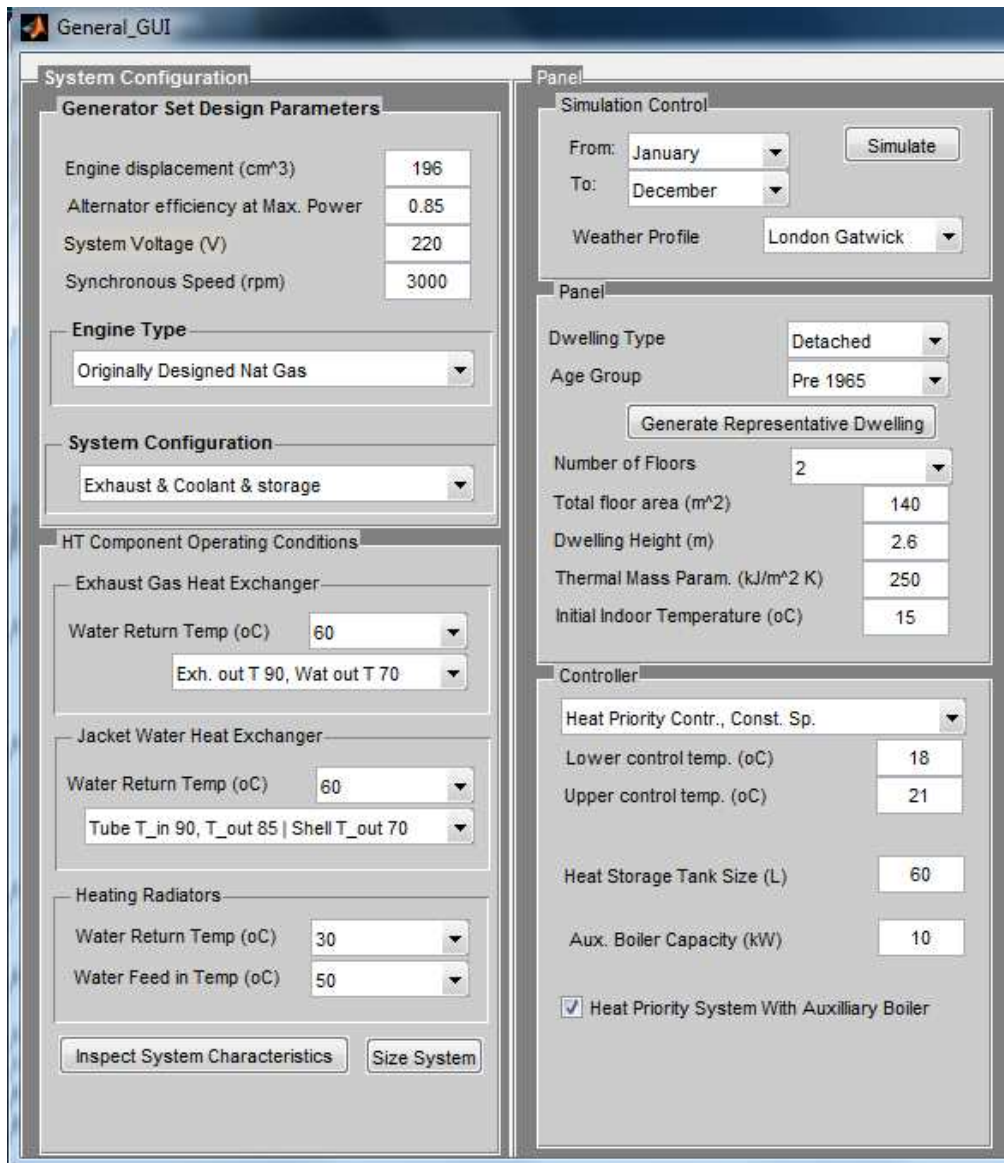


Figure 7.16 System configuration panel

### 7.2.1.15. System inspection panel

The system inspection panel shown in Figure 7.17 enables the researcher to inspect the main static performance characteristics of the CHP system under consideration for the minimum and maximum allowable loads. Within these characteristics, the sizes of both heat exchangers, as well as of the radiators are displayed.



System Inspection					
Eligible for F.I.T. scheme	Pmax	Pmin		Pmax	Pmin
Q <sub>fuel</sub> in (kW)	5.68214	2.74804			
Electrical Output (kW)	1.64244	0.492732	Oal. Conv. Efficiency	0.289053	0.179303
ICE Mech. Output (kW)	1.93229	0.571571	Alternator Conv. Eff.	0.849999	0.862066
CHP Total Thermal Output	4.0397	2.25531	ICE Conv. Efficiency	0.340063	0.207992
Exh. Heat (kW)	1.41527	0.629946			
Exhaust Mass Rate (kg/s)	0.0018857	0.0009119			
Exh. Temp (oC)	655.974	609.411			
Recovered Exh. Heat (kW)	1.2578	0.577838	Exh. Heat Recov. Eff.	0.89092	0.919739
ICE Convection (kW)	1.90538	1.2682			
ICE Friction (kW)	0.426177	0.426177			
Coolant Heat (kW)	1.76636	1.27172	Coolant Heat Recov. Eff.	1	1
Recov. Coolant Heat (kW)	1.76636	1.27172			
Radiation Heat (kW)	0.568214	0.274804			
Recov. Rad. Heat (kW)	0	0			
Rad. Heat Recov. Eff. (%)	0	0			
Total Recovered Heat (kW)	3.02416	1.84956	Heat Recovery Efficiency	0.74861	0.82009
Overall System Efficiency	0.821275	0.852349			
Space Heating Capacity (kW)	6.02404				
Exhaust HE size (Number of tubes)		10.7755			
Jacket Water HE size (Number of Elements)		40.7239			
Radiator Network Size (Number of Heating Elements)		73.9104			

Figure 7.17 System inspection panel

### 7.3. Total required thermal capacity of heating systems

A function that sizes the CHP as well as the auxiliary boiler with the objective of meeting the total thermal demand of the dwelling is included in the software package. This is not an optimal sizing routine, but it rather involves the calculation of the necessary total thermal capacity needed to meet the total dwelling space heating and DHW demand. In the case of the heat priority controller, "Size System" button sizes the engine to produce a thermal output that supplements the selected thermal capacity of the auxiliary boiler to meet the dwelling thermal demand.

The first step in this procedure executed by the developed Matlab code, regardless of engine type and system configuration, is the calculation of the total system thermal capacity. A method used in the sizing of conventional boilers as found in Fred Hall et al. [116] will be applied in this case. Appendix 4 contains the Location Factors ( $L.F.$ ) used for sizing heating systems for different UK locations compiled in Table A.4.1.

The system thermal capacity for space heating only is calculated from:

$$\dot{Q}_{total\_cap} = UAL.F. \quad (kW) \quad (7.16)$$

Where  $L.F.$  is the location factor found in Table A.4.1

When the system is designed to supply DHW, the total system thermal capacity is calculated from:

$$\dot{Q}_{total\_cap} = (UAL.F.) + 2 \quad (kW) \quad (7.17)$$

The second step is the calculation of the engine displacement per unit thermal output rate  $V_{dpq}$  of the engine ( $cm^3/kW$  in our case). In order for this segment of code to work correctly, the desired engine type and inlet and outlet temperatures of the heat recovery system must be selected. The selected engine displacement  $V_{d\_ini}$  at this point does not matter and can be of any positive value.

$$V_{dpq} = \frac{V_{d\_ini}}{\dot{Q}_{total\_recov\_ini}} \quad (cm^3/kW) \quad (7.18)$$

The third step depends on the system configuration and control strategy:

### 7.3.1. Case 1 HPC, no auxiliary boiler, no heat storage

Under this design, the thermal capacity of the CHP unit must equal the calculated required total space heating capacity as seen in equation ( 7.19 ).

In this case, a separate DHW boiler will meet this demand. Therefore the sized engine displacement will be:

$$V_{d\_sized} = V_{dpq} \dot{Q}_{total\_cap} \quad (cm^3) \quad (7.19)$$

### 7.3.2. Case 2 HPC with auxiliary boiler, no heat storage

In this case, the system is undersized and works in tandem with an auxiliary boiler of a thermal capacity  $\dot{Q}_{aux\_cap}$  which supplements the CHP unit and in addition provides DHW when necessary. The engine displacement of the unit is calculated from:

$$V_{d\_sized} = V_{dpq} (\dot{Q}_{total\_cap} - \dot{Q}_{aux\_cap}) \quad (cm^3) \quad (7.20)$$

### 7.3.3. Case 3 HPC with auxiliary boiler and heat storage

Due to the storage tank supplying both space and DHW heat, an additional  $2kW$  must be added to the total system capacity [116]. Therefore, the system may still be sized by using:

$$V_{d\_sized} = V_{dpq} (\dot{Q}_{total\_cap} + 2kW - \dot{Q}_{aux\_cap}) \quad (cm^3) \quad (7.21)$$

### 7.3.4. Case 4 EPC systems

Unless an auxiliary boiler of a suitable capacity supplements the micro-CHP unit, the thermal output of the system will be unable at times to meet the thermal demand. Therefore, systems using an electricity priority controller will be always combined with an auxiliary boiler. Again, the sizing of an electricity priority system, including the heat storage tank (if applicable), and the auxiliary boiler thermal capacity are all potential subjects of optimization. For the above reason, in the case of the electricity priority controller, the sizing function will initially size the auxiliary boiler as if the boiler operated on its own.

#### 7.4. Post Processing Window

When a simulation session is complete, the simulation data post processing window pops up. Interactive panels that are part of this window can be seen in Figure 7.18 and Figure 7.19.

The panel “Large Scale Electricity Production” in Figure 7.18 is used for inputting the fuel conversion efficiency, the power transmission efficiency and the specific CO<sub>2</sub> emissions of conventional centralized power supply.

The panel “Boiler Characteristics” is used to input the efficiencies of the auxiliary and the conventional boiler. According to 2000 ASHRAE HVAC and Equipment [117], Boiler efficiency ranges from 78% to 96%. Similar values are provided by Fred Hall et al [116] who give values of 75% for non condensing modern boiler, 88% for condensing boiler while for older boilers as low as 58%.

The panel “Energy Prices” is used to choose the electricity import scheme (constant and five variable electricity price schemes are available). Electricity import and export prices as well as the natural gas price can be set.

The screenshot displays three panels from the post processing window. The 'Large Scale Electricity Production' panel has three input fields: Fuel conversion efficiency (0.4), Power Transmission efficiency (0.93), and Emitted CO2 per kWh of produced electricity (0.489). The 'Boiler Characteristics' panel has two input fields: Aux. Boiler efficiency (0.9) and Main Boiler Efficiency (0.9). The 'Energy Prices' panel features a dropdown menu set to 'Constant Electricity Price', a checked checkbox for 'Standing Charge (£/day)' with a value of 0.20, and five other input fields: Constant Electricity Price (£/kWh) (0.1379), Economy Electricity Price High (£/kWh) (0.189), Economy Electricity Price Low (£/kWh) (0.155), Feed in Tariff £/kWh (only for Pe<2kWe) (0.1324), Natural Gas Price (£/kWh) (0.048), and Electricity Export Prices (£/kWh) (0.0477).

Figure 7.18 Segment of the post processing window

The panel of Figure 7.19 contains a plot tool that facilitates the generation of relevant plots such as monthly energy consumption, CO<sub>2</sub> emissions, costs, heat rejection, and daily indoor temperature and engine speed profiles. In addition, the payback period can be set, and the inclusion of the FIT scheme

can be excluded or included in the calculations on the unit economic performance.

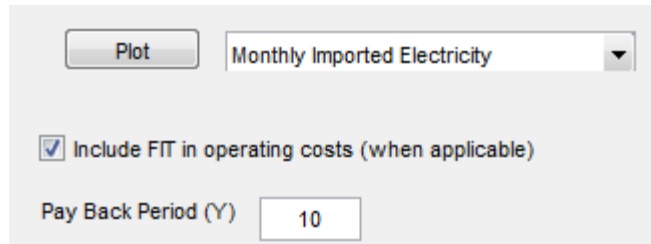
The image shows a software interface for selecting a plot. It features a 'Plot' button, a dropdown menu currently set to 'Monthly Imported Electricity', a checked checkbox for 'Include FIT in operating costs (when applicable)', and a 'Pay Back Period (Y)' input field with the value '10'.

Figure 7.19 Plot selection panel

A virtual button on the Simulation Data Post Processing Window discussed above calls a function that performs economical and environmental evaluation of the simulated micro-CHP system using the parameters entered through the panels of Figure 7.18 and Figure 7.19. Finally, it generates a report that contains a full description of the simulated system, and is accompanied by the following calculated performance indicators:

- Monthly and yearly CO<sub>2</sub> production
- Monthly and yearly consumed fuel
- Monthly and yearly produced electricity
- Monthly and yearly consumed electricity
- Monthly and yearly imported electricity
- Monthly and yearly exported electricity
- Monthly and yearly generated heat
- Monthly and yearly recovered heat
- Monthly and yearly used heat
- Monthly and yearly rejected heat
- Monthly and yearly fuel utilization efficiency
- Monthly and yearly energy costs
- Monthly and yearly generated primary energy savings
- Monthly and yearly CO<sub>2</sub> savings
- Monthly and yearly engine and auxiliary boiler ignitions

- Monthly and yearly operating time
- Monthly and yearly cost savings
- Unit Marginal Cost

### 7.5. Model functionality

The following graphs are plotted in order to present the functionality of the complete model. The plot of Figure 7.20 contains the indoor temperature profile obtained through the simulation of a model of a post-1967 mid-Terraced home during a March workday in Birmingham, heated by an HPC micro-CHP unit. The graph segments in which indoor temperature drops are intervals of no space heating during which the radiators are switched off. The radiator circuit pump is switched off, either due to no active occupants being in the dwelling (two time intervals in Figure 7.20 from 0 sec to  $2.6 \times 10^4$  sec and from  $3.2 \times 10^4$  sec to  $6.4 \times 10^4$  sec), or due to indoor air reaching the upper set temperature limit ( $7.8 \times 10^4$  sec to  $8.64 \times 10^4$  sec). As can be observed in Figure 7.20 and Figure 7.22, the longer the dwelling stays without heating, the longer it takes for the heating system to heat the indoor air up when a space heating demand occurs.

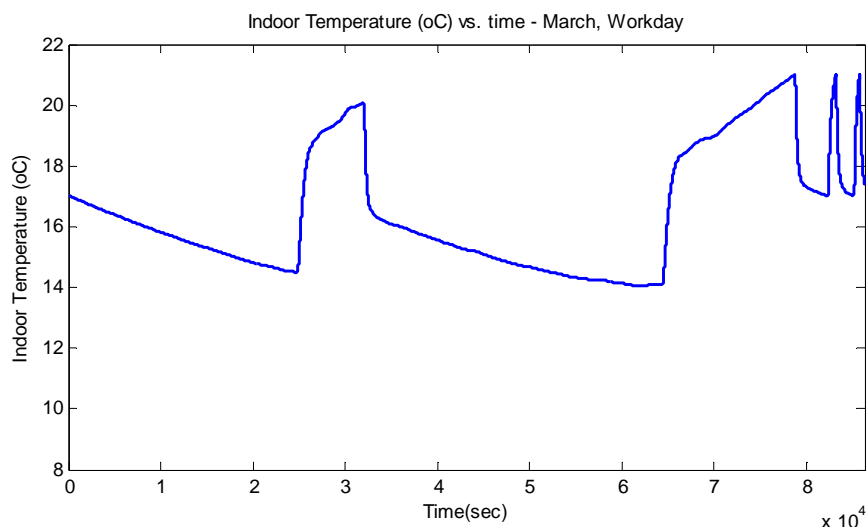


Figure 7.20 Simulated indoor temperature profile of a workday in March

The same indoor temperature plot along with the plots of the wall layer temperatures and the outdoor temperature can be seen in Figure 7.21. The temperature difference between the inner and the outer wall layers and the effect of the layered wall model in giving realistic indoor temperature profiles is visible. The heating up and cooling down of the dwelling fabric and the effects of its thermal inertia may also be observed.

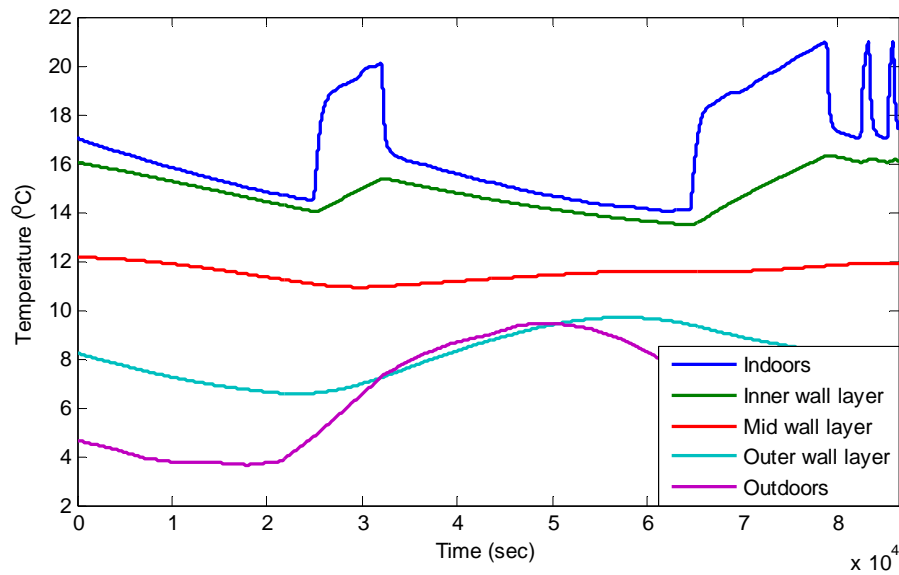


Figure 7.21 March workday outdoor, indoor, and wall layer temperature profiles

In the plot of Figure 7.22, the indoor temperature of the same dwelling at the same location and month during a holiday is plotted against time showing a similar behaviour, but following different heating patterns due to the difference in the occupancy profiles can be seen.

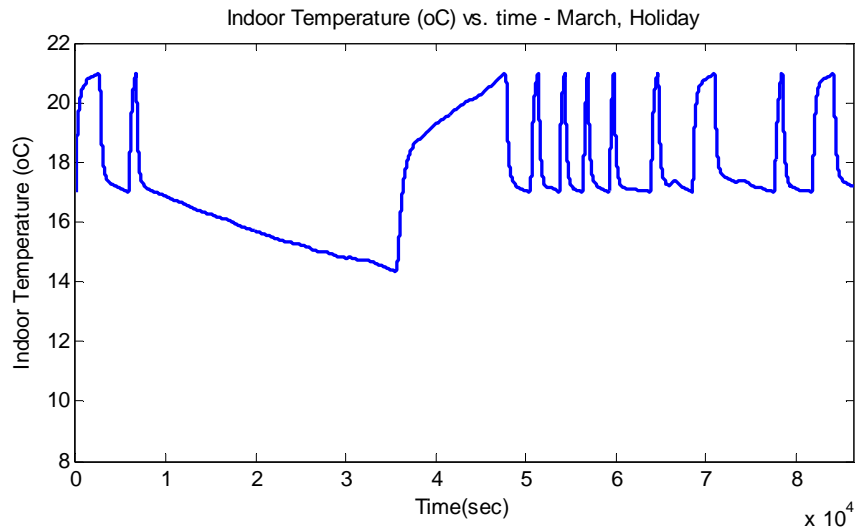


Figure 7.22 Simulated indoor temperature profile of a holiday in March

Figure 7.23 and Figure 7.24 show the plots of the daily engine speed profiles corresponding to the simulations of Figure 7.20 and Figure 7.22 respectively.

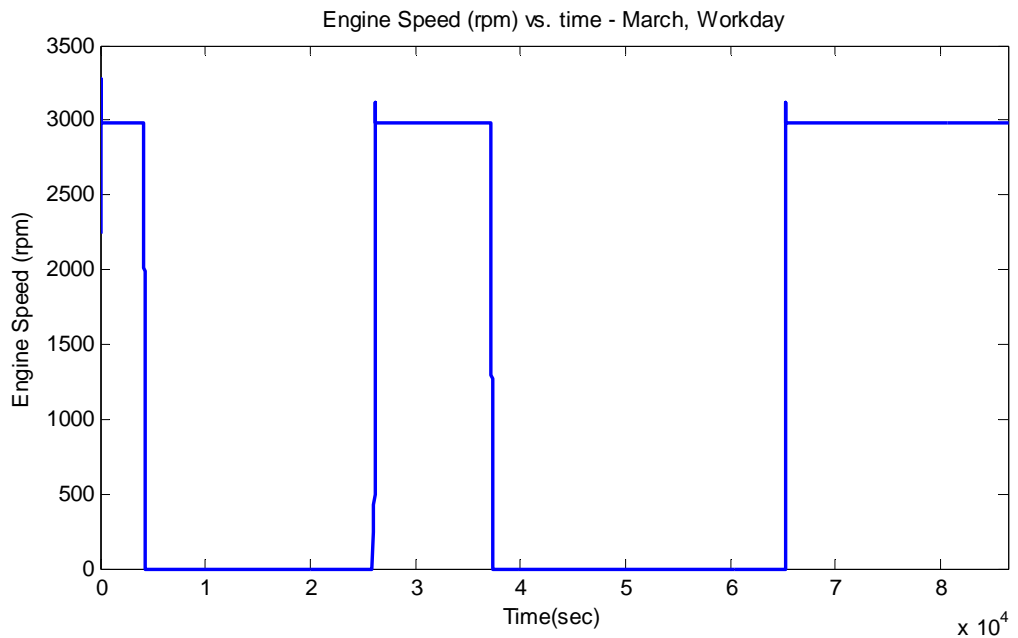


Figure 7.23 Simulated engine speed profile of a March workday

The longer engine operation during holidays observed by comparing Figure 7.23 to Figure 7.24, can be attributed to the greater duration of heating due



to the longer periods for which an active occupant is in the dwelling during holidays.

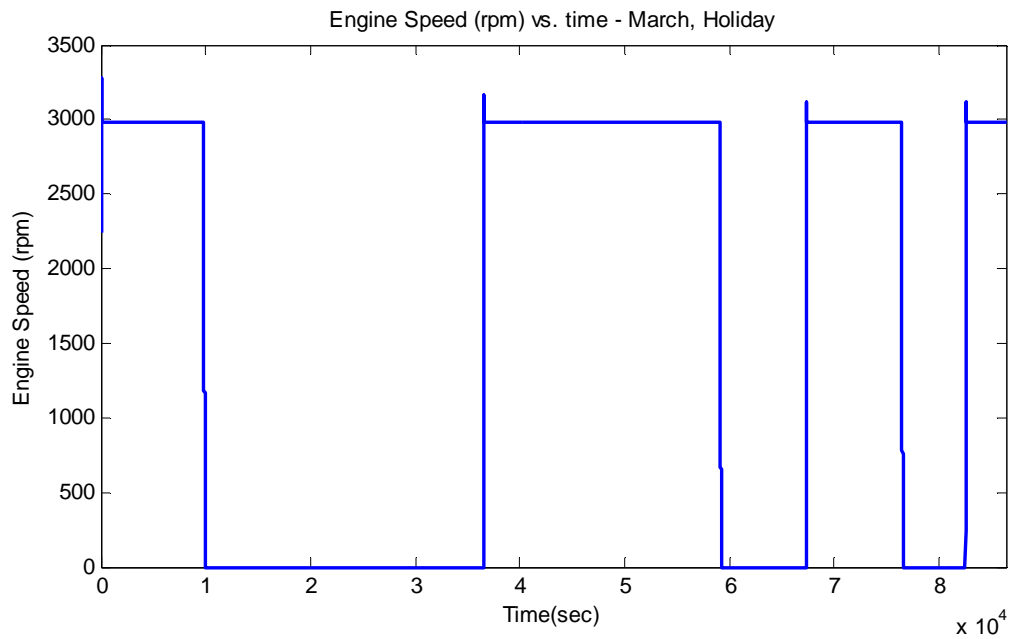


Figure 7.24 Simulated engine speed profile of a March holiday

The plot of the storage tank temperature profile during a workday under the same dwelling and weather profile can be seen in Figure 7.25. By comparing the contour of this plot to that of Figure 7.20, it can be observed that when the radiators are switched on to supply heat to the indoors, the tank temperature exhibits a sharp drop until it reaches its lower limit. From Figure 7.23 and Figure 7.25, it may be observed that the engine operates when the storage tank temperature crosses its lower temperature limit.

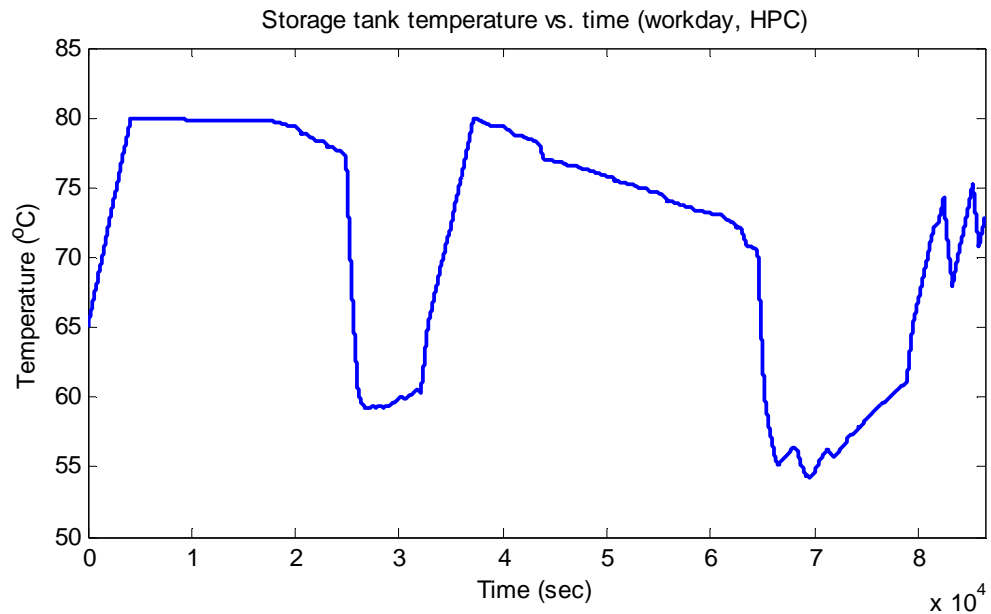


Figure 7.25 Storage tank temperature profile under heat priority control during a March workday

The graphs of Figure 7.26 and Figure 7.27, are plotted from data of the model simulated under electricity priority control operation. Figure 7.26, shows the engine speed profile throughout a March workday. It can be observed that the operating period of the engine is considerably longer than in the HPC case of Figure 7.23, as the engine operation depends on the electrical load rather than the indoor temperature and the occupancy profile. While the electrical load does depend on occupancy, there are no moments of zero electrical load due to the operation of appliances such as the refrigerator and the washing machine. The engine is turned off only when the electrical load drops below the minimum level (0.2x10<sup>4</sup> sec to 2.4 x10<sup>4</sup> sec).

The storage tank temperature profile under the electricity priority control operation is shown in Figure 7.27. During heating periods, the tank temperature exhibits a drop similar to that of the heat priority control. It can also be observed that the engine operation during periods of low thermal demand lead to the rise of the tank temperature to the level of the upper temperature limit “T\_st\_lim3”. This triggers the heat rejection mechanism until the temperature crosses the lower heat rejection threshold “Tin\_rej\_l” where heat rejection mechanism is switched off (4.2x10<sup>4</sup> sec to 6.4x10<sup>4</sup> sec).

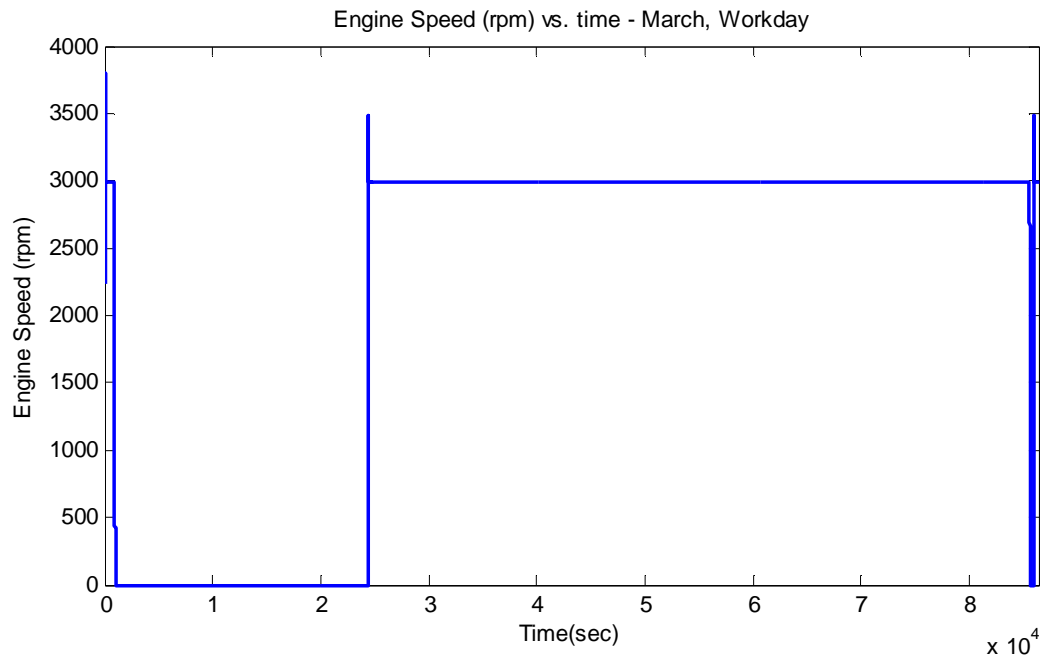


Figure 7.26 Simulated engine speed profile under an EPC operation

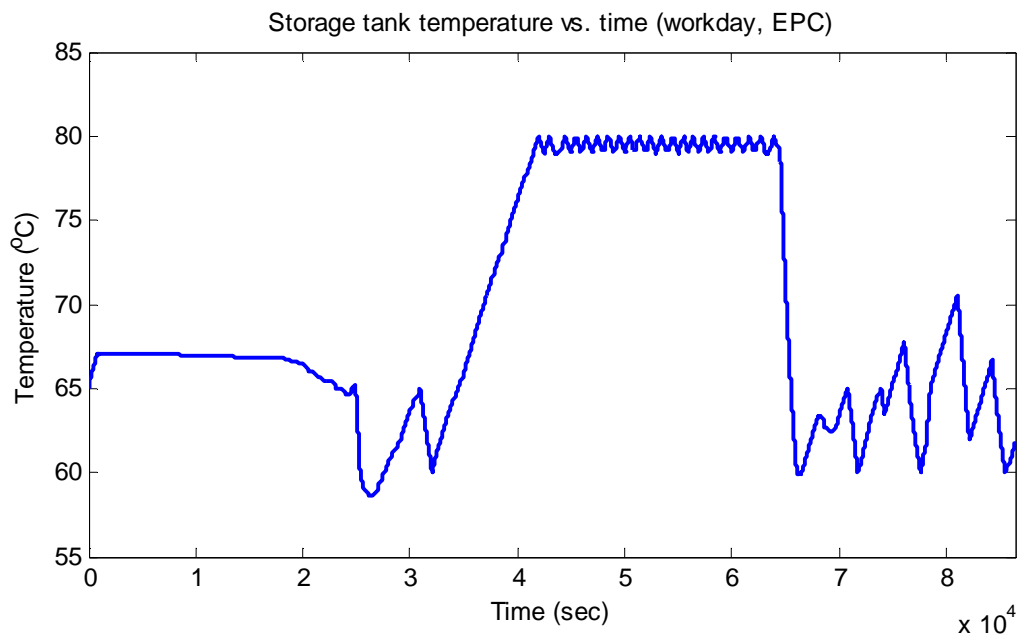


Figure 7.27 Storage tank temperature under EPC strategy during a March workday

## **7.6. Summary**

The developed simulation tool has been found to perform as intended. The model combines a number of novel features in terms of layout and characteristics. The component models developed in the previous chapters have been observed to integrate easily and without problem in the main model. The generator set and heat exchanger models offer a high degree of realism, and have a number of advantages not encountered in their counterparts from the reviewed literature. The developed graphical user interface constitutes a user friendly, time conserving, and well organized interface by means of which an array of simulation parameters can be configured and the simulation procedure controlled. The tool is characterized by a high degree of configurability and covers the most influential factors on system performance as discussed in section 3.1. The generated representative dwelling models make the selection and setup of a dwelling of relevant thermal characteristics a straightforward procedure. The ability to adjust the circuit temperatures allows for the study of their effect on system performance and cost of heat transfer components.

The post processing window that follows the completion of the simulation enables the user to process the simulation data and calculate the main performance indicators of the simulated micro-CHP system with minimal complexity.

From the above, it can be concluded that the simulation tool developed in the current chapter is particularly useful for applications in which the performance of the DES is the main focus of research. It is a viable alternative, and under certain circumstances, can be a more suitable platform than the more common building oriented simulation software for studying DES performance. Following the completion of the current chapter, the developed tool will be used in the following chapters for an in depth investigation of micro-CHP system performance and favourable system design characteristics.

## Chapter 8 Heat Priority Control Analysis

In this chapter, the effect of four different parameters on heat priority controlled (HPC) system performance will be investigated for an array of different system sizes. Since in the case of HPC systems the auxiliary boiler is sized to supplement the engine so that their collective heat output equals the design thermal load, the system performance indicators will be plotted against the thermal output ratio of the auxiliary boiler and the CHP:

$$R_q = \frac{\dot{Q}_{rec\_b}}{\dot{Q}_{rec\_CHP}} \quad (8.1)$$

As two different applications that share the same  $R_q$  number are characterized by the same proportion of thermal contribution by the CHP unit, the use of this term enables the direct performance comparison of applications that are characterized by different design loads such as in the comparison of two dwelling types.

### 8.1. Engine Grade

As discussed in section 3.1.5, system fuel conversion efficiency is an important factor in order to achieve high energy savings. In the current section, the effect of engine grade on system performance will be investigated. For this purpose, two different ICE model variants developed in section 4.11 will be simulated. The low compression ratio (LCR), low efficiency engine group represents the industrial heavy duty type engines typically encountered in stationary applications. The high compression ratio (HCR), high efficiency engine group represents engines originally designed to optimally operate on natural gas, and exhibit a considerable improvement in fuel conversion efficiency when compared to their LCR counterparts.

The effects of engine efficiency on the energetic performance of HPC systems can be observed on the plots of Figure 8.1 where  $PES$  are plotted against  $R_q$ . For all  $R_q$  values, the HCR engine generates higher savings than the LCR engine. This is attributed to the larger amounts of electricity generated by the HCR engine for a given amount of generated waste heat which results to lower amounts of imported electricity. Very low  $R_q$  values which correspond to larger engines result to low  $PES$  due to higher amounts of imported electricity. The increased electricity import is attributed to the shorter operating duration of the unit, as the time required by the engine to thermally saturate the storage tank is shorter. From  $R_q = 0$  to  $R_q = 2.9$ , the two engine types exhibit a similar behaviour with the  $PES$  of the LCR engine being approximately 0.1 to 1 percentage point lower than those generated by the HCR engine. This difference is increased considerably for  $R_q > 2.9$ , and while the maximum  $PES$  of 7.7% for the LCR engine is encountered for  $R_q = 4.5$ , the HCR engine yields a  $PES$  maximum of 9.1% at  $R_q = 6.4$ . The ratio between the two  $PES$  maxima is 1.18. By looking at the plots of Figure 8.2, it is observed that these points correspond to the same engine displacement. This indicates a weak dependence of the optimum engine size on engine grade in the case of HPC systems, while the dependence on  $R_q$  is stronger.

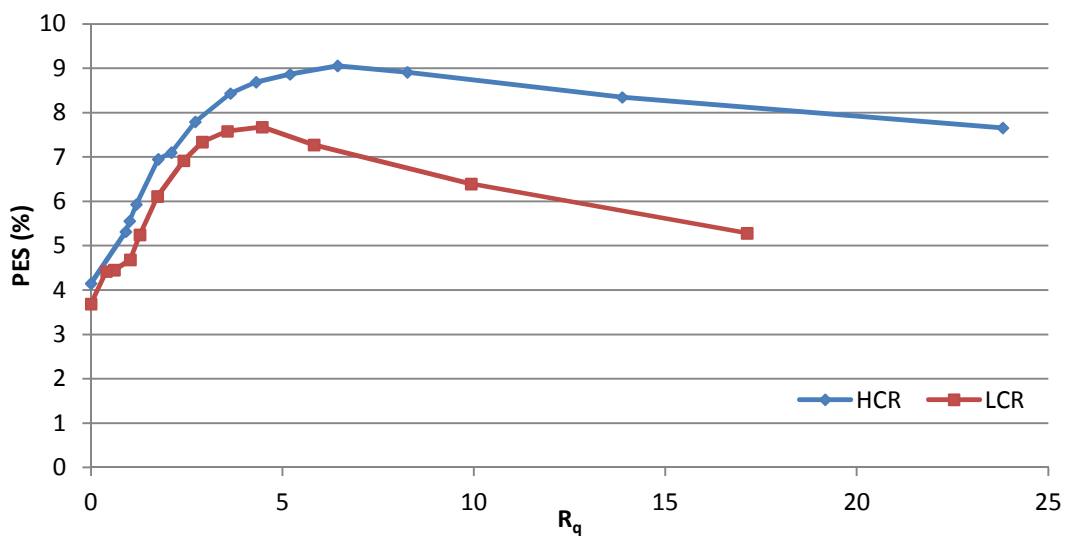


Figure 8.1 PES vs.  $R_q$  (Engine comparison, HPC)

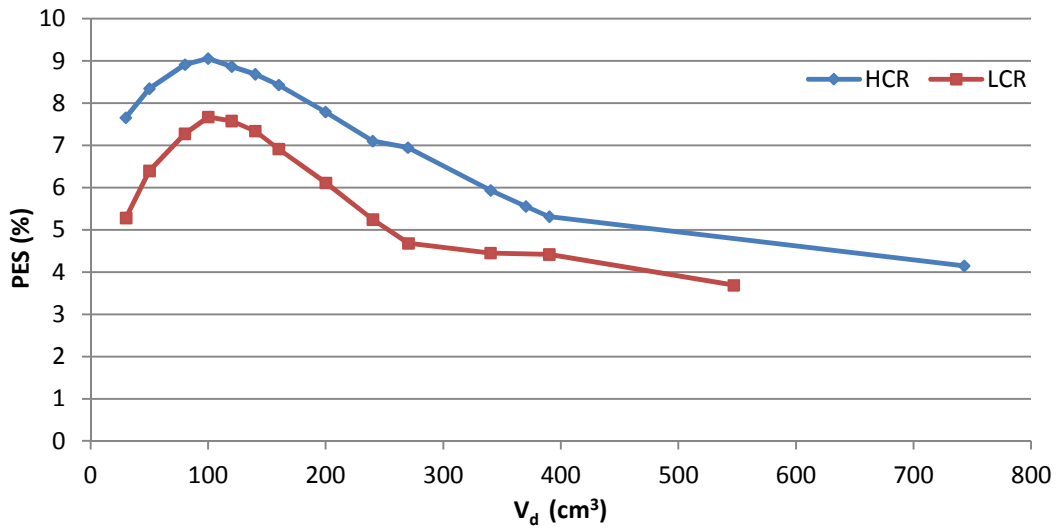


Figure 8.2 PES vs.  $V_d$  (Engine comparison, HPC)

$CO_2$  savings curves of Figure 8.3 follow the same contour observed in the  $PES$  curves of Figure 8.1, with maximum values of 11% and 9.2% for the HCR and LCR engines respectively, which is a ratio of 1.2. The  $CO_2$  savings maxima are positioned at 1.5 percentage points higher for the LCR engine, and 1.9 percentage points higher for the HCR engine than the respective  $PES$  maxima due to the low carbon content of natural gas compared to coal which is a commonly encountered fuel in centralized power stations.

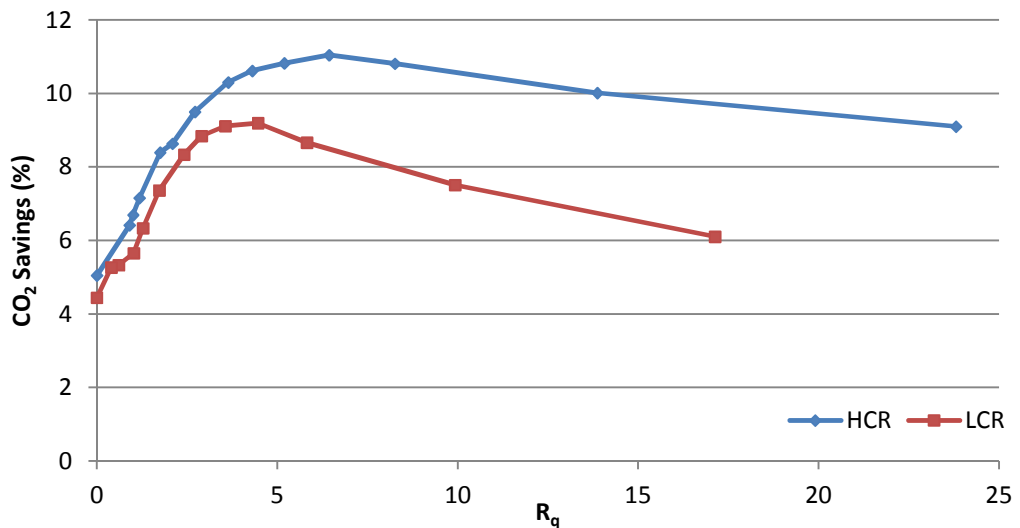


Figure 8.3  $CO_2$  savings vs.  $R_q$  (Engine comparison, HPC)

The engine and boiler start up frequency and duration with respect to  $R_q$  are identical between any tested engine type under HPC strategy, and for this reason no comparative graphs for these indicators are plotted for the HPC system in the current section.

In terms of cost savings in FIT eligible HPC systems, Figure 8.4 shows that for the tested dwelling, CHP/boiler combinations with  $R_q \geq 2.4$  for LCR and  $R_q \geq 4.3$  for HCR engines are characterized by FIT eligibility. This corresponds to engines of 160cc or smaller for LCR, and 140cc or smaller for HCR engines, as FIT is granted for units with a maximum electrical output of  $2kW$ . Since the HCR engine generates more electricity than the LCR engine for the same value of  $R_q$ , the FIT revenues (especially revenues due to the generation tariff) will be higher and hence the approximately 10 percentage point difference between the FIT eligible segments of the two curves. Maximum cost savings of 37% and 45% are observed for the minimum FIT eligible  $R_q$  values which is a ratio of 1.22. For the  $R_q$  values that yield maximum  $PES$ , cost savings drop to 39.1% and 31.7% for the HCR and LCR engines respectively, which is a ratio of 1.23.

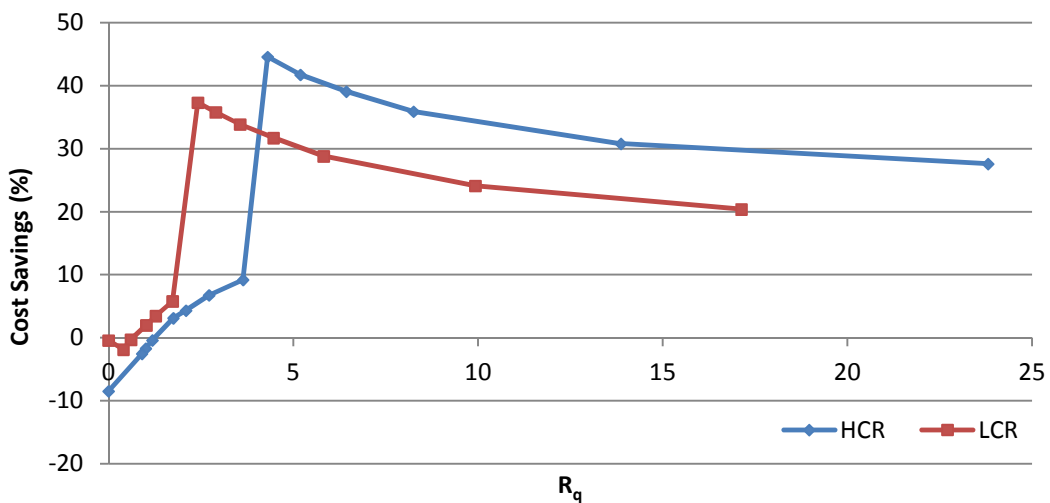


Figure 8.4 Cost savings (With FIT) vs.  $R_q$  (Engine comparison, HPC)



If it is assumed that no government funded monetary incentives such as the FIT are in place, calculated cost savings curves for the HPC system take the form of Figure 8.5. For  $R_q < 4.5$ , the LCR engine is the more cost effective choice. This can be attributed to the fact that the low prices normally encountered when power export is considered reduce the cost effectiveness of the process. For  $R_q < 1$ , both systems operate at a loss. For  $R_q > 4.5$ , the negative effect of power export on savings is reduced due to the engine size being reduced, and the cheaper production of electricity of the HCR engine compared to the LCR engine makes the HCR engine the more cost effective option. For the LCR engine, maximum savings of 11.7% are observed for  $R_q = 5.8$  which corresponds to an engine displacement of 80cc. For the HCR engine, maximum savings of 13.9% are observed for  $R_q = 13.9$  which corresponds to an engine displacement of 50cc – both smaller displacements than the maximum *PES* yielding 100cc engine. The ratio between the maximum cost savings of the two engine types is 1.18. Under the  $R_q$  values that generate maximum *PES*, cost savings of 12.7% and 11.3% for HCR and LCR engines respectively are observed which translates to a ratio of 1.12.

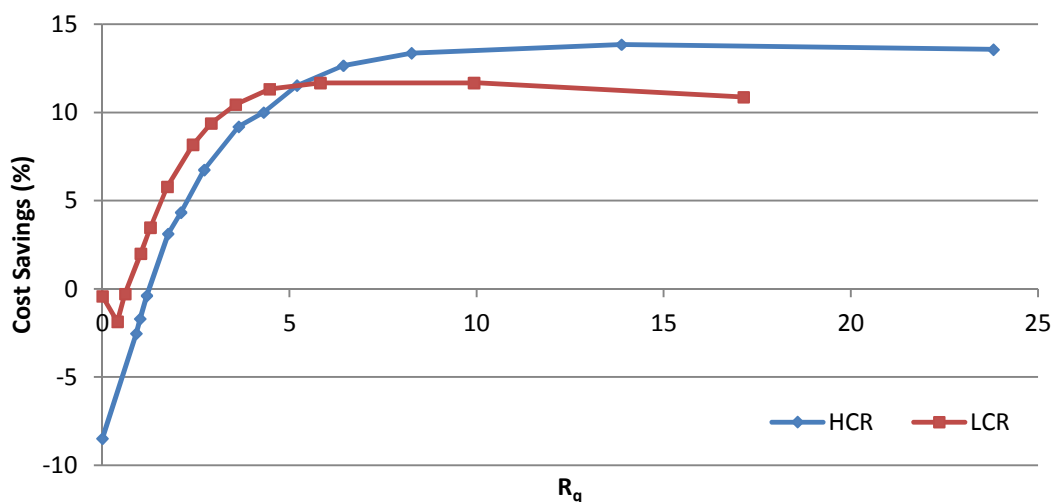


Figure 8.5 Cost savings (No FIT) vs.  $R_q$  (Engine comparison, HPC)

## 8.2. Dwelling Type

A detached and a mid-terraced dwelling both of the pre-67 group will be simulated for Leuchars weather profile to study the effect of dwelling type in the performance of micro-CHP systems. The dwellings are different not only in terms of size, but also in terms of geometry since they have a different number of exposed walls as shown in Chapter 6. In all cases, a high compression ratio (HCR) engine will be used in the following sections of the current chapter.

The *PES* vs.  $R_q$  curves of the two dwellings are shown in Figure 8.6. As can be observed, the energetic performance may vary significantly with  $R_q$ . In both cases, the lowest savings are observed when the engine is sized to cover the totality of the thermal load without auxiliary boiler operation ( $R_q = 0$ ). This is attributed to the fact that the oversized engine will heat up the storage tank at a very fast rate, and remain switched off for most of the time, thus not being available to meet the electrical demand which must be met by importing electricity from the non-cogenerating source of the centralized power plant. For  $R_q = 0$ , the detached house exhibits almost double the savings of the mid-terraced house. The reason for this being that the higher HPR of energy consumption of the mid-terraced house (the annual HPR of the mid terraced dwelling is 5.1 and of the detached is 4.3) translates to a higher proportion of the total energy demand being contributed by the boiler than from the grid in the case of conventional heat and power supply. Considering the fact that the boiler has higher utilization efficiency than the grid supplied power, the overall efficiency of the conventional solution of the higher HPR application is expected to be higher than that encountered in the lower HPR applications. Since the CHP device efficiency is not expected to vary to any appreciable degree, the savings generated by the higher HPR application are expected to be lower than of the lower HPR application. As  $R_q$  increases, this difference in performance is attenuated, and for  $R_q > 6.4$ , savings in the mid-terraced house are higher. This is attributed to the fact that for larger values of  $R_q$ , the engine is operated for a longer time period meeting a larger proportion of the electricity

demand. Since the mid-terraced house is characterized by proportionally lower electricity consumption, the amount of imported electricity keeps being reduced up to the smallest tested engines, and as a result, *PES* keeps increasing as well. On the other hand, the proportionally higher electricity loads of the detached house lead to a power deficiency for the smaller engines that must be met by the grid, and this leads to a reduction in *PES* for  $R_q > 6.4$ .

In the case of the detached house, maximum *PES* = 9.1% occur for  $R_q = 6.4$  and corresponds to an engine size of 100cc. For the same  $R_q$  value, the mid-terraced house generates identical savings. Maximum *PES* = 10.6% for the mid-terraced house occur for  $R_q = 14.5$  corresponding to the smallest simulated engine size of 30cc. The ratio between the maximum observed savings is 1.16. The above illustrates that the main component that negatively impacts energy savings in HPC systems is electricity import.

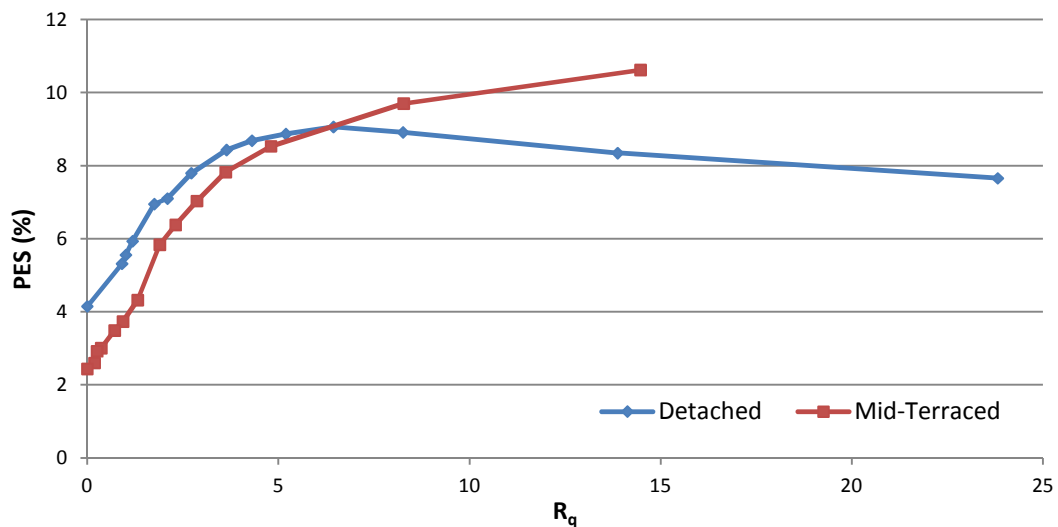


Figure 8.6 PES vs.  $R_q$  (Dwelling comparison, HPC)

CO<sub>2</sub> savings vs.  $R_q$  curves are shown in Figure 8.7, and are observed to follow the trend of the *PES* curves of Figure 8.6 which shows the dependence of CO<sub>2</sub> savings on imported electricity, and the analysis of the *PES* curves is also valid for the interpretation of the CO<sub>2</sub> savings curves. The curve of the detached home exhibits a maximum value of 11% and a turning point for

$R_q = 6.4$ , while maximum CO<sub>2</sub> savings of 13.2% for the mid terraced home occur for  $R_q = 14.4$ . The ratio between the two maxima is 1.2.

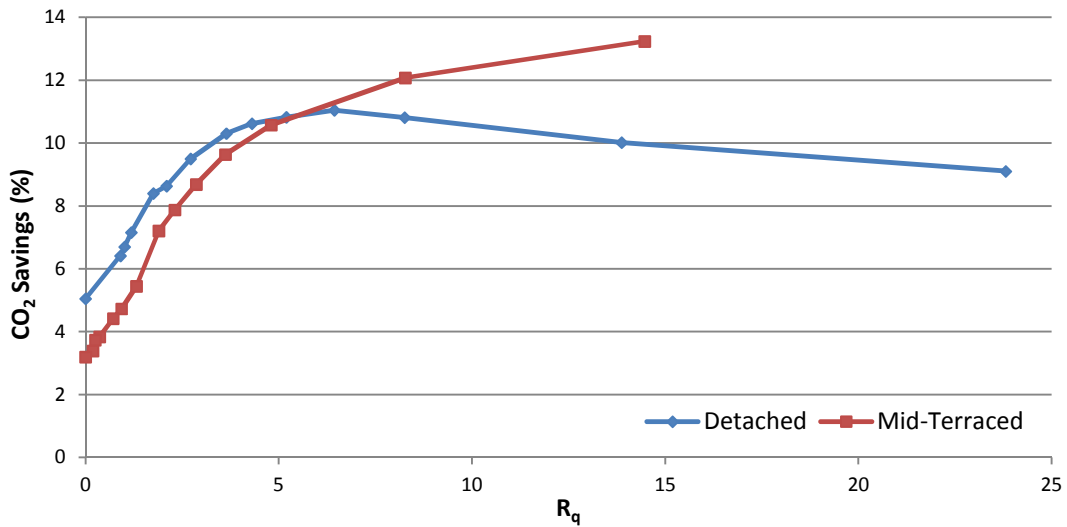


Figure 8.7 CO<sub>2</sub> Savings vs.  $R_q$  (Dwelling comparison, HPC)

The annual number of engine starts plots can be seen in Figure 8.8. It can be observed that the maximum engine start up frequency occurs for both dwelling types for  $R_q = 0$ , with 1450 and 1356 starts per year for the detached and mid-terraced house respectively. For low  $R_q$  values the engine becomes the principal source of heat and in this case, for  $R_q < 3.6$ , the detached home exhibits a higher engine start up frequency than the mid-terraced home. This is attributed to the fact that while the same thermal storage tank size of 200L is used for both house types, the thermal load encountered in the case of the detached house, and thus the engine size, are higher than of the mid-terraced house, resulting to a shorter time period for the storage tank water to transition from the engine switch on to the switch off temperature trigger limit and vice versa. As  $R_q$  is increased and the engine size is reduced, the heat storage tank is thermally saturated less frequently and difference in engine start up frequency is reduced considerably, and for the most efficient engine sizes of 30cc to 100cc ranges between 540 and 680 engine starts per year.

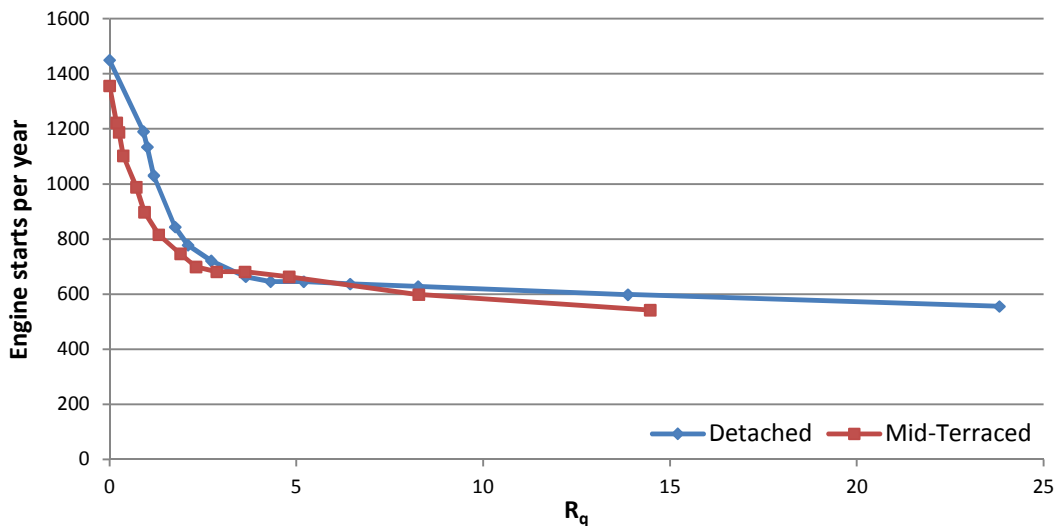


Figure 8.8 Engine starts vs.  $R_q$  (Dwelling comparison, HPC)

The annual engine operating duration plotted against  $R_q$  can be seen in Figure 8.9. It can be observed that for  $R_q = 0$  (maximum engine size without an auxiliary boiler), the annual engine operating duration is very short, with 2024 and 1767 operating hours per year for the detached and mid – terraced house respectively.

As  $R_q$  is increased, the engine operating duration increases as well due to the longer period of time necessary for the smaller engine to thermally saturate the heat storage tank, once the boiler is switched off for a given thermal demand. Considering that the demand for hot water is present throughout the year, and that for both dwellings a 100L per day hot water consumption is assumed, once space heat demand is not present, the smaller engine of the mid-terraced house operates for a longer period of time than in the case of the detached house for a given  $R_q$  value. The above comes in agreement with the observation that when engine operating duration is plotted against engine displacement as shown in Figure 8.10, annual engine operating hours do not detract significantly between the two house types for a given engine size, especially in the smaller more efficient sizes of 30cc to 100cc, and the difference in the largest engine sizes is attributed to the higher thermal load placed by the detached house on an engine that is the principal source of heat.

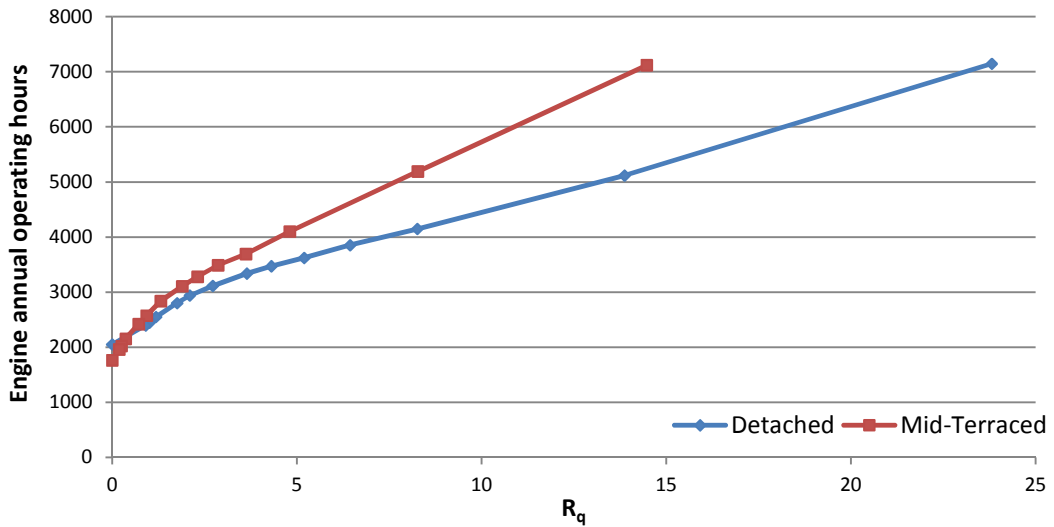


Figure 8.9 Engine operating hours vs.  $R_q$  (Dwelling comparison, HPC)

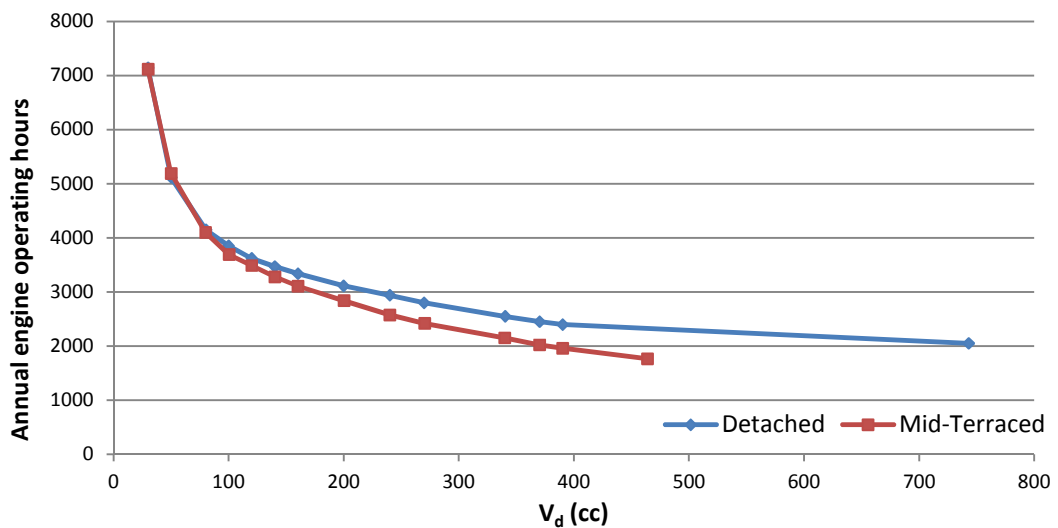


Figure 8.10 Engine oper. hours vs.  $V_d$  (Dwelling comparison, HPC)

Annual number of auxiliary boiler starts per year for the two house types plotted against  $R_q$  can be seen in Figure 8.11. As  $R_q$  is increased, the number of auxiliary boiler starts is increased as well due to the reduction of the amount of heat recovered from the smaller engines, which allows for the thermal load to reduce the thermal storage tank temperature below the boiler switch-on temperature limit at a higher frequency. The auxiliary boiler start up frequency is higher for the detached than for the mid-terraced house

throughout the tested  $R_q$  range with a difference of 200 to 700 engine starts. For engines displacements of 100cc and smaller, the boiler start up frequency in the case of the detached house stabilizes at 3500 annual start ups. Under the  $R_q$  values that give maximum  $PES$ , 3500 and 3290 engine starts for the detached and the mid-terraced house respectively are observed, which is a difference of 210 starts per year, and a ratio of 1.06. This difference between the frequencies of the two dwelling types can be attributed to the higher thermal loads and auxiliary boiler capacity of the detached house combined with the fact that both houses are simulated for the same storage tank size of 200L.

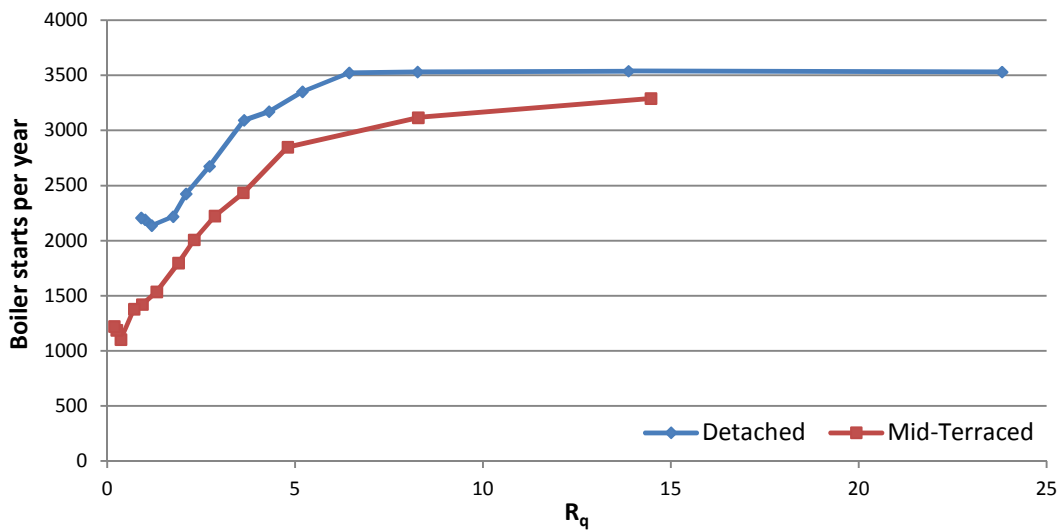


Figure 8.11 Boiler starts vs.  $R_q$  (Dwelling comparison, HPC)

The annual operating duration of the auxiliary boiler plotted against  $R_q$  for the two simulated building types can be seen in Figure 8.12. It can be observed that boiler operating duration for the smaller  $R_q$  values is low due to the larger engines meeting a greater fraction of the total thermal load than the smaller engines. For the smallest boiler capacities, the boiler operates for 724 and 1175 hours per year for the mid-terraced and the detached house respectively. As  $R_q$  is increased and engine size and recovered waste heat subsequently reduced, the boiler must meet a larger fraction of the thermal load, and as a result, boiler operating duration is gradually increased to 1373

and 1590 hours per year for the mid-terraced and the detached house respectively.

The boiler operating duration curve of the detached house is located approximately 200 hours above the curve of the mid-terraced house throughout the simulated  $R_q$  range, and for the  $R_q$  values that generate maximum  $PES$ , the boiler in the detached house operates 1.09 times longer than the boiler in the mid-terraced house. This behaviour can be attributed to the fact that the hot water load in the case of the detached house comprises a lower fraction of the total thermal load, and since total design thermal capacity includes an added  $2kW$  of hot water capacity, a larger fraction of the combined engine and boiler thermal capacity is dedicated for space heating applications. Since the combined boiler and engine thermal capacity is proportionally closer to the space heating design load in the case of the detached house, the thermal load is expected to remain proportionally higher and therefore the boiler is expected to work for longer periods during space heating before the storage tank temperature reaches the boiler switch off temperature than in the case of the mid-terraced house.

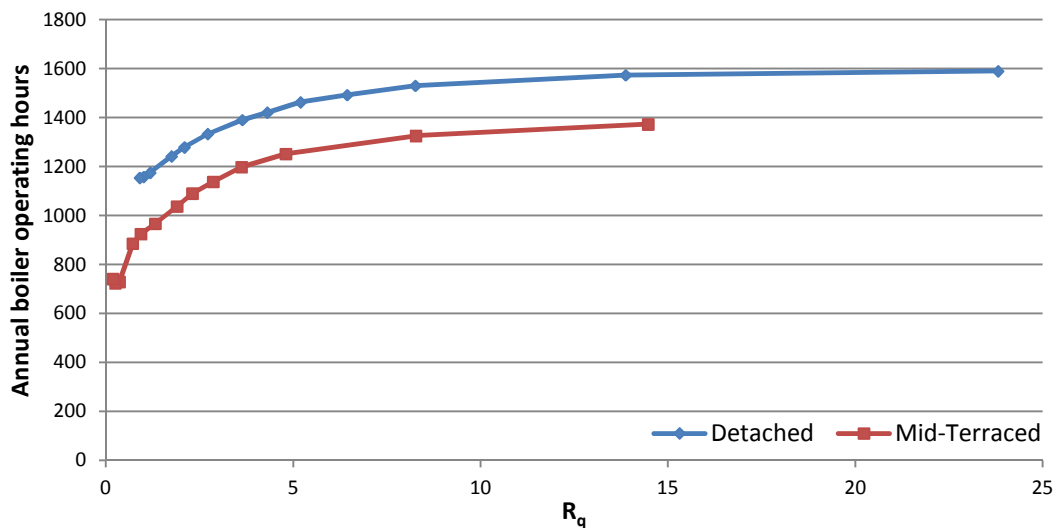


Figure 8.12 Boiler operating hours vs  $R_q$  (Dwelling comparison, HPC)

The economic performance of the simulated micro-CHP system under FIT scheme for the two tested house types can be seen in the annual cost



savings plots of Figure 8.13. The mid-terraced house under FIT scheme is observed to be generating higher savings than the detached house. The higher *HPR* exhibited by the mid-terraced house leads to the generation of proportionally higher amounts of electricity than in what is observed in the detached house. As the FIT scheme subsidizes not only power export, but also power generation, with generation tariff being almost three times the rate of the export tariff, the difference in cost savings between the two house types is well justified. In both cases, system sizes of 140cc and under are FIT eligible, but the same engine size results to different  $R_q$  values for houses of a different design thermal load. In the mid-terraced house, systems are FIT eligible for  $R_q > 2.3$ , while in the detached house, FIT eligibility starts for  $R_q > 4.3$ . Maximum cost savings of 61.3%, and 44.6% for the mid-terraced and detached houses respectively occur for the minimum FIT eligible  $R_q$  values. This is a difference of 16.3 percentage points and ratio of 1.37 between the two maxima. As  $R_q$  is increased and engine size reduced, cost savings are gradually reduced, and in the case of the smallest simulated engine size of 30cc ( $R_q = 14.5$  for mid-terraced, and  $R_q = 23.8$  for detached), cost savings drop to 40.8% and 27.6% for the mid-terraced and detached houses respectively. For the  $R_q$  values that generate maximum *PES*, cost savings of 40.8% and 39.1% for the mid-terraced and the detached house respectively are observed, which is a difference of 1.7 percentage points and a ratio of 1.04.

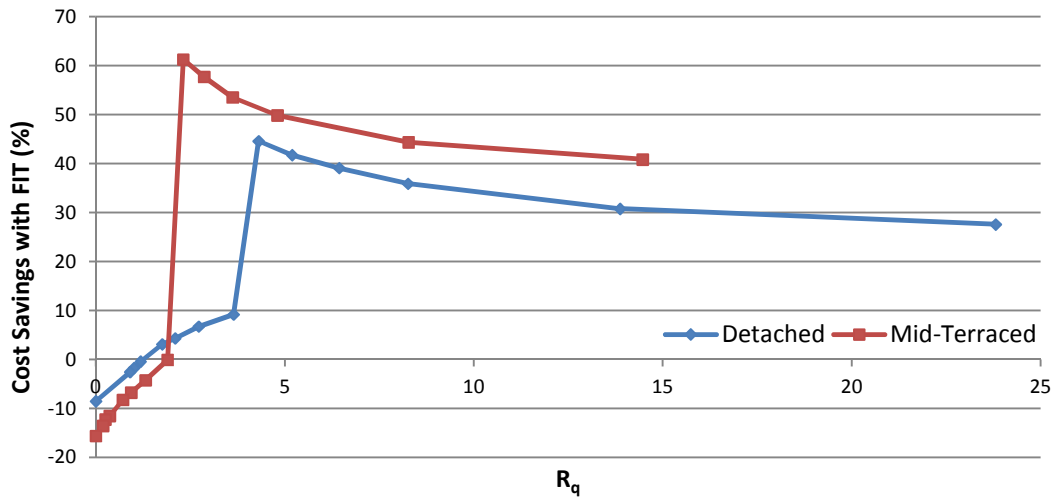


Figure 8.13 Cost savings vs.  $R_q$  (Dwelling comparison, HPC)

When cost savings are calculated under a no government subsidy regime, the resulting values are considerably reduced as can be seen in Figure 8.14. Maximum savings of 13.8% for  $R_q = 13.9$ , and 15.6% for  $R_q = 14.5$  are observed for the detached and the mid terraced house respectively. Compared to the FIT scheme regime, a no subsidy regime generates maximum cost savings that are reduced by 30.8 percentage points for the detached, and by 45.6 percentage points for the mid-terraced home, and the maxima occur for smaller engine sizes of 50cc and 30cc respectively. For  $R_q < 1.9$ , the system is observed to operate at a loss for the mid terraced house, while for the detached house, the system generates losses for  $R_q < 1.2$ .

The detached house performs better throughout the largest segment of the simulated engine size range. The higher HPR of the mid-terraced house leads to proportionally higher amounts of exported electricity than the detached house, and due to the low export price of electricity, the detached house exhibits higher cost savings for  $R_q < 10$ .

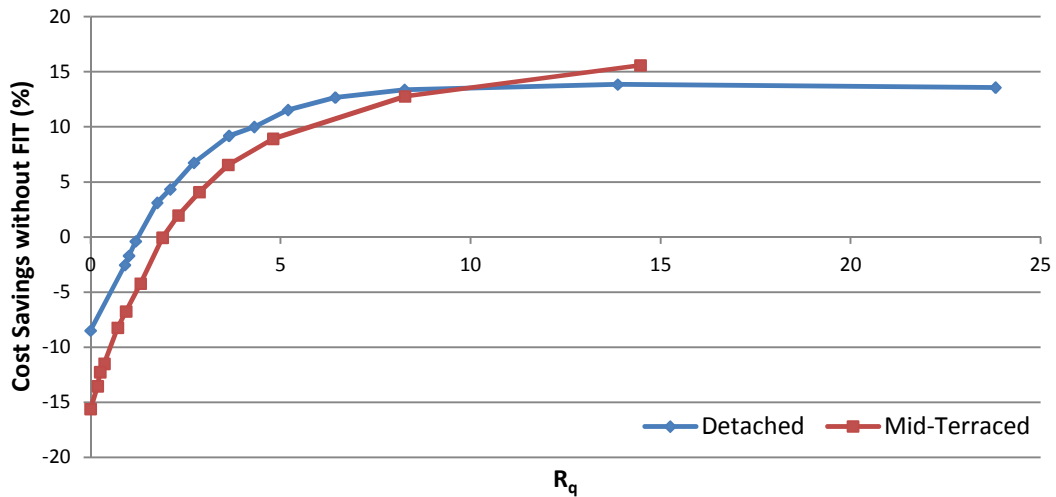


Figure 8.14 Cost savings vs.  $R_q$  (Dwelling comparison, HPC)

### 8.3. Dwelling Location

Since in some cases geographical location can be an important factor for system technical and financial feasibility, and since this document focuses on the investigation of micro-cogeneration performance in the geographical area of UK, the extent to which system performance can vary between two locations within the United Kingdom of significantly different geographical latitude will be investigated. For this purpose, the model of a pre-67 detached dwelling is simulated under the weather profiles of London Gatwick and Leuchars.

The difference in energetic performance between the two locations can be seen in Figure 8.15. It can be observed that the simulation results of the colder climate (Leuchars) exhibit *PES* that are 1.5 to 0.7 percentage points lower than those under the warmer climate of London Gatwick due to the fact that the higher HPR of the energy composition under the colder climate translates to a higher overall fuel utilization efficiency of the conventional boiler & grid solution than in the warmer climate, whereas the micro-CHP device efficiency remains almost constant regardless of climatic conditions, thus having a higher impact on the warmer climate application. Maximum savings of 9.8% and 9.1% occur for London Gatwick and Leuchars weather

profiles for  $R_q$  values of 6.1 and 6.4 respectively, both corresponding to an engine size of 100cc. This is a difference of 0.7 percentage points and a ratio of 1.08 between the two maxima.

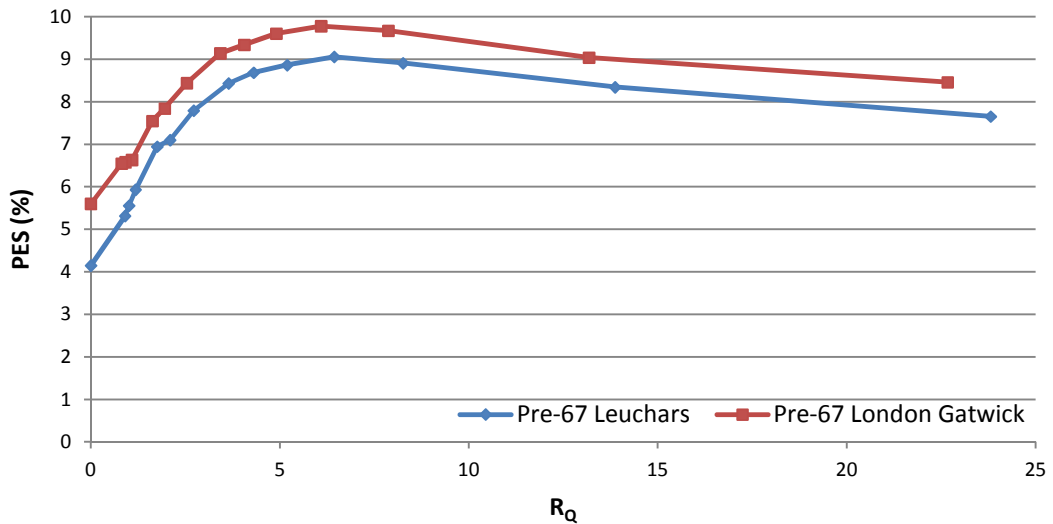


Figure 8.15 PES vs.  $R_q$  (Geog. comparison, HPC)

CO<sub>2</sub> savings curves as shown in Figure 8.16, follow the trend of the *PES* curves. The difference in CO<sub>2</sub> savings between the two locations ranges from 0.6 to 1.3 percentage points with maximum savings of 11.9% and 11% (a 0.9 percentage point difference, and a ratio of 1.08) for London Gatwick and Leuchars respectively, occurring for  $R_q$  values that maximum *PES* are also observed.

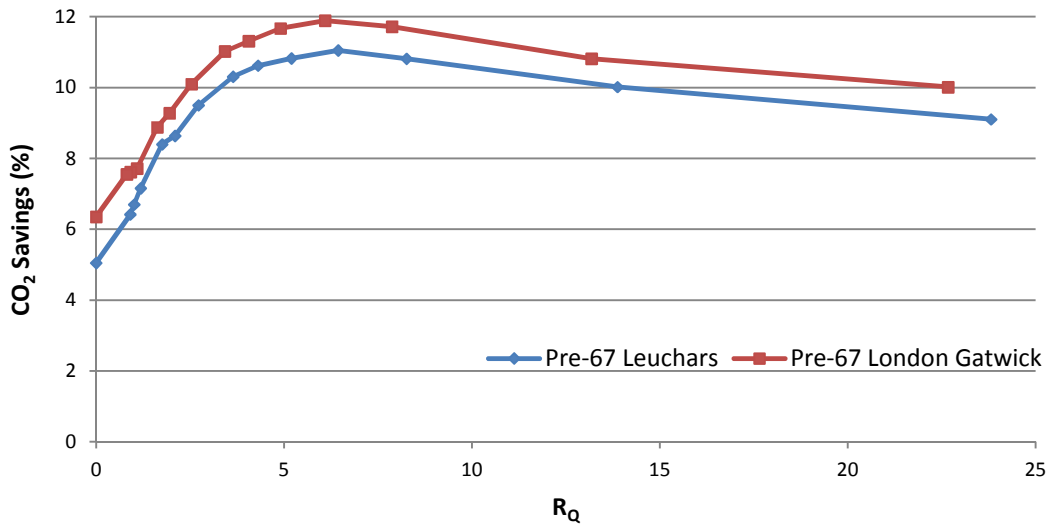


Figure 8.16 CO<sub>2</sub> Savings vs.  $R_q$  (Geog. comparison, HPC)

The annual number of engine starts recorded for the two locations plotted against  $R_q$  can be seen in Figure 8.17. Due to the higher thermal demand of the colder weather and the fact that the two simulations were performed under the same heat storage tank size, a more frequent engine start up frequency is observed for the Leuchars weather profile. The widest difference is observed for  $R_q < 1$  where the large engine contributes most of the heat to the dwelling with 318 starts per year difference for  $R_q = 0$ . For larger  $R_q$  values (smaller engines), this difference is attenuated and does not exceed 50 annual starts as the engine tends to operate for longer periods of time in order to thermally saturate the thermal storage tank. For the  $R_q$  values that result to maximum *PES*, the engine is started 587 and 637 times per annum for the London Gatwick, and the Leuchars weather profiles respectively, which is a difference of 50 starts and a ratio of 1.09.

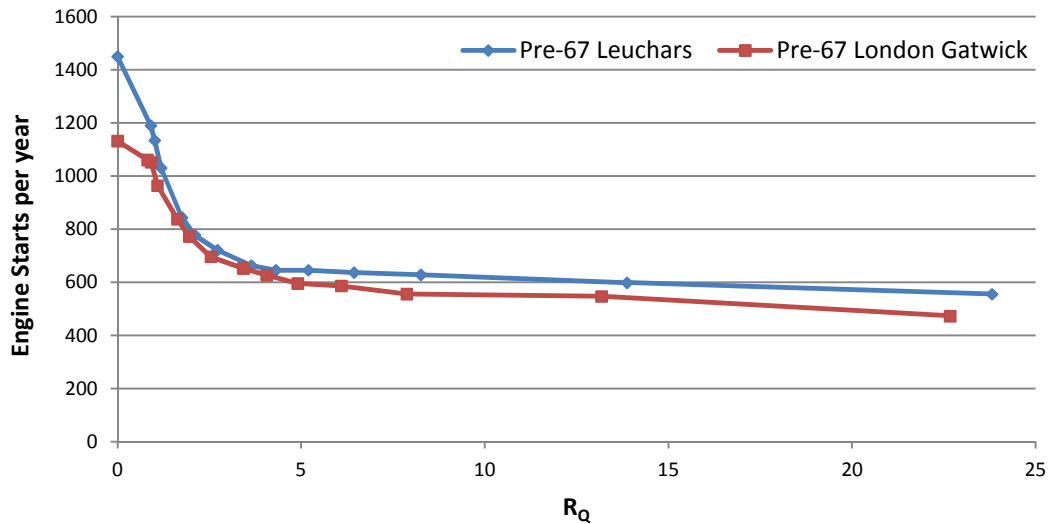


Figure 8.17 Engine starts vs.  $R_q$  (Geog. comparison, HPC)

The effect of location on annual engine operating duration can be seen in Figure 8.18. The annual engine operating duration curve under the Leuchars weather profile is located above the London Gatwick curve for the complete simulated engine size range. The difference in operating duration ranges between 300 to 500 hours for  $R_q = 0$  to  $R_q = 2.5$  respectively, and the difference tends to stabilize for  $R_q > 2.5$ . The longer engine operating time exhibited by the Leuchars profile is attributed to the higher thermal demand placed on the system by the colder weather profile. Minimum annual operating duration of 2053 and 1751 hours for the Leuchars and the London Gatwick profiles respectively is observed for  $R_q = 0$  where the engine supplies heat without being supplemented by an auxiliary boiler, while a maximum engine operating duration of 7114 and 6331 hours per year occurs for  $R_q$  values of 22.8 and 23.7 for Leuchars and London Gatwick weather profiles respectively. For the  $R_q$  values that result to maximum  $PES$ , the engine operates for 3305 and 3854 hours per year for the London Gatwick, and the Leuchars weather profiles respectively, which is a difference of 549 hours and a ratio of 1.17.

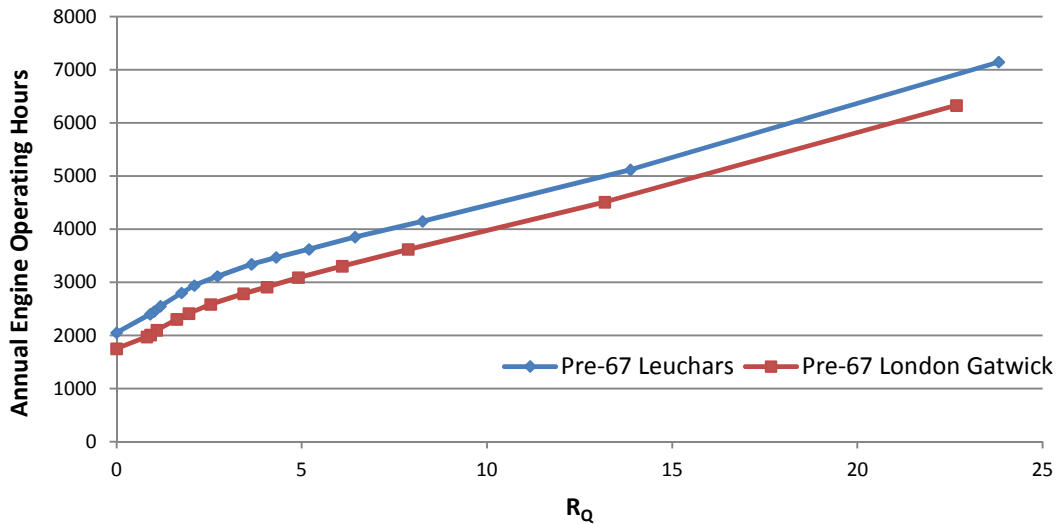


Figure 8.18 Engine operating hours vs.  $R_q$  (Geog. comparison, HPC)

The difference in the annual number of boiler starts between the two locations as can be observed in Figure 8.19 is considerably more noticeable than the difference in engine starts, with the colder climate of Leuchars resulting to a higher boiler start-up frequency than the London Gatwick profile throughout the complete simulated engine size range. Since for small  $R_q$  values, the principal source of heat is the engine, the difference in start-up frequency is relatively small (80 annual starts difference for  $R_q = 1$ ) as the engine is powerful enough to prevent the heat storage tank temperature from entering the boiler operating band for most of the time. As  $R_q$  is increased, the boiler start-up frequency and the distance between the two curves is increased as well. Under  $R_q$  values that generate maximum *PES*, 3500 and 2500 starts per year for Leuchars and London Gatwick respectively are observed. This is a difference of 1000 boiler starts and a ratio of 1.4 between the two locations. These start-up frequencies remain nearly constant for  $R_q > 6$  as the boiler becomes the principal source of heat, and the storage tank temperature lies within the boiler operating limits for most of the time. The significantly higher boiler start-up frequency observed in the case of the colder climate is attributed to the lower temperature the dwelling mass tends to fall to during non heating periods which during heating periods tends to

reduce the storage tank temperature to the boiler actuation limit more frequently.

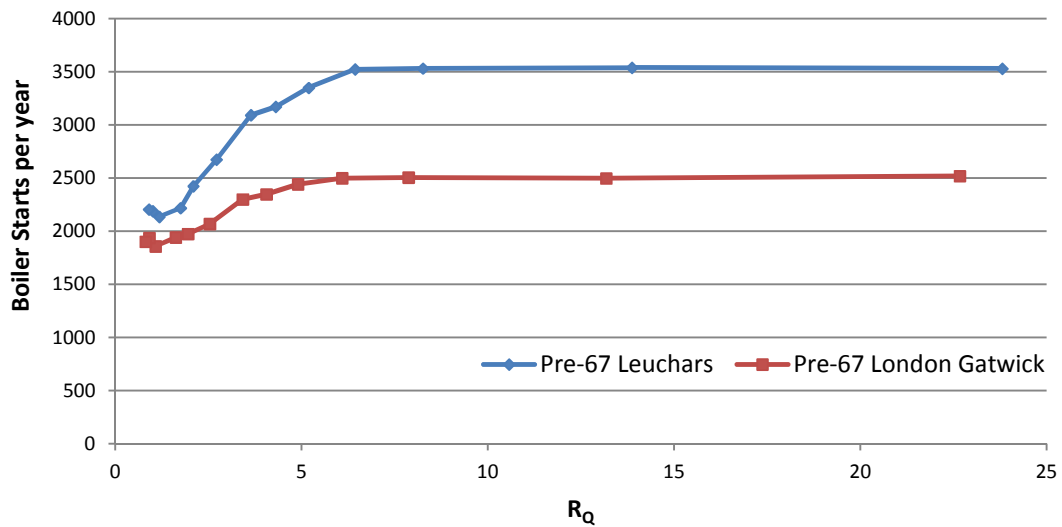


Figure 8.19 Boiler starts vs.  $R_q$  (Geog. comparison, HPC)

A considerable difference in annual boiler operating duration is also being observed between the two simulated locations, especially in the case of higher  $R_q$  values (smaller engines) as shown in Figure 8.20. The operating duration for the Leuchars weather profile is longer throughout the simulated engine size range with minimum operation of 1176 hours per year under  $R_q = 1.19$ , and 1065 hours per year under  $R_q = 0.82$  for Leuchars and London Gatwick for respectively. As engine  $R_q$  is increased and boiler gradually becomes the principal source of heat, the operating duration is increased, and the difference between the curves amplifies. For the  $R_q$  values that give maximum *PES*, the boiler operates for 1492 and 1286 hours per year for Leuchars and London Gatwick respectively, a 206 hour difference and a ratio of 1.16. Maximum boiler operating duration of 1590 and 1364 hours per year occurs for  $R_q = 23.8$  and  $R_q = 22.7$  for Leuchars and London Gatwick respectively, which is a difference of 226 hours and a ratio of 1.17. The significant difference in boiler duration is attributed to the fact that during non heating periods, the dwelling thermal mass temperature under a colder climate tends to drop below that encountered in the warmer



climate and this translates to the prolonged heat load periods of the colder climate keeping the heat storage tank water temperature in the boiler operating dead band for longer periods of time.

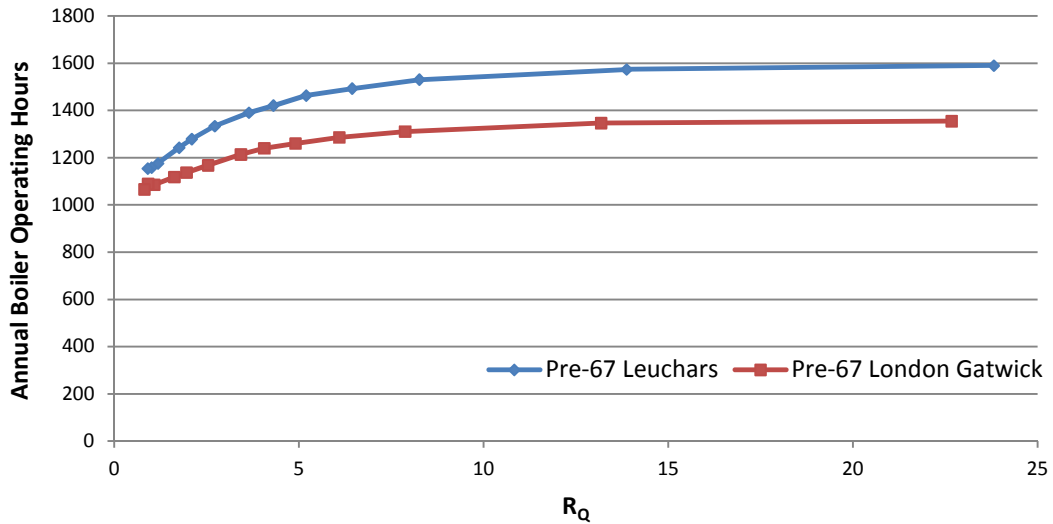


Figure 8.20 Boiler operating hours vs.  $R_q$  (Geog. comparison)

The economic performance of the CHP unit under FIT regime is very similar for both locations as can be observed in Figure 8.21 with the Leuchars curve being located above the London Gatwick curve throughout the complete FIT eligible  $R_q$  range due to the higher power generation tariff revenues associated with a higher thermal demand under HPC strategy. Highest savings of 42.8% and 44.6% - a difference of 1.8 percentage points and a ratio of 1.04 - occur under  $R_q = 4.1$  and  $R_q = 4.3$  (the largest FIT eligible engine size of 140cc) for London Gatwick and Leuchars respectively, the widest observed difference between the two FIT eligible curve segments. For the  $R_q$  values that maximize  $PES$ , cost savings of 38.2% and 39.1% for London Gatwick and Leuchars respectively are observed, which is a difference of 0.9 percentage points and a ratio of 1.02. Minimum savings of 27.6% occur for  $R_q = 22.7$  in London Gatwick, and for  $R_q = 23.8$  in Leuchars.

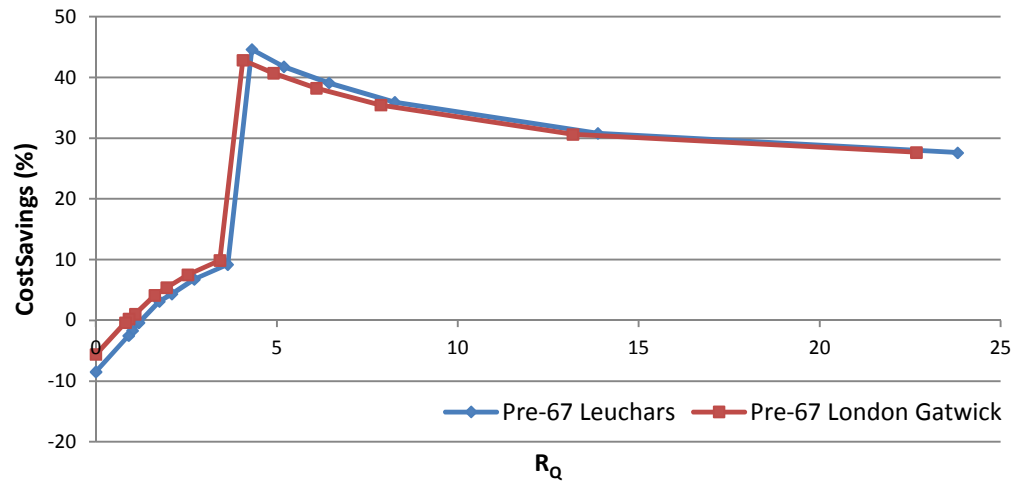


Figure 8.21 Cost Savings (With FIT) vs.  $R_q$  (Geog. comparison, HPC)

Cost savings under a no subsidy regime are also observed to be in close proximity between the two simulated locations as can be seen in Figure 8.22. Maximum annual cost savings of 14% occur under  $R_q = 13.2$  for London Gatwick, and under  $R_q = 13.9$  for Leuchars, both corresponding to a 50cc engine which is 50% of the engine size that generates maximum *PES*. Under  $R_q$  values for which maximum *PES* occur, savings of 13% for London Gatwick and 12.7% for Leuchars are observed. This is a difference of 0.3 percentage points and a ratio of 1.02.

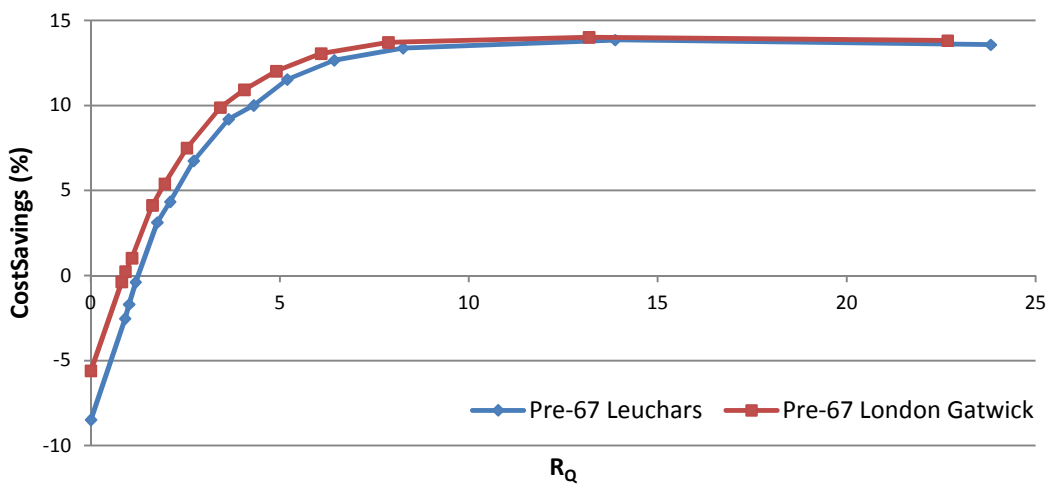


Figure 8.22 Cost Savings (No FIT) vs.  $R_q$  (Geog. comparison, HPC)

#### 8.4. Summary

The current chapter involved the investigation of the effect of system and energy consumption characteristics on the performance and operating patterns of HPC systems.

Imported electricity has been found to be the main cause of performance deterioration in HPC systems. The high efficiency HCR engine has been found to outperform the LCR engine in terms of *PES* and CO<sub>2</sub> Savings under all tested engine sizes, with a more pronounced difference in the smaller engine sizes, as the higher amounts of generated electricity reduce the need for electricity import from the grid. Maximum savings in both cases occurred for the same engine displacement. While system performance with the HCR engine is higher, the LCR engine operation generated savings that could still make this option attractive due to the lower cost and potentially higher service life of LCR engines. In terms of cost savings generated under FIT scheme, the higher amounts of electricity generated with an HCR engine lead to a considerable difference over the LCR counterpart due to the high rate of the generation tariff. FIT eligibility extends to a larger engine in the case of the LCR system. Under no government subsidy, the difference in cost savings between the two engine types is attenuated and the LCR system is the more cost effective option for medium and large engine sizes due to the fact that the higher amounts of power export under low export prices associated with the HCR engines reduce the economic performance of the system. On the other hand, the costs of electricity import in the case of the smaller LCR engines makes system operation less profitable than the HCR system where a larger percentage of electricity is generated on site.

The HPR of the power demand defines the engine size for which maximum *PES* and CO<sub>2</sub> savings are observed. Houses with a low HPR exhibit maximum savings for a midsized engine while smaller and larger engines lead to an increase of the amount of imported electricity, as a result, reduce savings. On the other hand, the savings of a dwelling with a high HPR keep increasing even for the smallest tested engines as the amounts of generated electricity are adequate for the importation of electricity to be prevented.

For a given  $R_q$  value, engine operating duration has been found to be longer for the smaller houses, as the smaller engine must work for longer periods to meet the hot water demand which was considered to be the same between the two dwellings. Due to the fact that in larger houses space heating comprises a larger fraction of the combined thermal capacity, the auxiliary boiler tends to operate for longer periods of time. Engines of the same displacement have been found to operate for almost the same duration.

Under the FIT scheme, the cost savings generated by the higher HPR dwelling are higher due the generation of proportionally higher amounts of electricity that are subsidized by the generation tariff. On the other hand, under no governmental subsidies, the higher amounts of exported electricity under very low export rates encountered in the case of the higher HPR dwelling reduce its economic performance below that of the low HPR dwelling.

In order to achieve similar engine and boiler start up patterns between different dwelling types, it is important that the thermal storage tank is sized in proportion to the modelled house.

The difference in performance between the tested locations was found to be small, with the warmer climate exhibiting higher savings due to the higher overall efficiency the conventional boiler & grid solution exhibits under colder climates combined with the practically constant device efficiency of the micro-CHP. The engine operating patterns were also similar but the engine and the boiler under the colder climate operated for a longer period of time mainly due to the lower temperatures the dwelling thermal mass dropped to during non heating periods which translated to longer heating periods. For the FIT eligible engine sizes, the colder climate generated higher cost savings due to the higher amounts of generated electricity. On the other hand, under no government subsidy, the low export rates made the colder climate generate lower savings.

## Chapter 9 Electricity Priority Control Analysis

The current chapter will investigate the effect of different system parameters and energy demand characteristics on the performance of a micro-CHP system operating under an electricity priority control (EPC) strategy using the same dwelling models and weather files as described in the HPC tests of Chapter 8. Since the auxiliary boiler capacity in this case is kept constant for all simulated engine sizes, all performance indicators are plotted against engine displacement  $V_d$  in  $cm^3$  rather than against  $R_q$ .

### 9.1. Engine Grade

The energetic performance of LCR and HCR engines operated under EPC strategy is shown in Figure 9.1. Maximum *PES* for both engine types is the highest for the smallest tested engine displacement of 30cc, and as engine size increases up to a point, *PES* are reduced as a result of the increase in generated and rejected waste heat. Once the minimum is reached, a further increase in engine size reduces the engine operating duration as the load falls more frequently below the minimum generator operating limit, resulting to a small increase in *PES*. The difference in *PES* between the two curves is 6 to 10 percentage points for smaller to medium engines, while for larger engines the curves tend to converge to the line of origin as only a fraction of the consumed electricity is produced on site, and the heat load is taken up by the auxiliary boiler, thus gradually approaching the performance of the traditional boiler & grid combination. As can be observed, a system using the LCR engine type under the EPC strategy will not generate any energy savings, but will rather operate at a loss for all but the smallest simulated 30cc engine. On the other hand, while HCR engines generate energy savings for the majority of simulated engine sizes, only small size units up to 80cc perform comparably to HPC systems, with *PES* for 30cc to 80cc engines ranging from 8.2% to 6.4% respectively. Maximum *PES* of 2.1% and

8.2% for LCR and HCR engines respectively are encountered, which translates to a difference of 6.1 percentage points and a ratio of 3.7. Minimum *PES* (or maximum loss of 10.4% ) occur for an LCR engine displacement of 160cc while in the case of the HCR engine, minimum *PES* of -2.3% (loss) occurs for a larger 200cc engine due to the lower power output an LCR engine exhibits for a given size.

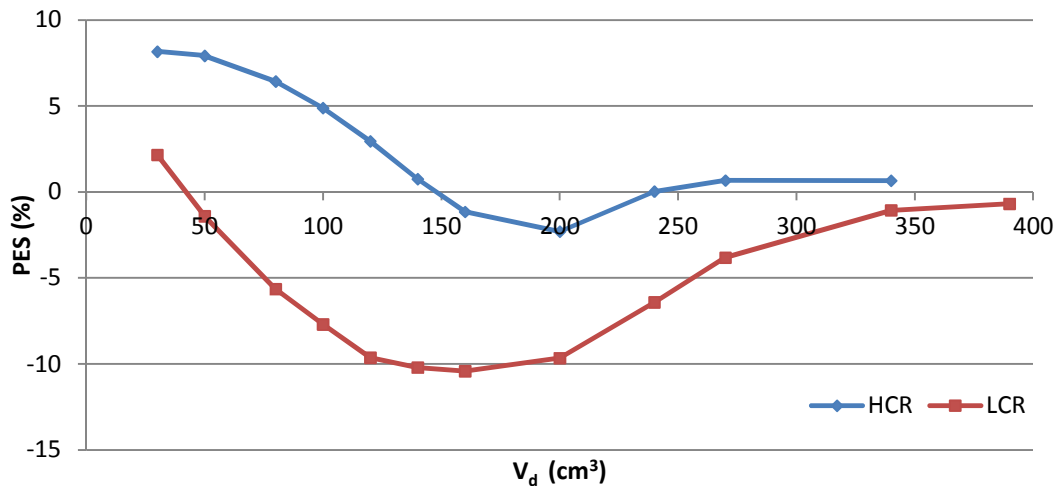


Figure 9.1 *PES* vs.  $V_d$  (Engine comparison, EPC)

As expected,  $\text{CO}_2$  savings curves shown in Figure 9.2 follow the trend of the *PES* curves of Figure 9.1, and the processes that lead to this behaviour are described above.  $\text{CO}_2$  savings curves for LCR engines retain a negative value throughout most of the simulated size range which translates to an increase in  $\text{CO}_2$  emissions compared to the commonly used grid & boiler combination. Minimum savings (Maximum emission increase) of -7.4% occurs under an LCR engine displacement of 160cc. On the other hand, the HCR curve has a positive value and generates  $\text{CO}_2$  savings for most of the simulated engine range, and leads to an increase in  $\text{CO}_2$  emissions of 0.7% only for an engine displacement of 200cc. In the case of an HCR engine, maximum  $\text{CO}_2$  savings of 10.5% are observed for an engine size of 50cc, while in the case of the LCR engine, maximum savings of 3.2% are observed under a 30cc engine, further highlighting the impact of excess waste heat generation on system performance. The ratio between the maximum values

of the two curves is 3.9. The 30cc to 100cc engine size range is of most interest due to a promising performance of the HCR engine. In this engine size range, the maximum difference in CO<sub>2</sub> savings between the HCR and the LCR curves is observed to be 12.6 percentage points. The considerable differences in CO<sub>2</sub> savings between the two engine types show the important role of engine efficiency in the performance of EPC systems.

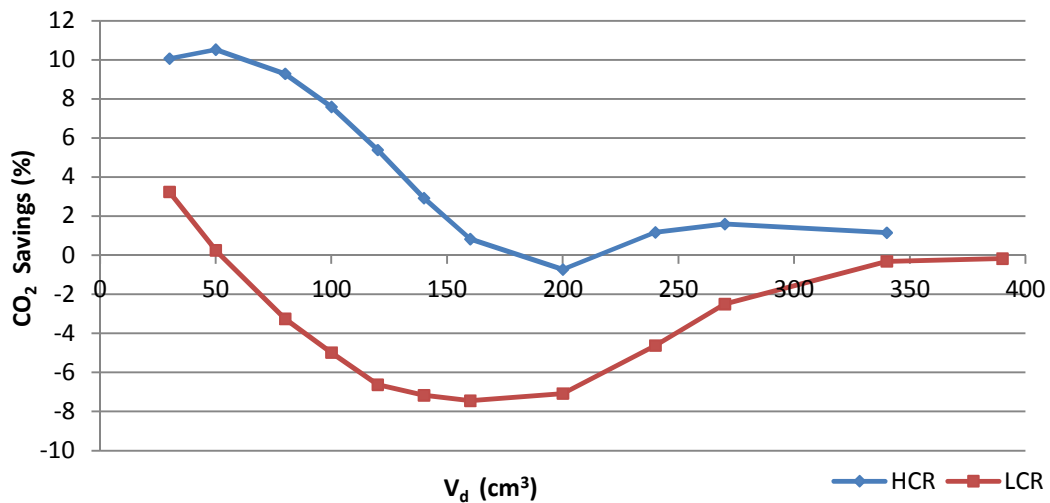


Figure 9.2 CO<sub>2</sub> Savings vs. V<sub>d</sub> (Engine comparison, EPC)

The effect of engine grade in engine start up frequency can be seen in Figure 9.3. As may be observed, both curves follow the same trend with minimum number of starts for the smaller engine sizes. As engine size increases, the frequency of the time intervals during which the electrical load is lower than the minimum generator load limit increases as well, and the engine is switched off and on more frequently. After a particular engine size, the generator minimum load becomes so high that it is switched on less frequently, thus reducing the annual number of engine starts.

The simulations for engine sizes of 30cc to 50cc yielded 0 engine starts for both LCR and HCR engine types as their small power output allows them to operate without stop to meet even the lowest encountered power demand. The maximum number of annual engine starts occurs for both engine types

for an engine size of 200cc (2044 starts/year for the HCR and 1859 starts/year for the LCR engine). For engine sizes of 200cc and below, the HCR engines exhibit a higher start up frequency than the LCR engines. This behaviour can be attributed to the fact that due to the higher power output of the HCR engine, load is found to be below the lower generator load limit more frequently for the HCR than the LCR engine, and thus the HCR system is expected to be switched off more frequently. For engine sizes greater than 200cc, the engine power output of the HCR engines (and the minimum generator load) becomes so high that the frequency of engine starts of the HCR engines are below those of LCR engines of the same size. The difference in engine starts between the two engine types ranges between 200 and 500 starts per year.

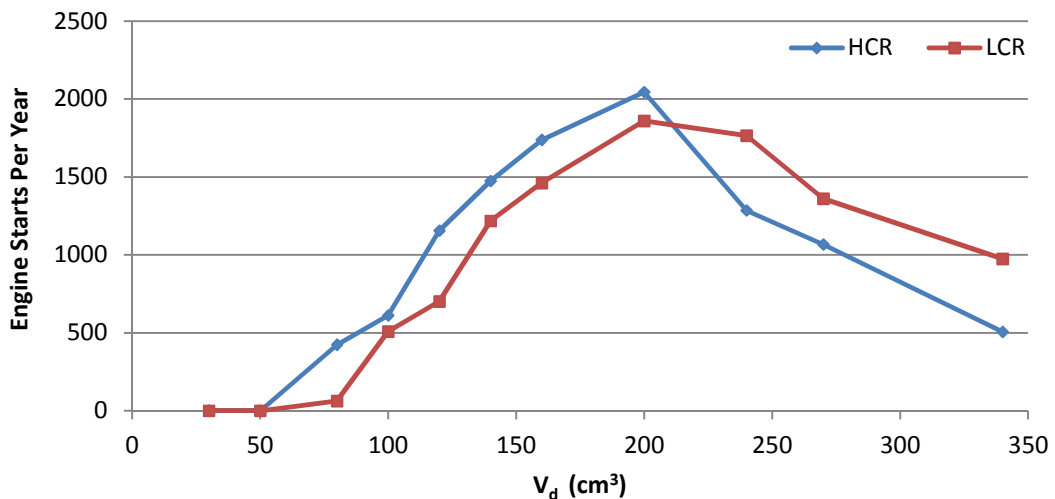


Figure 9.3 Engine starts vs.  $V_d$  (Engine comparison, EPC)

In terms of the annual operating duration of the two engines, Figure 9.4 shows that the HCR engines operate for fewer hours per year than the LCR engines of the same size for all the simulated engine size range but the 30cc and 50cc engines, for which the system operates 24 hours a day. For engines with a displacement greater than 50cc, the HCR engine operates for fewer hours per year as the minimum generator load limit is set higher than the LCR engine and this limit is located above the electrical load demand for



longer periods of time. The most notable difference in operating time between HCR and LCR engines is observed for an engine displacement of 200cc at 1125hours/year.

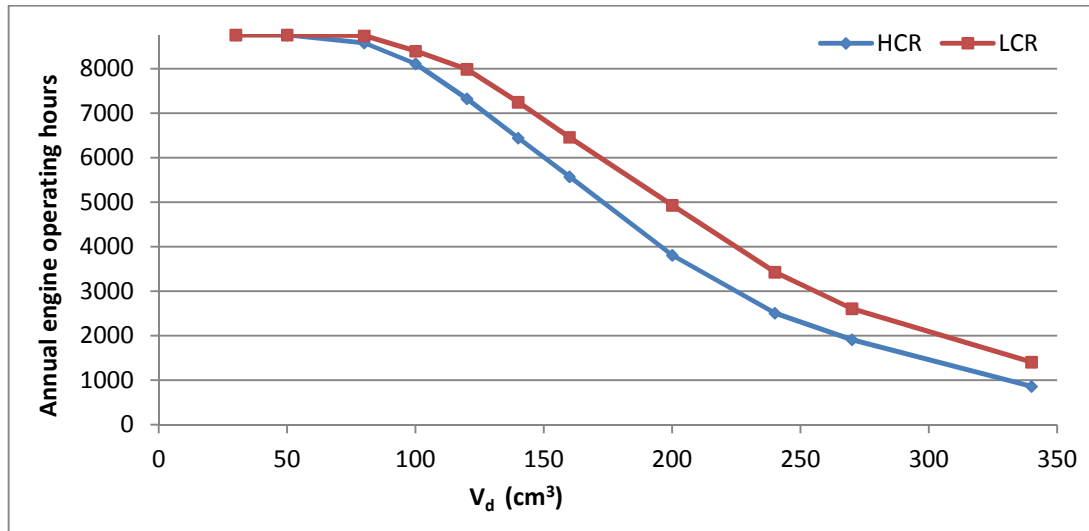


Figure 9.4 Engine operating hours vs.  $V_d$  (Engine comparison, EPC)

Engine type has been found to influence the operating patterns of not only the engine but also of the auxiliary boiler. As can be seen in Figure 9.5, a system equipped with an LCR engine of a given size exhibits a higher boiler start up frequency than the HCR counterpart of the same engine size. As the LCR engine generates larger amounts of waste heat than the HCR engine, a shorter period of time is required for the storage tank temperature to be elevated to the boiler switch off temperature limit, and for this reason, the boiler of the LCR engine equipped system is expected to be switched off and on more frequently than the boiler of the HCR system. Maximum number of annual boiler starts occurs for an engine displacement of 160cc for both engine types. For the LCR and HCR systems, a maximum of 3185 and 2911 respectively boiler starts per year are observed. Small engine sizes generate waste heat at a lower rate due to their inherently small thermal output. For a 30cc engine, 1880 and 1728 starts for the LCR and HCR engines respectively are observed, which is a ratio of 1.09. For a 50cc engine, 2398

and 1959 starts for the HCR and LCR engines respectively is observed (a ratio of 1.22). Larger engines generate lower amounts of waste heat due to being operated for a shorter amount of time. The lower amount of waste heat leads to the boiler being operated for a longer period of time until the upper boiler operating limit is reached which results to a reduction in the boiler start up frequency.

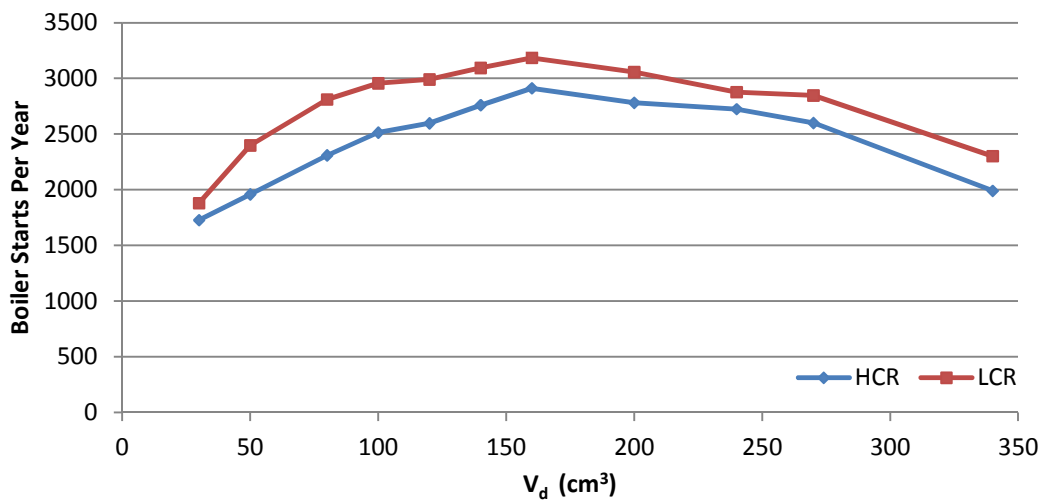


Figure 9.5 Boiler starts vs.  $V_d$  (Engine comparison, EPC)

Curves of annual boiler operating duration plotted against engine displacement for the two simulated engine types are shown in Figure 9.6. As can be observed, the HCR curve is located above the LCR curve for the complete range of simulated engine sizes. This can be attributed to the fact that for a given engine size, the LCR engine generates waste heat at a higher rate than the HCR engine and this displaces some of the thermal demand that the boiler would have to meet in the case of the HCR system. The minima of both curves occur at 160cc of engine displacement, for which also the maxima of annual number of boiler starts shown in Figure 9.5 occur. Such behaviour can be attributed to the fact that maximum waste heat is generated for engines of 160cc. Minimum operating duration of the HCR and LCR engines is 1177 and 1028 hours per year respectively. The higher boiler

operating duration for engines smaller and larger than 160cc is the result of the reduced generated waste heat. For the majority of simulated engine sizes, the difference between the annual boiler operating hours encountered in LCR and HCR based systems ranges between 150 to 200 hours per year, while for smaller engines the two curves tend to converge as the boiler becomes the main source of heat supply. Under a 30cc engine, the auxiliary boiler operates for 1449 and 1396 hours for the HCR and LCR engines respectively, which is a ratio of 1.04. For a 50cc engine, 1372 and 1292 hours for the HCR and LCR engines respectively are observed, a ratio of 1.06.

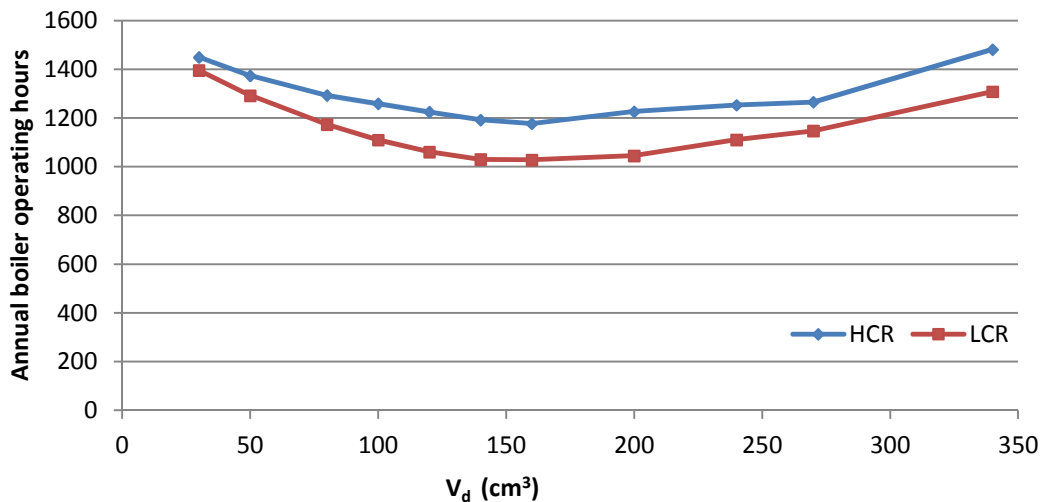


Figure 9.6 Boiler operating hours vs.  $V_d$  (Engine comparison, EPC)

The effect of engine type on the financial feasibility of EPC systems under FIT scheme can be seen in Figure 9.7. For almost all the simulated engine size range, the HCR engine generates higher cost savings than the LCR engine. The only exception to this trend is the displacement of 160cc where the LCR engine is covered by the FIT scheme while the HCR is not due to the HCR generator having a maximum output higher than the maximum FIT eligible of  $2kWe$ . Maximum cost savings for both engine types occur for a displacement of 80cc with the HCR and LCR engine types yielding annual

cost savings of 48.6% and 34.9% respectively which translates to a ratio of 1.39. Under a 30cc engine, savings are reduced to 32.8% and 24.4% for the HCR and LCR engines respectively, which is a ratio of 1.34.

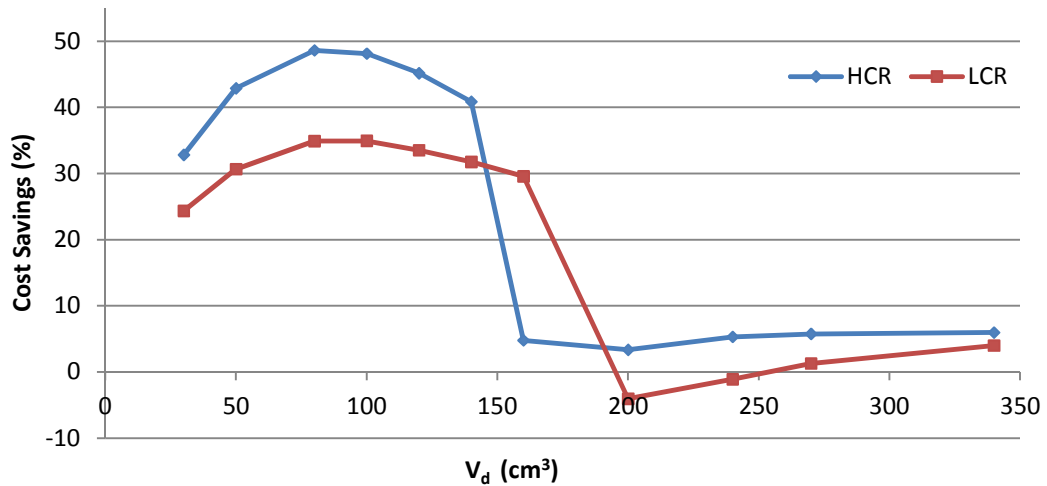


Figure 9.7 Cost savings (With FIT) vs. V<sub>d</sub> (Engine comparison, EPC)

If FIT revenues are not taken into account, cost savings are represented by the curves of Figure 9.8. Again, the cost savings generated by the HCR engine type are considerably higher than the values calculated for the LCR engine type, and for the majority of tested engine sizes, the difference ranges from 5 to 10 percentage points. HCR engines are observed to generate savings for the complete range of simulated engine sizes with a maximum of 14% for an engine displacement of 50cc, while in the case of the LCR engine, maximum cost savings of 7.7% occur under a 30cc engine and the ratio between the maximum savings is 1.82. The LCR engine operates at a loss for engine displacements that range from 120cc to 240cc. Minimum savings for the HCR engine type of 3.5% occur for a displacement of 200 cc while for the LCR engine type, minimum savings (or highest losses) of -4.5% occur for a smaller engine displacement of 160cc. As engine size increases, the effect of engine grade is reduced and the two curves tend to converge as the operating duration of the engine and its

economic effect are gradually diminished. Engine sizes for which maximum heat rejection occurs yield minimum cost savings.

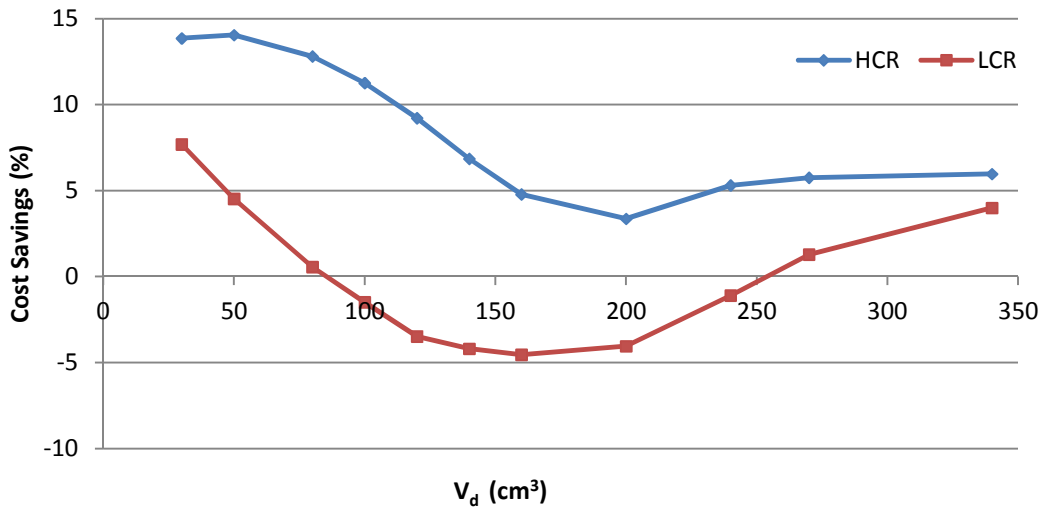


Figure 9.8 Cost savings (No FIT) vs.  $V_d$  (Engine comparison, EPC)

## 9.2. Heat Storage Size

Heat storage tank size is another system parameter whose influence on system feasibility will be investigated. For this task, the model of an electricity priority controlled system with a low compression ratio engine is simulated with a post-67 detached dwelling model under the weather profile of London Gatwick for an array of heat storage tank sizes varying from 50L to 350L in 50L increments, and the main performance indicators as well as the system operating duration and start up frequencies are recorded for further analysis.

As can be observed in Figure 9.9, thermal storage tank size can have a strong effect in the energetic performance of an electricity priority controlled system. The increase in storage size from 50L to 350L shifted *PES* upwards by 9.3 percentage points for a 50cc engine, while for an 80cc engine, this difference is increased to 10.2 percentage points. For the smallest engine size of 30cc, *PES* are increased from  $-3.1\%$  to  $5.6\%$  which is a 8.7 percentage point increase. While this is a substantial increase, the *PES* value

is still very low compared to the LCR HPC counterpart, and this is an indication that unless a very efficient engine is used, storage tank selection alone is not enough to elevate the EPC strategy to the HPC level of performance.

As the engine size increases past 160cc, the effect of heat storage tank size is attenuated as the larger engine is operated for fewer hours per year (as shown in Figure 9.12) than the smaller engine due to the use of the minimum generator load at 40% of the maximum output.

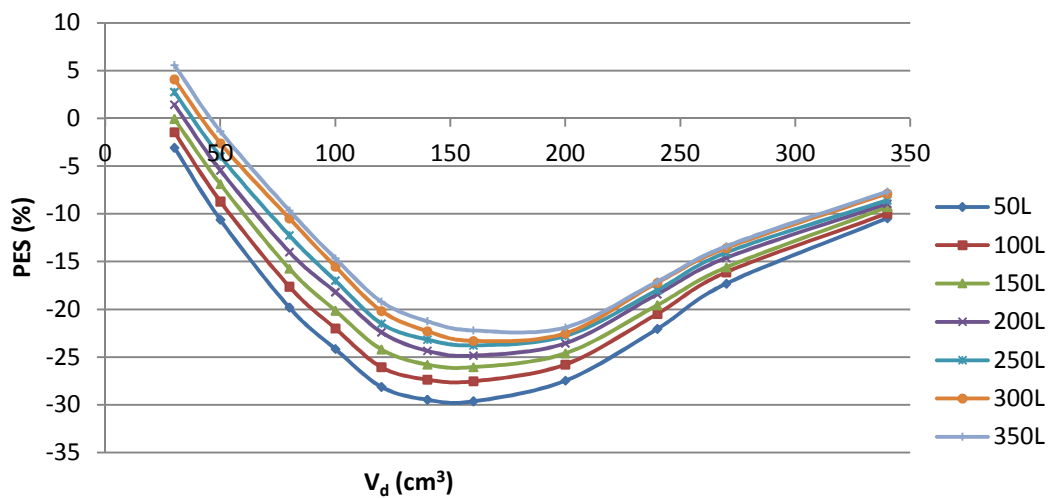


Figure 9.9 PES vs. V<sub>d</sub> (Tank size comparison, EPC)

As expected, CO<sub>2</sub> savings curves of Figure 9.10 follow the contour of the PES curves of Figure 9.9. For smaller engines of 30cc to 80cc, the transition from a 50L to a 350L tank increases CO<sub>2</sub> savings by 8.8 to 8 percentage points, while for larger engines the effect of storage tank size is attenuated with the minimum difference between the generated savings of the largest and the smallest tank being 1.9 percentage points for the 340cc engine.

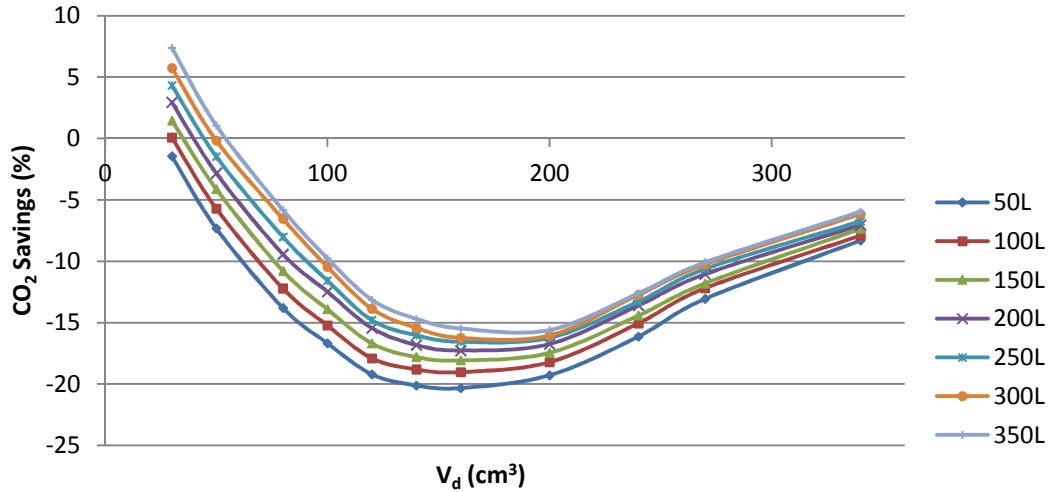


Figure 9.10 CO<sub>2</sub> savings vs. V<sub>d</sub> (Tank size comparison, EPC)

While storage tank size has no effect on the engine operating patterns of an electricity priority controlled system whose plots of start up frequency and operating duration are shown in Figure 9.11 and Figure 9.12 respectively, it has been found to heavily influence the operating patterns and duration of the auxiliary boiler.

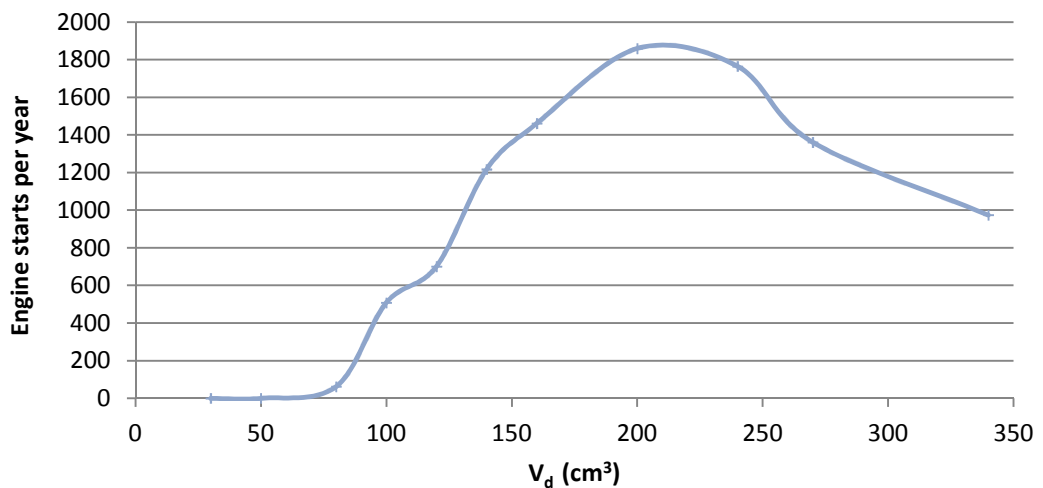


Figure 9.11 Engine starts vs. V<sub>d</sub> (Tank size comparison, EPC)

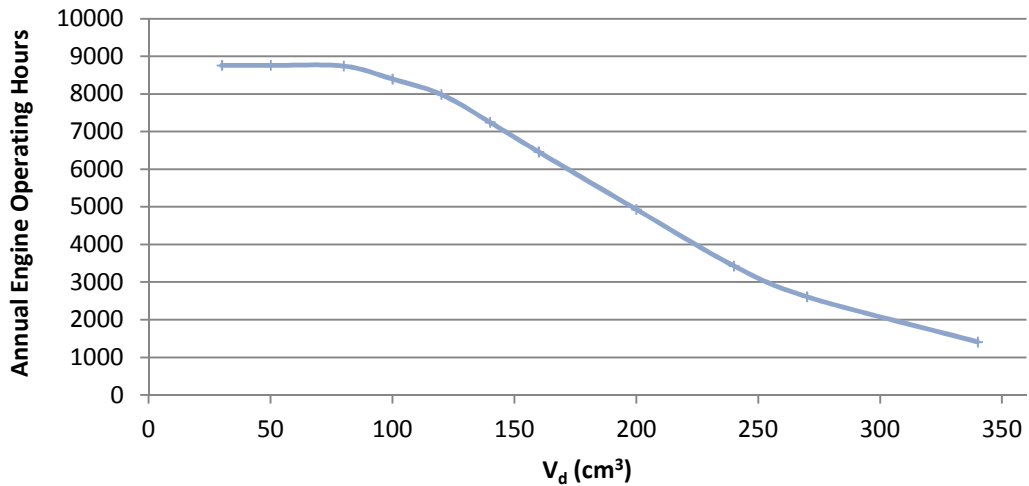


Figure 9.12 Engine operating hours vs.  $V_d$  (Tank size comparison, EPC)

As can be seen in the plots of Figure 9.13, the larger the heat storage tank capacity, the lower the curve of annual boiler starts is located on the graph. For the medium sized 160cc engine, the difference in boiler cycling frequency between the 50L and 350L tank is maximized, with the frequency exhibited under a 350L tank being 0.13 times that of the 50L tank system. In the better performing engine size of 30cc, 1394 and 635 boiler starts are observed for the 50L and 350L tanks respectively, which gives a ratio of 0.46. The reason for this shift is the fact that for a given thermal load magnitude, a larger thermal storage mass will require a longer period of time before its temperature falls to the boiler ignition trigger temperature. Similarly, when the auxiliary boiler is switched on, the time required for a given boiler thermal output to elevate the temperature of the heat storage tank to the boiler switch off trigger temperature level will be longer for higher heat storage sizes.

As may also be observed from the plots, the smaller the storage tank capacity, the higher the influence of engine size on the ignition patterns of the boiler. As engine size increases from small to medium size, the boiler start up frequency tends to increase. This is attributed to the increasing rate of generated waste heat leading to a reduction of the time interval required for the tank temperature to reach the boiler switch off temperature level. In



addition, the increase in engine start up frequency translates to more frequent instances during which thermal load is present while both the engine and the boiler are switched off. Increasing the engine size past a certain point (160cc for most under 250L curves), leads to a reduction in boiler ignitions as the engine is operated for fewer hours due to electrical load being below the minimum set value of the generator for a longer period of time. The reduction in engine operating time results in a reduction in generated waste heat, and this leads to a larger proportion of the thermal load being covered by the auxiliary boiler. Thus, the time required for the tank water to get elevated to the boiler switch off trigger limit is longer, and this in turn results to a less frequent boiler cycling. For the larger storage tank sizes, the effect of engine size on boiler start up frequency is gradually attenuated, since larger thermal capacities tend to dampen the frequent surges in generated waste heat from the mid-sized engines, and as can be observed, for the tested house, systems with tank sizes over 200L exhibit a considerably smaller variation in boiler ignitions throughout the tested engine size range.

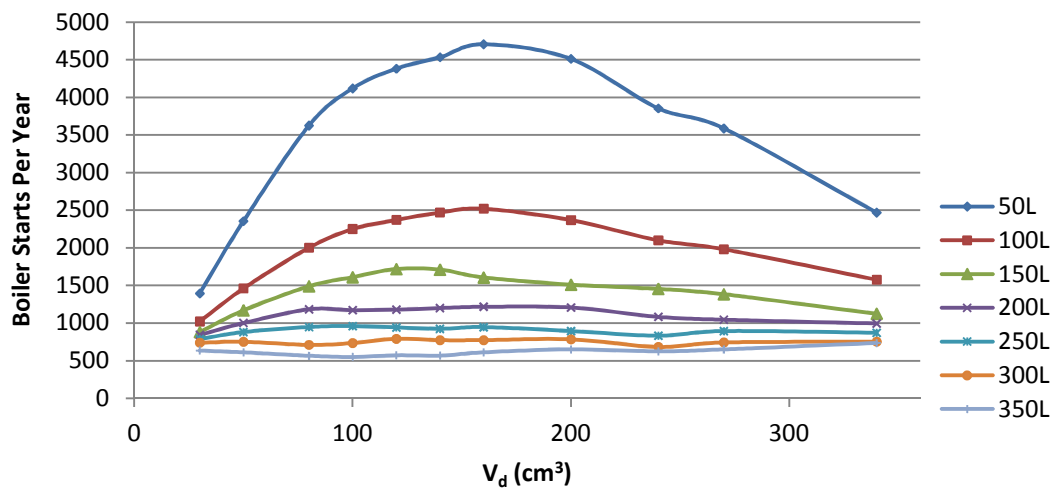


Figure 9.13 Boiler starts vs.  $V_d$  (Tank size comparison, EPC)

The strong effect of heat storage tank size on auxiliary boiler annual operating duration can be seen in Figure 9.14. The influence of tank size is stronger for smaller to medium sized engines where a transition from a 50L

tank to a 350L tank results to a reduction in annual boiler operating time by 32% to 50%. As engine size increases and engine operating time is reduced, the available waste heat from the engine is reduced as well and the boiler becomes the main source of heat supply. Since the boiler operation follows thermal demand, and since the amount of waste heat from the engine gradually diminishes as engine size is increased, boiler operating time tends to increase past 140cc – 160cc. In addition, the effect of tank size on boiler operating time is reduced for larger engines due to the reduction in the amount of uncontrollable generated heat by the engine. For the engine size of 30cc that yields maximum *PES* and CO<sub>2</sub> savings, boiler annual operating duration drops from 1152 to 781 hours a year, which is a ratio of 0.68. Minimum boiler duration tends to occur close to the engine size that generates the highest amount of waste heat. The size, for which this minimum occurs, is shifted from 160cc under a 50L tank, to 140cc under a 350L tank. Minimum boiler duration of 760 and 380 hours for the 50L and 350L tanks is observed respectively, which is a ratio of 0.5.

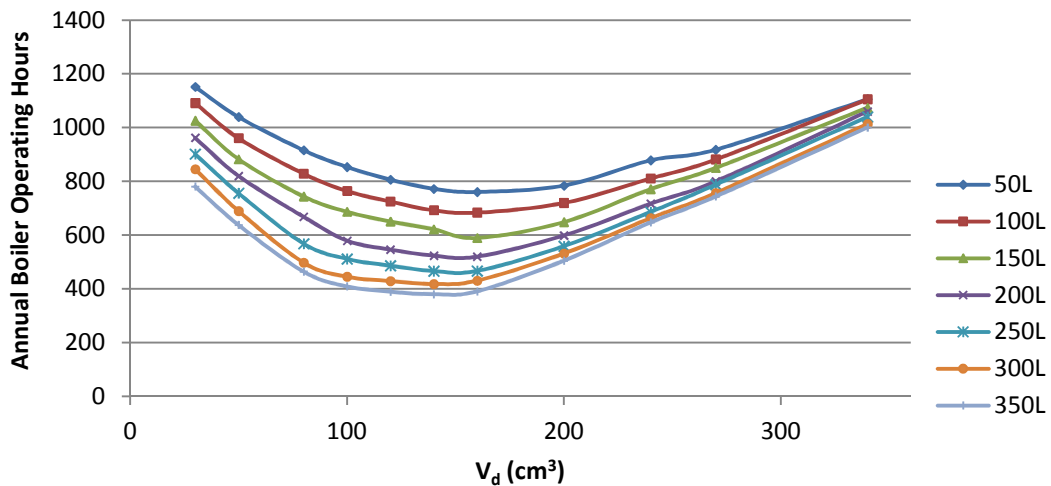


Figure 9.14 Boiler operating duration vs.  $V_d$  (Tank size comparison, EPC)

The effect of thermal storage tank size on FIT eligible system generated cost savings can be seen in Figure 9.14. While maximum *PES* and CO<sub>2</sub> savings

occur for an engine size of 30cc, maximum cost savings under FIT eligibility occur under a considerably larger 80cc engine due to the generation tariff favouring the larger engine, regardless of the storage tank size. The transition from a 50L to a 350L storage tank results to an increase in maximum cost savings from 37.7% to 44.9%. This is a 7.2 percentage point change and a ratio of 1.19. For the engine size that results to maximum *PES* and CO<sub>2</sub> savings of 30cc, the transition from a 50L to a 350L tank increases cost savings from 25.2% to 32.8%, which is a difference of 7.6 percentage points and a ratio of 1.3.

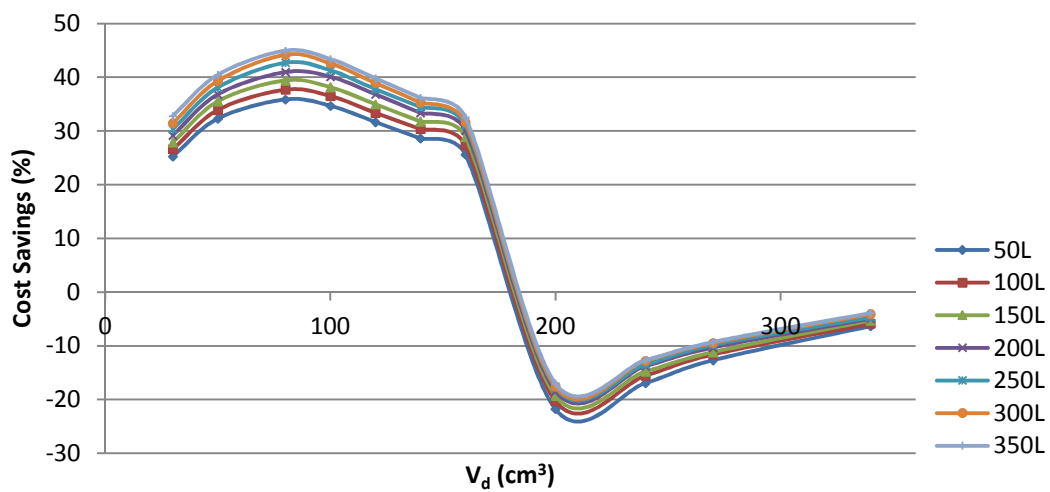


Figure 9.15 Cost savings (With FIT) vs. V<sub>d</sub> (Tank size comparison, EPC)

On the other hand, under a no government subsidy financial regime, cost savings curves shown in Figure 9.16 are observed to follow the trend of the *PES* and CO<sub>2</sub> savings curves of Figure 9.9 and Figure 9.10 respectively, with maximum cost savings occurring under the 30cc engine size that also gives maximum *PES* and CO<sub>2</sub> savings. The transition from a 50L to a 350L tank results to an increase in cost savings from 2.7% to 8.8%, which is a difference of 6.1 percentage points and a ratio of 3.21. Minimum cost savings occur under a 160cc engine size (*PES* and CO<sub>2</sub> savings minima occur under this engine size as well) for all tested storage tank sizes. The above indicate a strong dependence of cost savings on the amount of rejected heat. As in the case of the *PES* and CO<sub>2</sub> savings, the improvement in economic

performance of an LCR system by increasing the thermal storage tank capacity is not significant enough to make the system viable enough when no government subsidy is in place.

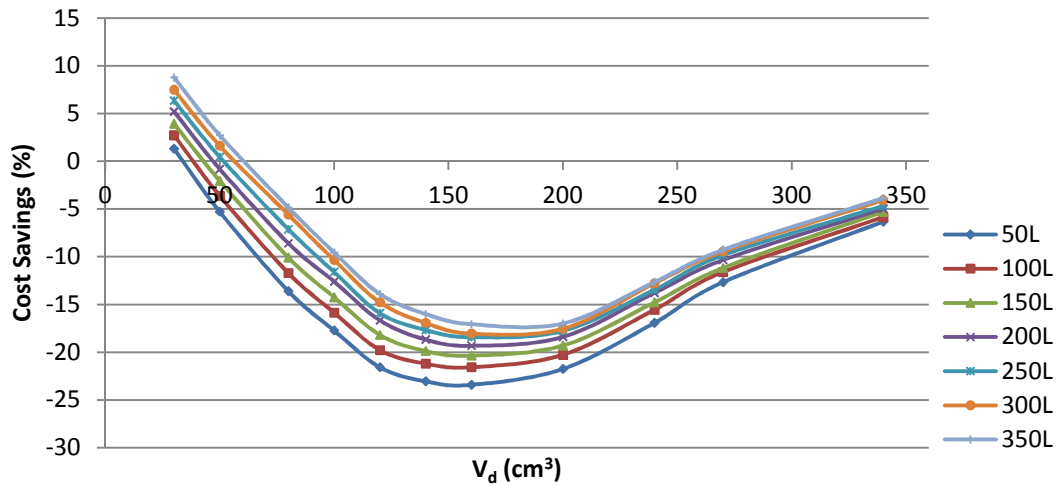


Figure 9.16 Cost savings (No FIT) vs.  $V_d$  (Tank size comparison, EPC)

### 9.3. Heat storage tank water temperature limits

In the current section, the effect of varying the thermal storage tank temperature operating limits will be investigated. For this purpose, an EPC system equipped with an LCR engine will be simulated under three storage tank limit combinations whose characteristics are illustrated in Figure 9.17.

The first simulated storage limit combination “Limit 1” uses a 10°C storage tank temperature band and the auxiliary boiler deactivation temperature limit is located in the middle of this band.

The second simulated storage limit combination “Limit 2” uses a 20°C storage tank temperature band and retains the boiler deactivation temperature in the middle of the band.

The third simulated storage limit combination “Limit 3” uses a 20°C storage tank temperature band and the boiler deactivation temperature is located 5°C above the boiler activation limit (lower band limit).

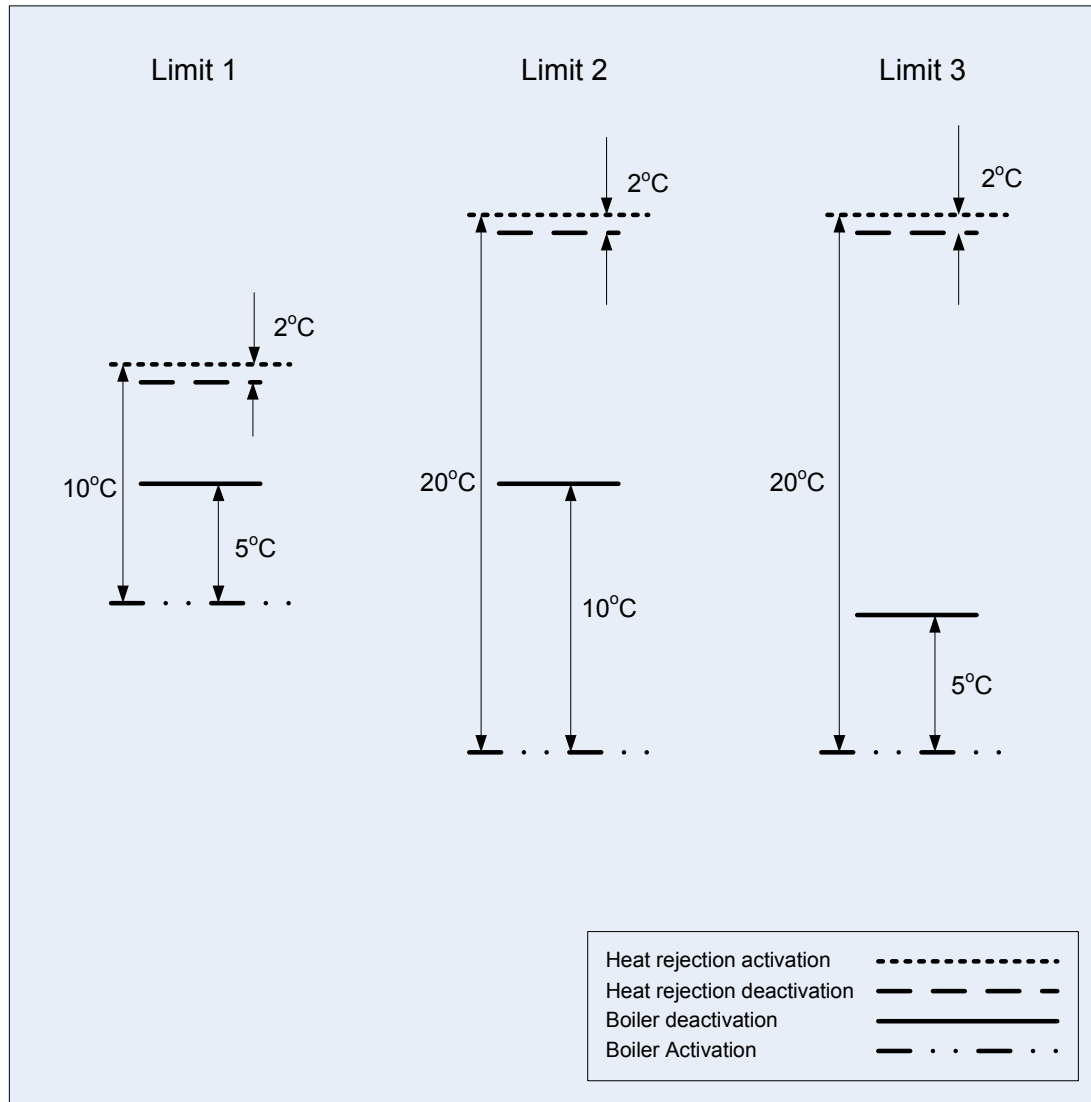


Figure 9.17 Tested storage tank temperature operating limits

The effect of varying the heat storage tank operating limits on the energetic feasibility of EPC systems can be seen in Figure 9.18, where it can be observed that the transition from “Limit 1” to “Limit 2” leads to an increase in *PES* throughout the complete range of simulated engine sizes by 2 to 5.5 percentage points. In the case of the 30cc engine, *PES* were increased from -3.6% to 1.8%. The reason for this improvement in performance is the fact

that the storage tank may now accumulate a larger amount of heat before the heat rejection switch-on limit is reached, and this allows the accumulation of waste heat for a longer period of time, during which, the probability of a coincident thermal load drawing the stored heat and averting heat rejection by keeping the tank temperature below the heat rejection limit is increased. On the other hand, the transition from “Limit 2” to “Limit 3” tank temperature limits appears to have little to no effect on *PES* for the smaller simulated engine sizes, while for larger engines, the increase is not greater than 1 percentage point. The small influence of the change in boiler switch off temperature is attributed to the fact that the wider storage limit band of “Limit 2” and “Limit 3” is more than adequate to accommodate the generated waste heat of the smaller engines before heat rejection is actuated. In the case of larger engines, while the total waste heat they generate is lower than that of the smaller to medium size engines due to being operated for a shorter period of time, their momentary heat generation rate is expected to be higher, and such a unit is benefited from the lower auxiliary boiler switch off temperature combination of “Limit 3” which can further help avoid surplus heat rejection by means of leaving a larger temperature dead band for the engine waste heat to cover before heat rejection is triggered. While the increase in *PES* can be characterized as notable, the system barely generates savings, an observation that indicates that while appropriate temperature limits could and should be used to improve on performance, this is not enough to bring a system to a viable status and should be used as a complimentary measure for performance enhancement to a high efficiency HCR engine.

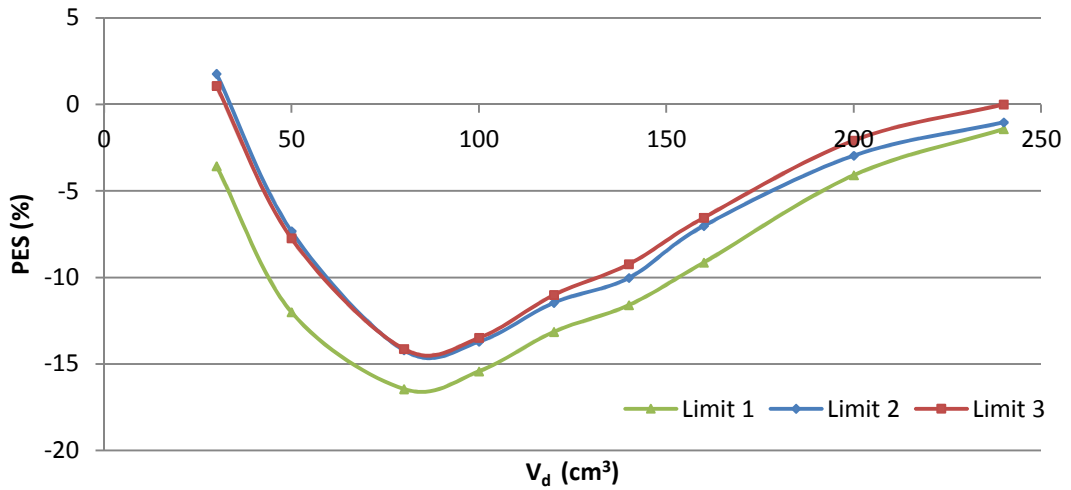


Figure 9.18 PES vs. V<sub>d</sub> (Temp. limit comparison, EPC)

In terms of CO<sub>2</sub> savings, the curves of the tested storage tank temperature limit combinations seen in Figure 9.19 follow the same pattern shown in the PES savings curves discussed above and the analysis of the PES curves is valid for this plot as well. The transition from “Limit 1” to “Limit 2” results in an increase in CO<sub>2</sub> savings by 5.3 percentage points in the case of the 30cc engine.

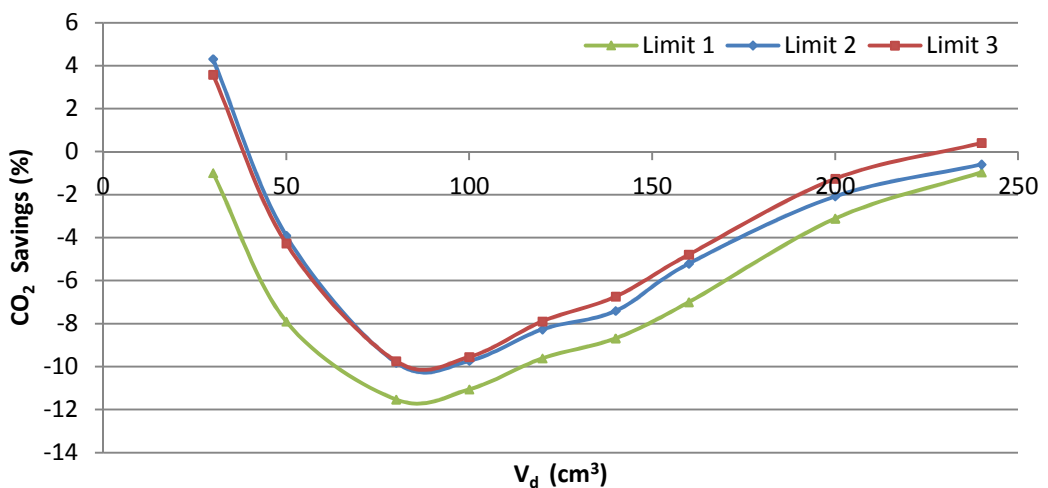


Figure 9.19 CO<sub>2</sub> savings vs. V<sub>d</sub> (Temp. limit comparison, EPC)

The combination of storage tank operating limits has been found to have a significant impact on the operating patterns of the auxiliary boiler as shown in the plots of Figure 9.20. The highest number of boiler starts is observed for “Limit 1” combination. The reason for this behaviour is attributed to the fact that the time required for the storage tank temperature to cross the narrower temperature dead band for given heat input rate and load is shorter than in the wider temperature dead band limits of “Limit 2” and “Limit 3” combinations, and as a result, the auxiliary boiler is switched on and off more frequently. The transition from “Limit 1” to “Limit 2” leads to a reduction in annual boiler starts from 849 starts per year to 619 starts per year for a displacement of 30cc. The minimum effect of increasing the temperature dead band from 10°C to 20°C occurs for a displacement of 80cc for which as discussed above, the engine generates waste heat in an almost continuous fashion, and the storage tank water is kept above the boiler switch off limit for most of the time. Therefore the boiler start up frequency is not affected significantly under the new wider limit dead band when compared to other engine sizes, for which the boiler is subject to more frequent waste heat surges and must also contribute a larger percentage of the total thermal load. The transition from “Limit 2” to “Limit 3” combination, results to an even more noticeable reduction in boiler cycling frequency due to the boiler deactivation temperature limit being located closer to the boiler activation limit. Thus, the time required by the engine alone to elevate the temperature from the boiler switch off level to the maximum boiler temperature operating limit is now longer, and as a result, boiler cycling frequency is reduced. A reduction of 130 to 273 boiler starts per year for engine displacements 140cc and 200cc respectively is observed with the transition from “Limit 2” to “Limit 3” curves, while for the smaller and best performing 30cc engine, boiler start up frequency is reduced from 619 to 469 annual starts, a reduction of 150 starts. The transition from “Limit 1” to “Limit 3” is observed to reduce the number of engine starts by 28% to 45%.



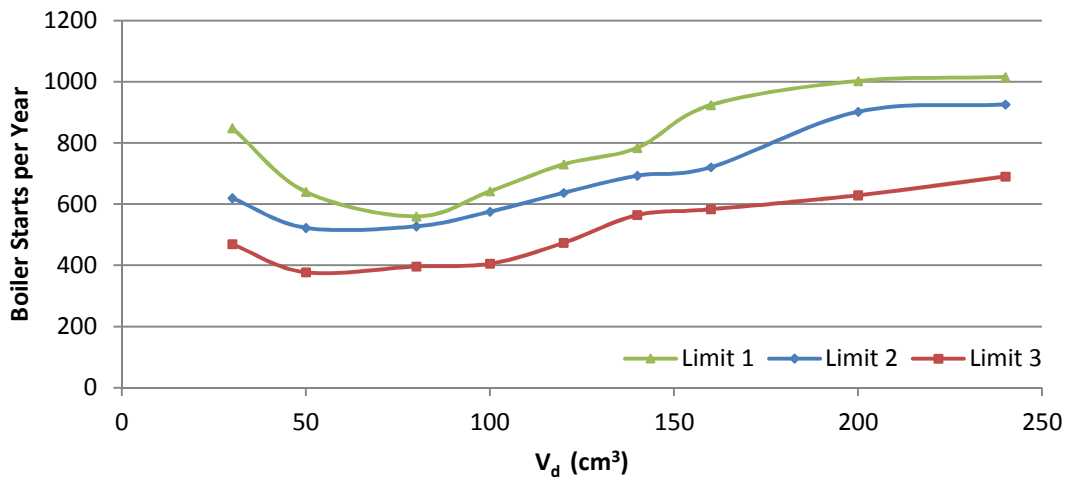


Figure 9.20 Boiler starts vs.  $V_d$  (Temp. limit comparison, EPC)

The impact of storage tank operating limit combination on the annual boiler operating duration is relatively small for engines with a displacement greater than 50cc as can be seen in the plots of Figure 9.21. The transition from “Limit 1” to “Limit 2” combinations is observed to have a stronger influence for the smaller engines. The reason for this behaviour is the fact that for engines greater than 80cc, the available waste heat from the engine is reduced as a result of the reduction in engine operating time, and the boiler must gradually supply a greater fraction of the thermal load. Since the boiler operation is controlled by the storage tank temperature limits, the lower the thermal contribution from the engine is, the less the boiler operating time is affected by the location of the temperature limits. The transition from “Limit 2” to “Limit 3” on the other hand has a negligible influence in annual boiler operating duration for engine displacements of 80cc or smaller, as heat from the engine is generated at a lower rate but in a more uniform pattern, and storage tank temperature is kept by the engine above the boiler operating temperature band for longer time periods, thus reducing the thermal contribution of the boiler in meeting the heat demand. As engine size is increased, the engine operates sporadically but when operated, it tends to thermally saturate the storage tank. By reducing the boiler switch off limit, the boiler is deactivated early in the tank heating process, and the engine must therefore cover a wider tank temperature band during which no heat rejection

occurs. This increases the contribution of the engine waste heat to the total usable heat while respectively decreasing the contribution of the boiler. The most noticeable reduction in boiler operating time from “Limit 1” to “Limit 3” curves has been observed to be 20% and 26% for 30cc and 50cc engines respectively, which corresponds to equal reductions in the amount of heat contributed by the boiler.

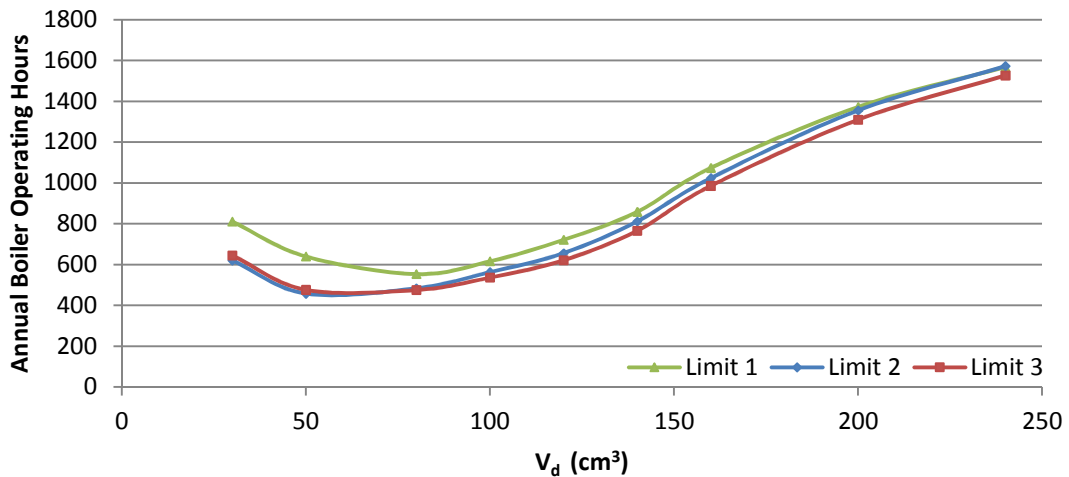


Figure 9.21 Boiler operating duration vs.  $V_d$  (Temp. limit comparison, EPC)

The effect of the change in storage tank operating limit combination on cost savings for FIT eligible units can be seen in Figure 9.22. For the majority of the simulated engine sizes, with the exception of 30cc and 50cc engines, the difference between the cost savings generated under “Limit 1” and “Limit 3” is no greater than 2 percentage points. For the larger units, the effect of storage tank temperature operating limits is gradually reduced as the engine operating time and therefore the engine generated waste heat are reduced. For the engine size of 50cc for which under “Limit 1” temperature limit, maximum cost savings of 41.6% occur, the transition to “Limit 3” results to an increase of 3.5 percentage points, and a gain of 1.084. It is observed that maximum cost savings occur for an engine size larger than the size that yields maximum *PES* and  $CO_2$  of 30cc. Under a 30cc engine, cost savings are increased from 40.2% to 43.9% with the transition from “Limit 1” to “Limit 3” which is a gain of 1.092.

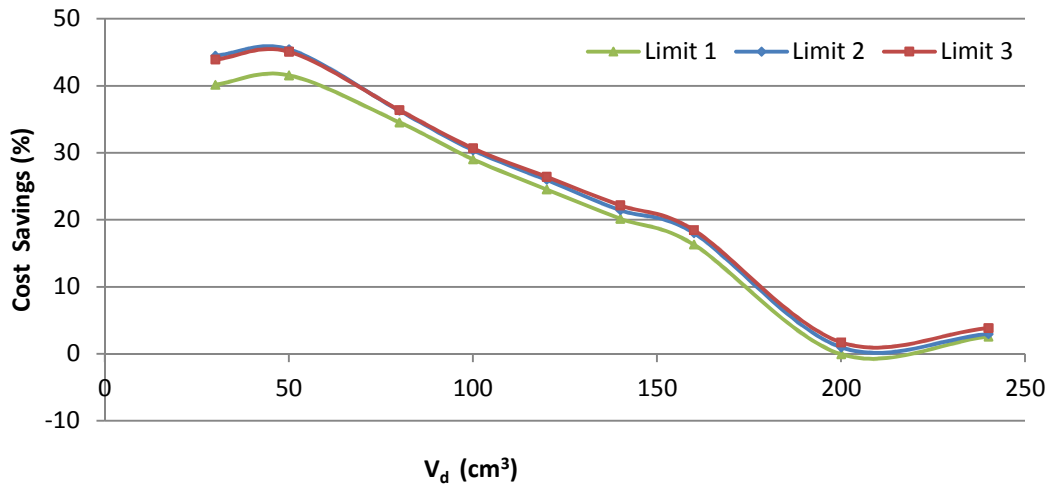


Figure 9.22 Cost savings (With FIT) vs.  $V_d$  (Temp. limit comparison, EPC)

Curves of cost savings calculated without FIT scheme revenues plotted against engine displacement for the tested heat storage tank temperature operating limit combinations can be seen in Figure 9.23. As can be observed, the three curves follow the trends of *PES* and  $\text{CO}_2$  savings curves plotted in Figure 9.18 and Figure 9.19 respectively. This indicates the strong dependence of cost savings on the amount of rejected heat and thus the analysis of the *PES* curves of Figure 9.18 is also valid for the curves of Figure 9.23. For smaller engine sizes of 30cc and 50cc, the transition from “Limit 1” to “Limit 3” leads to an increase of 4 percentage points in cost savings. For larger engines, this difference is reduced to 2 percentage points.

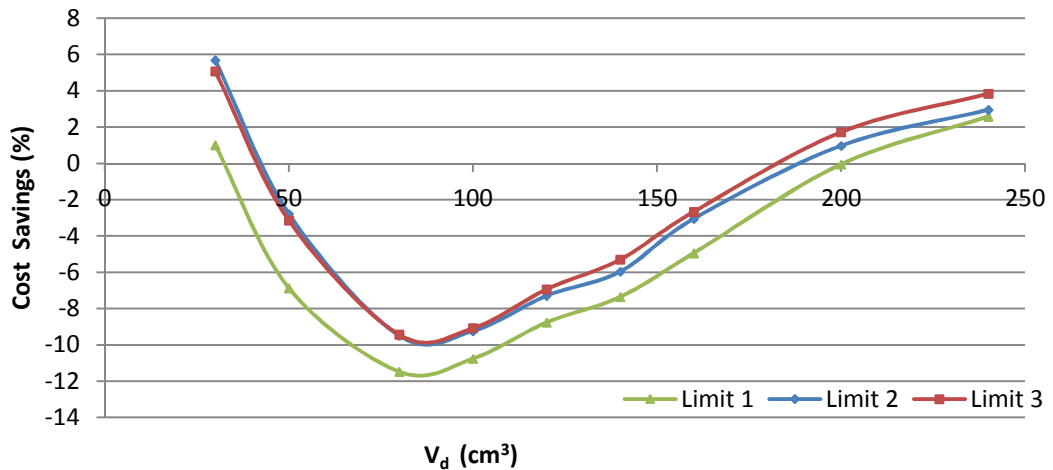


Figure 9.23 Cost savings (Without FIT) vs.  $V_d$  (Temp. limit comparison, EPC)

#### 9.4. Dwelling Type

The energetic performance of the EPC unit under two different dwelling types for an array of engine sizes can be seen in Figure 9.24. As can be observed, maximum savings of 12.2% under a 30cc and 7.9% under a 50cc engine are observed for the mid-terraced and the detached house respectively, which is a difference of 4.3 percentage points and a ratio of 1.54. For both cases, *PES* exhibit a steep decline as engine size is increased as a larger engine leads to higher amounts of heat being rejected into the atmosphere unutilized. For both dwellings, minimum savings occur for a 200cc engine size, while a further increase beyond this point results to a small increase in *PES* due to a reduction in engine operating time (as minimum generator load is increased) and therefore in generated waste heat. For the largest segment of the simulated engine size range the unit exhibits higher savings for the mid-terraced house due to the higher *HPR* of the energy demand of this dwelling type that reduces the amounts of rejected heat. The difference between the ratio of rejected heat over the used heat for the two dwelling types can be seen in Figure 9.25. Another reason behind the better performance of the mid-terraced house is the fact that for a given engine size, a proportionally higher amount of electricity is imported in the case of the larger detached house.

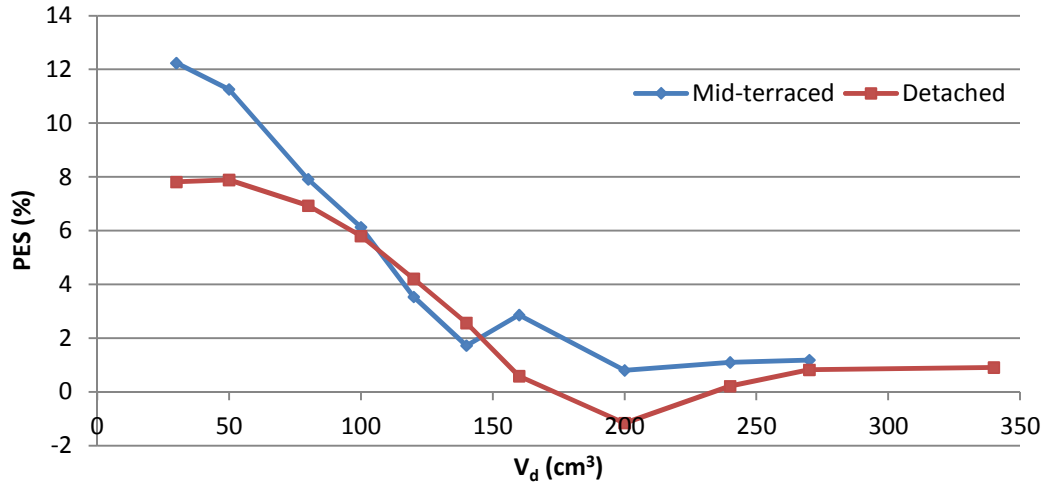


Figure 9.24 PES vs.  $V_d$  (Dwelling comparison, EPC)

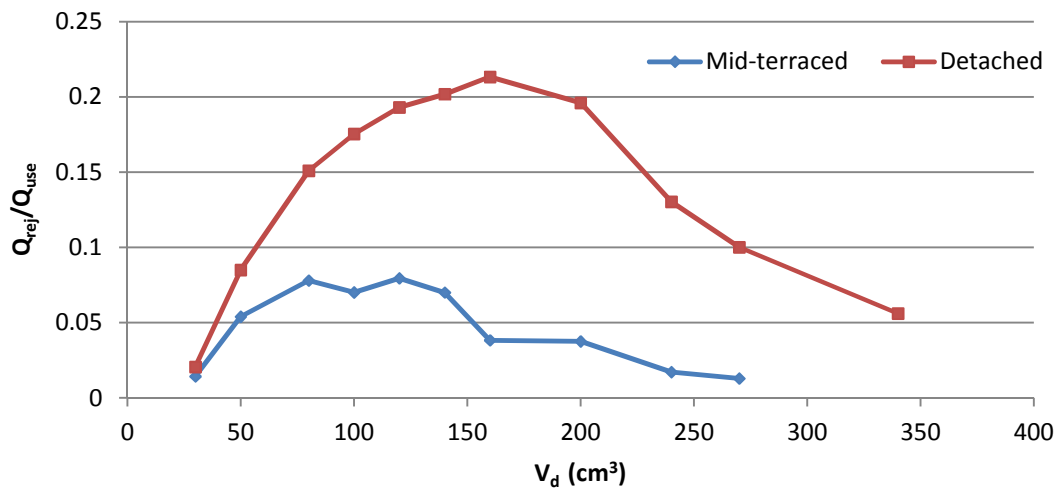


Figure 9.25  $Q_{rej}/Q_{used}$  vs.  $V_d$  (Dwelling comparison, EPC)

The trends of the *PES* curves of Figure 9.24 are also followed by the CO<sub>2</sub> savings curves of Figure 9.26, and therefore the analysis of the curve behaviour of Figure 9.24 is also valid for the CO<sub>2</sub> savings curves. Maximum CO<sub>2</sub> savings of 15.7% for a 30cc engine and 10.3% for a 50cc engine are observed for a mid-terraced and a detached house respectively, which corresponds to a difference of 5.4 percentage points and a ratio of 1.52.

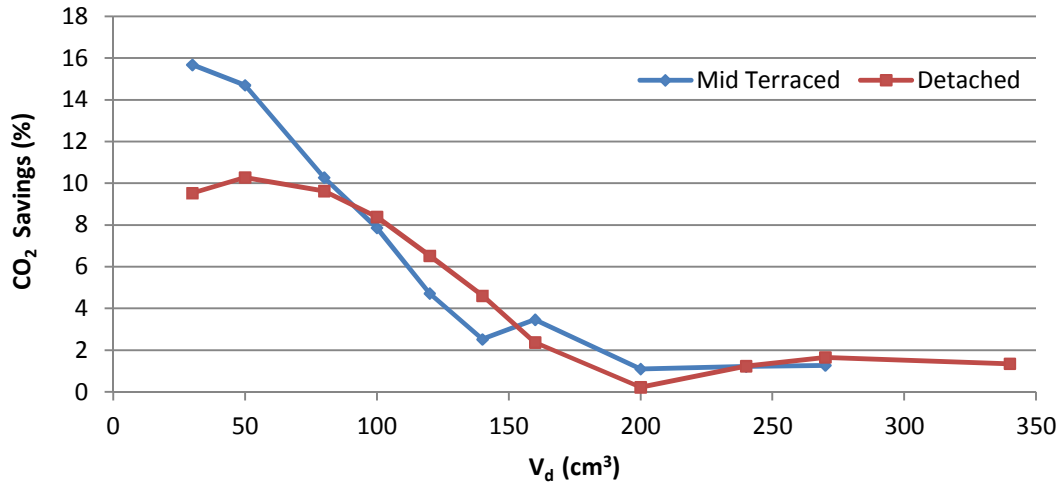


Figure 9.26 CO<sub>2</sub> Savings vs.  $V_d$  (Dwelling comparison, EPC)

Engine start up frequency exhibits a significantly different behaviour from one house type to the other. As can be seen in Figure 9.27, while the shape of the two curves is similar and both curves share a common point for an engine displacement of 30cc, the maximum number of 1852 annual engine ignitions for the mid terraced house occurs for an engine displacement of 100cc, while in the case of the detached house a maximum of 2044 starts per year occurs for a 200cc engine. For the better performing smaller engine sizes, the engine start up frequency encountered with the mid-terraced house is higher than the one exhibited under the detached house, and for engine sizes of 140cc and larger, the engine start up frequency for the detached house is higher than for the mid-terraced house. Under engine displacements that generate maximum *PES*, the engines operate continuously. The above behaviour is attributed to the higher electrical loads encountered in the detached house that lead to a less frequent generator deactivation for the smaller engine sizes. For the larger engine sizes, the small loads of the mid-terraced house lead to a lower engine start up frequency, as the instances where the load is equal or higher than the minimum generator load become less and less frequent, while for the same engine size, the higher loads of the detached house keep activating the

CHP. As a result, the turning point is shifted towards larger engines for larger houses.

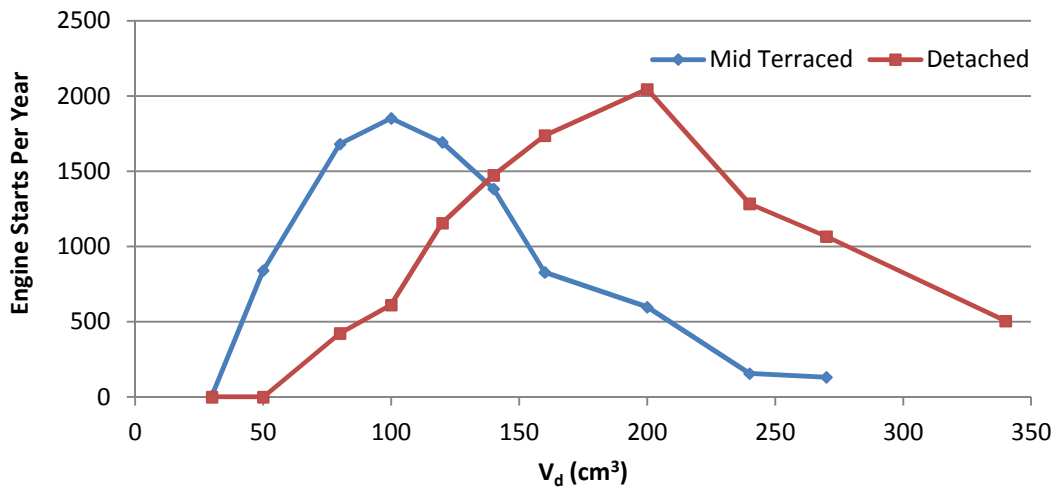


Figure 9.27 Engine starts vs.  $V_d$  (Dwelling comparison, EPC)

Significant differences are also observed in the annual engine operating duration between the two simulated dwellings as shown in Figure 9.28. While both dwelling types yield the same engine duration for the smallest simulated engine size of 30cc due to the engine being small enough to be operated continuously, as engine size is increased, a difference between the engine operating duration for the two dwellings appears and increases rapidly. The detached house yields a longer operating duration than a mid-terraced house for the same engine size for all simulated engine sizes but the 30cc. Maximum difference of 4527 hours between the two curves occurs for an engine displacement of 140cc, under which, the engine operates for 6443 and 1916 hours per year in the detached and the mid-terraced house respectively, which translates to a ratio of 3.4. Smaller but significant differences are also encountered for the more efficient, smaller engine sizes of 50cc to 100cc, with the engine operating duration in the detached house being 1.1 to 2.1 times respectively longer than the duration observed for the mid-terraced house. This difference in annual engine usage time from one house type to another has important implications on the difference in system economic viability between different dwelling types, as it directly affects the

system service life, and therefore the payback period (PBP) considered during the planning phase of an investment.

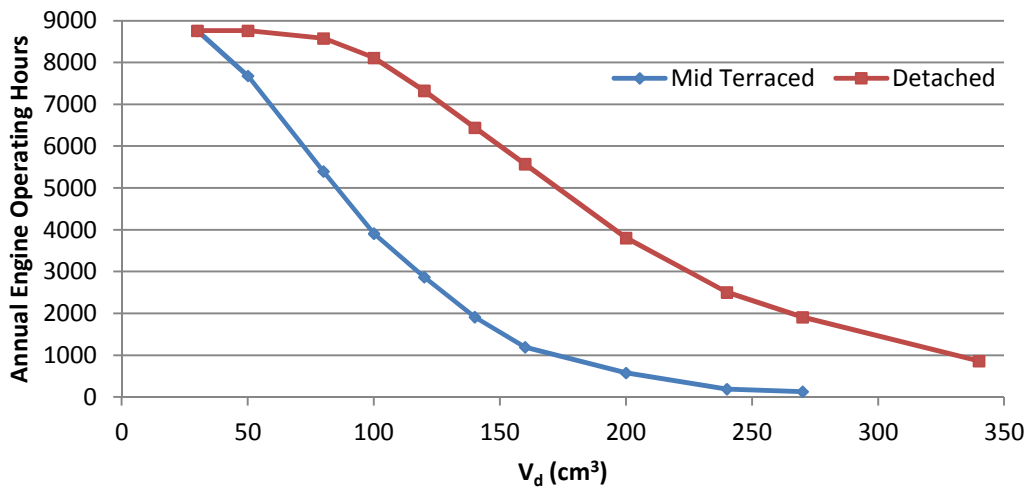


Figure 9.28 Engine operating hours vs.  $V_d$  (Dwelling comparison, EPC)

The effect of the different engine operating patterns on the fraction of used electricity imported from the grid can be seen in Figure 9.29.

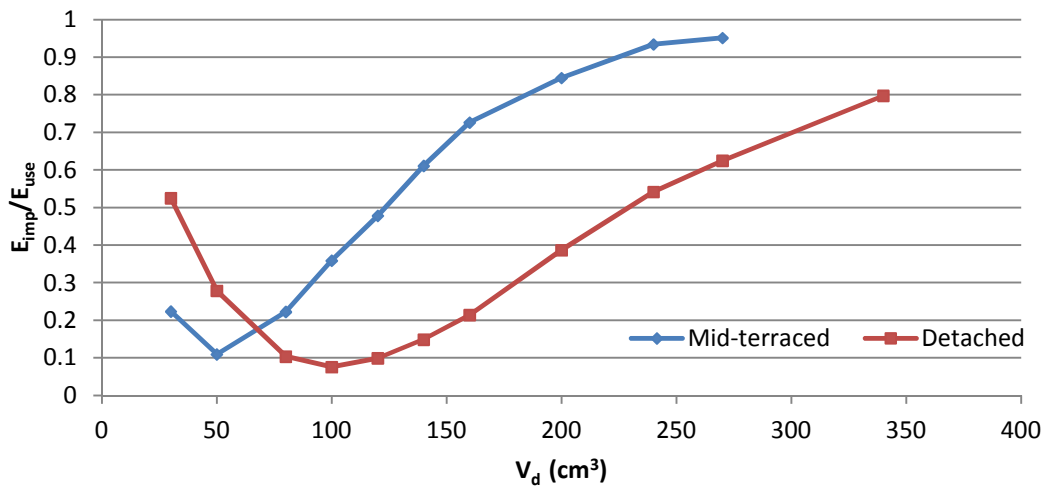


Figure 9.29  $E_{imp}/E_{use}$  vs.  $V_d$  (Dwelling comparison, EPC)

A considerable difference in the annual auxiliary boiler start up frequency can be observed in Figure 9.30 between the two simulated dwelling types. The boiler is found to exhibit a higher annual start up frequency under a detached



house than under a mid-terraced house throughout the complete simulated engine size range. As shown in section 9.2, the smaller the thermal storage tank on a given EPC application, the higher the boiler start-up frequency. In addition, the boiler start-up curve exhibits a wider range of values for the smaller storage tank sizes. While in this case the two dwellings are different, the fact that the boiler of the detached house is sized to meet the higher design thermal load when no electrical demand is present, combined with the fact that the two dwelling types share the same heat storage tank size of 200L makes the storage tank in the detached house proportionally smaller than in the mid-terraced house. As a result, the time for the storage tank temperature to transition from the boiler switch on to switch off temperature limits and vice versa is shorter in the case of the detached house during surges in engine generated waste heat and thermal load, resulting to a higher boiler start up frequency.

For the smallest simulated engine sizes of 30cc and 50cc, the engine provides a low but constant thermal output in both houses, and as a result, storage tank water temperature tends to not fluctuate to a great extent and remains above the boiler activation temperature limit, unless a thermal demand for space heating occurs. Since the space heating schedule does not differ between the two houses, the boiler start up frequency is observed to exhibit small differences for small engine sizes, with 2664 and 2528 boiler starts per year for the detached and the mid terraced house respectively under a 30cc engine displacement. The transition to larger engine sizes amplifies the difference, as the proportionally larger tank size of the mid-terraced house, manages the surges in thermal load and waste heat generation better. Maximum boiler operating frequency of 2701 and 3895 starts per year occur for the mid terraced house at 50cc, and for the detached at 160cc respectively.

By inspecting the engine sizes for which maximum amounts of rejected heat occur, it is observed that they are close to but smaller than the sizes that give maximum engine start-up frequencies. Maximum value of boiler start-up frequency in the mid terraced house is observed to occur for a considerably smaller engine size than in the detached house. Considering the

proportionally larger storage tank size of the mid-terraced house, the above behaviour comes to agreement with the observations of section 9.2, where it is shown that the engine size that results to a maximum boiler start-up frequency is subject to storage tank size with maxima of smaller storage tanks occurring for larger engine sizes. The above reinforces the need for the sizing of the heat storage tank for the given application in order to achieve similar results.

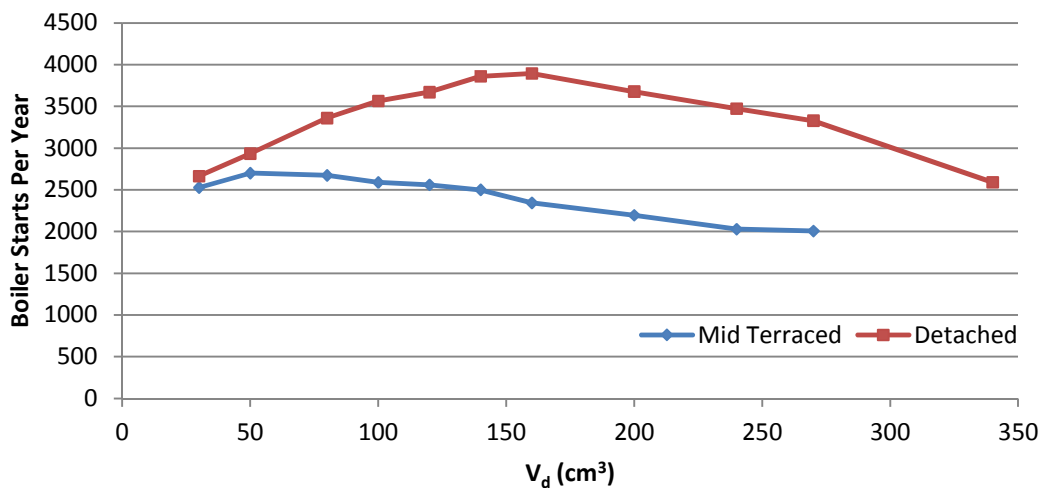


Figure 9.30 Boiler starts vs.  $V_d$  (Dwelling comparison, EPC)

The annual operating duration of the auxiliary boiler for the two dwelling types plotted against engine displacement can be seen in Figure 9.31. By comparing these plots to the plots of Figure 9.30, it is observed that the engine displacements for which minimum values of annual boiler operating duration of 1472 and 1402 hours per year for the mid-terraced and detached house occur, are the same displacements for which maximum boiler start up frequency occurs, an observation that highlights the displacement of the boiler capacity by abundant amounts of engine generated waste heat. While the two curves exhibit different shape and minimum values appear for different engine sizes, the range of their values is very similar, especially in the more energy efficient sizes of 30cc to 80cc. For a 50cc engine, 1617 and 1472 starts for the detached and the mid-terraced house respectively are observed, which is a difference of 145 hours and a ratio of 1.1. The longer

operating duration of engines larger than 80cc in the case of the mid-terraced house is attributed to the significantly longer operating duration of the engine observed in the detached house.

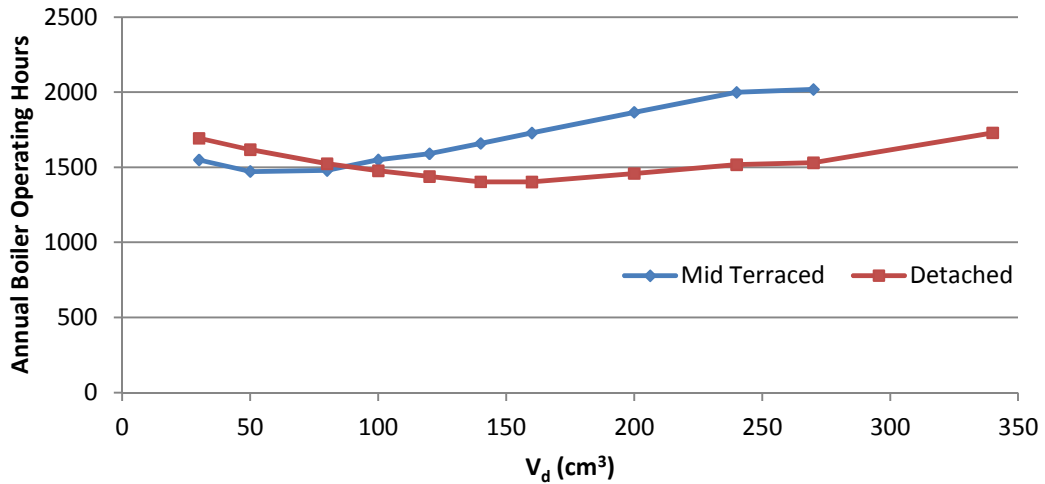


Figure 9.31 Boiler operating hours vs.  $V_d$  (Dwelling comparison, EPC)

The economic performance curves of the system for two dwelling types under an FIT regime plotted against engine displacement is shown in Figure 9.32. It is observed that for both house types, maximum cost savings of 46% are achieved but under engine displacements of 50cc and 80cc for a mid-terraced and a detached house respectively. In the case of the mid-terraced house, savings exhibit a steep decline past the 50cc engine size, and for the largest FIT eligible engine size of 140cc, savings drop to 20.3%. On the other hand, the detached house retains considerably higher cost savings under larger FIT eligible engine sizes, which for a 140cc engine reach 39.4%, almost double the savings of the mid-terraced house. The main reasons for this difference in the behaviour of the two curves are the longer operating duration exhibited by an engine of a given size under a detached dwelling, as well as the lower HPR of the detached dwelling which both allow for the generation of proportionally higher amounts of electricity and result to proportionally higher revenues due to the high rate of the generation tariff.

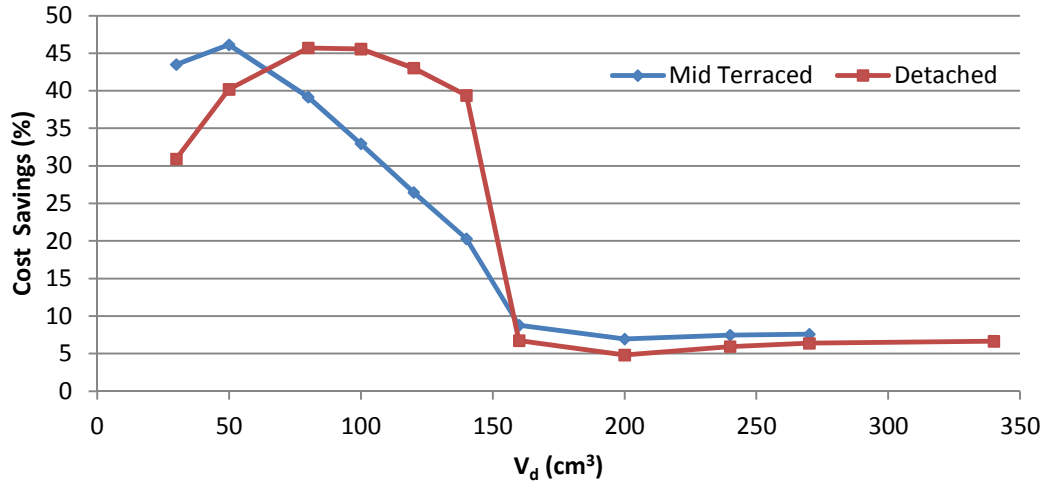


Figure 9.32 Cost savings (with FIT) vs.  $V_d$  (Dwelling comparison, EPC)

Under a no government subsidy regime, cost savings for otherwise FIT eligible engine sizes are considerably lower than under FIT regime. As can be observed in Figure 9.33 cost savings curves follow the trend of the *PES* curve of Figure 9.24 and this similarity indicates a strong dependence of system economic performance on the amount of rejected heat. Maximum savings of 18.5% and 14.3% occur for the mid-terraced with a 30cc engine, and the detached house with a 50cc engine respectively, which is a difference of 4.2 percentage points and a ratio of 1.29. For the engine sizes of 30cc to 100cc, cost savings of 12.4% to 18.5% for the mid-terraced, and 12.4% to 14.3% for the detached house are observed.

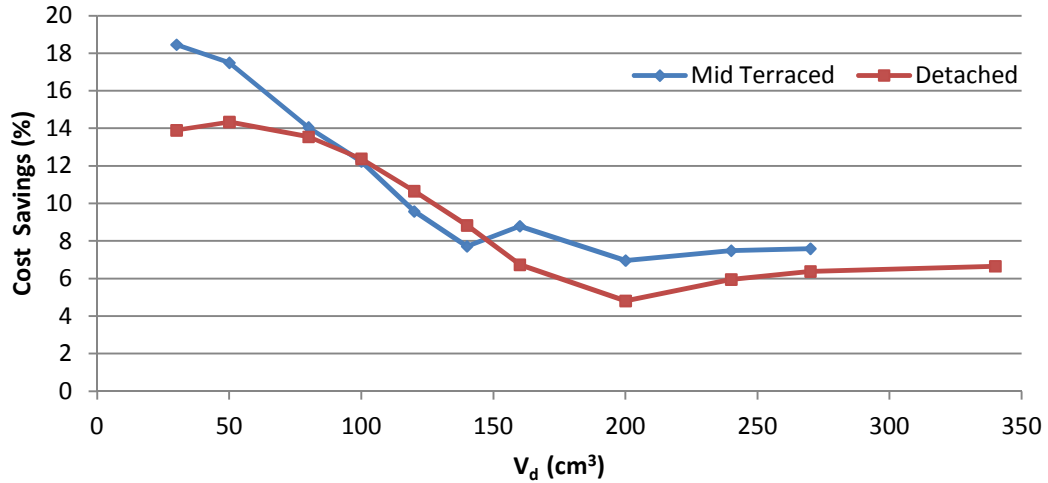


Figure 9.33 Cost savings (No FIT) vs.  $V_d$  (Dwelling comparison, EPC)

### 9.5. Dwelling Location

Geographical location has been found to have the opposite effect on system energetic performance on EPC systems with the simulation performed under ‘Leuchars’ weather profile being characterized by higher primary energy savings than the ‘London Gatwick’ simulations for almost all engine sizes as can be observed in Figure 9.34. Such behaviour can be attributed to the fact that waste heat generation under an electricity priority control is independent of heat demand, and systems that make use of this control strategy perform better when the heat demand is high enough to prevent the rejection of surplus heat into the atmosphere. As a result, the colder the climate, the less heat is rejected into the atmosphere and the greater the energy savings. For the Leuchars weather profile, maximum savings of 7.9% occur with a 50cc engine (identical with London Gatwick for the same engine size). For the London Gatwick weather profile, maximum savings of 8.2% occur with a 30cc engine which is 0.4 percentage points, higher than the savings encountered under Leuchars weather profile for the same engine which translates to a ratio of 1.05. For both locations, minimum *PES* occur for a 200cc engine. The difference in *PES* between the two curves is amplified for medium sized engines. The reason for which the warmer climate generates more savings than the colder climate for the smallest simulated engine is the

fact that the contribution of the CHP is reduced to the extent that the application approaches the conventional boiler & grid solution energy wise.

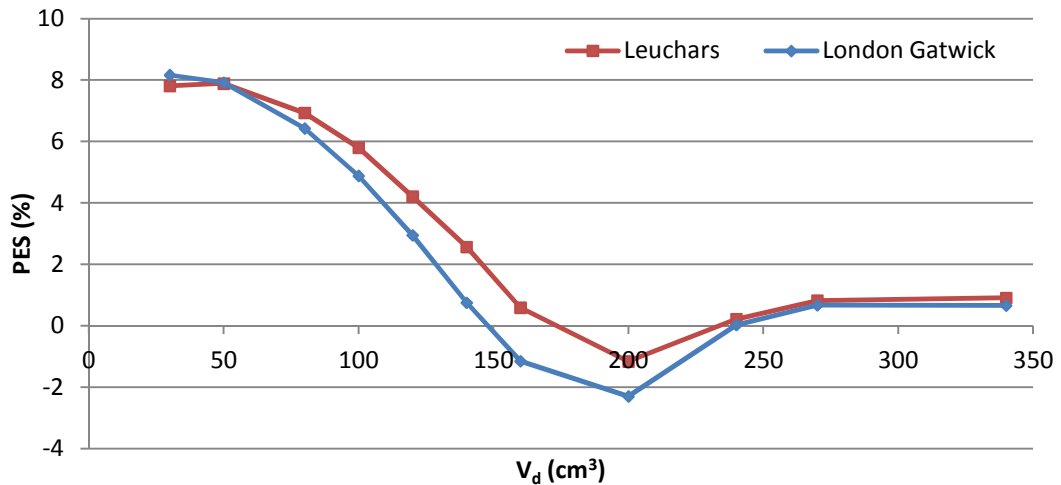


Figure 9.34 PES vs.  $V_d$  (Geog. comparison, EPC)

CO<sub>2</sub> savings curves of Figure 9.35 are observed to follow the trend of *PES* curves of Figure 9.34 with the two locations generating similar values. For both locations, maximum CO<sub>2</sub> savings occur for a 50cc engine with 10.5% for London Gatwick and 10.3% for Leuchars, which is a 0.2% percentage point difference and a ratio of 1.02. For engine sizes between 80cc and 240cc, this difference amplifies and maximizes for a 140cc engine at 1.7 percentage points.

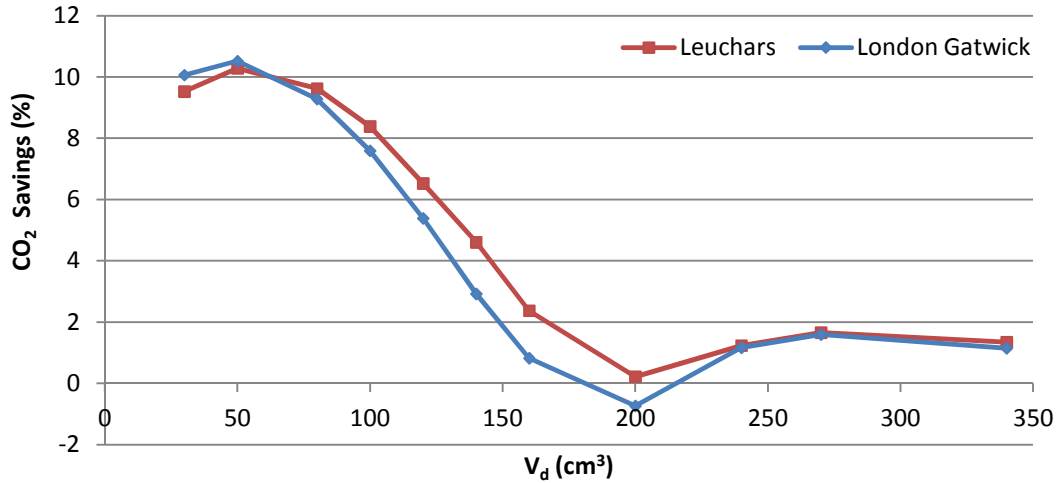


Figure 9.35 CO<sub>2</sub> Savings vs. V<sub>d</sub> (Geog comparison, EPC)

While the differences in energetic and emissions performance between the two different UK locations for the better performing engine sizes has been found to be small, the operating patterns of the auxiliary boiler exhibit considerable differences both in terms of start-up frequency and operating duration. From Figure 9.36, it is observed that the auxiliary boiler in Leuchars completes 600 to 1100 boiler starts per year more than the boiler under a London Gatwick weather profile due to the higher thermal demand associated with a colder climate reducing the dwelling thermal mass temperature to lower levels during non heating periods. For a 50cc engine size, the boiler is switched on 2934 and 1959 times per year for Leuchars and London Gatwick respectively, which is a difference of 975 start-ups and a ratio of 1.5. Maximum boiler start-up frequency of 3895 and 2911 starts per year for Leuchars and London Gatwick – a difference of 984 starts and a ratio of 1.3 – occurs for a 160cc engine.

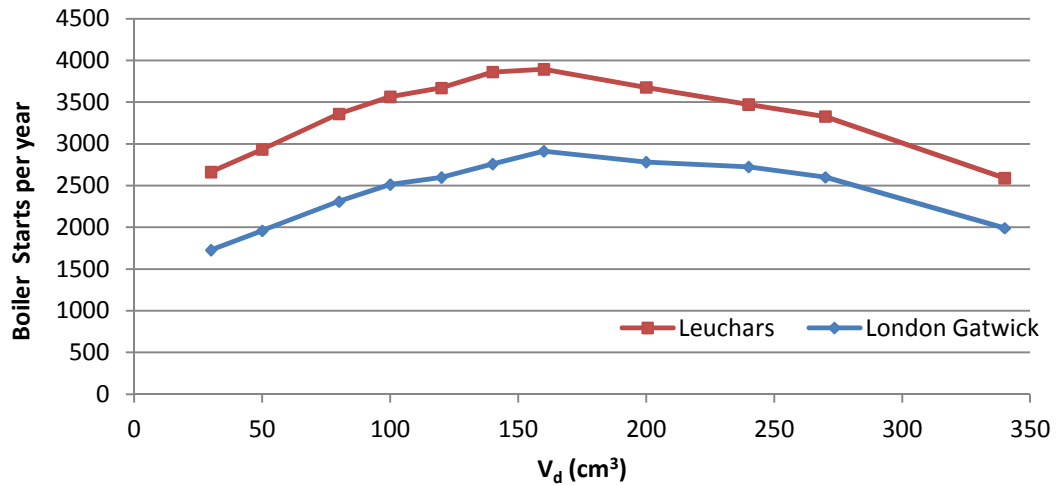


Figure 9.36 Boiler starts vs.  $V_d$  (Geog comparison, EPC)

From the boiler operating duration plots of Figure 9.37, it is observed that the boiler under the colder Leuchars weather profile operates for 200 to 260 hours per year longer than the boiler under the London Gatwick profile due to the higher thermal demand placed on the system by the colder climatic conditions of the former. The higher thermal demand is a result of not only the higher steady state load, but also the lower temperatures the dwelling mass falls to under the colder climate during non heating periods. For an engine displacement of 50cc, the boiler is operated for 1618 and 1374 hours under Leuchars and London Gatwick profiles respectively, which is a difference of 244 hours and a ratio of 1.18. Minimum operating hours occur for both locations under an engine size of 160cc with 1402 and 1177 hours per year of boiler operation observed for Leuchars and London Gatwick, which a difference of 225 hours and a ratio of 1.19.



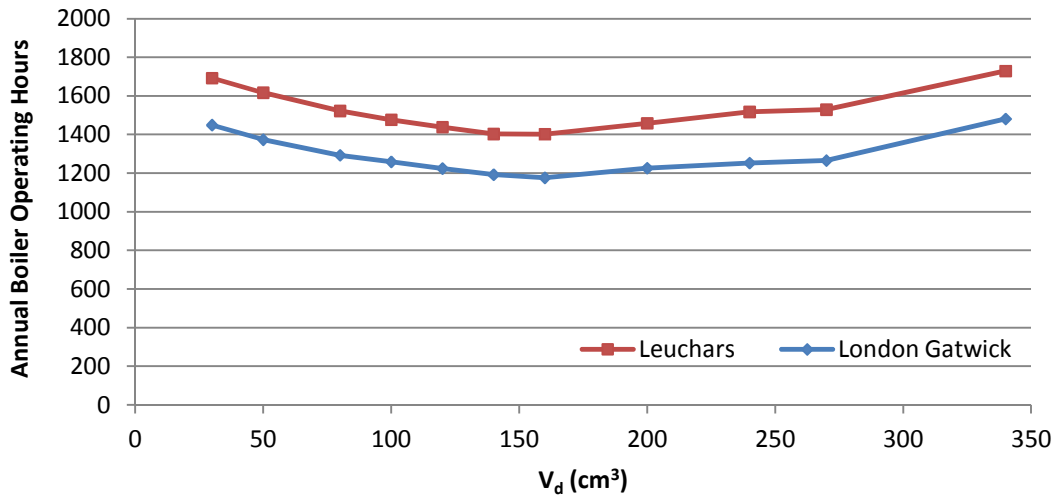


Figure 9.37 Boiler operating hours vs.  $V_d$  (Geog. comparison, EPC)

Cost savings generated by the EPC system under a FIT economic regime plotted against engine displacement for the two simulated locations can be seen in Figure 9.38. As can be observed, the generated cost savings under FIT eligibility between the two locations are close in value with cost savings for the London Gatwick weather profile being located higher than the cost savings generated for Leuchars for all FIT eligible units. This can be attributed to the fact that electricity revenues are equal for both cases, while the operating costs under the colder climate are higher than the warmer climate. An equal reduction on two different values of operating costs favours the lower cost in terms of relative reduction, in this case the warmer climate of London Gatwick. Maximum cost savings of 48.6% and 45.7% for London Gatwick and Leuchars respectively occur for both locations under an 80cc engine, which is a 2.9 percentage point difference and a ratio of 1.06. Minimum savings of 32.8% and 30.9% for London Gatwick and Leuchars respectively occur for both locations under a 30cc engine – a 1.9 percentage point difference and a ratio of 1.06. Under a 50cc engine displacement, savings of 42.9% and 40.2% are observed for London Gatwick and Leuchars respectively, which is a 2.7 percentage point difference, and a ratio of 1.07.

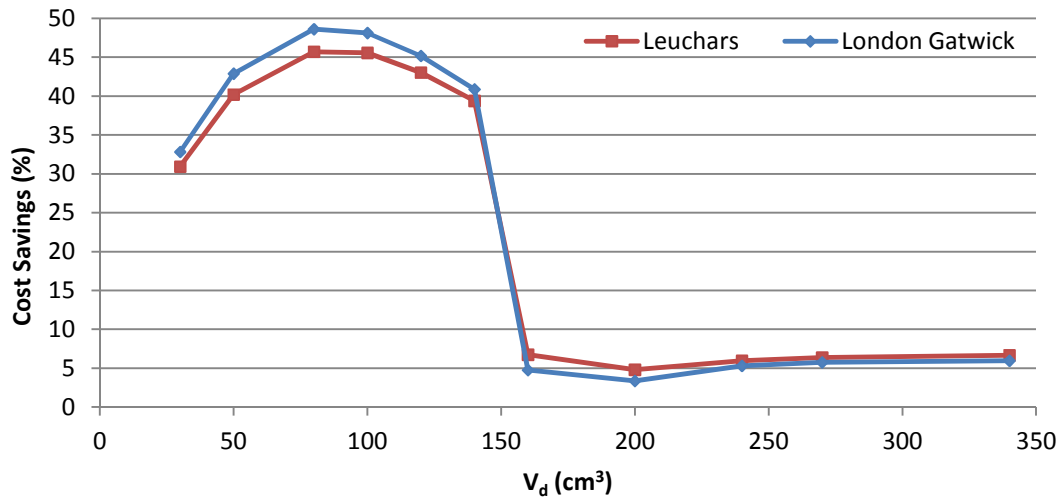


Figure 9.38 Cost Savings (With FIT) vs.  $V_d$  (Geog. comparison, EPC)

If no government subsidy is in place, cost savings curves take the shape shown in Figure 9.39 and follow the *PES* curve trend of Figure 9.34. Cost savings generated under the Leuchars weather profile are higher than the savings generated under London Gatwick due to the higher thermal demand of the colder climate leading to a reduction in the amount of rejected heat. As can be observed, for the smaller more efficient engine sizes of 30cc to 80cc, generated cost savings between the two locations are quite similar. Maximum savings of 14.3% and 14% for Leuchars and London Gatwick respectively occur under a 50cc engine size – a 0.3 percentage point difference and a ratio of 1.02. Identical cost savings of 13.9% for both locations occur under a 30cc engine size. For larger engine sizes the difference in cost savings between the two locations is amplified, and under a 80cc engine size, savings of 13.5% and 12.8% for Leuchars and London Gatwick respectively are observed, which is a 0.7 percentage point difference and a ratio of 1.05. Minimum savings of 4.8% and 3.4% occur for Leuchars and London Gatwick respectively under a 200cc engine size.

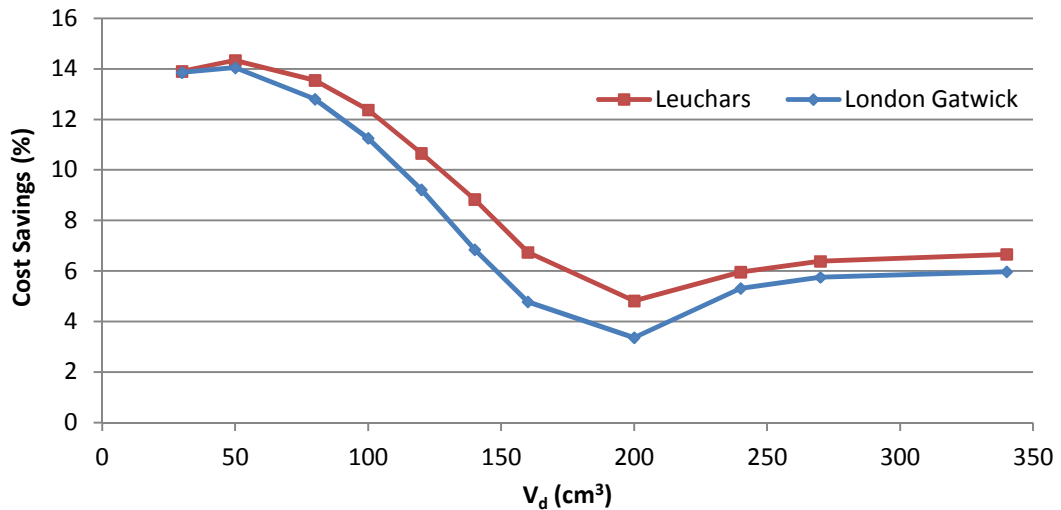


Figure 9.39 Cost Savings (Without FIT) vs.  $V_d$  (Geog. comparison, EPC)

## 9.6. Summary

The current chapter investigated the effects of different system parameters as well as energy demand characteristics on the performance of EPC systems. In all cases, highest *PES* and CO<sub>2</sub> savings are observed for the smallest simulated engine sizes of 30cc to 50cc for both houses as the amount of rejected heat as well as imported electricity are kept to a minimum.

In terms of the effect of engine grade on performance, it has been observed that the system generates considerably higher the *PES* and CO<sub>2</sub> savings for the more efficient HCR engine type. While the HCR engine generates savings comparable to those encountered under an HPC strategy (for the very small engines), the savings generated by the LCR engine are very low and hardly justify the replacement of the boiler & grid solution. In addition, the LCR engine equipped system operated at a loss for most of the medium and larger engine sizes. Thus, it is concluded that system performance under this control strategy is very sensitive to the fuel conversion efficiency as well as the size of the used engine, and only high performing, small engines must be used.

The extent to which an LCR EPC system performance can be improved by changing the thermal storage tank size and operating temperature limits has been investigated. While *PES* and CO<sub>2</sub> savings showed an impressive increase with the transition from the smallest to the largest tank size, the improved performance indicators still fell short from making LCR engine equipped EPC micro-CHP systems a competitive option. A smaller but impressive nonetheless improvement in system performance was observed when the storage tank operating temperature limits were widened, but such measures failed to elevate the system to a competitive status. The effect of the lowering of the boiler deactivation temperature limit was negligible for the small engine sizes. Boiler start up frequency as well as operating duration showed a significant reduction with larger boiler sizes and the new operating limits, and this is of great importance in the longevity and the emission quality of the boiler. Therefore the above measures must be used in conjunction with a high performing engine.

In terms of the effect of load characteristics on EPC system performance, it has been observed that the higher HPR of a dwelling, the higher the *PES* and CO<sub>2</sub> savings are. Different electrical load magnitudes lead to different engine start-up patterns, and the curves peak under different engine sizes. Small engines were found to operate without a stop under both tested house types. Engines of medium and larger sizes operate for considerably longer periods in the larger dwelling. Thermal storage tank must be sized in proportion to the house type in order to achieve similar performance as well as auxiliary boiler operating patterns.

Under the FIT scheme the system was found to generate cost savings even in the larger engines for the larger houses, while for smaller houses, savings are reduced at a fast pace due to the faster reduction in engine operating duration. Cost savings without government subsidies are considerably less than with FIT and follow the trends of the *PES* indicating the strong dependence of costs on rejected heat, and favouring the dwelling with the higher HPR and proportionally larger thermal storage tank size.

A colder climate was observed to generate higher savings, as the higher HPR of the total energy consumption reduces waste heat rejection. While the differences in savings were relatively small between the two tested UK locations, significant differences were observed in the operating patterns of the auxiliary boiler, with the boiler operating under the colder climate being started more frequently and operated for longer periods of time than in the case of the warmer climate. This observation is attributed to the lower temperatures the dwelling under the colder climate falls to during non heating periods.

## Chapter 10 Results and Strategy Comparison

Control strategy can play a very important role in the technical and economic feasibility of a micro-cogeneration system. In this chapter, heat priority control (HPC) strategy will be compared in terms of performance, as well as in terms of engine and boiler operating patterns to the electricity priority control (EPC) strategy. The used engine type is of high compression ratio (HCR), and the dwelling type post-1967 detached, which is simulated under a London Gatwick weather profile. Thermal storage tank size for both cases is 200L.

Section 10.1 compares the *PES* and CO<sub>2</sub> savings the two strategies generate over the conventional method of heat and power supply of boiler & grid. Section 10.2 compares the operating patterns (start-ups and operating duration) of the engine and the auxiliary boiler of a  $\mu$ CHP system operated under the two tested strategies, while the cost savings under an FIT subsidy and without a governmental subsidy, generated by the EPC and HPC strategies are compared in Section 10.3.

### 10.1. Energetic and Environmental Performance

The energetic performance of the two strategies can be seen in the curves plotted in Figure 10.1. It can be observed that while the HPC strategy generates *PES* throughout the complete tested engine range and the maximum spread of the savings is no more than 2.6 percentage points from maximum to minimum value, the EPC system generates energy savings comparable to those obtained by the HPC system only for the very small engine sizes of 30cc and 50cc, and operates at a loss for engine sizes larger than 100cc with a peak value of 9.7% for an engine displacement of 200cc. The HPC strategy is found to outperform the EPC strategy for all simulated engine sizes with a maximum difference of 20 percentage points for an engine displacement of 200cc. Maximum *PES* for the HPC strategy of 11.6% occur for an engine displacement of 80cc, while in the case of the EPC

strategy, maximum *PES* of 10.6% occur for the much smaller engine displacement of 30cc. The *PES* of the EPC strategy for the 30cc engine may be very close to those generated by the HPC strategy for the same engine size, but as engine size increases, a steep drop in *PES* is observed for the EPC systems due to the increase in the amount of rejected heat. A further increase in engine size beyond 200cc gradually reduces the engine generated waste heat in the EPC system, and heat rejection follows this reduction resulting to an increase in *PES* which reach a value of  $-3.5\%$  (3.5% loss) for a 340cc engine displacement. It is therefore safe to conclude that the energetic performance of the EPC strategy is very sensitive to engine size selection while the HPC strategy can generate savings even for the largest engines.

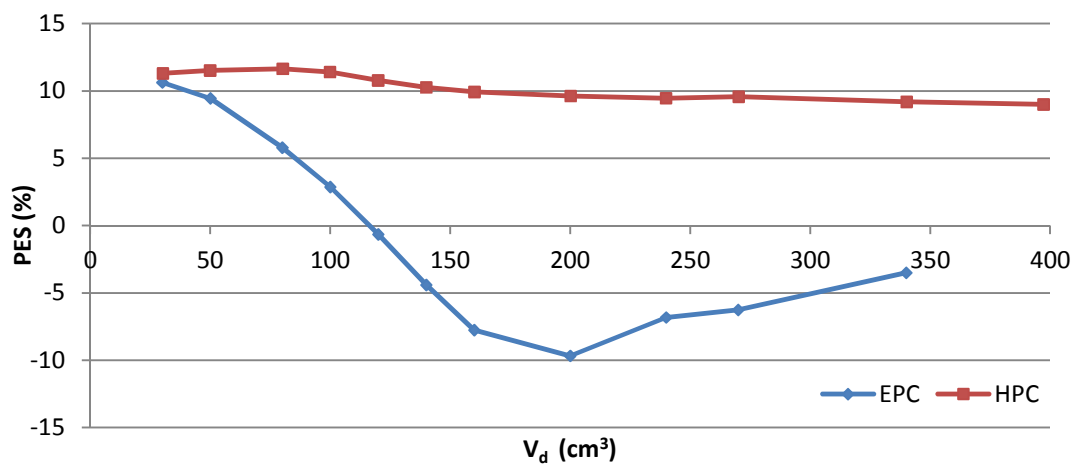


Figure 10.1 *PES* vs.  $V_d$  (Strategy comparison)

A comparison between the seasonal variation of *PES* of the two strategies under a 100cc engine can be seen in Figure 10.2. As can be observed, the HPC strategy outperforms the EPC strategy throughout the whole year. Maximum *PES* in the case of the HPC system occur during the warmer months of the year, as the overall efficiency of the conventional boiler & grid solution drops significantly due to the consumption consisting mainly of imported electricity. On the other hand, the EPC strategy exhibits its lowest performance during the warmer months, and the unit operates at a loss due

the increased amounts of rejected heat. From the above, it can be seen that switching between strategies would not improve system performance, and HPC should be the strategy of choice if saving primary energy (and reducing CO<sub>2</sub>) is the main objective of the operator.

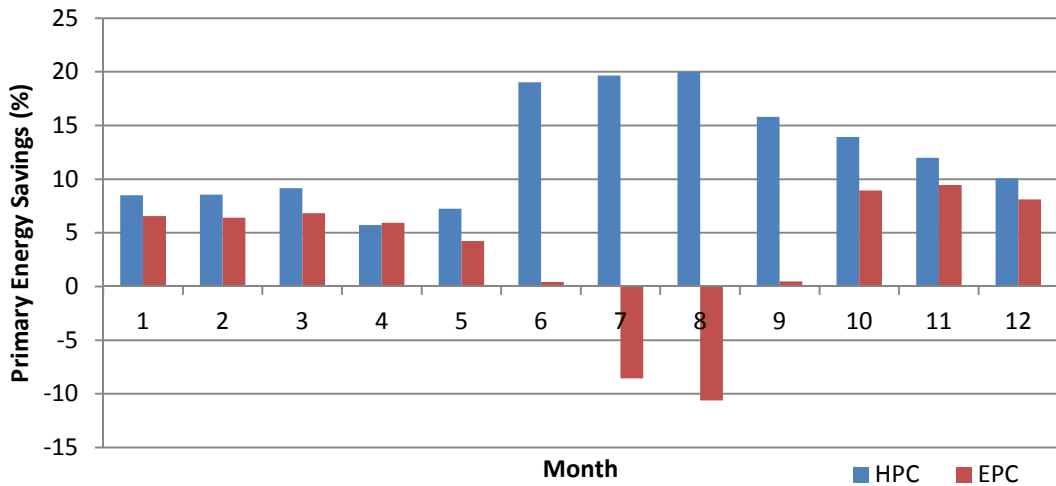


Figure 10.2 PES vs. month of the year (Strategy comparison)

The trend of the *PES* plots of Figure 10.1 is followed by the CO<sub>2</sub> savings plots of Figure 10.3 where the two performance indicators behave in a very similar manner. For engine sizes of 30cc to 50cc, CO<sub>2</sub> savings generated by EPC and HPC strategies are very similar. For larger engine sizes, the difference between the performance of the two strategies increases rapidly with EPC performance exhibiting a significantly steeper drop in performance than the HPC system. CO<sub>2</sub> savings for the HPC strategy range from 14.2% for an engine displacement of 80cc to 9.9% for a 400cc engine. For the EPC strategy, CO<sub>2</sub> savings of 13.7% for 30cc to -6.7% (6.7% increase in CO<sub>2</sub> emissions compared to the boiler-grid case) for a 200cc engine are observed. Under EPC strategy, engine sizes greater than 120cc generate more emissions than the boiler and grid solution. Maximum difference in emissions performance between the two strategies occurs for a 200cc engine displacement with 17.8 percentage points.



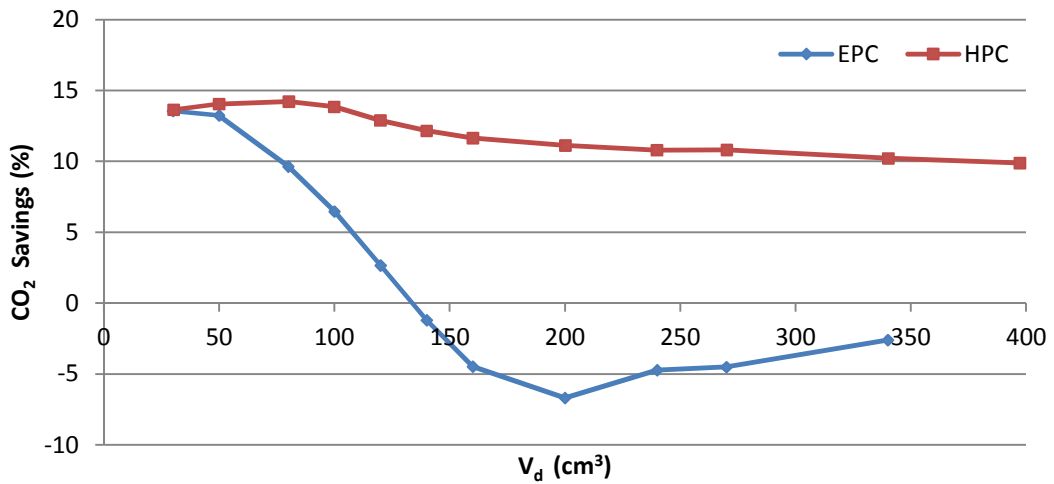


Figure 10.3 CO<sub>2</sub> vs.  $V_d$  (Strategy comparison)

## 10.2. Operating Patterns

Engine operating patterns for the two strategies are characterized by a considerably different behaviour as can be seen in Figure 10.4. The annual number of engine starts in the case of an HPC system exhibits a relatively slow increase as engine size increases. 508 and 862 annual engine starts for 30cc and 400cc respectively have been observed which translates to a ratio of 1.7. The gradual increase of engine start up frequency of HPC systems with engine size is attributed to the fact that the greater the engine size is, the shorter the time for the storage tank temperature to transition from the engine switch-on temperature trigger limit to the switch-off engine temperature limit. On the other hand, the engine operating patterns of EPC strategy deviate significantly from those of HPC strategy. The engine start-up frequency is 0 for the 50cc and 80cc engines as they operate continuously due to their minimum generator load limit being always lower than the minimum electrical load. As engine size is increased and electrical load is more frequently found to be below the generator minimum load, the engine is switched off more frequently, thus increasing the annual number of engine starts which crosses the HPC curve at the engine displacement of 100cc. Engine start-up frequency under EPC strategy reaches a maximum of 2044 starts per year for an engine size of 200cc which is a 2.7 times higher

frequency than the one exhibited by the HPC system of the same engine size. An increase in engine size past 200cc decreases the engine start up frequency rapidly, crossing the HPC curve again at the capacity of 300cc, as the frequency of the instances for which the electrical load is equal or higher than the minimum generator load is reduced.

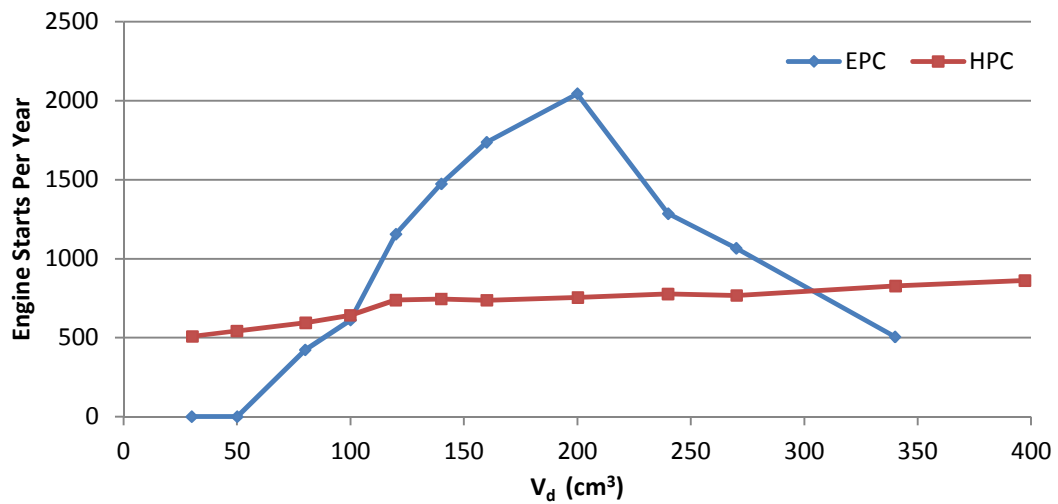


Figure 10.4 Engine starts vs.  $V_d$  (Strategy comparison)

Considerable difference in the annual engine operating time can be observed in Figure 10.5 between the two operating strategies for a given engine size throughout the largest segment of the simulated engine size range. While both curves are characterized by a significant drop as engine size is increased, the implementation of the EPC strategy results in a longer annual engine operating duration than the HPC system up to an engine size of 300cc. The most notable difference in operating duration occurs for an engine displacement of 80cc (which incidentally is the engine size that generated maximum *PES* and  $\text{CO}_2$  savings for the HPC system) where the engine operates for 8579 and 3120 hours per year under EPC and HPC strategies respectively, which translates to a 2.7 times longer engine operating duration of the EPC compared to that of the HPC strategy. Such a difference in engine operating duration is an important factor in the financial feasibility of the system as it directly affects the necessary payback period.

The drop in engine annual operating duration for the EPC system is attributed to the fact that the larger the engine size, the longer the period of time during which the electrical load magnitude is located below the minimum generator load. EPC systems with engine displacements of 30cc and 50cc operate continuously, and thus exhibit the maximum possible engine annual operating time of 8760 hours.

In the case of the HPC system, as engine size is increased, its operating duration is reduced due to the higher engine waste heat output saturating the storage tank within a shorter period of time. The maximum engine annual operating duration of 5748 hours occurs for a 30cc engine.

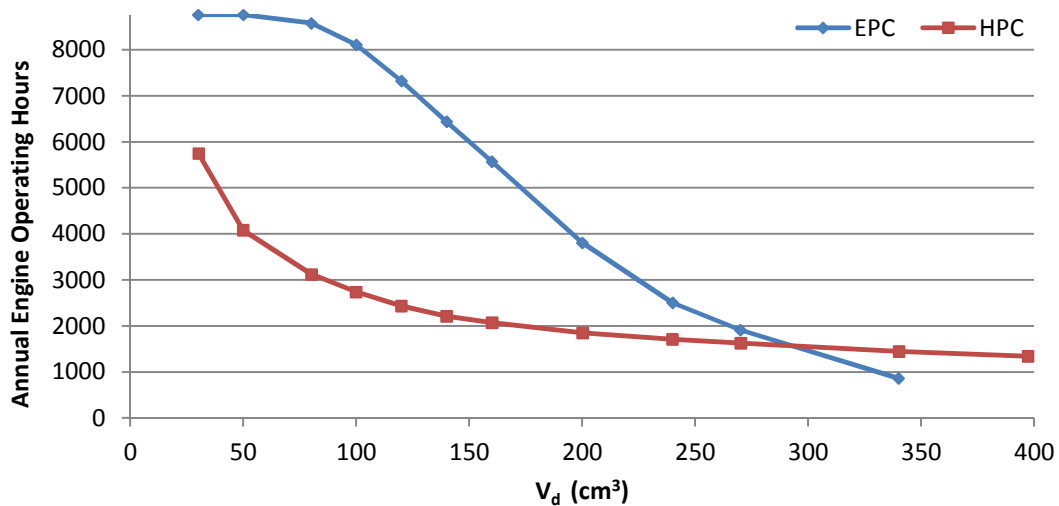


Figure 10.5 Engine operating duration vs.  $V_d$  (Strategy comparison)

The control strategy of the CHP system influences not only the engine but also the boiler operating patterns and its effect can be seen in Figure 10.6. For the smaller, more efficient engine sizes of 30cc to 100cc, the auxiliary boiler of an HPC system exhibits a larger annual number of starts than of an EPC system, and the ratio of HPC/EPC annual boiler starts ranges from 1.6 to 1.05. For engine sizes larger than 100cc, the boiler of the EPC system operates for a longer period of time. The maximum number of 1244 annual boiler starts for the HPC system occurs for the smallest simulated engine size of 30cc, and as the engine size is increased, the boiler start up

frequency is gradually reduced to 836 starts per year for the largest simulated engine displacement of 340cc.

The EPC system powered by the smallest simulated engine size of 30cc, exhibits the minimum number of 766 annual boiler starts in the simulated engine size range. As engine size is increased, the frequency of occurrence of engine shut down periods during which heat must be supplemented by the boiler, and therefore the number of annual boiler starts increases as well, crossing the HPC curve at 110cc engine displacement and reaching a maximum value of 1220 starts per year for an engine displacement of 140cc. A further increase in engine size leads to a gradual increase in the fraction of total thermal load that must be covered by the boiler, and a slow reduction in boiler start up frequency takes place dropping to 1068 starts per year for a 340cc engine displacement.

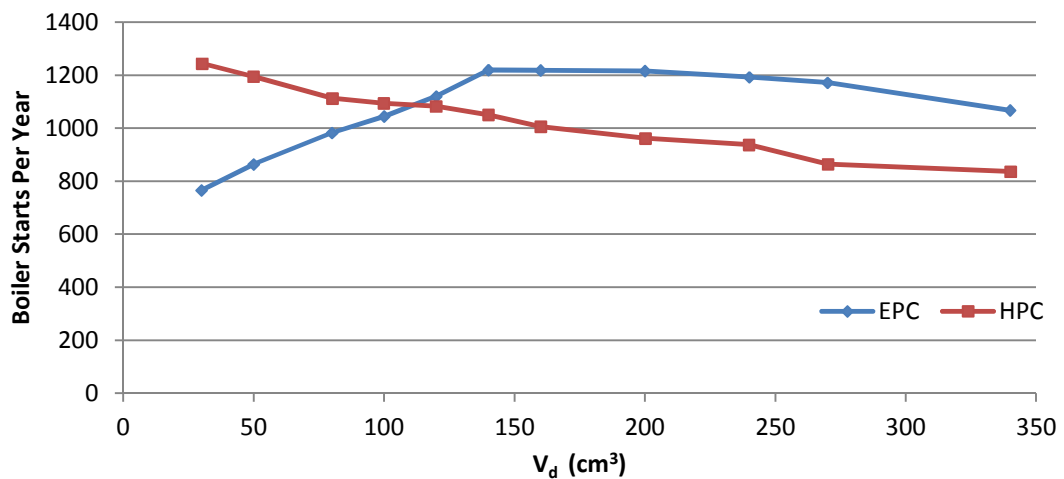


Figure 10.6 Boiler starts vs.  $V_d$  (Strategy comparison)

Auxiliary boiler annual operating duration exhibited by the two control strategies for a range of tested engine sizes is shown in Figure 10.7. For the smaller, better performing engine sizes of 30cc to 100cc, the resulting boiler operating duration does not exhibit a significant difference between the two control strategies, and for a 50cc engine displacement, the boiler operating duration is almost identical. While boiler operating duration in the case of

HPC strategy exhibits a slow reduction as engine size increases, with the maximum value of 934 hours per year being observed for the minimum simulated displacement of 30cc and the minimum value of 734 hours per year for a 340cc engine, boiler operating duration under the EPC strategy is more sensitive to the selected engine size and follows a different trend than the HPC curve. Starting from the smallest simulated engine size, the increase in displacement leads to a steep reduction in boiler operating duration as waste heat from the engine meets a larger fraction of the total thermal load. The minimum number of 704 boiler operating hours per year for the EPC system occurs under the engine displacement of 140cc. As engine size is increased beyond 140cc, the amount of engine waste heat that contributes to the thermal load is reduced due to the reduction in the engine operating duration of the engine, and as a result, the heat demand placed on the auxiliary boiler is increased, thus increasing its duration of operation, which crosses the HPC curve for the engine displacement of 200cc, and reaches 1272 hours per year for a 340cc engine.

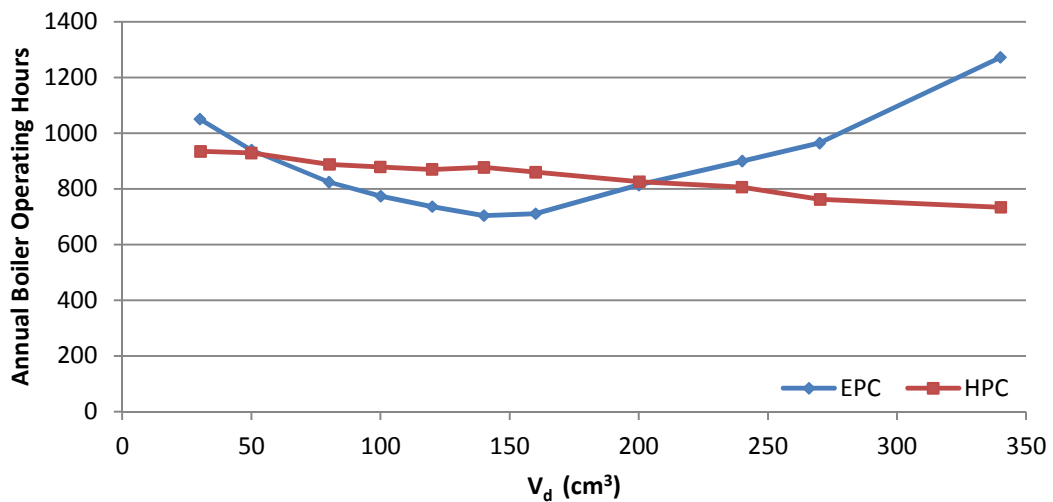


Figure 10.7 Boiler operating duration vs.  $V_d$  (Strategy comparison)

### 10.3. Economic Performance

The difference in cost savings between the two tested control strategies operating under FIT scheme can be seen in Figure 10.8. It may be observed

that the EPC system is the more cost effective control strategy of the two throughout the FIT eligible engine size range despite the fact that for engine sizes greater than 50cc, its energetic and environmental performance is considerably lower than of the HPC system. The better economic performance of the EPC system under FIT scheme can be attributed to the fact that subsidies are provided not only for power export but also for the amount of generated electricity, and since the generator under EPC strategy operates for a considerably longer period of time than the HPC system – especially in the smaller engine sizes - , the electricity generation revenues are expected to be higher in the case of the EPC system as the generation tariff is almost three times higher than the export tariff.

Under the FIT scheme regime, the EPC system generates maximum cost savings of 62.5% for an engine size of 80cc, while the HPC system with the same engine size generates savings of 40%, which is a difference of 22.5 percentage points and a ratio of 1.6 in favour of the EPC strategy. On the other hand, the CO<sub>2</sub> savings for the EPC and HPC systems for the same engine size are 9.6% and 14.2% respectively, which translate to a difference of 4.6 percentage points and a ratio of 1.6 in favour of the HPC strategy. It is also observed that while the 140cc engine is covered by the FIT, and the EPC strategy is more cost effective than the HPC unit of this engine size, its CO<sub>2</sub> savings are located 13.4 percentage points below the HPC generated value, and it generates 1.2% higher CO<sub>2</sub> emissions than the traditional boiler-grid solution.

From the above, it can be seen that in some cases, a CHP unit may be eligible for a government subsidy program, while at the same time generating more CO<sub>2</sub> emissions than the boiler-grid solution as well as a less profitable CHP alternative.

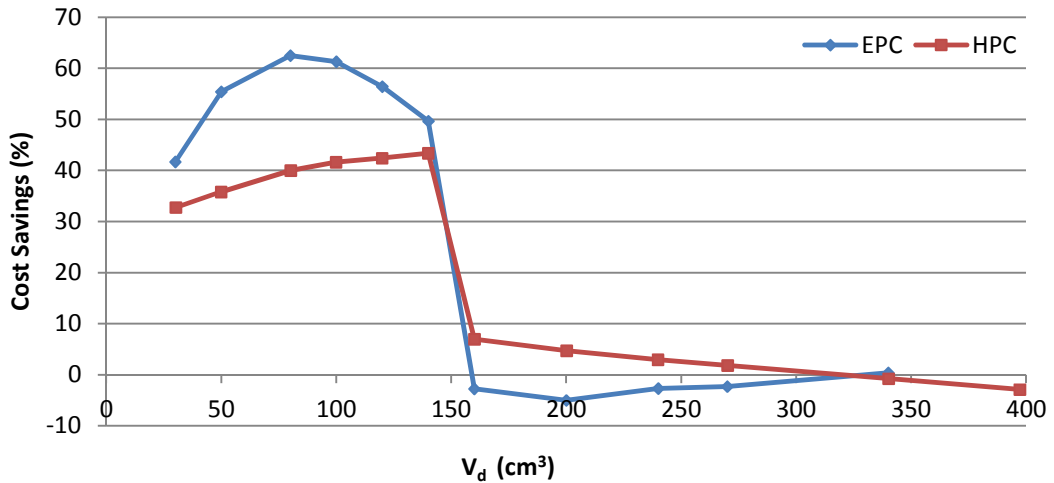


Figure 10.8 Cost savings (With FIT) vs. V<sub>d</sub> (Strategy comparison)

The economic performance of the two strategies under a no governmental subsidy regime can be seen in Figure 10.9. It can be observed that for both strategies, cost savings are significantly reduced for the otherwise FIT eligible engine size range of 50cc to 140cc compared to savings calculated with FIT revenues in place. For both strategies, maximum savings of 14.5% occur at the minimum simulated displacement of 30cc. For the smaller simulated engine sizes of 30cc and 50cc, the cost savings exhibited by the two strategies are almost identical, but as engine size is increased, the savings generated by the EPC strategy exhibit a steep decline compared to those generated by the HPC system and as a result, the EPC cost savings curve is located below the HPC curve for most of the simulated engine size range. In addition, for engine sizes of 160cc to 340cc the EPC system is found to operate at a loss with a maximum loss rate of 5% occurring for an engine displacement of 200cc which coincides with high amounts of heat rejection.

By comparing the results of Figure 10.9 to those of Figure 10.8, it can be observed that FIT revenues could in some cases enhance the cost effectiveness of an inherently less environmentally friendly and less cost effective system to the point that it is more attractive option for the end user

than a system that would normally be more profitable and generate lower emissions.

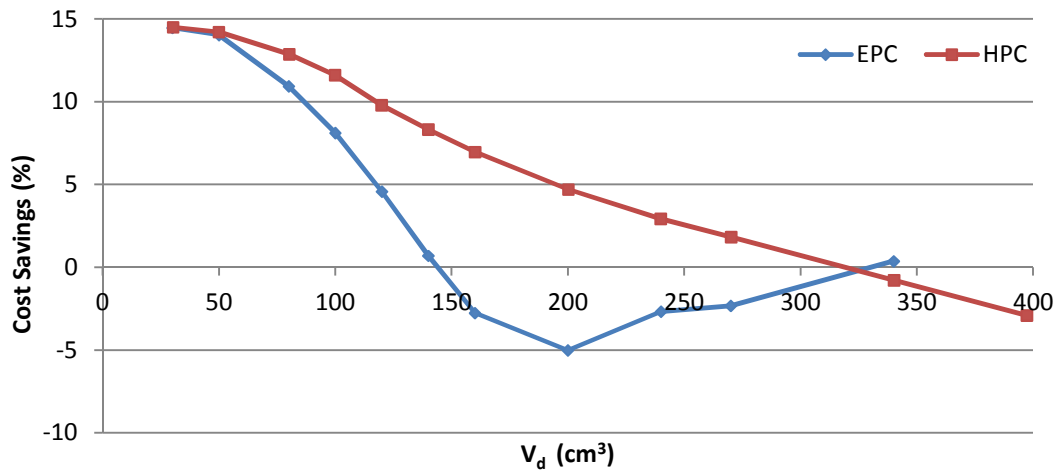


Figure 10.9 Cost savings (Without FIT) vs.  $V_d$  (Strategy comparison)

#### 10.4. Summary

The current chapter compared the performance of the HPC and EPC strategies, and the HPC strategy has been found to outperform the EPC strategy throughout the tested engine size range. The EPC strategy exhibited a comparable performance only when very small engines were simulated, with savings dropping sharply for larger engine sizes. On the other hand, the HPC strategy generated savings even for the larger engine sizes, and its performance was observed to be less affected by engine size and grade. Therefore, the EPC system performance is highly sensitive to the selected engine grade and size. In addition, the operating duration of the engine under EPC strategy with an engine size that performs comparably to the HPC strategy in terms of savings leads to considerably longer engine duration, and this constitutes a significant drawback as it reduces the required system payback period. Thus, a properly sized HPC system will outlive the EPC system by exhibiting approximately three times the life, an observation that must be taken into account when planning an investment on micro-CHP technology. While EPC strategy has been found to work well only



for engines of 50cc or smaller, the recommended range of engine sizes in the case of the HPC strategy is significantly larger and more practical with 80cc to 120cc giving best results. In all cases, storage tank size has been found to play an important role in system performance, and it is important to size the tank to fit the particular application, especially in the case of the EPC systems.

In terms of cost savings under FIT scheme, it has been observed that while the EPC system exhibits an energetic and environmental performance that is generally inferior to that of the HPC system, under government subsidies it has been found to outperform the HPC system in economic terms, and there is even the possibility that an EPC unit that operates at an energetic loss, and generates more CO<sub>2</sub> emissions than the conventional boiler & grid solution, be highly profitable, even more than a high performing HPC system.

## **Chapter 11 Conclusions and Recommendations for Future Work**

The current PhD thesis involved the thermo-economic modelling of micro-cogeneration systems as a central process in the development of a DES centred energy simulation software package with the ultimate aim of simulating micro-CHP systems under load profiles commonly encountered in the United Kingdom in order to expand the existing knowledge on micro-CHP system performance, and to identify design characteristics that ensure system sustainability within this geographical region.

### **11.1. Observations**

A comparison of the main characteristics of power generator technology most commonly encountered in existing literature revealed that the reciprocating internal combustion engine remains the most suitable type of prime mover for micro-cogeneration applications, while alternative power generator technologies are still underdeveloped for this application, and for this reason, a decision to focus on ICE based technology was made.

Through the review of existing literature on micro-cogeneration systems, the following parameters have been identified as having a strong effect on system performance and viability.

- Geographical location
- Building characteristics
- System heat to power ratio and electrical efficiency
- Load pattern morphology
- Device fuel utilization efficiency
- Fuel utilization efficiency of the conventional boiler & grid combination
- Control strategy of the CHP system
- System size
- Energy prices
- Electricity export prices

- Potential governmental subsidies
- System thermal inertia and thermal cycling and
- System useful operating life.

Due to the fact that cogeneration technology has been applied in the micro scale relatively recently, the energetic, environmental, and economic effect of the application under residential loads has not been thoroughly explored yet. The above, combined with the dependence of micro-CHP system performance on geographical location makes country specific research necessary, and this thesis started with the intent to expand the existing knowledge on the performance of ICE based micro-cogeneration under the geographical area of the United Kingdom through simulation.

The review on simulation based DES studies showed that the majority of researchers used dedicated building simulation software that rely on sophisticated 3-D dwelling models. While these packages describe building behaviour in great detail (necessary when research focuses on the dwelling fabric and the HVAC system), their overly complex to setup procedure, the need for operators to have a strong civil engineering background, and the high associated computational load they place on the computer make them less than ideal for researchers of DES, for whom the generation of a high volume of data is of a higher priority than running the most accurate case specific building model. Research on DES can benefit from an easier simulation configuration procedure and a faster running model than those encountered in existing building centred software tools, which would allow to resources to be funnelled on the study of the DES itself in order to generate a large volume of data in a short period of time – a highly desirable trait for sensitivity analyses. Thus, in order to address the need for such a tool and facilitate the generation of data for the current study, it was decided to develop a DES oriented energy simulation software that uses a 1-D building model and features a greatly simplified simulation setup procedure that allows for the generation of a high volume of simulation data specific to the evaluation of the performance of DES. The developed software in its current configuration is centred on ICE based micro-cogeneration systems.

During the developmental phase of the software tool, several areas of potential improvement, especially in the modelling of the micro-CHP system and the dwelling have been identified and contributions to these areas have been made in the process.

Readily available CHP models from literature lacked flexibility and did not take into consideration the effect of water temperature on heat recovery efficiency. A more flexible micro-CHP model using separate engine, electric machine, and heat exchanger sub-models, and taking into consideration the return water temperature in the calculation of recovered heat has been proposed and developed.

The resulting engine model is easy to scale and simple to connect to other subsystems, describes mass flows and the distribution of waste heat components in detail throughout the complete engine operating range, and is capable of describing the dynamic behaviour of the moving parts – all desirable engine model characteristics in CHP applications that have not been encountered integrated all in one existing engine model. Due to the above, it is highly suitable for use in variable speed or constant speed variable output CHP system simulation and constitutes a useful addition to the toolbox of the CHP modeller.

As a response to the lack of a ready to use true, computationally light heat exchanger model in literature, a map based heat exchanger model has been developed. It is useful in applications in which heat exchanger mass flow rates and inlet temperatures vary with time while at the same time being computationally light. Models of CHP systems or other installations involving heat exchanger networks are applications that can benefit from the use of the developed heat exchanger model. In order to populate the maps of the models, a complete heat exchanger simulation and mapping software tool based on discretised heat exchanger models has been developed, which while being a by-product of this project, it can be a very useful standalone piece of software that can serve in the role of heat exchanger rating, design, model generation and even for educational purposes.

In addition, while information on the thermal performance of UK dwellings has been encountered in existing literature, it was found to be sporadic and not readily useable. For this reason, the development of representative heat transfer models of UK dwellings has been of a high priority in this project. The developed UK dwelling model gives the researcher the flexibility to easily approximate the thermal characteristics of a given dwelling type that follows a given method of construction for the desired floor area, thus removing additional modelling effort were he or she need to change the dwelling size.

The resulting DES centred energy simulation software is a highly modular, easy to configure platform capable of accelerating the study of micro-cogeneration systems by allowing for the generation of a large volume of data under a diverse set of system configurations and operating conditions. It has been the main tool used in the generation of data presented and analysed in Chapter 8, Chapter 9, and Chapter 10, and it can be considered as a very promising alternative to dedicated building simulation software, whose use can be highly beneficial when the DES is the main area of focus of the study.

## **11.2. General Conclusions**

Simulations were carried out for different dwelling types, dwelling locations, engine grades, operating strategies, boiler operating limits, and boiler sizes under a range of engine sizes in order to investigate the effect of their variation on system performance and component operating patterns. In all cases, CO<sub>2</sub> savings curves have been found to closely follow the trend of the *PES* curves.

HPC systems have been found capable of generating *PES* and CO<sub>2</sub> savings under both low and high performing engines, and engine grade has not been found to influence the engine size under which maximum *PES* and CO<sub>2</sub> savings occur. For both HCR and LCR engine types, savings have been observed for even the largest simulated engine sizes showing a relatively low sensitivity of performance on engine size, but the use of engines larger than

120-140cc is not recommended due to the steep increase in both imported and exported electricity which negatively affect the environmental and economic system performance respectively.

For HPC systems, the higher the HPR of the demand, the lower the generated *PES*, and CO<sub>2</sub> savings are due the higher overall efficiency of the conventional boiler & grid solution, and due to the fact that the CHP device efficiency remains almost constant. For this reason, the mid-terraced house was found to generate higher *PES* and CO<sub>2</sub> savings than the Detached house. Similarly, an HPC system operated under a warmer climate performs better than under a colder climate, but the difference in savings between the two simulated UK locations has not been found to be significant.

EPC strategy performance is very sensitive to the power generation efficiency of the CHP unit and has been found to be very low under LCR engines, operating at a loss for most engine sizes. Even under a high performing HCR engine EPC system, only the smallest simulated engine sizes of 50cc and below yield comparable results to those encountered under HPC strategy. Performance has been observed to be very sensitive with respect to engine size under both HCR and LCR engines with a dramatic reduction in savings for engine sizes of 100cc and above.

Under EPC strategy, the higher the HPR of the total energy demand, the lower the amount of heat rejected into the atmosphere. For this reason, higher *PES*, CO<sub>2</sub>, and cost savings are observed under the colder simulated climate. For the smaller engine sizes, higher *PES* and CO<sub>2</sub> savings have been recorded for the smaller house due to the negative effect of the proportionally higher amount of imported electricity encountered in the case of the larger house.

The widening of the storage tank temperature band can have a strong effect on EPC system performance as it increases *PES*, CO<sub>2</sub> savings, and cost savings to a considerable extent, while at the same time boiler start up frequency and operating duration are reduced. On the other hand, the shift in the boiler switch off temperature limit closer to the boiler switch on temperature limit has negligible effects on *PES* and CO<sub>2</sub> savings while it has

a strong influence on boiler operating patterns. Increasing heat storage tank size can increase *PES*, CO<sub>2</sub> savings, and cost savings considerably while reducing boiler start up frequency and operating duration. While the increase in thermal storage tank size and the selection of appropriate operating temperature limits may improve the performance of an EPC system, the effects of these changes have not been found sufficient to make a system equipped with a low performing LCR engine to be a viable option, and this shows the importance of engine efficiency for EPC applications. Therefore, the general design characteristics of an EPC system must involve a high performing engine that is no larger than 80cc, a thermal storage tank sized for the particular house type, and carefully selected storage tank temperature limits with a wide operating temperature dead band.

When comparing the two strategies, it can be observed that maximum *PES* and CO<sub>2</sub> savings for the HPC system tend to occur for a larger engine size than in the case of the EPC system. In both cases, in order to have reproducible results in different house types, it is important to size the storage tank to match the particular application.

For LCR engines, while the HPC strategy generates considerable *PES*, CO<sub>2</sub> savings and cost savings, EPC systems are marginally profitable, and only for the smallest engines. For most of the engine size range they operate at a loss. Operating patterns of the auxiliary boiler on the other hand do not detract significantly between the two strategies.

In terms of the seasonal variation of generated savings, the HPC strategy has been found to generate savings under all seasons with highest observed savings during the summer months. On the other hand, the EPC strategy has been observed to operate at a loss during the warmer months of the year as a result of the reduced thermal load leading to large amounts of rejected heat. In addition, the HPC strategy has been found to outperform the EPC strategy in terms of *PES* and CO<sub>2</sub> savings throughout the whole year, and this leads to the conclusion that the HPC strategy is the better strategy throughout the whole year.

While the difference in system performance between the two tested UK locations has been found to be small under both tested strategies, the operating patterns of the auxiliary boiler were observed to exhibit significant variations with location.

The FIT eligibility specifications are in place to prevent the use of excessively large units by disqualifying all systems that generate a maximum power output greater than  $2kW$  which corresponds to an engine displacement ranging between 140cc and 160cc. The simulation results showed that while this specification works reasonably well for all tested FIT eligible HPC systems, the EPC strategy has been found to exhibit a performance comparable to that of the HPC strategy only under engine sizes of 50cc and below, and only when the fuel conversion efficiency of the generator set is high. Even under an HCR engine, FIT eligible EPC systems with an engine size of 100cc and above generate no *PES* and  $CO_2$  savings, but at the same time have been found to have a very profitable operation, more so than the HPC system of the same size generating high *PES* and  $CO_2$  savings. For both control strategies, cost savings under FIT scheme occur for a larger than optimum engine size due to the high revenues provided by the generation tariff which favour systems that produce larger amounts of electricity (larger systems and EPC strategy). Due to the high export and generation tariffs present under the FIT scheme, cost savings tend to be higher for the system that generates proportionally larger amounts of electricity, even when the generated *PES* and  $CO_2$  savings are lower compared to those encountered under a system that generates proportionally smaller amounts of electricity. Thus, from the above, it is concluded that the FIT scheme for micro-CHP systems does not always promote the most environmentally friendly solution, but in many cases provides incentives for the acquisition of a system that generates the highest amount of electricity under the given maximum allowable power output which for both strategies can be characterised as excessive.

Under no government subsidy, cost savings curves tend to follow the trends of the *PES* curves and the low export prices make power export an



economically damaging process. The comparison of the non subsidized economic outcome of the two strategies under an HCR engine showed that the HPC strategy is an inherently better performing control scheme not only in terms of energetic and environmental performance criteria, but also in terms of annual cost savings throughout the complete simulated engine size range.

The LCR engine type (under which the HPC outperforms the EPC strategy by a great margin) is the most common, affordable, and readily available of the two, and in reality it is uncommon to find an engine of such high efficiency in the small scale. In addition, the engine under the EPC strategy operates for considerably longer periods than under the HPC strategy for engine sizes that generate comparable savings. The above, combined with the fact that under no governmental subsidies, the HPC system outperforms the EPC system in terms of cost savings make HPC a more viable strategy for residential applications under UK residential energy demands.

### **11.3. Recommendations for future work**

Due to the time constraints present in the delivery of all projects, there are a number of areas that have not been explored in the current thesis, but will be listed in the following paragraphs as recommendations for future work.

While in the current project the engine efficiency has been assumed to be the same for all engine sizes belonging to the same engine family, in reality, engine efficiency tends to drop as engine size is reduced. It is recommended that studies on the variation of engine waste heat are undertaken, and a mathematical relationship that scales the various waste heat component tables for a given engine size is created for use in future studies.

Research on the effect of the number of engine and boiler start up processes on component operating life can allow for a better planning of an investment on a CHP system.

As the developed engine model describes the engine operation for the complete operating range of the engine, a controller algorithm that sets the engine speed at an optimum value for a given electrical load, thus operating

the engine at a variable speed control scheme can be added in the main model. The model under a variable speed, variable output operating strategy can then be simulated, and its performance be evaluated and compared to that of the constant speed HPC and EPC strategies.

The addition of a battery to the unit is expected to influence the non-subsidized economic performance of the HPC strategy – especially in the case of the larger engine sizes – to an extent, as it would ensure that a larger fraction of onsite generated electricity is consumed by the operator. In the case of the EPC strategy, it would allow for larger engines to be used efficiently for a shorter annual operating duration. The extent to which the addition of a battery enhances system performance can be investigated by means of developing and adding a battery model to the existing general model layout, combined with updated controller algorithms to accommodate the battery model, and simulating the battery equipped models under the parameter combinations tested on Chapter 8, Chapter 9, and Chapter 10, and comparing the resulting performance to the existing findings.

A new hybrid strategy is suggested for future evaluation that combines characteristics of both HPC and EPC strategies in order to avert the importation of electricity as well as rejection of surplus heat. Under this proposed strategy, the system will operate as an electricity load following generator, recovering waste heat from the engine, and adding it to the heat storage tank only when the storage tank temperature lies between a specified temperature band. Once the upper limit of this temperature band is reached, the system will be switched off, and electrical demand will be met by the grid until the storage tank temperature falls to the lower band limit, where the unit will be switched on again, and the system will resume operating as a load following EPC system. This strategy would therefore take the best of both worlds by combining the shorter engine operating duration and no heat rejection of the HPC strategy, with the reduced amounts of electricity imports of the EPC strategy.

Simulations can be carried out for all dwelling types developed in Chapter 6 under all engine types and control strategies tested in Chapter 8 to Chapter

10, as well as the system variations and control strategies proposed in the current section. Data obtained by this procedure would help the CHP designer select the most suitable system combination for a given application.

The simulation tool could be further developed to an intelligent online energy optimization platform. Real time weather data, energy prices available from online sources, along with the schedule and performance objectives of the occupant acquired through a smart phone application would be utilized to enable the tool to generate the most suitable control code and upload it to a real time CHP system controller through the internet. This network would give the occupier the capability of scheduling the operation of the micro-CHP installation remotely in a way that the house reaches the desired temperature at the expected time of the occupant arrival while following an optimal control schedule in terms of energy, CO<sub>2</sub>, and cost savings, depending on the set objective, and address the volatility in energy prices, and the day to day differences in weather and occupancy.

Finally, while the FIT scheme has been found to be quite effective in promoting the proliferation of low carbon footprint DES such as micro-CHP, a further development of its set of specifications could ensure that all subsidized units generate *PES* and CO<sub>2</sub> savings. It is recommended that FIT eligibility requirements become specific to the selected control strategy, dwelling type and size. Specifying the thermal storage tank size and boiler operating temperature limits would further ensure that performance does not fall below a certain level, especially in the case of the EPC strategy, and that the engine and boiler start up frequencies are kept to a minimum. A more radical approach to the subsidy of micro-CHP systems would be a scheme that rewards the CHP operator for a calculated annual amount of CO<sub>2</sub> reduction rather than for power generation and export, thus enhancing the incentive to invest in the most efficient and environmentally friendly CHP system combination.

## References

- [1] T. Korakianitis, A. M. Namasivayam and R. J. Crookes, "Natural-gas fueled spark-ignition (SI) and compression-ignition (CI) engine performance and emissions," *Progress in Energy and Combustion Science*, vol. 37, pp. 89-112, 2010.
- [2] F. Caresana, C. Brandoni, P. Feliciotti and C. M. Bartolini, "Energy and economic analysis of an ICE-based variable speed-operated micro-cogenerator," *Applied Energy*, vol. 88, p. 659–671, 2011.
- [3] K. Gluesenkamp, Y. Hwang and R. Radermacher, "High efficiency micro trigeneration systems," *Applied Thermal Engineering*, vol. 50, no. 2, p. 1480–1486, 2013.
- [4] L. M. Chamra, P. J. Mago, N. Stone and J. Oliver, "Micro-CHP (Cooling, Heating, and Power): Not Just Scaled Down CHP," in *ASME 2006 Power Conference*, Atlanta, Georgia, USA, 2006.
- [5] B. Sicre, A. Buhning, B. Platzer and K. H. Hoffmann, "Energy and cost assessment of Micro-CHP plants in high performance residential buildings".
- [6] M. Cadorin, P. R. Spina and M. Venturini, "Feasibility analysis of Micro-CHP systems for residential building applications. (2010)," in *EUCOS 2010 International Conference*, Lausanne, 2010.
- [7] A. D. Hawkes and M. A. Leach, "The capacity credit of micro-combined heat and power," *Energy Policy*, vol. 36, pp. 1457-1469, 2008.
- [8] J. Abedin, S. Firth and P. Eames, "SIMULATION OF DOMESTIC HEAT DEMAND SHIFTING THROUGH SHORT TERM THERMAL STORAGE," in *Conference of International Building Performance Simulation Association*, Chambéry, France, 2013.

- [9] “Feed-In Tariffs,” [Online]. Available: <http://www.fitariffs.co.uk/FITs/principles/export/>. [Accessed 31 03 2015].
- [10] “Energy Saving Trust,” [Online]. Available: <http://www.energysavingtrust.org.uk/Generating-energy/Getting-money-back/Feed-In-Tariffs-scheme-FITs>. [Accessed 21 01 2015].
- [11] A. Moran, P. J. Mago and L. M. Chamra, “Thermoeconomic modeling of micro CHP (micro – cooling, heating and power) for small commercial applications,” *INTERNATIONAL JOURNAL OF ENERGY RESEARCH*, vol. 32, pp. 808-823, 2008.
- [12] Y. A. Cengel and M. A. Boles., *Thermodynamics: An Engineering Approach* 5th edition, McGraw-Hill Companies, 2005.
- [13] B. Linder, *Thermodynamics and introductory statistical mechanics*, New Jersey: John Wiley & Sons, Inc., 2004.
- [14] R. Saidur, M. Rezaei, W. K. Muzammil, M. H. Hassan, S. Paria and M. Hasanuzzaman, “Technologies to recover exhaust heat from internal combustion engines,” *Renewable and Sustainable Energy Reviews*, vol. 16, no. 8, pp. 5649-5659, 2012.
- [15] J. S. Jadhao and D. G. Thombare, “Review on Exhaust Gas Heat Recovery for I.C. Engine,” *International Journal of Engineering and Innovative Technology (IJEIT)*, vol. 2, no. 12, pp. 93-100, 2013.
- [16] C. R. Ferguson and A. T. Kirkpatrick, *Internal Combustion Engines: Applied Thermosciences*, New York: John Wiley & Sons. Inc., 2001.
- [17] J. Heywood, *Internal Combustion Engine Fundamentals*, London: Mcgraw-Hill, 1989.
- [18] H. Onowwiona and V. Urgusal, “Residential Cogeneration Systems: Review of the current technology,” *Renewable and Sustainable Energy*

*Reviews*, vol. 10, pp. 389-431, 2006.

- [19] H. I. Onovwiona, V. I. Urgusal and A. S. Fung, "Modelling of internal combustion engine based systems for residential applications," *Applied Thermal Engineering*, vol. 27, pp. 848-861, 2007.
- [20] C. D. Aussant, A. S. Fung, I. V. Urgusal and H. Taherian, "Residential application of internal combustion engine based cogeneration in cold climate-Canada," *Energy and Buildings*, vol. 41, p. 1288–1298, 2009.
- [21] A. Thumann and D. P. Mehta, *Handbook of Energy Engineering* 5th edition, Exeter, DEV, United Kingdom: Fairmont, 2001.
- [22] M. Badami, M. Mura, P. Campanile and F. Anzio, "Design and performance evaluation of an innovative small scale combined cycle cogeneration system," *Energy*, vol. 33, p. 1264– 1276, 2008.
- [23] A. A. Aliabadi, M. J. Thomson and J. S. Wallace, "Efficiency Analysis of Natural Gas Residential Micro-cogeneration Systems," *Energy Fuels*, vol. 24, pp. 1704-1710, 2010.
- [24] G. Angrisani, C. Roselli and M. Sasso, "Distributed microtrigeneration systems," *Progress in Energy and Combustion Science*, vol. 38, pp. 502-521, 2012.
- [25] A. Canova, C. Cavallero, F. Freschi, L. Giaccone, M. Repetto and M. Tartaglia, "Comparative economical analysis of a small scale trigenerative plant: a case study," in *Industry Applications Conference, 2007. 42nd IAS Annual Meeting.*, New Orleans, LA, 2007.
- [26] E. S. Barbieri, P. R. Spina and M. Venturini, "Analysis of innovative micro-CHP systems to meet household energy demands," *Applied Energy*, vol. 97 , p. 723–733, 2012.
- [27] O. A. Shaneb, G. Coates and P. C. Taylor, "Sizing of residential  $\mu$ CHP systems," *Energy and Buildings*, vol. 43, pp. 1991-2001, 2011.

- [28] H. Cho, R. Luck, S. D. Eskioglu and L. M. Chamra, "Cost-optimized real-time operation of CHP systems," *Energy and Buildings*, vol. 41, pp. 445-451, 2009.
- [29] Y. Takita, S. Kono and A. Naoi, "Study of Methods to Enhance Energy Utilization Efficiency of Micro Combined Heat and Power Generation Unit-Equipped with an Extended Expansion Linkage Engine and Reduction of Waste Energy," *SAE International*, 2011.
- [30] H. Ren, W. Gao and Y. Ruan, "Optimal sizing for residential CHP system," *Applied Thermal Engineering*, vol. 28, p. 514–523, 2008.
- [31] Y. Huangfu, J. W. Wu, R. Z. Wang, X. Q. Kong and B. H. Wei, "Evaluation and analysis of novel micro-scale combined cooling, heating and power (MCCHP) system," *Energy Conversion and Management*, vol. 48, pp. 1703-1709, 2007.
- [32] M. De Paepe, P. D'Herdt and D. Mertens, "Micro-CHP systems for residential applications," *Energy Conversion and Management*, vol. 47, p. 3435–3446, 2006.
- [33] V. Kuhn, J. Klemes and I. Bulatov, "MicroCHP: Overview of selected technologies, products and field test results," *Applied Thermal Engineering*, vol. 28, p. 2039–2048, 2008.
- [34] A. Martens, "A. The energetic feasibility of CHP compared to the separate production of heat and power," *Applied Thermal Engineering*, vol. 18, pp. 935-946, 1998.
- [35] X. Q. Kong, R. Z. Wang, J. Y. Wu, X. H. Huang, Y. Huangfu, D. W. Wu and Y. X. Xu, "Experimental investigation of a micro-combined cooling, heating and power system driven by a gas engine," *International Journal of Refrigeration*, vol. 28, p. 977–987, 2005.
- [36] N. J. Kelly, J. A. Clarke, A. Ferguson and A. Burt, "Developing and testing a generic micro-combined heat and power model for simulations

of dwellings and highly distributed power systems,” *Proceedings of the Institution of Mechanical Engineers Part A Journal of Power and Energy Impact Factor & Information*, vol. 222, pp. 685-695, 11 2008.

- [37] J. L. Silveiraa, A. C. d. S. Walter and C. A. Luengo, “A case study of compact cogeneration using various fuels,” *Fuel*, vol. 76, no. 5, p. 447–451, 1997.
- [38] “Electricity: chapter 5, Digest of United Kingdom energy statistics (DUKES),” Department of Energy and Climate Change, London, 2014.
- [39] K. R. Voorpools and W. D. De Haeseleer, “The evaluation of small cogeneration for residential heating,” *International Journal of Energy Research*, vol. 26, no. 13, p. 1175–1190, 2002.
- [40] R. Jablko, C. Saniter, R. Hanitsch and S. Holler, “Technical and economical comparison of micro chp systems,” in *Future Power Systems*, Amsterdam, 2005.
- [41] S. J. Chapman., *Electric Machinery Fundamentals Fifth Edition*, Mc Graw-Hill, 2011.
- [42] A. Piacentino and F. Cardona, “An original multi-objective criterion for the design of small-scale polygeneration systems based on realistic operating conditions,” *Applied Thermal Engineering*, vol. 28, pp. 2391-2404, 2008.
- [43] M. Bianchi, A. De Pascale and P. R. Spina, “Guidelines for residential micro-CHP systems design,” *Applied Energy*, vol. 97, p. 673–685, 2012.
- [44] “U.S. Department of Energy,” ASHRAE, [Online]. Available: [http://apps1.eere.energy.gov/buildings/energyplus/cfm/weather\\_data3.cfm/region=6\\_europe\\_wmo\\_region\\_6/country=GBR/cname=United%20Kingdom](http://apps1.eere.energy.gov/buildings/energyplus/cfm/weather_data3.cfm/region=6_europe_wmo_region_6/country=GBR/cname=United%20Kingdom).



- [45] M. Bianchi, A. De Pascale and P. R. Spina, "Best practice in residential Micro-CHP systems design," in *Proceedings of the Thrid International Conference on Applied Energy*, Perugia, Italy, 2011.
- [46] H. Cho, R. Luck and L. M. Chamra., "Dynamic Simulation of a Micro-CHP Facility: A Case Study (2007)," in *Proceedings of Energy Sustainability 2007*, Long Beach, California, 2007.
- [47] The Government's Standard Assessment Procedure for Energy Rating of Dwellings, 2005, Revision 3 ed., Garston, Watford: BRE, 2005.
- [48] J.-P. Zimmermann, M. Evans, J. Griggs, N. King, L. Harding, P. Roberts and C. Evans, "Household Electricity Survey: A study of domestic electrical product usage," Milton Keynes, 2012.
- [49] "24-Hour Profile Chooser," 2011.
- [50] W. Pulkrabek, *Engineering Fundamentals of the Internal Combustion Engine*, New Jersey: Prentice Hall, 2003.
- [51] N. Hill, C. Dun, R. Watson and K. James, "2014 Government GHG Conversion Factors for Company Reporting: Methodology Paper for Emission Factors," Department of Energy & Climate Change, London, 2014.
- [52] H. M. Cho and B.-Q. He, "Combustion and Emission Characteristics of a Natural Gas Engine under Different Operating Conditions," *Environ. Eng. Res.*, vol. 14, no. 2, pp. 95-101, 2009.
- [53] M. S. Rocha, R. Andreos and J. R. Simões-Moreira, "Performance tests of two small trigeneration pilot plants," *Applied Thermal Engineering*, vol. 41, pp. 84-91, 2012.
- [54] Y. Li and X. Zhang, "Parametric Optimization of a Power System for a Micro-CCHP system," in *6th International Symposium on Heating, Ventilating and Air Conditioning*, Nanjing, China, 2009.

- [55] S. Scesa, "Analysis of a cogeneration system," *Energy Conversion and Management*, vol. 31, no. 5, pp. 489-493, 1990.
- [56] "Office of Gas and Electricity Markets," [Online]. Available: <https://www.ofgem.gov.uk/ofgem-publications/87074/rpiadjustedtariffsnon-pvapril2014.pdf>. [Accessed 19 01 2015].
- [57] X. L. Zhao, L. Fu, S. G. Zhang, Y. Jiang and H. Li, "Performance improvement of a 70 kWe natural gas combined heat and power (CHP) system. (2010)," *Energy* 35, vol. 35, p. 1848–1853, 2010.
- [58] M. Houwing, R. R. Negenborn and B. De Schutter, "Demand Response With Micro-CHP Systems," in *Proceedings of the IEEE | Vol. 99, No. 1*, January 2011.
- [59] A. D. Peacock and M. Newborough, "Controlling micro-CHP systems to modulate electrical load profiles," *Energy*, vol. 32, p. 1093–1103, 2007.
- [60] J. Zavala, P. R. Sanketi, M. Wilcutts, T. Kaga and J. K. Hedrick, "SIMPLIFIED MODELS OF ENGINE HC EMISSIONS, EXHAUST TEMPERATURE AND CATALYST TEMPERATURE FOR AUTOMOTIVE COLDSTART," in *Fifth IFAC Symposium for Advances in Automotive Control*, Pajaro Dunes/Seascap, California (USA), 2007.
- [61] L. Fu, X. Zhao, S. Zhang, Y. Li, Y. Jiang, H. Li and Z. Sun, "Performance study of an innovative natural gas CHP system," *Energy Conversion and Management*, vol. 52, p. 321–328, 2011.
- [62] J. A. Caton, "The thermodynamic characteristics of high efficiency, internal-combustion engines," *Energy Conversion and Management*, vol. 58, pp. 84-93, 2012.
- [63] W. Wang, I. Beausoleil-Morrison, M. Thomas and A. Ferguson, "VALIDATION OF A FULLY-MIXED MODEL FOR SIMULATING GAS-FIRED WATER STORAGE TANKS," in *Building Simulation 2007*,

2007.

- [64] Z. Liao and A. L. Dexter, "The potential for energy saving in heating systems through improving boiler controls," *Energy and Buildings*, vol. 36, pp. 261-271, 2004.
- [65] R. Parsons, 1997 Ashrae Handbook Fundamentals SI Edition, Amer Society of Heating, 1997.
- [66] "Energy Saving Trust," [Online]. Available: <http://www.energysavingtrust.org.uk/Heating-and-hot-water/Thermostats-and-controls>. [Accessed 25 10 2014].
- [67] R. Yao and K. Steemers, "A Method of formulating energy load profile for domestic buildings in the UK," *Energy and Buildings*, vol. 37, pp. 663-671, 2005.
- [68] K. T. Yun, H. Cho, R. Luck and P. J. Mago, "Modeling of reciprocating internal combustion engines for power generation and heat recovery," *Applied Energy*, vol. 102, pp. 327-335, 2013.
- [69] T. Heß, J. Seifert and P. Schegner, "COMPARISON OF STATIC AND DYNAMIC SIMULATION FOR COMBINED HEAT AND POWER MICRO-UNITS," in *17th Power Systems Computation Conference*, Stockholm, Sweden, 2011.
- [70] C. C. Lela and J. J. White, "DURABILITY OF LOW-EMISSIONS SMALL OFF-ROAD ENGINES," SOUTHWEST RESEARCH INSTITUTE, San Antonio, Texas, 2004.
- [71] R. A. Parsons, 2000 ASHRAE Handbook Heating, Ventilating and Air-Conditioning Systems and Equipment (SI Edition), American Society of Heating, Refrigerating & A-C Engineers, 2000.
- [72] J. Cadafalch, D. Carbonell, R. Consul and R. Ruiz, "Modelling of storage tanks with immersed heat exchangers," *Solar Energy*, vol. 112,

pp. 154-162, 2015.

- [73] G. Angrisani, M. Canelli, C. Roselli and M. Sasso, "Calibration and validation of a thermal energy storage model: Influence on simulation results," *Applied Thermal Engineering*, vol. 67, pp. 190-200, 2014.
- [74] R. D. C. Oliveski, A. Krenzinger and H. A. Vielmo, "Comparison between models for the simulation of hot water storage tanks," *Solar Energy*, vol. 75, pp. 121-134, 2003.
- [75] T. Schütz, R. Streblow and D. Müller, "A comparison of thermal energy storage models for building energy system optimization," *Energy and Buildings*, vol. 93, pp. 23-31, 2015.
- [76] V. Badescu, "Optimal control of flow in solar collector systems with fully mixed water storage tanks," *Energy Conversion and Management*, vol. 49, pp. 169-184, 2007.
- [77] A. C. Celador, M. Odriozola and J. M. Sala, "Implications of the modelling of stratified hot water storage tanks in the simulation of CHP plants," *Energy Conversion and Management*, vol. 52, pp. 3018-3026, 2011.
- [78] I. Richardson, M. Thompson, D. Infield and C. Connor, "Domestic electricity use: a high-resolution energy demand model," *Energy and Buildings*, vol. 42, no. 10, p. 1878–1887, 2010.
- [79] "United Kingdom Time Use Survey, 2000," Statistics, Ipsos-RSL and Oddice for National, Colchester, Essex.
- [80] S. Robinson and L. Smith, "Concept for exhaust energy recovery using a turbine electrical generator on a turbocharged spark ignition engine," 2011.
- [81] I. B. Morrison, "Annex 42 Domestic Hot Water Profiles for Use in Simulating the Performance of Residential Cogeneration Systems,"

International Energy Agency.

- [82] I. Knight, N. Kreutzer, M. Manning, M. Swinton and H. Ribberink, "European and Canadian non-HVAC Electric and. DHW Load Profiles for Use in Simulating the. Performance of Residential Cogeneration Systems," International Energy Agency, Ottawa, 2007.
- [83] I. B. Morrison, "ECBCS," [Online]. Available: <http://www.ecbcs.org/annexes/annex42.htm>. [Accessed 12 02 2014].
- [84] I. Richardson, M. Thompson and D. Infield, "A high-resolution domestic building occupancy model for energy demand simulations," *Energy and Buildings*, vol. 40, no. 8, pp. 1560-1566, 2008.
- [85] D. C. Karnopp, D. L. Margolis and R. C. Rosenberg, *System Dynamics: A Unified Approach*, Wiley Interscience, 1990.
- [86] D. C. Karnopp, D. L. Margolis and R. C. Rosenberg, *System Dynamics: Modeling, Simulation, and Control of Mechatronic Systems*, New Jersey: John Wiley & Sons, 2012.
- [87] W. J. Palm III, *System Dynamics Second Edition*, New York: McGraw-Hill, 2005.
- [88] C. L. Yaws, *Handbook of Thermodynamic Diagrams Volume 3: Organic Compounds – C8 to C28*, Houston, Texas: Gulf Publishing Company, 1996.
- [89] C. L. Yaws, *Handbook of Thermodynamic Diagrams Volume 1: Organic Compounds – C1 to C4*, Houston, Texas: Gulf Publishing Company, 1996.
- [90] L. Eriksson, "Mean Value Models for Exhaust System Temperatures," in *SAE 2002 World Congress & Exhibition*, Detroit, Michigan, 2002.
- [91] A. E. Fitzgerald, C. J. Kingsley and S. D. Umans, *Electric Machinery*,

6th ed., New York: Mc Graw-Hill, 2003.

- [92] M. U. Aslam, H. H. Masjuki, M. A. Kalam and M. A. Amalina, "A Comparative Evaluation of the Performance and Emissions of a Retrofitted Spark Ignition Car Engine," *Journal of Energy & Environment*, vol. 4, pp. 97-110, 2005.
- [93] T. I. Mohamad, H. H. Geok, S. Abdullah, Y. Ali and A. Shamsudeen, "Comparison of Performance, Combustion Characteristics and Emissions of a Spark Ignition Engine Fuelled by Gasoline and Natural Gas," *Technology Today Quarterly Journal*, vol. 2, no. 2, pp. 173-182, 2010.
- [94] M. A. Sera, R. A. Bakar and S. K. Leong, "EFFECT OF FUEL DENSITY ON THE PERFORMANCE OF A CNG FUELLED ENGINE," Fakulti Kejuruteraan Mekanikal Universiti Teknologi Malaysia.
- [95] P. M. Darade and R. S. Dalu, "Investigation of Performance and Emissions of CNG Fuelled VCR Engine," *International Journal of Emerging Technology and Advanced Engineering*, vol. 3, no. 1, pp. 77-83, 2013.
- [96] I. Sezer, "Gaseous Fuels in PFI Spark Ignition Engines," in *6th International Advanced Technologies Symposium (IATS'11)*, Elazığ, Turkey, 2011.
- [97] K. Resapour, B. A. Mason, A. S. Wood and M. K. Ebrahimi, "Bi-fuel SI Engine Model for Analysis and Optimization," *Universal Journal of Mechanical Engineering*, vol. 2, pp. 71-82, 2014.
- [98] E. Ramjee and K. V. K. Reddy, "Performance analysis of a 4-stroke SI engine using CNG as an alternative fuel," *Indian Journal of Science and Technology*, vol. 4, no. 7, pp. 801-804, 2011.
- [99] H. H. Geok, T. I. Mohamad, S. Abdullah, A. Yusoff and A. Shamsudeen, "Experimental Investigation of Performance and

Emissions of a Sequential Port Injection Compressed Natural Gas Converted Engine,” SAE Japan, 2009.

- [100] A. Das and H. C. Watson., “Development of a natural gas spark ignition engine for optimum performance (1996),” *Journal of Automobile Engineering*, vol. 211, pp. 361-378, 1997.
- [101] R. Ebrahimi and M. Mercier, “EXPERIMENTAL STUDY OF PERFORMANCE OF SPARK IGNITION ENGINE WITH GASOLINE AND NATURAL GAS,” IJE, 2010.
- [102] E. Tribbett, E. Froehlich and L. Bayer, “Effects of Ignition Timing , Equivalence Ratio and Compression Ratio on RDH Engine Performance,” [Online]. Available: [http://rescomp.stanford.edu/~efroeh/papers/RDH\\_Engine\\_Performance.pdf](http://rescomp.stanford.edu/~efroeh/papers/RDH_Engine_Performance.pdf).
- [103] S. Kakac and H. Liu, Heat Exchangers: selection, rating, and thermal design - Second Edition, London: CRC Press, 202.
- [104] D. Q. Kern, Process Heat Transfer - International Student Edition, London: McGraw-Hill International Book Company, 1983.
- [105] J. I. H. Lienhard and J. V. H. Lienhard, A Heat Transfer Textbook, Third ed., Cambridge, Massachusetts: Phlogiston Press, 2003.
- [106] F. P. Incropera, D. P. DeWitt, T. L. Bergman and A. S. Lavine, Fundamentals of Heat and Mass Transfer, 6th ed., New Jersey: John Wiley & Sons, 2007.
- [107] F. Kreith, Mechanical Engineering Handbook, Boca Raton: CRC Press, 1999.
- [108] C. Depcik and S. Assanis, “A Universal Heat Transfer Correlation for Intake and Exhaust Flows in an Spark-Ignition Internal Combustion Engine,” in *SAE 2002 World Congress & Exhibition*, 2002.

- [109] S. A. Ngy, "Exhaust Heat Exchange in a Pipe of an Internal Combustion Engine. EGR Cooler and Passenger Compartment Heating Applications," *Society of Automotive Engineers*, 2000.
- [110] P. F. Chapman, "A geometrical model of dwellings for use in simple energy calculations," *Energy and Buildings*, vol. 21, pp. 83-91, 1994.
- [111] "National Statistics - English Housing Survey: Housing Stock Report 2008," Department for Communities and Local Government, London, 2008.
- [112] The Government's Standard Assessment Procedure for Energy Rating of Dwellings 2012, Garston, Watford: BRE, 2012.
- [113] Y. McNally, P. Griffiths and T. Hyde, "Energy efficiency of dwellings and their impact on CO<sub>2</sub> reduction targets in Northern Ireland," in *CIBSE Technical Symposium*, Liverpool, 2013.
- [114] "National Statistics - English Housing Survey: Housing Stock Report 2009," Department for Communities and Local Government, London, 2009.
- [115] "Energy Consumption in the UK 2013," Department of Energy & Climate Change, London.
- [116] F. Hall and R. Greeno, *Building Services Handbook*, Fourth ed., Oxford: Butterworth-Heinemann, 2007.
- [117] R. A. Parsons, *22000 ASHRAE Handbook Heating, Ventilating and Air-Conditioning Systems and Equipment (SI Edition)*, American Society of Heating, Refrigerating & A-C Engineers, 2000.
- [118] T. Wang, Y. Zhang, J. Zhang and G. Shu, "Analysis of Recoverable Exhaust Energy from a Light-Duty Gasoline Engine," *Applied Thermal Engineering*, vol. 53, no. 2, pp. 414-419, 2013.



- [119] D. A. Arias, T. A. Shedd and R. K. Jester, "Theoretical Analysis of Waste Heat Recovery from an Internal Combustion Engine in a Hybrid Vehicle," *SAE 2006 Transactions Journal of Engines*, vol. 115, no. 3, 2006.
- [120] S. Mavridou, G. C. Mavropoulos, D. Bouris, D. T. Hountalas and G. Bergeles, "Comparative design study of a diesel exhaust gas heat exchanger for truck applications with conventional and state of the art heat transfer enhancements," *Applied Thermal Engineering*, no. 30, pp. 935-947, 2010.
- [121] Y. Ismail, D. Durrieu, P. Menegazzi and P. Chesse, "Potential of Exhaust Heat Recovery by Turbocompounding," in *SAE 2012 International Powertrains, Fuels & Lubricants Meeting*, 2012.
- [122] J. Martins, L. M. Goncalves, J. Antunes and F. Brito, "Thermoelectric Exhaust Energy Recovery with Temperature Control through Heat Pipes," in *SAE 2011 World Congress & Exhibition*, 2011.
- [123] Q. Hussain, D. Bringham and D. Maranville, "A MODEL BASED APPROACH TO EXHAUST HEAT RECOVERY USING THERMOELECTRICS," Ford Motor Company.
- [124] G. Shu, J. Zhao, H. Tian, H. Wei and X. Liang, "Theoretical Analysis of Engine Waste Heat Recovery by the Combined Thermo-Generator and Organic Cycle System," in *SAE 2012 World Congress & Exhibition*, 2012.

## **Appendix 1 Types of micro-CHP**

The following main  $\mu$ CHP technological branches have been identified on existing literature.

### **A.1.1 Stirling**

Stirling engines belong in the general family of external combustion engines, have multi-fuel capabilities [15], [24] and may even operate under solar power supply [4]. They are characterized by a quiet operation, low emissions, and low maintenance requirements [26].

Stirling based m-CHP units are usually operated under heat priority control and have predetermined discrete power levels. Heat to power ratio is well suited for residential use [33]. According to V. Kuhn et al. [33], Stirling based CHP electrical efficiency is highly dependent on the input temperature and may reach 25 – 30% LHV when fuelled by natural gas. Similarly, L. M. Chamra et al. [4] report an electrical efficiency range between 12% and 25% with a further potential for increase using recuperators. On the other hand, N. J. Kelly et al. [36] report electrical efficiency to be in the order of 8% – 9% LHV with device efficiency reaching levels as high as 88% to 95% LHV. In addition to the above, Stirling systems are characterized by a good part load performance [24].

While Stirling technology does have a number of advantages as shown above, it is still considered to be underdeveloped [26], [24] and expensive [20] to be considered a viable  $\mu$ CHP platform.

### **A.1.2. Rankine**

Micro-CHP systems that operate based on a variant of Rankine cycle are durable and have a low initial cost [4]. In addition, they are characterized by a low noise operation [26]. On the other hand, their electrical efficiency is relatively low and ranges from 5% to 20%. They are still considered underdeveloped for micro-CHP applications [4].

### **A.1.3. Micro Turbines**

Gas turbines as prime movers have some inherent advantages such as a multi-fuel capability, a high reliability and simplicity. For large scale units, electrical efficiency lies between 25% and 30% [4]. Due to the high temperature of the exhaust gasses, high grade waste heat can be used to successfully power a bottoming cycle thus increasing the system fuel conversion efficiency.

In the case of micro scale units, the available systems exhibit a less than favourable performance since gas turbines have been found to lose efficiency fast as unit size falls below  $30kW$  and the typical micro-CHP power output is in the order of  $3kW$ . Therefore, for the smaller scale Micro-Turbines, electrical efficiency is relatively low and in the order of 12% LHV [26]. This technology has also been characterized as underdeveloped [24] with poor part load efficiency [33], and therefore not very suitable for small scale applications [4].

### **A.1.4. Fuel Cells**

Fuel Cells have certain operating characteristics that could potentially make the technology a good candidate platform for micro-cogeneration applications. Their very high electrical efficiency [24] which ranges between 45 – 55% LHV means that they can generate savings even during warmer months. At the same time, they are characterized by a fast electrical response, noiseless operation and a high reliability [33].

While the above advantages of Fuel Cells increase their attractiveness, at the same time their very high initial cost, their short service life [20],[24], their fuel sensitivity, and the fact that they are still underdeveloped [107], [24] compared to competing systems such as ICE and SE based systems [36], are serious obstacles in the proliferation of such systems in the  $\mu$ CHP industry.

### **A.1.5. Thermo - Photovoltaic**

While this category of cogeneration is probably the simplest as it is pretty similar in construction to the conventional boiler with a part of its internal surface fitted with thermo-photovoltaic (TPV) elements, it is also the least likely to encounter in micro-CHP applications.

E.S. Barbieri et al. [26] investigated the performance characteristics of a Thermo-Photovoltaic micro-CHP unit and encountered values of electrical efficiency that ranged between 2% to 5% LHV, and an overall fuel utilization efficiency higher than 90%. As in the case of the competing technologies discussed above, further development has been suggested in order for this technology to be made marketable.

### **A.1.6. ICE based systems**

The reciprocating internal combustion engine (especially NG fuelled variants) is currently the most popular prime mover type used in micro-cogeneration systems due to a number of very favourable characteristics such as a high electrical efficiency, a low investment cost, and a high reliability [2]. Other notable advantages of this prime mover type are its fast electrical response, its fast start-up, its capability to power equipment other than the electric machine, its high level of technological maturity [4], and its relatively good part load performance [22].

Due to their relatively high exhaust temperatures, ICEs generate waste heat of a high grade [4] and the use of this heat for powering a bottoming cycle is not uncommon [22], [118].

Electrical efficiency of ICE powered micro-CHP systems usually ranges from 20% to 26% [26] but in some cases may exceed 30% depending on the engine and electric machine characteristics [4]. Compared to competing distributed energy technologies, ICEs are more efficient at small scale than MTs, and have a shorter payback period (PBP) than that of Photovoltaic cells [20]. In terms of the device fuel utilization efficiency of ICE based  $\mu$ CHP systems, in some cases it may exceed 90% LHV [26].

Due the many advantages of the reciprocating ICE compared to the competition, and the disadvantages of the competing systems, internal combustion engines are considered to be the most suitable of the available technologies for small scale cogeneration applications [35] and for the above reasons, they are the most widespread prime movers in the industry [24].

## Appendix 2. A discussion on Bottoming cycles

### A.2.1. Rankine Cycle

The most common bottoming cycle type used for the increase of the fuel conversion efficiency of ICE based power generators is the closed Rankine cycle, be it based on a steam turbine as shown in Figure A.2.1, or a reciprocating steam engine.

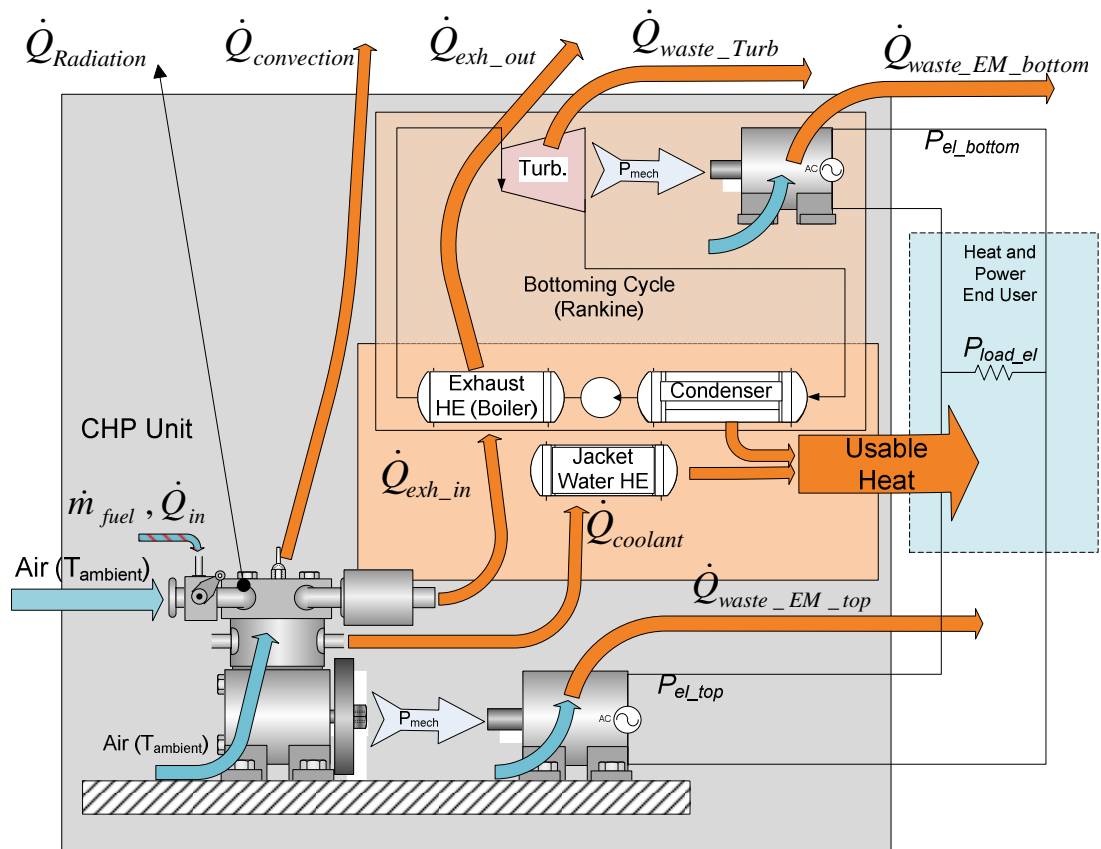


Figure A.2.1 Schematic of the energy flow taking place between the components of a combined ICE-Rankine cycle based CHP system

Depending on the selected working medium, waste heat of high and low grades may be recovered. Diego Arias et al. [119] reported that the amount of waste heat converted to mechanical power amounted up to 5.5% of fuel input power when heat from the exhaust and the engine coolant was used. A

similar improvement in fuel conversion efficiency was observed by M. Badami et al. [22] whose ICE/RC system used recovered exhaust heat to power the Rankine cycle and showed an increase in fuel conversion efficiency of approximately 4% LHV compared to that of the ICE only variant. In addition, efficiency was reported as less sensitive throughout the system operating envelope. Comparable were the findings of S. Mavridou et al. [120] who observed 10% to 12% reduction in *bsfc* at 100% of maximum load. Similarly, Tianyou Wang et al. [118] observed an increase in fuel conversion efficiency of up to 14% and fuel savings of up to 34% compared to the stock engine.

Non usable (low grade) amounts of waste heat from the condenser of the Rankine cycle as well as the coolant heat from the ICE jacket can be recovered at a temperature of approximately 90°C for space heating purposes [22].

### **A.2.2. Turbocompounding**

Turbocompounding is the utilization of the enthalpy of the exhaust gasses to power a turbine which is mechanically engaged with the engine main shaft [121], [15]. Youssef Ismail et al. [121] modelled and simulated a diesel turbocompound engine and observed a gain in fuel conversion efficiency in the order of 5% to 10%. A disadvantage of the turbocompound technology is the fact that it affects engine backpressure significantly [15].

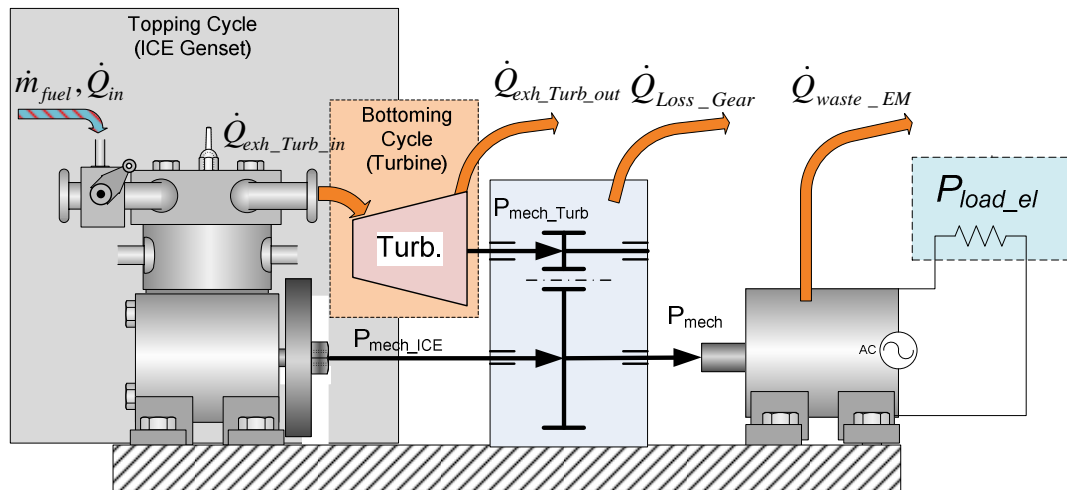


Figure A.2.2 Schematic of the energy flow taking place between the components of a turbo-compound prime mover supplying power to an electric machine

### A.2.3. Turbo generator

A less common but interesting nonetheless type of bottoming cycle fitted on a reciprocating internal combustion engine is the turbo generator as seen in S. Robinson and L. Smith [80] who conducted a study on the recovery and conversion of waste heat contained in the exhaust gasses of an SI ICE to electrical power using a turbo generator which is similar in principle to a turbocharger. The sum of the electrical power from the engine crank and the turbine shaft supply the battery of the hybrid car.

Since turbine efficiency is in excess of 60%, and the heat rejected in the exhaust is over 30% of the fuel input LHV, the recovered energy in mechanical form can reach or exceed 18% of fuel input. The efficiency of the generator can reach or exceed 90% of the input. As a result this configuration can lead to a reduction in the *bsfc* of the system by 10% or more.



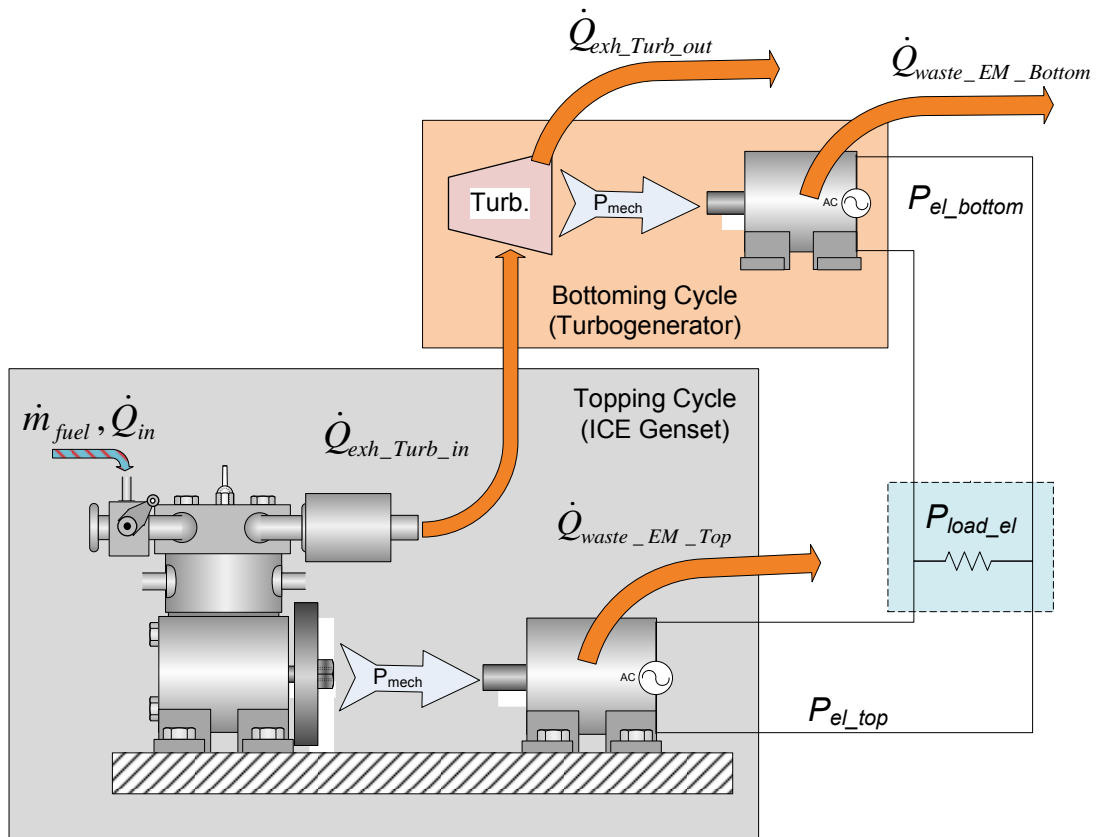


Figure A.2.3 Schematic of the energy flow taking place between the components of an internal combustion engine with a turbogenerator

#### A.2.4. Thermoelectric Exhaust Heat Recovery

Thermoelectric generators recover heat from the exhaust and coolant and convert it to electricity using thermocouples [122]. They work on the seebeck effect [14], which is the same principle used by TPV systems [123] as discussed in Appendix 1. Heat is converted to electricity, provided there is a temperature gradient between the ends of a semiconductor [14], [15]. Currently energy savings of 6% have been observed in the automotive industry [122].

One of their main advantages is the lack of moving parts [123] while the main disadvantage of this technology is its low conversion efficiency which ranges between 2% to 5% [15] and its low level of technical maturity [14].

#### **A.2.5. A combination of technologies**

A combination of the technologies discussed above, may further increase the system fuel conversion efficiency. One such case is the system modelled and simulated by Gequn Shu et al. [124] consisting of an SI engine, a thermoelectric generator and an ORC bottoming cycle the fuel conversion efficiency of which reached 45% LHV.

### Appendix 3 Sensible Enthalpy Plots

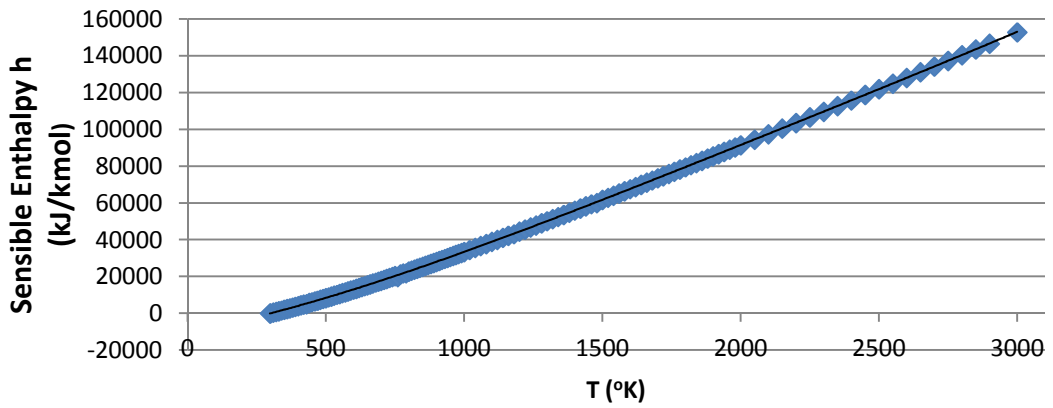


Figure A.3.1 Sensible Enthalpy of CO<sub>2</sub> vs. temperature

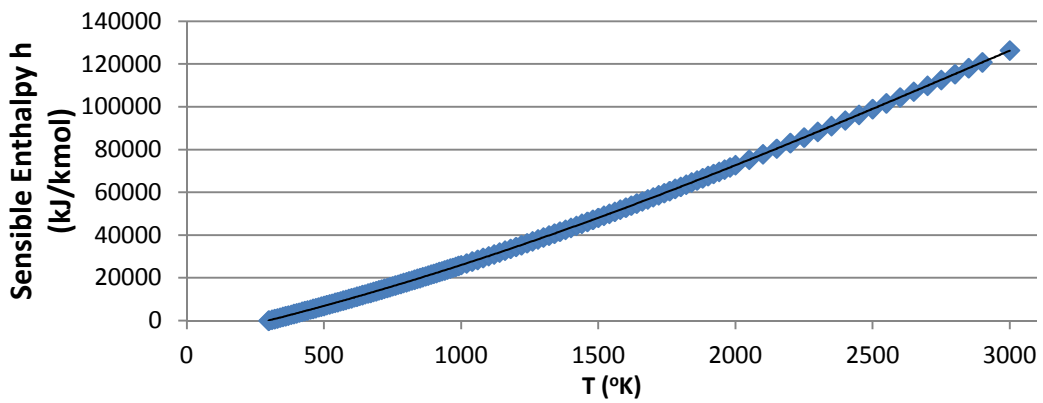


Figure A.3.2 Sensible Enthalpy of H<sub>2</sub>O vs. temperature

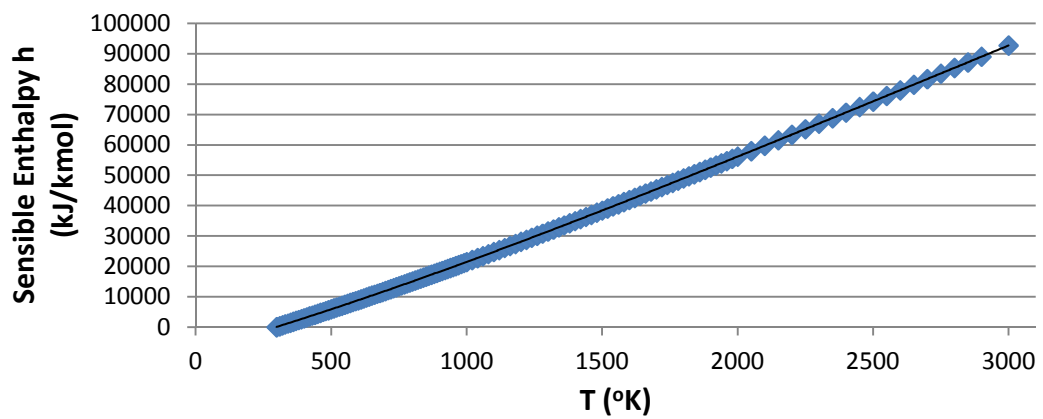


Figure A.3.3 Sensible Enthalpy of N<sub>2</sub> vs. temperature

## Appendix 4 UK Location Factors

Table A.4.1 Table of UK Location Factors [116]

UK Location		Location Factor <i>L.F.</i> (°K)
Available Locations in Fred Hall et al. [116]	IWECS weather profile locations	
North & Midlands	Aughton	29
	Birmingham	
	Finningley	
Scotland	Aberdeen	28.5
	Leuchars	
	Oban	
South East	Hemsby	27
	London, Gatwick	
Wales	-	27
Northern Ireland	Belfast	26.5
South West	Jersey *	25
* While Southwest may not include Jersey, it is the closest from the available locations in Fred Hall et al. [116]		